COMPACT MULTIBAND ANTENNAS WITH POLARIZATION DIVERSITY AND WIDEBAND CHARACTERISTICS USING ARTIFICIAL ELECTROMAGNETIC STRUCTURES

Thesis

Submitted in partial fulfillment of the requirements for the degree of
DOCTOR OF PHILOSOPHY

by

PRINCY MARIA PAUL

DEPARTMENT OF ELECTRONICS AND COMMUNICATION ENGINEERING,
NATIONAL INSTITUTE OF TECHNOLOGY KARNATAKA,
SURATHKAL, MANGALORE -575025

JANUARY, 2019

DECLARATION

I hereby ***declare*** that the research Thesis entitled **Compact Multiband Antennas with Polarization Diversity and Wideband Characteristics using Artificial Electromagnetic Structures** which is being submitted to the ***National Institute of Technology Karnataka, Surathkal*** in partial fulfillment of the requirement for the award of the Degree of ***Doctor of Philosophy*** in **Department of Electronics and Communication Engineering** is a ***bonafide report of the research work carried out by me***. The material contained in this research Thesis has not been submitted to any University or Institution for the award of any degree.

Princy Maria Paul
Register No: 155060EC15F05
Department of Electronics and Communication Engineering.

Place: NITK-Surathkal.
Date:

CERTIFICATE

This is to certify that the Research Thesis entitled **Compact Multiband Antennas with Polarization Diversity and Wideband Characteristics using Artificial Electromagnetic Structures** submitted by **Princy Maria Paul** (Register Number:155060EC15F05) as the record of the research work carried out by her, is accepted as the *Research Thesis submission* in partial fulfillment of the requirements for the award of degree of **Doctor of Philosophy**.

Dr. Krishnamoorthy Kandasamy
Research Guide
Assistant Professor
Dept. of Electronics and Communication Engg.
NITK Surathkal - 575025

Dr. Mohammad Sharawi
Research Co- Guide
Professor
Dept. of Electrical Engg. and Poly-Grames Research Center
Polytechnique Montreal, QC H3V 1A2, Canada

Chairman-DRPC
(Signature with Date and Seal)

To the pursuit of knowledge
And the thrill of discovery

For Dad, Mom, Roby, Pappa, Mummy and Simmu

Acknowledgements

First and foremost, I take this opportunity to thank the Lord Almighty for enabling me to work persistently in pursuit of this research work, and for empowering me with the strength and perseverance towards the fruitful accomplishment of the task.

Next, I offer my deepest gratitude to my research supervisor, Dr. K. Krishnamoorthy who has been a constant source of support and encouragement to me. His timely counseling has always guided me technically and morally. His profound knowledge and thorough patience have always been a beacon of light for me throughout the course of my journey.

I would like to sincerely acknowledge the immense support provided by my co-advisor Prof. Mohammad Sharawi without whom the realization of this work would not have been possible. I thank him for his invaluable advices, kind words and patient guidance whenever approached. His in depth technical know-how, enthusiasm, and spirited support have always kept the wheels of my work going, His ready willingness to spare his time and his wise mentoring have always ensured the timely completion of my works. I also thank the administration of King Fahd University of Petroleum & Minerals (KFUPM) and Prof. Sharawi in particular for providing me with the opportunity to undergo a research interaction there and for giving me access to the lab facilities at KFUPM for fabrication and measurement purposes. I would like to sincerely acknowledge the technical support the students at KFUPM have provided me for the same. I am grateful to them for their kind gesture and valuable inputs which have helped me during the course of my work. I also wish to acknowledge the technical exposure received during the period of my research interaction at the University of Texas Dallas (UTD) and would like to thank Prof. Lakshman Tamil for having hosted me there.

I owe my sincere thanks to Prof. M. S. Bhat and Prof. U. Shripathi Acharya, former heads and Prof. T. Laxminidhi, the present head, Department of Electronics and Communication Engineering for their valuable advice and administrative support. I would also like to acknowledge the encouragement, guidance and useful evaluation provided by my RPAC members, Prof. M. Kulkarni and Dr. P. Parthiban. I take this opportunity

to thank all the teaching and non teaching staff and the lab technicians for offering their valuable expertise at all times which has helped me realize the goals of my work at a faster pace.

I particularly thank my fellow scholars who have been a part of my journey and helped me technically and motivated me. I take this opportunity to genuinely thank all my friends from far and near who have always been with me, never failing to support me and lift me up at times of need. I will forever be indebted to them for their invaluable friendship, care, concern and timely interventions. A special word of thanks to Meryl Lopez for proofreading my thesis and extending unforgettable companionship during the final days of my course.

Throughout the different phases of my Ph.D., the love and support provided by my family know no bounds, I thank them for always having worked behind the scenes for me. Their silent prayers and gentle chiding have molded me into the person I am today. A special word of thanks to my husband and family, my sisters, brother-in-law and nephew for their benevolence and guidance at every juncture of my course. I specially wish to acknowledge the unparalleled support my parents have provided me, for the sacrifices they have made, and for always believing in me.

Abstract

With the rapid changes in the technological advancements of wireless communication, the design and development of advanced diverse antennas that are smaller in size but higher in performance with enhanced bandwidth and independently controllable multiple bands of operation has become a challenging need. In addition, the features of circular polarization (CP) at the multiple resonant frequencies and provision for control in sense of polarization at each of the CP bands of the antenna are desired. The different performance parameters and radiation characteristics of these antenna designs play a significant role in the optimum realization of the concerned wireless devices. Hence, this thesis presents novel antenna designs that offer radiating bands at frequencies pertaining to various applications related to wireless technology, radar systems, satellite communication devices among many other applications.

In order to obtain the desired characteristics, artificially synthesized metamaterials (MTMs) have been used whose properties can be easily tuned and controlled so as to obtain superior performance in MTM based antennas.

The thesis presents MTM based slot antennas that are designed to operate at multiband frequencies and offer easy opportunity for independent tuning of the frequency bands. The different types of MTM unit cells used include the split ring resonators (SRRs) and copper strip arrays whose properties have helped design slot antennas that operate with triband, quadband and pentaband frequencies with compact antenna geometries.

The other designs presented in the thesis include compact slot antenna geometries that operate at multiple frequency bands having at least one band of operating bandwidth greater than 50%. A fictitious short circuit is excited in a quarter wavelength slot using a suitably designed microstrip feed line to obtain the wideband compact design. Multiple bands are obtained by introducing SRR and modified SRR structures.

The concept of transmission line is also briefly introduced in the thesis and a novel compact UWB slot antenna design is discussed where rows of artificially dispersed transmission lines are used to obtain the various

resonance modes that combine with the fundamental slot modes to give the UWB resonance. The remaining designs included in the thesis involve slot antennas that offer the feature of circular polarization at multiple frequency bands. This is obtained by altering the slot structure and by introducing different MTM-based structures, inclined copper strip strips, U-strips and meandered slots. The different frequency bands can be tuned according to the application by changing the sizes of the structures and also the sense of polarization at the different bands can be altered.

All the designs are fabricated and the different parameters are compared based on simulated and fabricated results. The last chapter presents a brief comparison of the proposed designs with the previous works and gives a brief idea on the scope for future works. The compactness, radiation efficiencies, peak gain values, operating bandwidths, axial ratio values are the various parameters looked into and compared with previous designs in literature.

Keywords: Slot antennas; Multiband; Metamaterials; Circular polarization; Ultra wideband; SRR.

Contents

List of Figures

List of Tables

Abbreviations

Abbreviation	Expansion
MTM	Metamaterials
UWB	Ultra Wide Band
CP	Circular Polarization
ARBW	Axial Ratio Band Width
LHCP	Left Hand Circularly Polarized
RHCP	Rightt Hand Circularly Polarized
SRR	Split Ring Resonator
CSRR	Complementary Split Ring Resonator
EBG	Electromagnetic Band Gap
TL	Transmission Line
LHM	Left Handed Materials
NRI	Negative Refractive Index
DNG	Double Negative

Chapter 1

INTRODUCTION

This chapter gives an introduction to the evolution of the different wireless communication standards and the need for novel antenna systems that can support these communication standards. Depending on the application requirements, various antenna designs have been developed, yet research gaps remain that need to be filled. These gaps are discussed in the work motivation followed by definition of the problem statement and formulation of the objectives. The work methodology utilised to fulfill these objectives is also discussed and an outline of the thesis is provided at the end of the chapter.

1.1 Evolution of Wireless Communication Standards and Antenna Systems

With the introduction of compatible transmission technology and new frequency bands over the past decades, the cellular wireless communication witnessed an explosive growth. The first move in the cellular wireless generation (G) started in 1979 by Nippon, Japan with an analog (1G) under the radio-frequency (RF) standards. This was the first generation of wireless cellular technology, which continued until replaced by digital (2G) telecommunications in 1981. The 2G technology was followed by the Wide Band (3G) Wireless Network, which supported the data transfer of 0.2 Mbits/S with mobile broadband access of several Mbits/s, video calls and mobile TV technologies in 1998. The 4G networks started its waves in 2008 with a massive feat for mobile technology, especially for smartphones, increased internet speeds up to 500

times faster than 3G and also supported HD TV on mobile, high quality video calls, and fast mobile browsing. The 5G with lot of advanced features like cloud computing is under pipeline which will be able to manage the huge number of connections and to make the Internet of Things (IoT) a real possibility. The evolution of the wireless mobile phone communication is pictorially depicted in Figure 1.1.

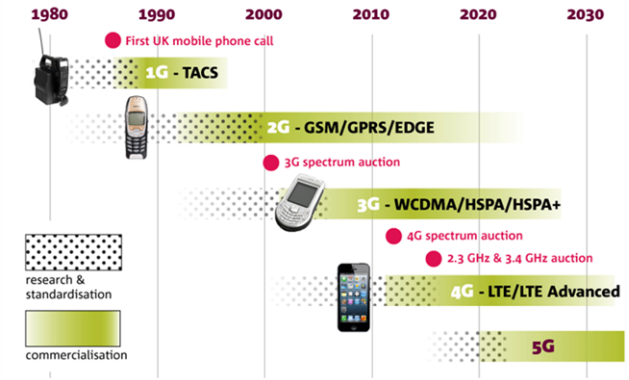

Figure 1.1: Evolution of mobile phone communications (Futter and Soler (2017))

The beginning of the 2G mobile phone technology saw an advancement in the wireless communication standards in the 1990s. Thus led to a growth in the invention of innovative antenna designs that comply with the various standards. The antenna came into existence with the discovery of the EM waves by Heinrich Hertz over a century ago. Since then, the antenna technology has witnessed various developments to keep in par with the growing demands of the different wireless RF standards (Luk (2011)).

The antenna was developed as an essential component of any wireless system to receive and transmit signals. Beginning from the large profile dish-like reflector antennas and the Yagi-Uda antennas, the compactness, efficiency, gain and bandwidths of the antenna systems have improved over the years in order to be easily mounted on the required systems and at the same time provide superior performance for various applications. Depending on the number of ports designated for the wireless system, SISO (Single-Input Single-Output) and MIMO (Multiple-Input Multiple-Output) technologies have evolved over the years to improve channel capacities using diversity techniques. The modern era foresees a demand in the development of low profile resonant antennas such as the dipole antennas, patch antennas, slot antennas and the DRAs (Dielectric Resonator Antennas) to serve as major components in the forthcoming

wireless systems. Much work can be seen in the antenna based literature related to the miniaturization, bandwidth enhancement, radiation pattern control, multi-band operation of these antennas (Lim *et al.* (2004)). Non resonant LWAs (Leaky Wave Antennas) have also been developed which find application in beam scanning and applications demanding highly directional beams. Moreover various technologies have been contemplated recently to promote innovative designs to introduce features such as frequency reconfigurability, polarization diversity, pattern diversity and the like.

The diversity in the existing wireless networks demands the design of antennas specific to the required application. This becomes a highly difficult task as each application offers one or more stringent constraints to the antenna designer in terms of size, bandwidth, efficiency and other performance parameters depending on the consumer requirement. For the cellular mobile networks, the handsets require low profile antennas that offer wide operating bands while the base stations require panel antennas with high side lobe suppression and low cross polarization effects. For devices that require Wi-Fi connectivity, the antennas for the access points demand high performance with low cost and ability to integrate multiple functions. The wireless communication networks that require high data rate performance at short range communication, UWB antennas have been developed that can operate approximately from 3 GHz to 10 GHz with stable gain and efficiency values. The RFID (Radio Frequency Identification) technology is used for wireless sensor networks to design tag antennas that are miniaturized and have high isolation between the different elements. Low profile tunable antennas find application for the digital television broadcasting in handheld devices. The GPS (Global Positioning Systems) require antennas that radiate circularly polarized waves with a wide beam width. Miniaturized implantable and body wearable antennas have been developed for various medical applications. This has provided a major boost in the growth of the e-healthcare technology.

Hence, the growth in the wireless communication technology has brought into light the need for innovative antenna designs that can operate suitably at the different standards. Each wireless system demands various application specific requirements which rely on a suitable antenna design that can be effectively co-designed and integrated with the internal circuit components and external mounting body of the system. Thus an effective integration of these technologies is required to foster the development of innovative designs that meet the needs of the rapidly evolving wireless communication system.

1.2 Work Motivation

As mentioned in the preceding section, in the present scenario, the need for the development of novel multiband antennas is on the rise as the current technological standards for various applications operate on multifunctional platforms. These application oriented novel designs are required to be suitably integrated into the wireless devices in order to be effectively incorporated into the present era. Thus, there has been a surge in the research for the design and development of antennas that can effectively operate over multiple bands with desirable radiation and resonance characteristics such as easy frequency tunability, presence of circularly polarized bands and controllable polarization states, and wideband characteristics with stable gain and efficiency values over the entire band. The need for the viability of these designs brings into light the easily mountable and low-profile slot antennas that can provide wideband features as well as exhibit simple geometry.

The multiple bands of operation can be easily achieved in slot antennas using different slit configurations or extended ground plane techniques using different shaped stubs. But the main drawbacks of such designs include extensive substrate sizes and most importantly the difficulty in controlling the resonance bands on account of the sensitivity of resonant frequencies to the precise slit/stub dimensions.

The wideband resonance characteristics in antennas is generally obtained on excitation of different modes that can suitably combine to produce a wide band with return loss characteristics below 10dB. This excitation of different modes can be done by carefully distributing the current densities over the proposed geometry so that different modes are excited. The conventional methods include introducing slits or stubs in the ground plane or by modifying the feed line design. Also, using stepped slots or slots with perturbed geometry help to create the necessary mode excitation for the required resonance characteristics. The modification of the ground plane and feed line geometry lead to widened bandwidth response but at the cost of a larger geometry and large cross polarization effects or unstable gain patterns over the entire bands.

The circular polarization characteristics have been significantly achieved by carefully controlling the current distributions and exciting orthogonal modes with 90° phase difference. This leads to the generation of the required phase shifted components that can combine to resonate at a CP mode thus generating the circularly polarized band. This generation of suitable current distribution is done convention-

ally by purposely modifying the slot and ground plane geometry along with the feed line so that the required modes are generated. But most of the methods proposed in literature either have a single operating band or multiple bands with very narrow axial ratio bandwidths. Also, the control of the sense of polarization at each of the bands becomes difficult or may not be possible as the resonance characteristics depend entirely on the precise geometry of the design.

To overcome the disadvantages in each case, and to allow for miniaturized designs that offer multiband, easily controllable resonances with circularly polarized or wideband characteristics, metamaterials (MTMs) are found to be a suitable candidate that can be integrated into the antenna geometry to produce novel designs with desirable operating characteristics and easy tunability.

MTMs are artificially engineered structures that exhibit physical properties usually not found in nature. It is quite a recent area of research that has been fast progressing since the nineteenth century. Works by Engheta and Ziolkowski (2006), Caloz and Itoh (2005) have already explored the various properties of metamaterials and research has been carried out in diverse fields to exploit these favorable features for the design of compact multiband antenna structures. Some examples can be seen in the works proposed by Caloz *et al.* (2008) and Sharawi *et al.* (2012). The MTMs have been studied in detail to put into use their interesting properties in order to formulate antenna designs that can suitably incorporate the metamaterial features into their operation and hence, produce structures that fulfill our goals. The basic MTM elements commonly used include the Split Ring Resonators (SRRs), Complementary Split Ring Resonators (CSRRs), Electromagnetic Band Gap (EBG) structures and metasurfaces. These MTM integrated designs offer desired characteristics for various applications but may have disadvantages in certain cases as low gain values attributing to the etching of the CSRRs from the metallic ground or bulky profiles due to the large EBG based or metasurface coupled designs. Besides, disturbance of the ground plane leads to disruption in the radiation and impedance characteristics. As an appropriate candidate for suitable incorporation in the slot antenna geometry, SRRs have been proved to offer the necessary permeability effects that provide for miniaturization as well as multiple frequency operation with easy tunability. They can be easily integrated with slot antennas on suitable loading and their geometries can be altered to generate circularly polarized (CP) and wideband designs. The orientation and placement of the SRR unit cells are carefully controlled to ensure maximum excitation and

resonance. Also, copper strip arrays that provide negative permittivity effects can be used to generate the multiple bands where the operation of the antenna changes depending on the design of the strips and their placement.

1.3 Problem Statement

Based on the work motivation discussed, it can be seen that over the past many years, the electronic industry has witnessed a steady growth in the demand for compact and low-profile devices capable of catering to multiple applications at a time. This requirement has called for a need to develop compact, low cost, multiband antennas that could be easily integrated with these devices. For further ease of use, features such as tunability of frequency bands as per required applications, presence of circularly polarized bands that relax the restriction on device orientation, provision for polarization reconfigurability and wideband operation are also desired to be incorporated into the antenna design. The existing literature presents various designs in line with these demands, but our extensive survey shows that certain gaps need to be filled. There still exists a requirement for simple and compact antenna structures that could provide these features and those that could be easily reconfigured as per need.

Thus, in order to fill the research gaps, the followong objectives have been formulated and listed in the next section.

1.4 Objectives

The objectives of this research work include:

1. To design compact multiband rectangular slot antennas covering at least three wireless bands and exhibiting independent frequency band tuning capabilities.

2. To develop compact wideband and ultra wide band slot antenna designs that radiate at resonance frequency bands of at least 60% impedance bandwidth providing stable gain and efficiency values over the entire operating bandwidth.

3. To design multiband circularly polarized slot antennas that offer the feature of independent control of the resonance bands and also selective assignment of polarization states for each of the frequency bands as required.

1.5 Work Methodology

For realizing the above mentioned objectives, the upcoming technology of MTMs is integrated with the already existent antenna technology to optimize and fabricate various slot antenna designs. The work methodology adopted for the same is described below:

- To design compact multiband slot antennas with independently controllable frequency bands, the slot is loaded with MTM inspired structures such as SRRs and array of thin copper strips. The slot geometry remains unaffected by the loading of the resonant MTM elements. Their excitation leads to additional resonance bands without affecting the fundamental slot resonance. Thus, multiple bands of resonance can be obtained at a compact antenna size. The placement and geometry of the MTM resonating structures determine the resonance characteristics of the antenna designs. The frequency bands can be independently tuned by suitably altering the MTM and slot dimensions.

- Compact slot antennas exhibiting ultra wide band (UWB) characteristics are designed using the concept of artificial transmission lines (TLs). The slot is loaded with rows of differently sized and periodically spaced TLs that can resonate at closely spaced frequencies. Each row of TL exhibits different dispersion characteristics and support propagation at different cut off frequencies. This gives rise to various modes that combine to give rise to a UWB response.

  A fictitious short circuit concept is used to design slot antennas with wideband properties. Here, an asymmetric microstrip feed line is used to excite a narrow rectangular slot. This leads to resonances at closely spaced frequencies which combine to give the wideband resonance. An open slot of quarter wavelength is used to obtain compactness of the antenna structure.

- To design compact slot antennas resonating at multiple CP bands, SRR and inclined copper strips arrays are precisely designed and loaded on the slot antenna. The resonance modes obtained from the slot and the strips combine to give the required CP characteristics. In another design, multiband CP resonance is achieved using a modified feed line that is offset from the centre and by loading the slot with an SRR and a meandered U-shaped copper strip. Easy control

and tuning of the CP resonance bands as well as of the polarization senses at each band is achieved by suitably orienting the SRR, feed and copper strips.

1.6 Outline of the Thesis

The thesis aims at presenting the design and analysis of the proposed MTM based antennas which exhibit multiple properties such as operation at multiple bands with CP and wideband characteristics. The thesis is divided into different chapters based on the applications obtained using the proposed novel MTM based antenna designs that include multiband operating capabilities with independently controllable frequency bands, development of compact devices that operate at circularly polarized and wideband frequencies. The introduction to the thesis gives the readers a basic idea on the importance of wireless communication and its evolution as well as the importance of different antenna systems. The work motivation, objectives, work methodology, and an outline of the thesis are provided. A background study on the different concepts including MTMs, slot antennas, artificial transmission lines, and a brief literature survey on the existing works in the areas pertaining to such applications are provided in the succeeding chapter.

The flow of the thesis can thus be outlined as follows:

In Chapter 2, a background study and a brief literature survey on the various works done for the design of multiband antennas are presented. The chapter first gives an introduction to the basic concepts related to the design and analysis of the proposed antenna geometries. This involves a study on MTMs, slot antennas and artificial transmission lines. Then, the various methods that have been used to develop antennas that operate at multiple bands are discussed which include conventional techniques as well as MTM based structures. The literature survey is divided into four sections where the first two sections deal with multiband and CP based multiband slot antenna designs whereas the last two discuss designs that offer wideband and UWB properties using the concept of artificial transmission lines.

In Chapter 3, investigation and presentation of three multiband designs with independent frequency tuning capabilities is done. The designs offer pentaband and triband resonance characteristics with compact structure and good gain and efficiency values. The desirable properties of MTMs have been used by incorporating SRR and copper strips on the slot antenna design which leads to miniaturized multiband de-

signs. For the SRR based design, multiple slits have been introduced in the SRR which is suitably positioned on the slot to obtain the required resonance bands. The higher frequency bands are obtained by loading the slot with two SRR structures that are optimally positioned within the slot. Thus, in this chapter the aim is to present the SRR and strip based square slot antennas with multi band operation and easy frequency tunability at the MTM controlled frequency bands, without affecting the main fundamental mode of the slot. Desired bands of operation can be obtained by either changing the SRR, strip or slot dimensions as each of the resonant band is either slot or MTM controlled.

In Chapter 4, MTM based wideband designs are proposed with independently controllable frequency bands. A fictitious short circuit concept is used to model a tapered microstrip feed line on an open slot to design a compact wideband antenna. The dual band property is obtained for the design by introducing an additional SRR resonant band. Further impedance bandwidth is improved on introduction of capacitor across the slot ends. The concept of using the tapered feed is also combined with the properties of a modified SRR to obtain a compact tri band slot antenna that exhibits wideband property at its first band of resonance.

In Chapter 5, the ultrawideband property is obtained by using the concept of artificial transmission lines on a microstrip fed square slot antenna. Rows of artificially engineered transmission line elements are loaded on a square slot to generate various resonance modes that combine to give an UWB response. Equivalent circuit analysis is done for the proposed model and current distributions are plotted over the wideband. The properties of microstrip transmission lines are used to evaluate the performance of the dispersion engineered transmission line loaded slot antenna.

In Chapter 6, MTM based multiband CP designs are presented. Array of copper strips and carefully oriented SRR structures are used to generate the multiple bands with CP characteristics. The slot corners are also modified to obtain CP at the fundamental slot resonance mode. The current distributions at each of the resonance bands are studied and different orientations are presented where the sense of polarization can be altered. For the final design proposed in this chapter, meanders are introduced in the feed line and in the loaded U-strips to obtain the necessary path lengths for the current distribution in order to generate CP bands.

Chapter 7 provides a conclusion for the work presented in the entire thesis and also discusses the future scope of the present work for further applications.

Chapter 2

BACKGROUND AND LITERATURE SURVEY

2.1 Background

The impinging of an EM wave on different systems brings into effect various kinds of responses which can be characterized by the effective permittivity and permeability of the constituent materials. Thus, based on the values and polarities of these parameters the materials can be broadly classified into different types such as Double Positive (DPS), Epsilon Negative (ENG), Double Negative (DNG) and Mu-Negative (MNG) media as depicted in Figure 2.1.

Most of the naturally occurring materials fall into either of the three classes that include double positive, epsilon negative or mu-negative media. The double negative media have both negative epsilon and mu values and are found to exhibit interesting properties in the presence of EM waves. These include artificially generated materials and are also termed as left-handed media (LHM), media with negative refractive index and backward-wave media (BW media) due to their inherent characteristics (Eleftheriades and Balmain (2005)). The negative refraction phenomena in DNG media is illustrated in Figure 2.2. Such media, when incorporated within suitable dielectric in the form of inclusions of novel geometries brings out a realizable material termed as the Metamaterial (MTM).

These MTMs when integrated with antennas appropriately, help modify the characteristics of the antenna structure and enhance its performance in terms of reduction in size, polarization, radiation efficiency, phase control, peak gain values, etc. Hence

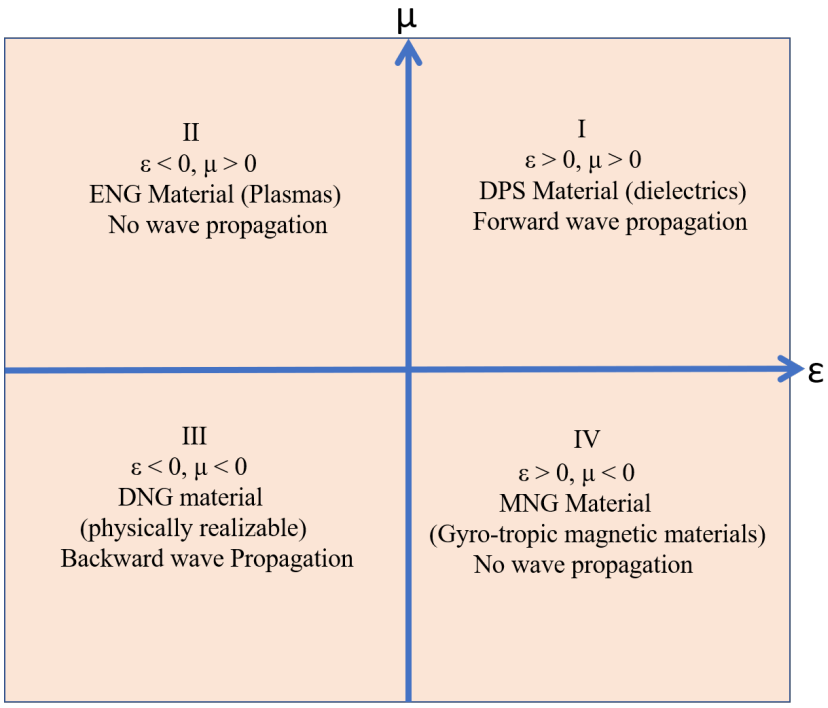

Figure 2.1: Classification of materials.

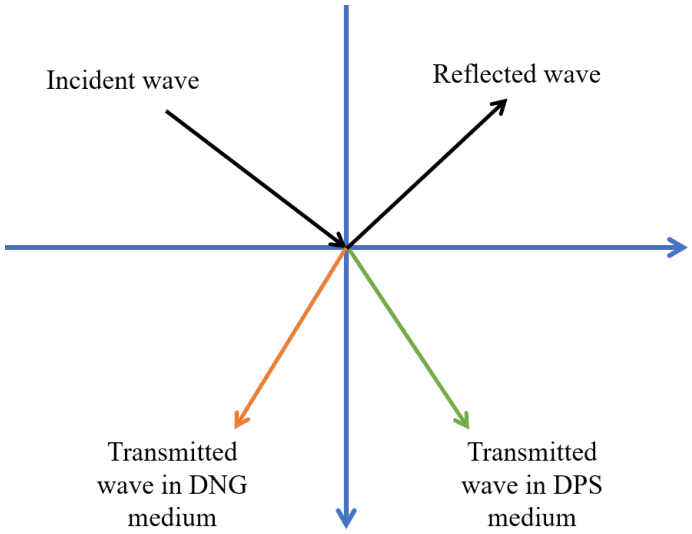

Figure 2.2: Negative Refraction in DNG medium.

novel designs have been developed that can be used for various applications that require radar cross-section (RCS) reduction, circularly polarized waves, ultra-wide bands of operation, multiple frequencies of operation and also for beam steering in phased

arrays. The control of its properties can be easily done by mechanically or electrically tuning the properties of the constituent metamaterial elements.

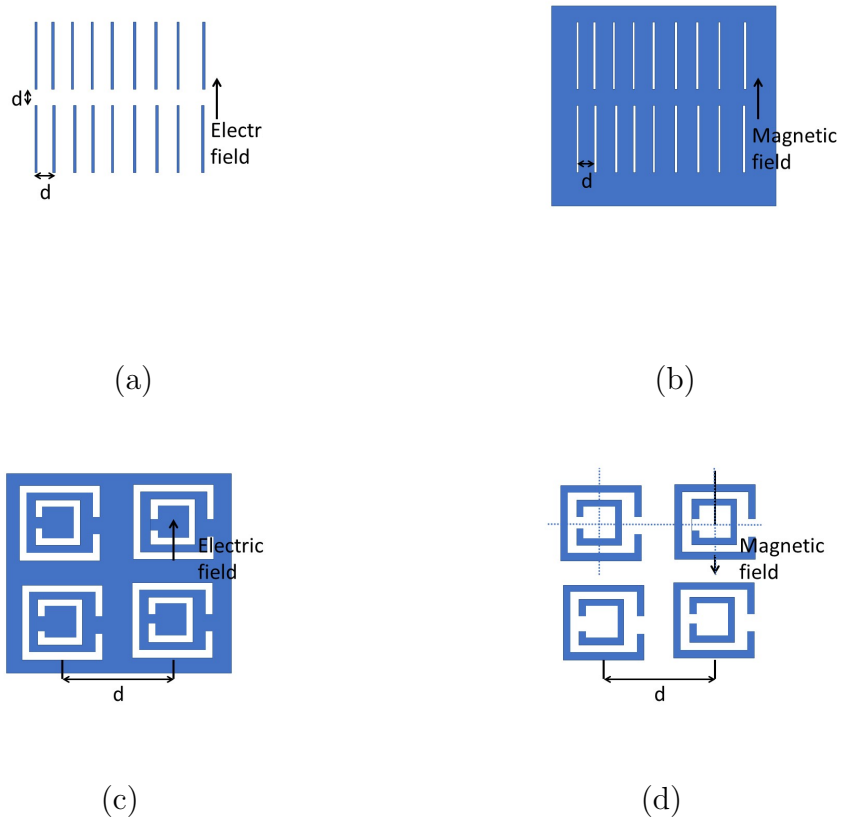

Figure 2.3: Types of metamaterials: (a) Copper strip array (b) Slot lines (c) CSRRs (d) SRRs

Depending on the exhibited electromagnetic properties, various types of metamaterials have been introduced in the literature, including SRR, CSRR, Metal wires, slot lines (Engheta and Ziolkowski (2006)) which are displayed schematically in Figure 2.3.

The SRRs and slot lines exhibit negative permeability effects in the presence of an axial magnetic field and hence can be termed as magnetic dipoles whereas the CSRRs and metal wires act as electric dipoles exhibiting negative permittivity effects in the presence of a time varying electric field along their axes. The first LHM as shown in Figure 2.4 was made using a composite of SRR unit cells and copper strips array in order to obtain a DNG media. It was made at the University of California, San Diego by Smith et al. in association with Pendrey (Pendry *et al.* (1999)).

Figure 2.4: An MTM media made of SRR and copper strips

2.1.1 Negative Refraction

The study carried out by Victor Vesalgo and his team in the 1960s led to the conclusion that the existence of a DNG media exhibiting negative values for both mu and epsilon was allowed by the Maxwells equations. However, the wave propagation through such media would follow a left-handed rule contrary to the right handed relationship followed in conventional media to describe the relationship between the E, H and k vectors as shown in Figure 2.5. Thus they were termed as the LHM. Moreover, the Poynting vector **S** is found to be anti-parallel to **k** in the case of such media, which in turn implies that **E**, **H** and **S** follow a right handed rule in this case. This nature of the LHM inspired researchers to investigate the possibility of a backward wave and hence consequently coined the term Backward media for the LHM. Backward wave propagation brings in the definition of a negative refractive index characterized by a reversal of the Snell's Law. In order to understand the concept of negative refraction, two media M1 and M2 are considered as shown in Figure 2.6. A plane wave travelling from M1(with wave vector **k1**) strikes the interface to propagate through M2 with wave vector **k2**. Keeping up with the law of conservation of momentum, the tangential components of the wave vectors are required to be equal at the interface. Thus the normal components can be envisaged in two ways: (i) directed towards interface (usually the case of reflection) (ii) directed away from the interface. Now, analysing the Poynting vectors, it is required that their normal components maintain the direction through the +x-axis in order to fulfill the law of conservation of energy. Thus if M2 is a RHM, case (i) holds good, whereas if M2 were to be a LHM, the case (ii) follows where **k2** is anti parallel to **S2** and hence, power propagates in a direction of phase advance so that a negative refractive index can be defined for the medium M2.

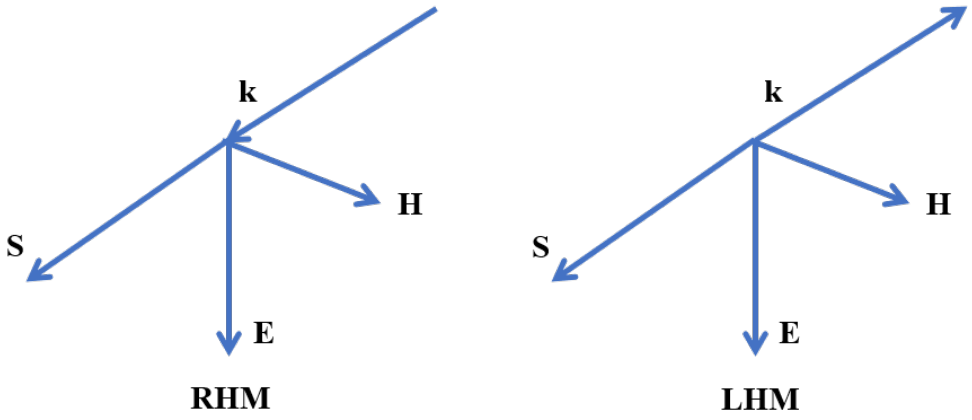

Figure 2.5: Orientation of field quantities in RHM and LHM media (Eleftheriades and Balmain (2005))

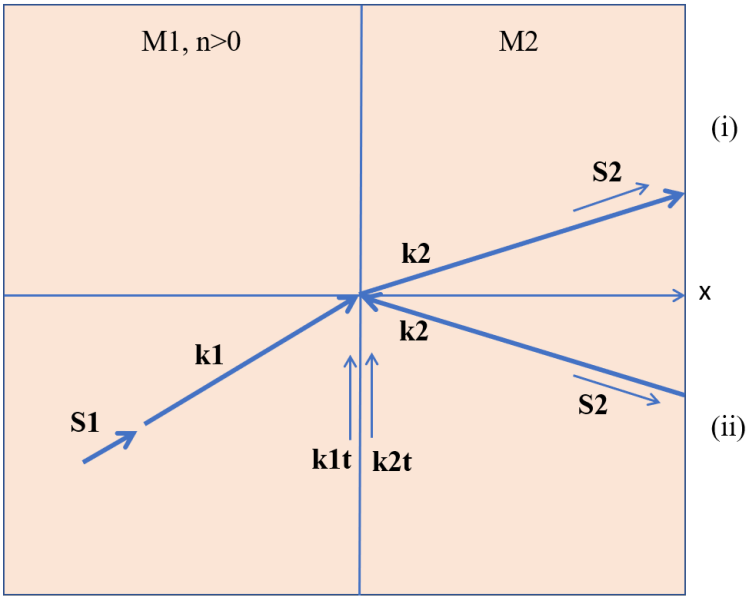

Figure 2.6: Refraction at two media interface (Eleftheriades and Balmain (2005)

2.1.2 Transmission Line Theory of LHM

A classic way of explaining the LHM wave propagation phenomena through a DNG media involves applying the distributed circuit concept. Any 3-D media can be described using L-C networks and the possibility of a negative permittivity and permeability media brings into light a possibility of negative L and C parameters to represent the network.

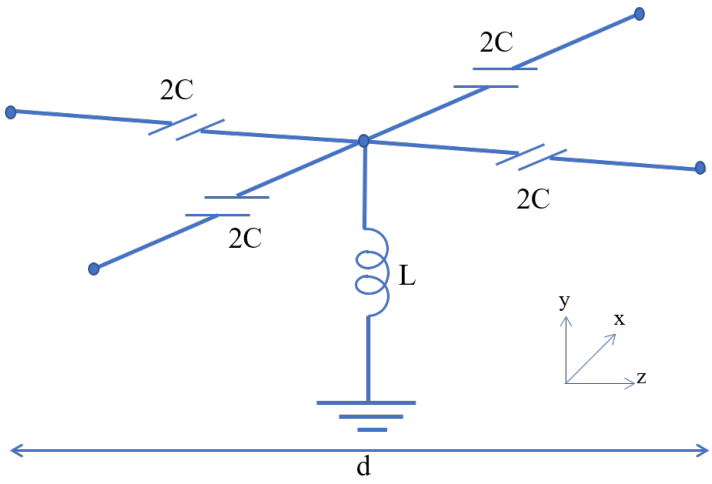

Figure 2.7: 2-D dual transmission line unit cell(Eleftheriades and Balmain (2005))

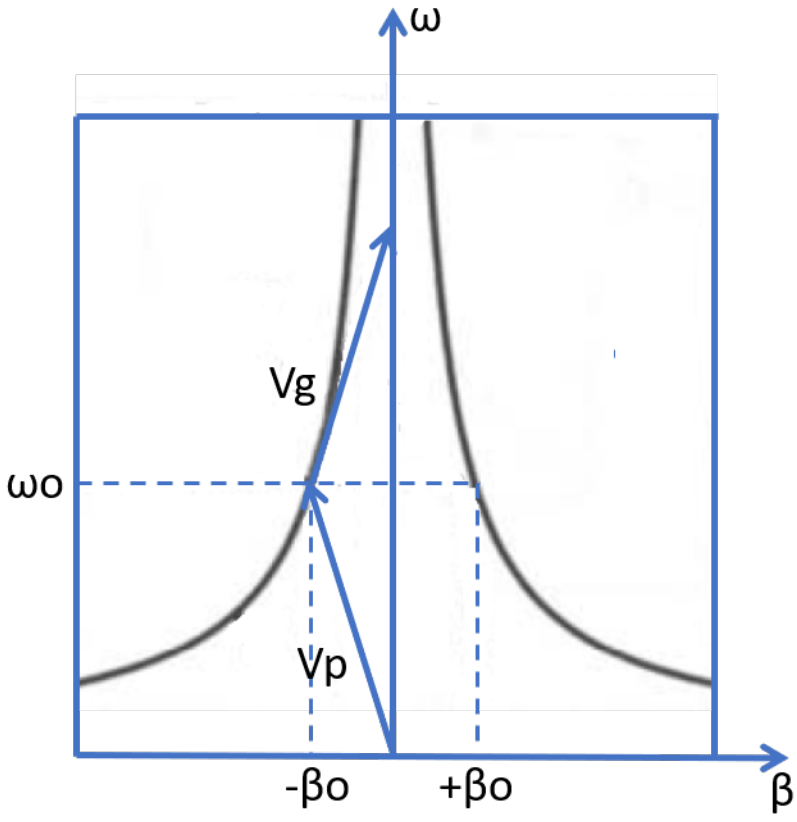

Figure 2.8: Dispersion diagram for media with negative mu and negative epsilon (Eleftheriades and Balmain (2005))

The TL unit cell of such a media can be obtained by imposing negative series impedance (shunt impedance) -j$\omega L^{'}$d and negative shunt capacitance (series capacitance) -j$\omega C^{'}$d in the circuit so that the roles of the inductive and capacitive elements are reversed compared to that of the L and C elements in the TL unit cell for a conventional media. This is shown in Figure 2.7. The effective permittivity and permeability are functions of frequency and can be described by the following equations:

$$\mu(\omega) = \frac{1/j\omega Cd}{j\omega} = -\frac{1}{\omega^2 Cd} \tag{2.1}$$

$$\epsilon(\omega) = \frac{1/j\omega Ld}{j\omega} = -\frac{1}{\omega^2 Ld} \tag{2.2}$$

Where L=Ld and C=Cd and C and L define the per unit length series capacitance and shunt inductance. Thus the left-handed behavior is satisfied and the effective material parameters can be observed to be simultaneously negative. The propagation constant associated with the structure can be given by:

$$\beta = -\omega\sqrt{\mu(\omega)\epsilon(\omega)} = -\frac{1}{\omega\sqrt{L'C'}} \tag{2.3}$$

And hence ω and β share an inverse relationship which can be seen in the dispersion diagram shown in Figure 2.8. Looking into the phase and group velocities, the phase velocity can be described as

$$v_{ph} = \frac{\omega}{\beta} = -\omega^2\sqrt{L'C'} = -\frac{\beta}{\omega}^{-1} = -v_g \tag{2.4}$$

This shows that the phase and group velocities share an antiparallel relationship, implying the possiblity of a backward wave phenomena. The phase is found to lead in the direction of positive group velocity (power flow) thus inidicating a negative index of refraction at the RHM-LHM interface. The refractive index is calculated as :

$$n = c/v_{ph} = -\frac{\sqrt{\mu(\omega)\epsilon(\omega)}}{\sqrt{\mu_0\epsilon_0}} = -\frac{1}{\omega^2\sqrt{L'C'\mu_0\epsilon_0}} \tag{2.5}$$

2.1.3 Split Ring Resonators

The discovery of a negative epsilon material led Veselago to explore the possibility of a negative mu substance. However, considering the thin wire media, further reduction

in the radius of the wire elements only shifted the permeability values to the free space value as expected in artificial dielectrics. Then, on modification of the cylindrical structure by introducing an internal electromagnetic layer, a model resembling a parallel plate capacitor was obtained as shown in Figure 2.9. This structure could be termed as the Split Ring Resonator (SRR). Thus, The SRRs consist of thin metallic ring structures of size smaller than the wavelength of an incident EM wave and with gaps between each other and splits at opposite ends. When excited by an axial magnetic field strong electric currents are produced along the thin rings thus producing high capacitive values between the rings. The large capacitance effects between the rings supports strong electric fields and the axial magnetic field applied induces currents in the rings. This natural inductance of the system along with the synthesized capacitance in the presence of a time varying field helps characterize an effective relative permeability for the system which defines the resonance behavior of the SRR. The effective permeability thus obtained can be made to assume negative values around the magnetic plasma frequency for an array of SRR. This frequency when placed at the microwave range can find application in antenna designs. This concept of SRRs was first introduced by Pendry et al. (1999) and was experimentally demonstrated by Shelby et al. (2001).

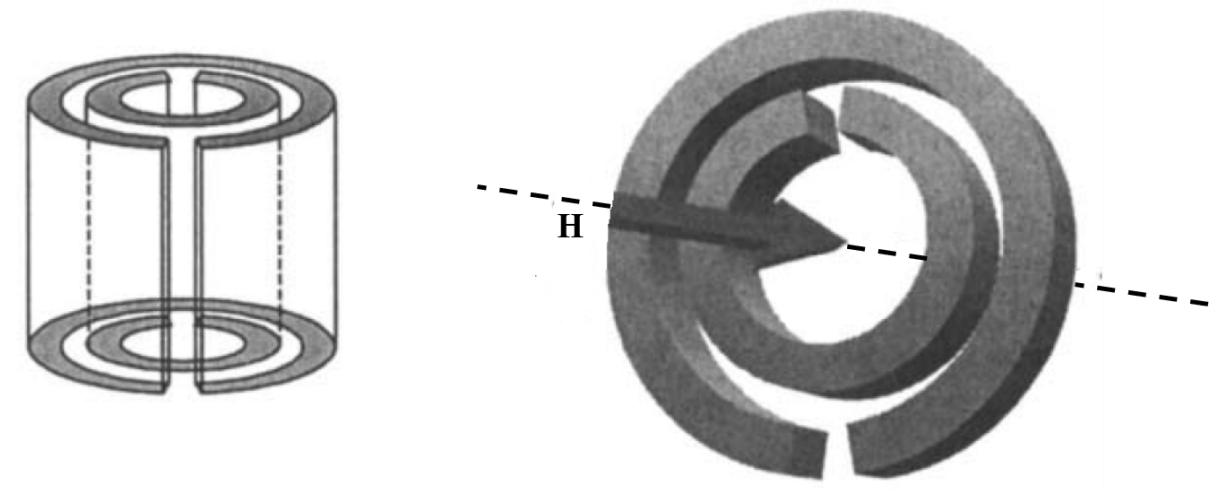

Figure 2.9: The SRR structure discovered by Pendrey in cylindrical and planar forms (Eleftheriades and Balmain (2005))

The SRR can be analyzed using an equivalent LC circuit and the resonance frequency can be given by

$$\omega = 1/\sqrt{(LC)} \tag{2.6}$$

where L is the inductance provided by the rings and C is the capacitance of the SRR due to the gap between the rings.

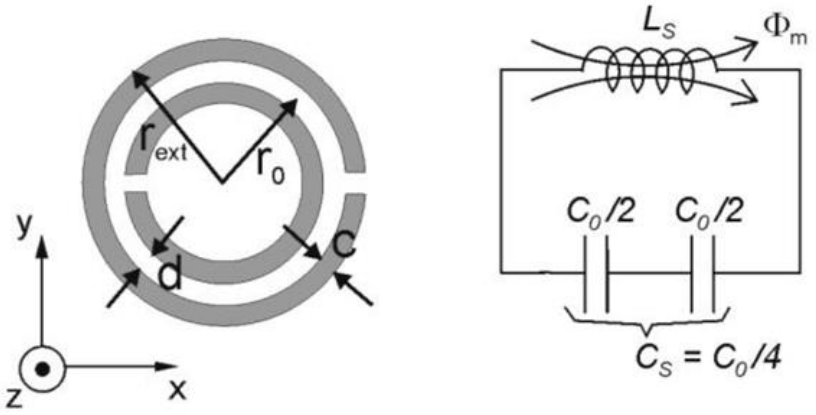

Figure 2.10: SRR unit cell and equivalent circuit

An SRR unit cell and its equivalent circuit is shown in Figure 2.10. When a large array consisting of such SRR structures are embedded within a dielectric and is excited by an axial magnetic field, it produces a large negative effective permeability effect near its frequency of resonance. Thus, these purely non-magnetic materials act like an effective artificial magnetic plasma providing negative permeability values at microwave frequencies.

When these SRR structures are introduced within a waveguide of cutoff frequency ω_c, an effective MTM structure can be designed. The waveguides are chosen for analysis as they have a high Q factor and exhibit negative permittivity effects below the cut off frequency. Thus, without synthesis of an artificial negative permittivity media, such a uniform structure is obtained devoid of inclusions and loss effects. This equation for the dispersion constant of the propagating modes within the waveguide is given by Engheta and Ziolkowski (2006)

$$k = \omega\sqrt{(\mu_r \epsilon_e f f)} \tag{2.7}$$

$$\epsilon_e f f = \epsilon_r(1 - \omega_0^2/\omega^2) \tag{2.8}$$

Where ϵ_r and μ_r are the effective permittivity and permeability values of the

substrate and ω_o is the cut off frequency for the operating mode, and the refractive index n is given by

$$n = \pm\sqrt{(}\mu_r \epsilon_e f f) \tag{2.9}$$

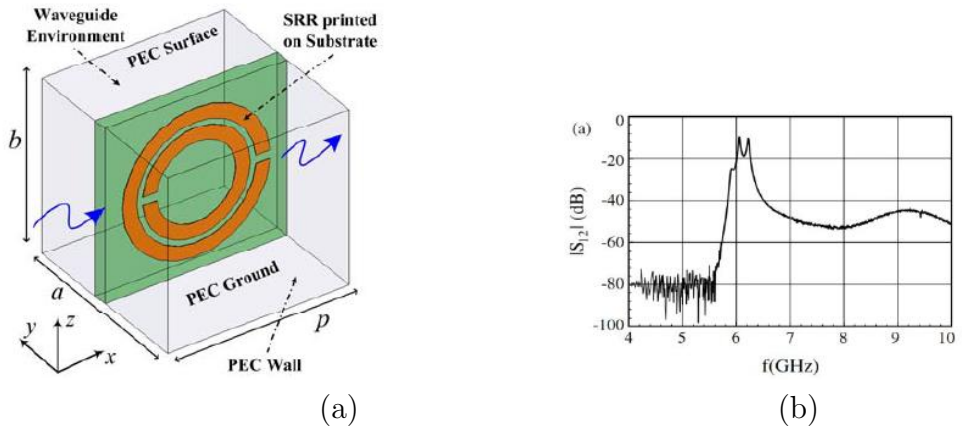

Figure 2.11: SRR unit cell analysis: (a) Experimental setup (b) Transmission coefficient characteristics

Now, the effect of embedding an SRR within the structure generates an LH pass band in the presence of an axial magnetic field and hence backward wave propagation is supported near the SRR resonance frequency. In Figure 2.11, an SRR of cut off frequency 6.25 GHz is introduced in the waveguide which is designed for a cut off frequency of 24 GHz. Hence in the frequency band below 24 GHz the waveguide exhibits the property of negative permittivity and the presence of the SRR introduces a negative permeability effect region around the resonance frequency of 6.25 GHz. This explains the presence of the transmission band in the graph showing $|S_{12}|$ versus frequency. Thus a DNG media is obtained and an LH band is observed around the resonance frequency of the SRR.

The response of the SRR to the external EM wave depends on the orientation of the structure with respect to the direction of the electric field **E**, magnetic field **H** as well as that of the wave vector **k** (Zhou *et al.* (2007)). Different configurations of **E**, **H** and **k** excite different responses in the SRR structure. This is shown in Figure 2.12. In the first case (a), the plane of SRR lies perpendicular to the direction of **H** and parallel to direction of **k**. This stimulates a magnetic response in the SRR which is responsible for its resonance. In the second case (b), the **E** field which is parallel to the SRR

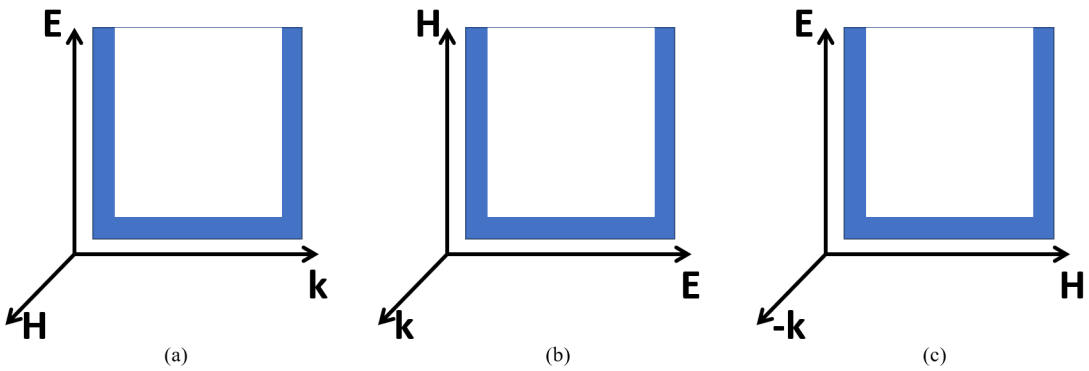

Figure 2.12: Different SRR configurations

excites an electric current in the SRR which in turn creates the magnetic resonance of the SRR This is called as the electric excitation coupled magnetic resonance (EEMR). The third configuration (c) shows the case where the E field is parallel to the side of the SRR. This excites a weak wire like electric response in the SRR.

Since the SRRs can be described using lumped Land C elements that determine its frequency of resonance, the structure of the ring can be modified to obtain additional inductive or capacitive effects that in turn shift the region of negative permeability to required band of interest, This has been investigated in a study whereby multiple splits are introduced within the split ring structure and the unit cell analysis is carried out to find out the resonant frequencies of the SRR structure. It can be seen that on addition of two and three micro splits the capacitive effects increase around the ring which in turn leads to a shift of the resonance frequency bands to higher values.

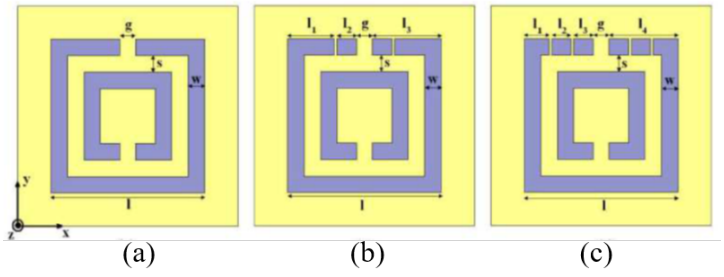

Figure 2.13: Schematic views of (a) Unit cell A, (b) unit cell B, and (c) unit cell C.

In the work by Ekmekci *et al.* (2009), micro splits were added on the outer ring of the SRR along the arm having the main split. The series capacitance effects thus introduced led to increase in the resonance frequency of the SRR. Transmission character-

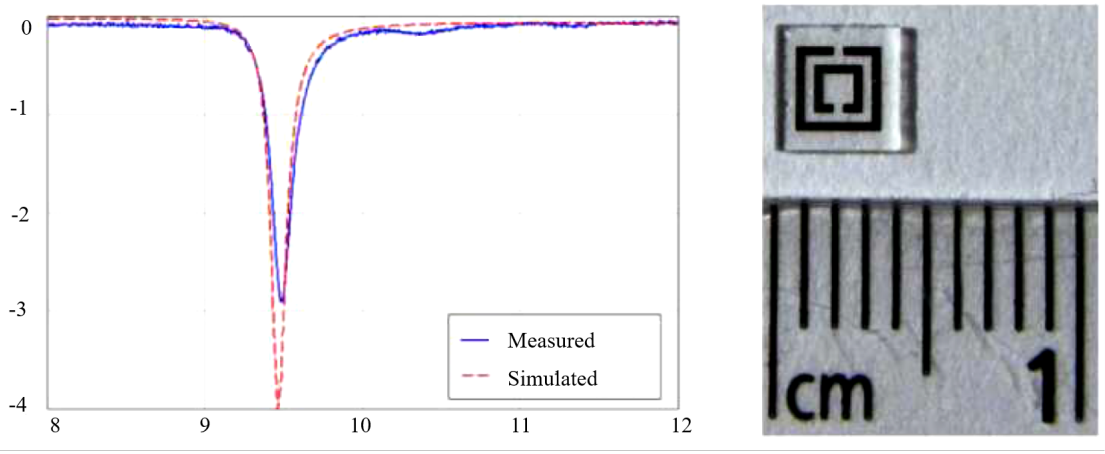

Figure 2.14: Transmission characteristics of the type A unit cell with photograph of the actual resonator.

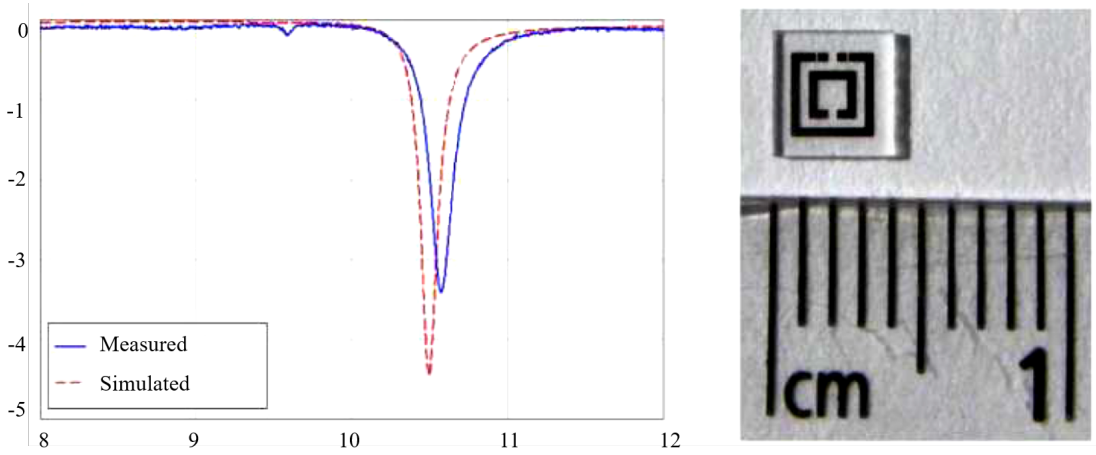

Figure 2.15: Transmission characteristics of the type B unit cell with photograph of the actual resonator.

istics of these MSSRR (micro-split SRR) structures were obtained and compared with the characteristics of the ordinary SRR structure. Figure 2.13 shows the schematic for the different unit cells analyzed where unit cell A is an ordinary SRR, unit cell B is an MSSRR with single micro split pair and unit cell C is the MSSRR with two pairs of micro splits. Figure 2.14-2.16 show the measured and simulated transmission characteristics obtained for each case along with photographs of the actual resonators. The resonance frequency is observed to shift to higher values on addition of micro-splits. Thus, it can be seen the geometry of the SRR structure can be modified as per

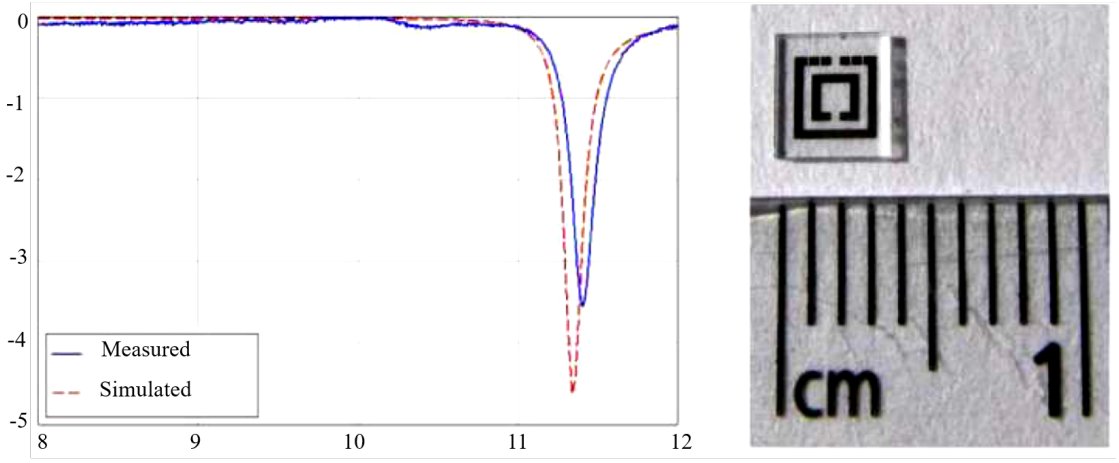

Figure 2.16: Transmission characteristics of the type C unit cell with photograph of the actual resonator.

application to tune the resonance to desired frequencies.

2.1.4 Copper Strips

Metals essentially fall into the category of plasmas as they are constituted of ionized gas that are made of free electrons. They have a cut off frequency of ω_p below which the bulk permittivity of the metal becomes imaginary and propagation is not supported. The negative permittivity effect is obtained below the plasma frequency and this can be utilized to obtain an effective MTM medium. Usually the plasma frequency lies within the ultra-violet (UV) region and thus would be difficult to obtain negative permittivity effects without dissipation effects within waveguides where long wavelengths are supported. Hence, very thin wires are arranged in a periodic lattice structure so that the plasma frequency is suppressed due to the lower effective electron concentration within the volume. Besides, due to the enhanced effective electron mass within the thin wire array arrangement, the self-inductance of the structure manifests itself greatly which shifts the effective plasma frequency to the Gigahertz range. Hence this array of thin wires can be used to develop a metamaterial media when suitably incorporated within the dielectric waveguide. When operated below the cut off frequency, the waveguide exhibits the negative permittivity effects. Below its plasma frequency, the wire array also exhibits similar characteristics and the combination of the two helps to provide an effective media exhibiting positive permittivity,

i.e., reversal of the permittivity effect occurs and thus a forward wave propagation is supported around the resonance frequency. From the Equations (2.7) and (2.9) it can be seen that a positive refractive index is required for propagation which can be obtained through engineering the material parameters such as effective permittivity and permeability effects. This is where the properties of MTMs become significant.

2.1.5 Slot Antennas

The slot antenna consists of a slot etched out of a metallic surface printed on a dielectric substrate. When excited using a suitably designed feed, voltage differences are developed across the slot. This generates electric field lines and axial magnetic field lines which leads to the excitation of different resonance modes across the slot. The radiating frequency is determined by the dimensions of the slot and the parameters of the substrate which can be tuned as per desired frequency of operation. Slot antennas are mainly used for operation in the UHF range and many of their applications lie under the areas of radar systems, surveillance aircrafts, desktop devices etc. They are popular due to their low profile, ease of fabrication and mounting and the wideband characteristic response. The radiation pattern obtained is similar to that of the dipole antenna. Slot antennas are commonly known as complementary dipole antennas and their principle of operation can be explained based on the Babinets principle which relates the radiation characteristics and impedance of the antenna with its dual antenna. In the case of the slot antenna, the dual antenna can be considered as the dipole antenna and hence the impedance, electric field distributions, etc, can be calculated for the antenna if the same are known for the dipole antenna. The principle of operation of the slot antenna and its properties based on the Babinets principle is given below in detail.

Consider a metal plane on a substrate over which a gap is etched of width $h << \lambda$ as seen in Figure 2.17. It is excited using a voltage source connected from one end of the slot to the other end and offset from the centre. Assuming the length of the slot to be half wavelength the voltage at the ends drop to zero and has peak value at the centre. The slot can be considered as a transmission line having two paths and short circuited at the ends. Hence, the current associated with the voltage is out of phase as seen in the voltage and current profiles along the slot length shown in Figure 2.18(a). The current flows through the top and bottom of the slot in opposite direction and cancels out effectively whereas the voltage distribution adds up in phase giving rise

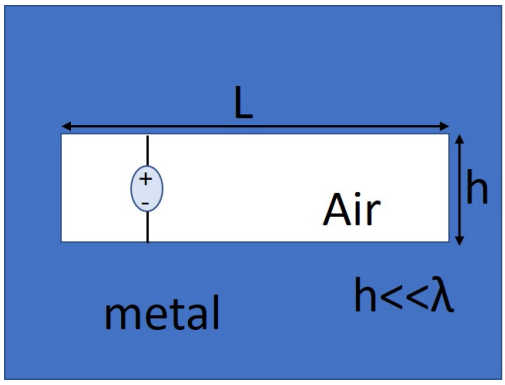

Figure 2.17: Slot Antenna schematic

to electric fields thus leading to radiation. Hence the slot can be termed as a voltage radiator, whereas the dipole acts as a current radiator.

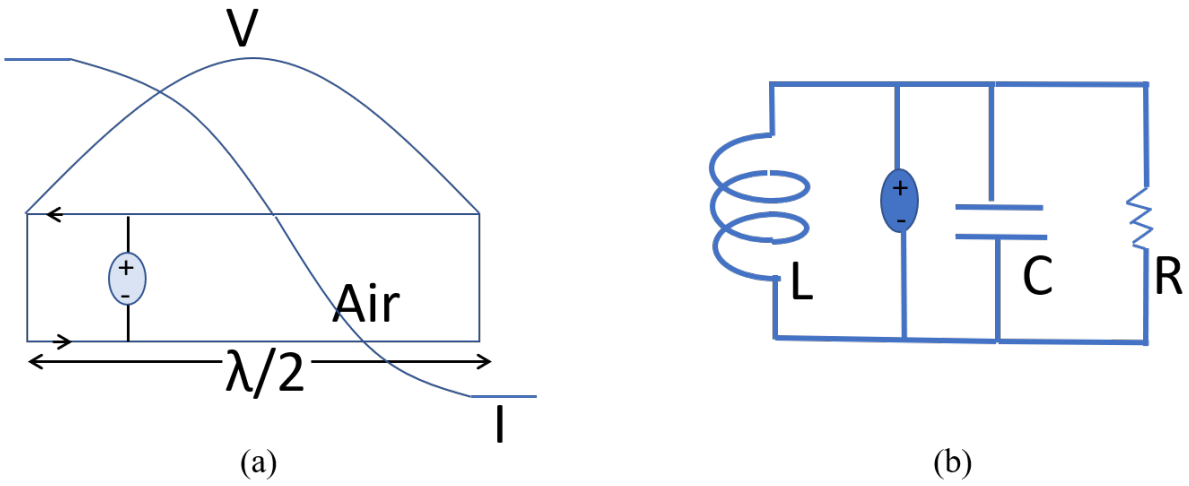

Figure 2.18: (a)V and I profile along the slot and (b) Equivalent circuit of slot antenna

In order to excite the slot, we offset the feed from the centre to obtain the point where 50 Ω impedance is obtained. At the ends, zero impedance points are observed and at the centre, impedance obtained is infinite as analyzed from the V and I profiles. The slot length to the left of the voltage source can be considered as a transmission line with length $l < \lambda/4$ and to the right, as a line with length $l > \lambda/4$. These can be considered as giving rise to inductive and capacitive effects and are thus represented as L and C elements in the equivalent circuit model. When fed appropriately, their effects cancel and only radiation resistance remains. The voltage adds up in phase

and the slot radiates. Thus, the equivalent circuit for the slot is obtained as shown in Figure 2.18(b).

Duality

The dipole is considered as wire fed in the center producing currents along its length that add up in phase producing radiation. If the air around it is replaced by metal in the single plane and the shape of the dipole is cut out, a slot antenna is obtained with feeding it across with a voltage source. Hence it is rightly called the complement of the dipole. The slot antenna and its complementary dipole structure is given in Figure 2.19.

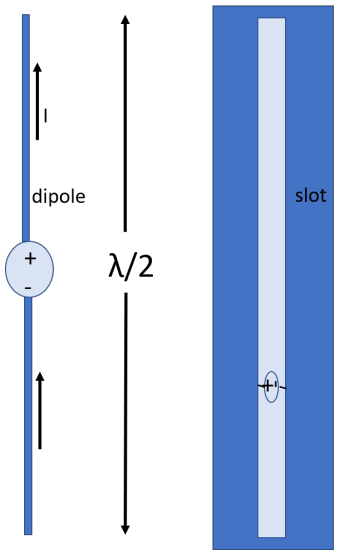

Figure 2.19: Babinet Principle: Slot antenna and its complementary dipole structure

From the duality principle, the radiation patterns in terms of magnitudes remain the same for both structures in the same plane but vary in polarization. The currents going through the dipole gives rise to radiating fields for the dipole that are vertically polarized, whereas the **E** fields across the slot give rise to horizontally polarized fields for the slot antenna. The Babinets Principle helps to relate the impedances of the two structures. If Z_d andZ_s are the impedance of the dipole and the slot respectively, and η is the intrinsic impedance of the medium then, the following relation holds good:

$$Z_d Z_s = \eta^2/4 \tag{2.10}$$

The bandwidths of both antenna are around 7%. Also, the slot can be of any shape and can radiate as long as it is fed across its ends and has a path around it

with perimeter $p \approx \lambda$.

2.1.6 Artificial Transmission Lines

Transmission lines operating in the microwave frequency range can be analyzed as a two port network used to carry energy or power from one end to the other. The length of the transmission line is required to be greater than the operating wavelength of the EM wave. The transmission line can be characterized using lumped elements and corresponding equivalent circuits can be modeled. They can be used to replace lumped elements in circuits and hence provide a low-cost solution for the design of microwave devices. The transmission line is generally designed for a cut off frequency ω_0 above which the line allows propagation with phase constant β. The expression for the wave propagation constant is given by (Martin (2015))

$$\beta = \omega\sqrt{LC} \tag{2.11}$$

where L and C are the per unit length inductance and capacitance for the transmission line.

The artificial transmission lines can be synthesized by loading the transmission lines with the lumped elements or by interrupting the uniformity by introducing certain periodicity or specific arrangements in the wave propagation direction. This includes periodically perturbed transmission lines or cases where certain inclusions or etchings are incorporated within the transmission line design to obtain the desired responses. Two types of such a class of artificial transmission line are studied and characterized. One type includes the transmission line periodically loaded with shunt vias and the other one wherein the transmission line is loaded with periodically dispersed gaps.

1. Line loaded with Periodic Vias

In this case, metallic shunt posts are loaded with a periodicity p on a lossless microstrip line defined by characteristic impedance Z_0 and phase velocity v_p. The vias are characterized by an inductance L_e and are spaced from each other at a distance much smaller than the operating wavelength. A schematic representation of the via loaded transmission line is shown in Figure 2.20. The corresponding circuit schematic and equivalent circuit are shown in Figure 2.21.

The propagation constant is given by Johnson and Jasik (1984) as

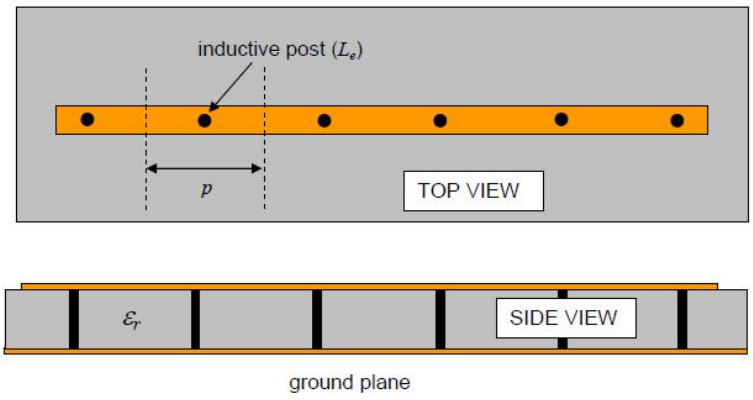

Figure 2.20: Line loaded with Periodic Vias.

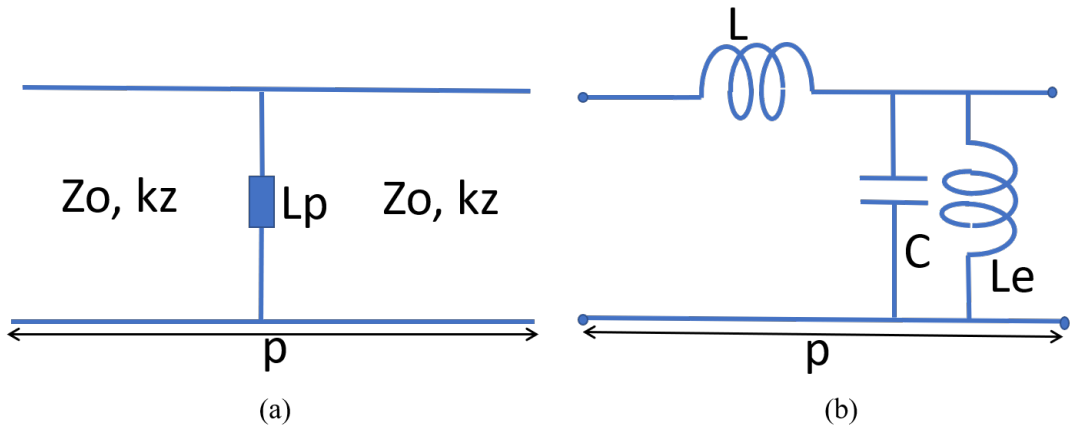

Figure 2.21: (a) Circuit schematic and (b) Equivalent circuit diagram for the via loaded line.

$$\gamma = j\omega\sqrt{LC}\sqrt{1 - \frac{1}{\omega^2 L_e p C}} \tag{2.12}$$

where critical frequency is defined as,

$$\omega_c = \frac{1}{\sqrt{L_e p C}} \tag{2.13}$$

The periodicity p, per unit length capacitance C and inductance of via L_e define the cut off frequency of the artificial transmission line. Above this critical frequency, pure propagation is supported (α=0) whereas below it evanescence occurs (β=0). This can be seen from the dispersion diagram shown in Figure 2.22.

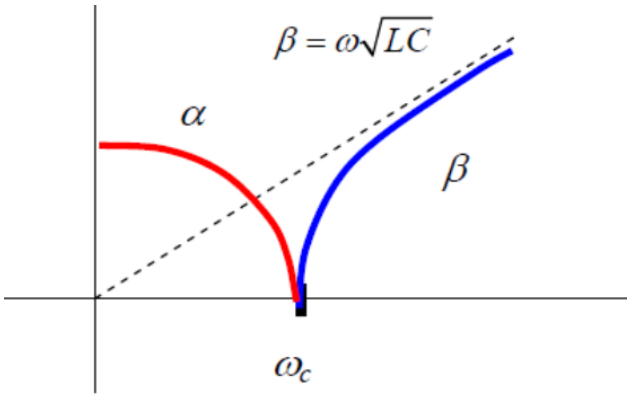

Figure 2.22: Dispersion diagram for the via loaded line

The attenuation and phase constants are defined as

$$\alpha = \omega\sqrt{LC}\sqrt{\frac{1}{\omega^2 L_e pC} - 1} \tag{2.14}$$

$$\beta = \omega\sqrt{LC}\sqrt{1 - \frac{1}{\omega^2 L_e pC}} \tag{2.15}$$

Here L and C define the per unit length inductive and capacitive effects which are given by

$$L = Z_0/v_p \quad and, \quad C = 1/Z_0 v_p \tag{2.16}$$

2. Periodically Gap loaded Artificial transmission line A similar analysis is carried out for the lossless microstrip line of characteristic impedance Z_0 and wavenumber k_z loaded with periodic gaps of period p much smaller than operating wavelength as shown in Figure 2.23. The gaps are defined by capacitance C_g. The equivalent circuit diagram for the gap loaded line is shown in Figure 2.24. The per unit length inductance and capacitance of the lines are given by

$$L = \frac{k_z Z_0}{\omega} \ , \ C = \frac{k_z}{\omega Z_0} \tag{2.17}$$

Then the propagation constant can be defined as:

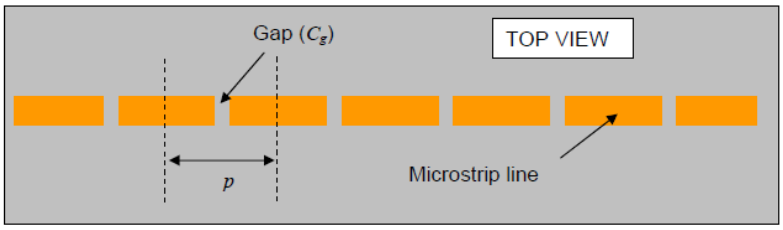

Figure 2.23: Periodically Gap Loaded Transmission Line.

$$\gamma = j\omega\sqrt{LC}\sqrt{1 - \frac{1}{\omega^2 C_g p L}} \tag{2.18}$$

where the critical frequency

$$\omega_c = \frac{1}{\sqrt{C_g p L}} \tag{2.19}$$

is determined by periodicity p, per unit length inductance L and the gap capacitance C_g.

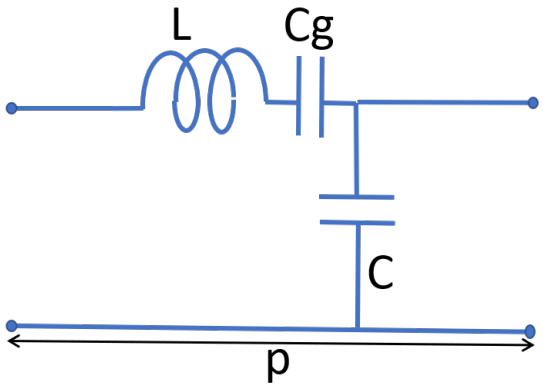

Figure 2.24: Equivalent circuit diagram for the gap loaded line.

The dispersion curve is plotted as shown below in Fig. 2.25 and the cut off frequency can be observed around ω=ω_c. The phase and attenuation constants as obtained from the propagation constant are given by:

$$\beta = \omega\sqrt{LC}\sqrt{1 - \frac{\omega_c^2}{\omega^2}}, \quad when\, \omega < \omega_c \tag{2.20}$$

$$\alpha = \omega\sqrt{LC}\sqrt{\frac{\omega_c^2}{\omega^2} - 1}\,, \quad when\, \omega > \omega_c \tag{2.21}$$

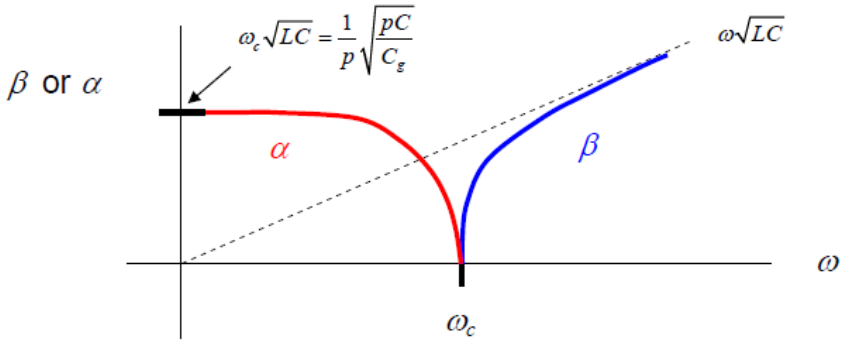

Figure 2.25: Dispersion diagram for the gap loaded line

2.2 Literature survey

This section gives a brief overview on the various works seen in literature until date using slot antennas and metamaterials for obtaining compact, multiband, circularly polarized and wideband antenna designs. A deep insight into the recent works carried out related to the design of each of the proposed slot antenna designs pertaining to the fulfillment of the formulated objectives is given below. In the first subsection, the previous works carried out in the area of multiband antennas and the different techniques used to achieve multiband operations, their advantages and setbacks and how the designs have evolved over time are reviewed. In the successive subsections, the literature related to wideband and circular polarization operation is discussed to look into the possibility of a multiband antenna design with suitable wideband and dual polarization characteristics too. Also, some earlier work related to artificial transmission lines is discussed to better understand the concept of integrating these novel materials with antennas to obtain different properties such as wideband operation.

2.2.1 Slot Antennas with Multiband Characteristics

In order to meet the demand of compact multiband antenna designs that can be easily integrated with other devices, various works are found in literature which use

different techniques to obtain multiband antenna designs. Introducing stubs and slits in the antenna structure help achieve multiband operation but at the cost of larger profiles and resonance bands that cannot be easily tuned as per application. Coplanar waveguide fed slot antenna and printed monopole antenna are respectively designed for WLAN/WiMAX applications in the works by Karimian *et al.* (2013), Sun *et al.* (2012). A tri-band CPW fed slot dipole antenna is designed by Chen *et al.* (2014). An efficient frequency adjustable pentaband slot antenna was designed using ridged stubs by Gholamrezaei *et al.* (2014). A quad-band slot antenna was designed using E and T shaped stubs by Cao *et al.* (2015). A quad band slot antenna was proposed using the proper design of stubs and slots on the ground plane by Piao *et al.* (2017). In different works carried out, compact quad band slot antennas have been designed for various applications (Karimian *et al.* (2013), Sun *et al.* (2012)).

The negative permittivity property of the CSRR can be used to design monopole and dipole antennas that operate at multiple bands of resonance. But, the introduction of the CSRR reduces the gain and efficiency of the system as it is etched out of the ground plane (Basaran *et al.* (2013)). In the work by Li *et al.* (2008), etching a set of CSRR s in the ground plane leads to the design of a dual-band compact linear polarized antenna. A dual band CP antenna is designed by Zhou *et al.* (2010) using spiral resonators. An Electromagnetic Band Gap (EBG) structure is used by Dong *et al.* (2011) for obtaining multiband operation, but this creates large antenna profile and bulky structures.

SRR loading in slot and monopole antennas to achieve multiband application is becoming increasingly popular nowadays.(Ntaikos *et al.* (2011)). Slight modification of the monopole parameters is required to achieve the multiband operation. An MTM based frequency reconfigurable monopole antenna is designed by Cheribi *et al.* (2013), which offers tri-band operation using two differently sized SRRs loaded in the antenna. Each band can be tuned by suitable design of the loaded SRRs. A compact multi-band antenna is designed by Rajkumar and Kiran (2016) for WLAN/WiMAX/ITU applications using a modied TSRR(Triangular Split Ring Resonator).

In the design proposed by Kandasamy *et al.* (n.d.), an SRR loaded square slot antenna is presented which offers circularly polarized dual bands that can be independently controlled. In the design proposed by Sarkar *et al.* (2014), loading a loop antenna with an SRR helped achieve tri band operation, along with miniaturization. However, independent tuning is not easily achievable in this design. The antenna

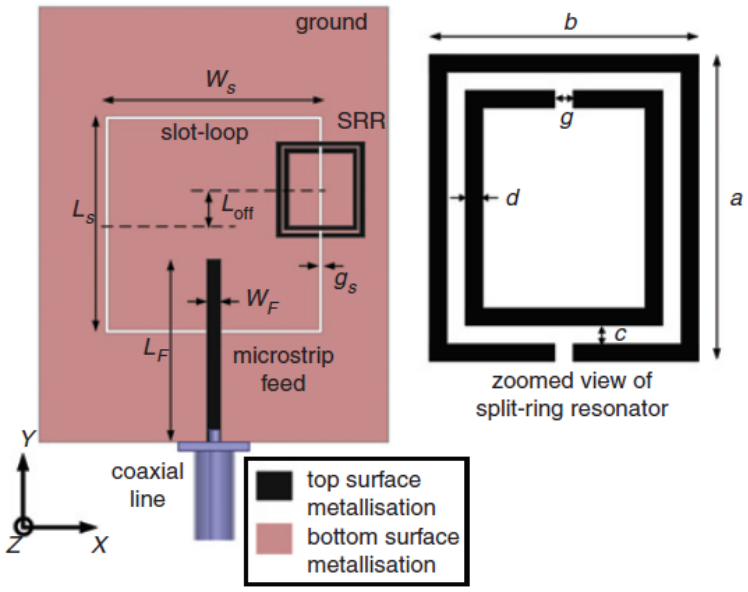

Figure 2.26: SRR loaded square slot loop antenna [Sarkar *et al.* (2014)].

geometry is shown in Figure 2.26.The reflection coefficient characteristics and surface current distributions are shown in 2.27 and 2.28. It can be seen that the presence of the SRR on the slot loop introduces two additional lower order resonance modes in the antenna. The geometry of the SRR and its position along the slot determine these frequencies of resonance. The dimensions of the SRR determine its fundamental resonant mode at 1.65 GHz. When the SRR is suitably offset, the additional resonant band is obtained at the intermediate frequency of 1.93 GHz. Hence the reflection coefficient characteristics are obtained as shown in Figure 2.27. The surface current distributions for the slot loop antenna at the three resonant frequencies shown in Figure 2.28 show that the resonances at the lower two frequencies are due to the excitation of the SRR modes.

The designs proposed in Chapter 3 of the thesis pertain to multiband slot antennas that are miniaturized and radiate at tunable frequency bands. In the first design proposed in Chapter 3, a triband SRR loaded slot antenna is designed which offers independent control of frequency bands. The second and third designs offer compact copper strip loaded square slot antenna designs with pentaband resonance operation.

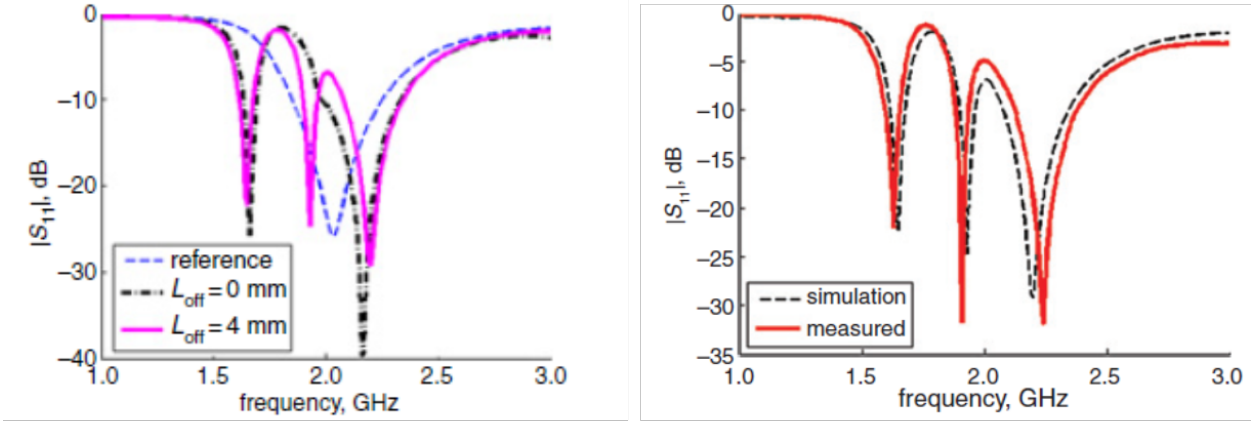

(a) (b)

Figure 2.27: (a) Simulated reflection coefficient characteristics on varying the offset (b) Simulated and measured reflection coefficient characteristics for the square slot loop antenna for the optimum offset [Sarkar *et al.* (2014)].

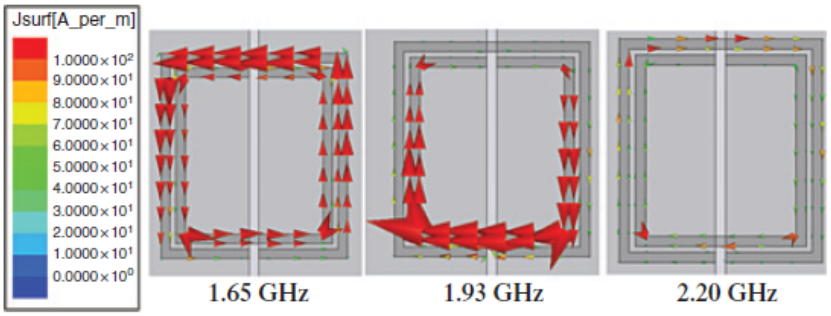

Figure 2.28: Surface current distributions for the slot loop antenna at the different frequencies [Sarkar *et al.* (2014)]

2.2.2 Slot Antennas with Wideband Characteristics

Various methods have been used to increase the bandwidth of a slot antenna, using straight slot, wide slot, L-shaped, inverted T etc.Chen *et al.* (2009), Jan and Su (2005), Latif *et al.* (2005), Zheng *et al.* (2011) show some works that use different techniques to achieve a UWB antenna where Jan and Su (2005) uses a fork shaped feed to excite the structure. The bandwidths can also be increased by exciting two types of resonant modes, namely the slot and monopole modes (Hu *et al.* (2016) and Latif *et al.* (2005)). In the design proposed by Lu and Zhu (2015), pairs of stubs are introduced along the slot near the electric field distribution nulls to excite the slot modes. All of them use

the conventional /2 slot resonators. Broadband filtering slot line antennas are designed using multimode resonators as seen in the work proposed by Hu *et al.* (2017). The slot structure can be modified to obtain a wide bandwidth response where multiple slots and step slots are used to introduce more than one resonant mode with adjacent frequencies which leads to a widened impedance bandwidth (Gopikrishna *et al.* (2009), Huang *et al.* (2012), Kumar *et al.* (2014), Lui *et al.* (2005)). Stepped slots are used by Gopikrishna *et al.* (2009) to obtain UWB characteristics. Notches are cut by Chen and Ku (2008) in an inverted L open slot antenna to enhance bandwidth. In Lee et al. (2002), a broadband planar antenna is designed using round corner rectangular wide slot. In the work proposed by Rao *et al.* (2000), a broad band antenna is designed for DCN/UMTS applications. A microstrip fed wideband slot array with finite ground is designed by Liang and Michael (2000). Isosceles triangular slots and circular slots are used byLee *et al.* (2009), and Jiang *et al.* (2013) respectively to obtain broadband dual polarization applications. These designs require multiple ports and comparatively larger dimensions of the ground plane. Microstrip slot line transitions and stubs have also been used to increase bandwidth (Verbiest and Vandenbosch (2006), Yoon *et al.* (2004) and Gopikrishna *et al.* (2008)). All of these show large cross polarization variation levels or have large area. The fictitious short circuit concept to obtain broad band radiation was introduced by Zhu *et al.* (2003) with bandwidth of 32%. A microstrip line of reduced width was used to realize a fictitious short circuit along the slot thus exciting two resonances and thus generate the wide band operation. The length and position of feed line are carefully chosen so that the multiple resonances excited are very close-by and hence wideband operation is obtained. Double rejection zeros are introduced in a slot antenna using a $\lambda/4$ resonator in the feeding network to obtain widened impedance bandwidth. This concept of fictitious circuit is used in Sadat *et al.* (2006, 2007) and Javan *et al.* (2008) for UWB applications.

The bandwidth was improved in the works by Behdad and Sarabandi (2005) and Behdad and Sarabandi (2004) to 37% and 43% respectively compared to the work proposed by Zhu *et al.* (2003). A modified feedline is used by Behdad and Sarabandi (2004) to achieve bandwidth enhancement. The designs had complex feeding structure and large size. To overcome these disadvantages, and also for obtaining high gain and unidirectional radiation, Majumder *et al.* (2015) introduced a design which gives wide band metasurface antenna. In order to further reduce the size of the slot resonator, a $\lambda/4$ resonator using the same concept of fictitious short circuit is proposed here.

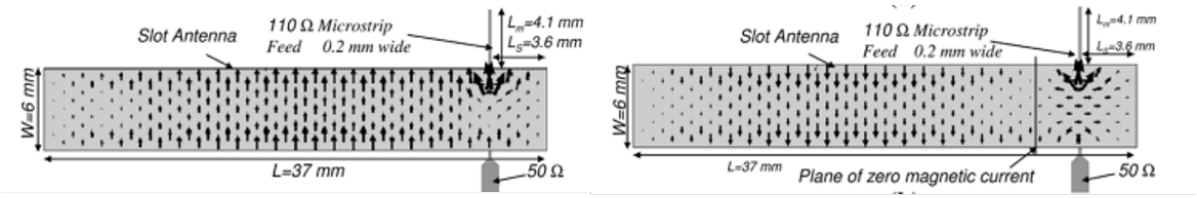

(a) (b)

Figure 2.29: Electric field distribution for the wideband slot antenna proposed by Behdad and Sarabandi (2005): (a) Normal distribution (b) Distribution at a slightly higher frequency (Fictitious short circuit concept)

Some of the other compact UWB designs include that proposed by Chen and Ku (2006) which has a disadvantage of high cross polarization, Li *et al.* (2010) uses a compact CPW fed rectangular slot which is excited by a simple square patch to exhibit wideband characteristics, Zheng *et al.* (2010) proposes a compact UWB slot antenna with two stepped slots. It is a modification of the design by Chen and Ku (2006) and also exhibits high cross polarization level, and Kanno (2007) uses an inductive resonant section along with a fictitious short circuit fed slot resonator to obtain compact UWB antenna. The fictitious short circuit concept is pictorially demonstrated in Figure 2.29 using the electric field distributions along the wideband slot antenna proposed by Behdad and Sarabandi (2005). The second resonance is basically generated due to the nulls created on cancellation of the fields created by the microstrip line and by the return current on the ground plane. Dual band and wide band operation can be obtained depending on the feed position and slot width which determine the frequency at which the null is obtained. The reflection coefficient characteristics obtained for both cases in shown in Figure 2.30. From Figure 2.29, it can be seen that the electric field distributions at both the frequencies follow a similar pattern and hence the radiation patterns at the two frequencies are also expected to be similar. This can be seen in Figure 2.31 which shows the E and H plane co and cross polarization patterns for the wideband antenna at (a) 3.077 GHz and (b) 3.79 GHz (Behdad and Sarabandi (2005)).

Artificial transmission lines are also used to obtain wideband characteristics. They are formed by modifying planar transmission lines, that is, by conveniently modulating their dimensions, or etching patterns on the metallic ground plane layer, or loading the line with reactive elements. This helps to achieve reduction in the device size, or improve the performance parameters and functionalities of the host device. Different

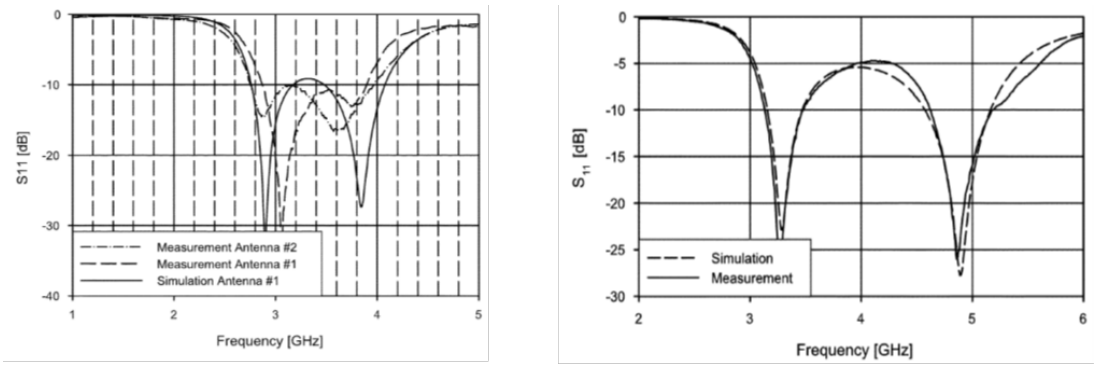

Figure 2.30: Reflection coefficient charcateristics for half wavelength slot antenna obtained on varying the feed position, hence exhibiting: (a) wideband and (b) dual band characteristics (Behdad and Sarabandi (2005)).

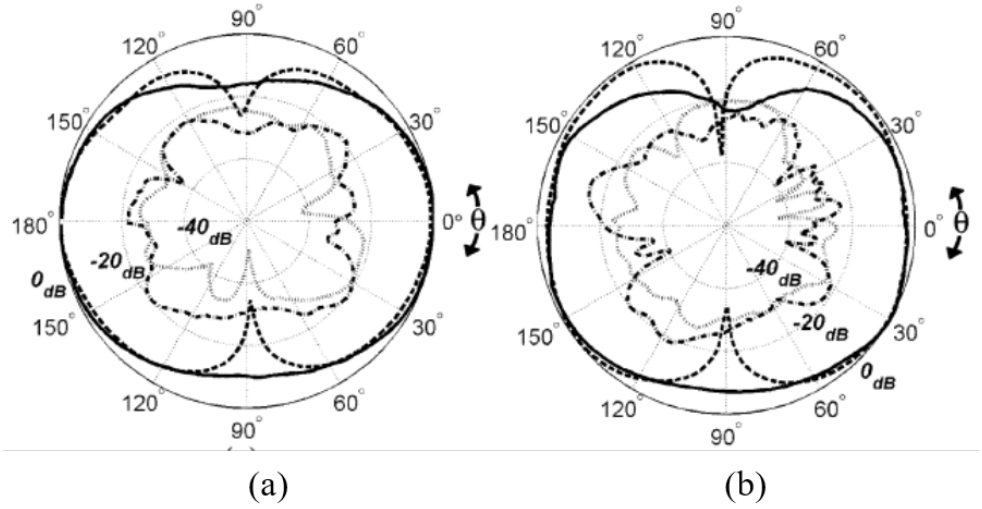

Figure 2.31: Radiation patterns for E-plane and H-plane (a) 3.077 GHz and (b) 3.79 GHz (Behdad and Sarabandi (2005)).

kinds of artificial line structures and their applications have been discussed in literature. Some of the earlier works involved the inclusion of a periodicity within the transmission line structures to obtain the desired properties. These include electromagnetic band gap (EBG) based and capacitive loaded lines. Wideband filtering has been achieved using periodic capacitive patch loaded transmission lines which give rise to wide stop bands (Garcia-Garcia *et al.* (2006)). Metamaterials (MTMs) are integrated with the microstrip lines to form another class of artificial lines called MTM

based artificial lines where the host lines are loaded with various resonating elements such as inductors, resonators or capacitors. Composite right and left handed (CRLH) based transmission lines have been used to design enhanced bandwidth microwave components and also band pass filters with UWB responses (Mo *et al.* (2007), Gil *et al.* (2007)). The phase shift experienced by the transmission lines for a nominal change in the frequency limits the bandwidth in distributed circuits. The phase shift at angular frequency ω_0 and phase velocity v_p for a transmission line of length l is given by (Martin (2015))

$$\phi_0 = \beta l = \omega_0 l / v_p \tag{2.22}$$

The bandwidth depends on the derivative of the phase with respect to frequency, or the group delay and hence, is inversely proportional to the length of the line. Therefore, it is not an easily controllable parameter in conventional transmission lines. However, on introducing metamaterial elements in the lines, possible degrees of freedom come into picture which could be varied in order to control the bandwidth of the line. Computing the derivative of the phase at the operating frequency for N number of unit cells, the following relation is obtained:

$$\frac{d\phi}{d\omega}|_{\omega_0} = \frac{2}{\omega_0} N \tan(|\phi_0|/2N) \tag{2.23}$$

Thus, as N increases, the derivative of phase reduces and bandwidth increases. The optimal case is hence obtained using an N-stage artificial transmission line with N tending to ∞ . Miniaturization and bandwidth enhancement of many microwave components are possible using artificial transmission lines. In Figure 2.32, a broadband series power divider is shown. Bandwidth enhancement is made possible using MTM based transmission lines. The MTM based cells are designed suitably so as to obtain values of L and C that optimize the phase shift and hence improve the bandwidth at the operating frequency with compact component dimensions. It can be seen that the metalines used are shorter than the conventional 2π transmission lines and hence the device area is significantly reduced.

Wideband filters have been designed using open resonant particles such as the open split ring resonators (OSRRs) and their complementary counterparts, the open complementary split ring resonators (OCSRRs) (Martel *et al.* (2007)). To further widen the propagation band for artificial transmission lines, lattice network and non-

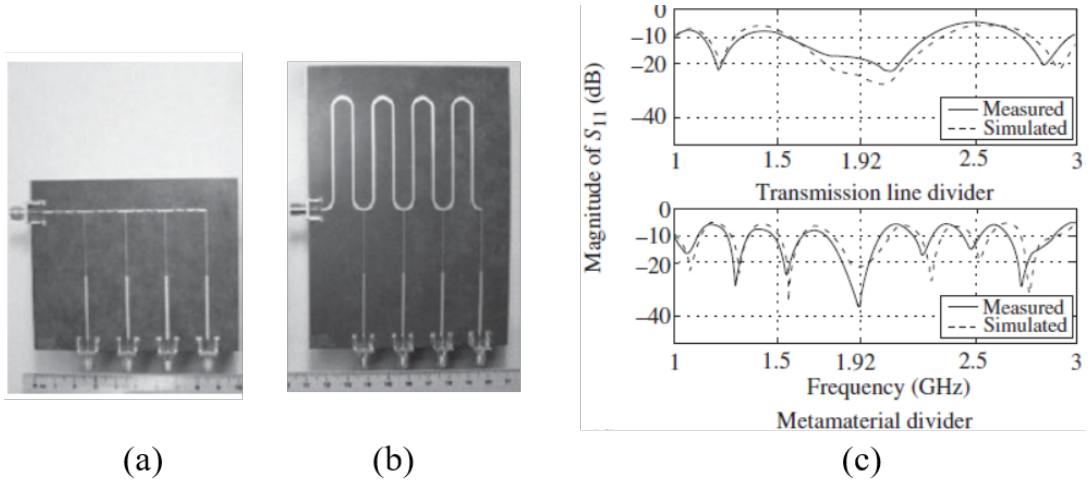

Figure 2.32: (a) MTM based TL power divider (b) Conventional TL series power divider (c) Reflection coefficient magnitude characteristics.

foster element-based transmission lines are also used by Perruisseau-Carrier *et al.* (2011) and Hrabar *et al.* (2013).

For designing compact devices that operate over a wide range of frequencies (wide-band opeartion) and that can cater to multiple applications, miniaturized multiband antenna designs are required which can give wideband operation over at least one resonant band. Various methods have been used for obtaining multiband properties within compact slot antenna structures, such as the insertion of strips or employing slots by Hu *et al.* (2016), Dang *et al.* (2010) to produce additional resonances. These traditional methods usually give low efficiency values and narrow bandwidth for multiband antennas. Also, independent frequency tuning is not possible.

As mentioned in the earlier works, in order to achieve multiband antenna designs with easy tunability of the frequency bands, the integration of metamaterials (or their unit cells) with antenna structures has become a very possible choice. Upon excitation, these structures behave as LC resonant tanks and thus provide negative permeability/permittivity near their resonance frequency as mentioned by Marques *et al.* (2002). Further, these structures allow for compact designs owing to their sub-wavelength dimensions. CSRRs (Complementary split ring resonators) have been used in different antennas to obtain multiband characteristics such as in the work carried out by Basaran *et al.* (2013). But the gain and efficiency are reduced due to the etching out of the main radiator. For slot antennas, SRRs have been used to obtain multiband characteristics as in designs proposed by Sarkar *et al.* (2014), Kandasamy

et al. (n.d.) and Paul *et al.* (2017). These designs are of large dimensions and are useful for narrow-band applications.

The Chapters 4 and 5 of the thesis discuss novel wideband slot antenna designs that are proposed to offer compact, multiband structures that can operate over a wide frequency band. In the first design proposed in Chapter4 of the thesis, a compact quarter length open slot structure is excited using a simple feed to exhibit wide band characteristic with constant radiation patterns and low cross polarization levels throughout the band of operation. The antenna is designed such that the operation covers the WiMAX / WLAN bands. Compactness is achieved compared to other single slot multiband antennas with wideband characteristics by using a quarter wavelength open slot. Besides, dual band characteristics can be incorporated by introducing a suitably oriented SRR at the open slot. Hence, a rectangular narrow slot multiband antenna with wideband characteristics using an SRR loading and using a fictitious short circuit microstrip line feed is proposed for the first time. Frequency reconfigurability could be achieved using active devices such as varactor diodes. In the second design, a similar structure is proposed with a modified SRR to obtain triband operation with independent tunability. The square slot design introduced in Chapter 5 uses the concept of artificial transmission line to produce multiple resonances that combine to produce an ultra-wideband resonance characteristic with good efficiency and gain values over the operating band.

2.2.3 Slot Antennas with Circularly Polarized Multiband Characteristics

The presence of circularly polarized (CP) resonance bands become an added advantage for mobile wireless devices because CP signal provides better propagation characteristics in multipath environment compared to the linear polarization. The circularly polarized (CP) antennas are less sensitive to the multipath effects and polarization mismatch between the transmitter and the receiver. Hence there has been an increased demand for the design of circularly polarized antennas, which can also exhibit multiband properties. Furthermore, tuning of the frequency bands and reconfigurability of the polarization states are desirable features which find application in various areas.

Different wide slot CPW fed antennas with circularly polarized radiation have been realized over the years. In the work proposed by Sze *et al.* (2003), a CPW

fed square slot antenna using T-shaped strips is designed for CP, while in the design proposed by Chou *et al.* (2007), a cross patch is loaded on the slot to obtain CP. In the works by Deng *et al.* (2007) and Wang and Chen (2009), grounded metallic strips are used to obtain circular polarization. A lightning shaped feed and grounded strip are used by Fries *et al.* (2003) to obtain CP. These designs have a large profile and use complicated designs where the frequency of operation and axial ratio are sensitive to the strip and sub dimensions. Perturbations are used for ring slot antennas for generating CP radiation (Fries *et al.* (2003), Wong *et al.* (2002), Bao and Ammann (2008)). A V- shaped coupling strip is used by Row *et al.* (2011) to obtain CP in the ring slot antennas.

Dual band slot antennas with circular polarization characteristics have been designed with good ARBW, gain and efficiency values at the different resonant bands. The conventional methods used to achieve this commonly involve introduction of carefully designed slits or stubs in the ground plane. This helps to modify the current distribution around the slot in order to generate 90° phase shifted orthogonal modes and hence, circularly polarized (CP) waves (Xu *et al.* (2017),Baek and Hwang (2013)). The antennas thus designed, offer dual bands of operation, but are of large size. Also easy tuning of the sense of polarization and resonant frequencies is not possible. These techniques to obtain dual band dual polarized antennas lead to large dimension structures and do not facilitate independent tuning and control of polarization sense for each band. In the work proposed by Hsieh *et al.* (2012), an annular slot antenna is designed to give circular polarization with ARBWs of 0.9% and 0.6% at the two operating bands.

Metamaterials (MTMs), due to their interesting resonant properties, can be used to obtain various desired characteristics such as miniaturization, multiband operation, circular polarization etc. when integrated with the antennas. The property of metamaterials can be used to obtain multiband and circular polarization operation in antennas. Multiband circularly polarized patch and monopole antenna designs are proposed by Zhou *et al.* (2010) using CSRRs. The gain and efficiency values of the antenna are reduced due to the etching of the CSRRs in the ground plane.

In works by Hoang *et al.* (2016) and Ko *et al.* (2013) Electromagnetic Band Gap (EBG) structures and metasurfaces are introduced for design of multiband CP antennas. These designs offer the disadvantages of large profile, and very low axial ratios. SRRs can be effectively used to generate the additional resonance to obtain multiband

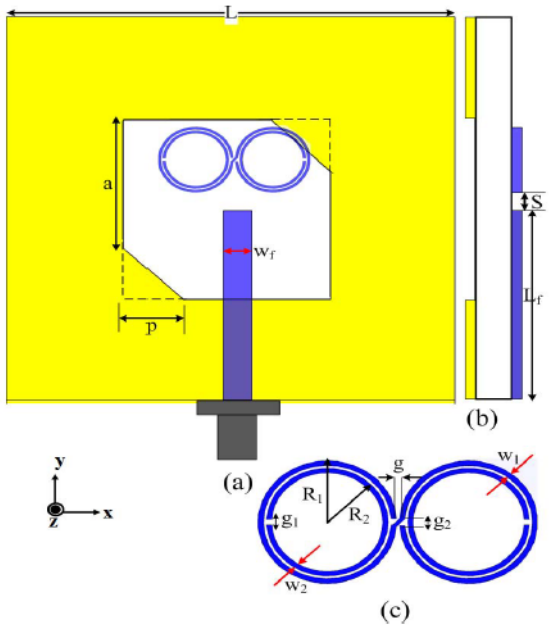

Figure 2.33: Connected SRR loaded dual band CP slot antenna (a) Top view (b) Bottom view (c) SRR geometry (a=24.4mm, L=70mm, L_f=22mm, p=10mm, S=4mm, W_f=3.4 mm) [Kandasamy *et al.* (2016)]

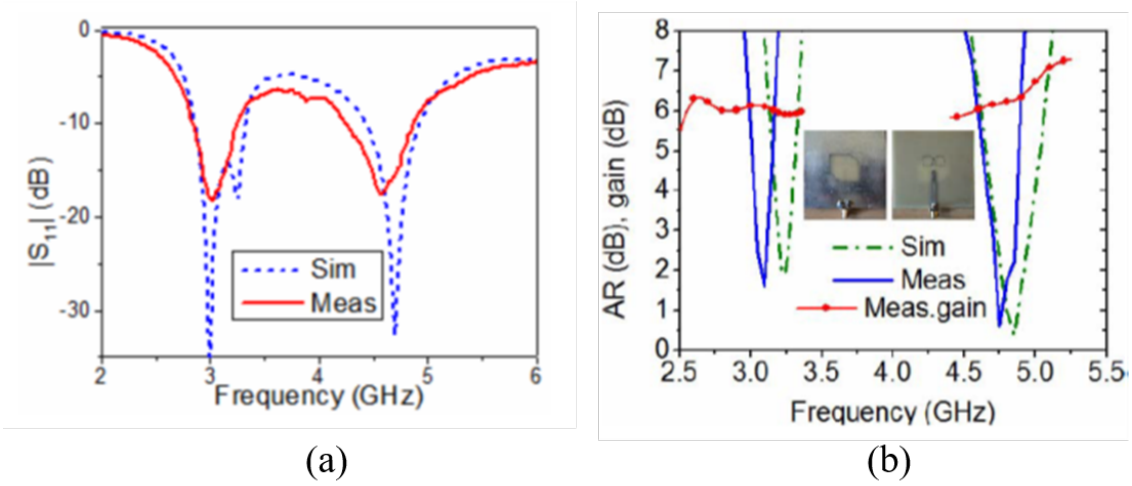

Figure 2.34: (a)Reflection coefficient magnitude characteristics for the dual band CP antenna (b) Axial ratio plots for the dual band CP antenna. (Kandasamy *et al.* (2016))

properties with tunability features, and the proper design and orientation of SRR can help to achieve CP properties. A dual band CP square slot antenna is designed using connected SRRs by Kandasamy *et al.* (2016) to obtain ARBWs of 3.1% and 4.2% at 3.1 GHz and 4.7 GHz respectively. Here, the polarization at each of the bands as well

as the sense of polarization can be controlled. S-shaped SRR is used to excite CP for the upper band. The Figure 2.33 shows the connected SRR loaded slot antenna that can operate at dual CP bands due to the truncation of the slot at the corners and the properties of the connected SRR. The reflection coefficient characteristics and axial ratio plots obtained on simulation and measurement of the antenna is shown in Figure 2.34. In the work byGhaffarian *et al.* (2017), a switchable dual/triple band circularly polarized slot antenna is designed using L shaped feeding stub, modified open SRR and CSRR. A dual band CPW fed SRR loaded slot antenna is proposed by Saraswat and Harish (2018) which offers circular polarization at the two operating bands. In the work by Chen *et al.* (2018), a dual band circularly polarized antenna is designed using artificial transmission line to obtain two operating bands with ARBWs of 10.2% and 7.7% respectively.

In the works proposed in Chapter 6, novel compact single, dual and tri-band slot antennas with CP characteristics are designed. The proposed designs provide CP resonance bands with wider ARBW values and compact size compared to other MTM based designs. Moreover, easy tunability of the frequency bands as well as the polarization senses at each band is possible. Also, a quad band slot antenna with circular polarization characteristic at one band is discussed.

2.2.4 Research Gap Analysis

Compact Multiband Slot Antenna with Independent Tunability: There lies a need for the design of compact slot antennas that can be easily integrated with wireless devices that require multiple functionalities. The antenna requires miniaturized designs that can operate at easily controllable multiple resonance bands with good impedance bandwidth, efficiency and gain values at each of the resonant bands.

Compact Wideband Slot Antenna: On investigation of existent designs, it is found that there is a scope for further miniaturization and improvisation of performance parameters for antennas operating at multiple bands with one or more bands exhibiting wide impedance bandwidth property. There lies a need for developing such novel antennas that can operate with good impedance bandwidths, peak gain values and stable radiation patterns at all the multiple bands and also provide the feature of independent frequency control.

Compact Multiband Circularly Polarized Slot Antenna with Independent Tunability: The research gap analysis points out the requirement for the design

of compact slot antennas that can operate at multiple circularly polarized bands and whose bands can be tuned independently. The antenna requires to operate at the resonance bands with good impedance bandwidth, AR bandwidth, efficiency and gain values. Also, the sense of polarization at the resonance bands are required to be tuned as per will.

Compact Ultrawideband Slot Antennas: The study on UWB slot antennas shows a majority of designs that use the differently shaped slot structures, stubs, slits and modified ground planes to obtain a wide resonance. Novel techniques that involve the concept of artificial transmission lines have not been investigated yet. Without modifying the slot antenna geometry and keeping the fundamental slot mode intact, it is required to obtain a compact design that offers an ultrawideband resonance characteristic with good gain and efficiency values over the entire operating bandwidth.

Chapter 3

COMPACT MULTIBAND SLOT ANTENNA DESIGNS

3.1 Introduction

This chapter discusses the various compact multiband antenna designs that have been developed using loading of SRR and metallic strip elements on the square slot. In the first section, a triband SRR loaded slot antenna design is presented which provides independently controllable bands of operation. The second section presents an SRR and copper strip array loaded square slot antenna design that offers operability at five different bands and provides a compact multiband design with higher bandwidth and efficiency values compared to earlier works. The third section explains a pentaband strip loaded slot antenna design where the square slot is loaded with a uniform array of thin vertical copper strips. The designs use the negative permeability and permittivity properties of MTMs such as the SRR and copper strip array to produce multiple bands of resonance that can be tuned depending on the MTM dimensions. The antenna geometry, principle of operation, measurement and simulated reflection coefficient characteristics and radiation patterns are presented and compared for each design. Fabricated prototypes are also shown.

3.2 Triband SRR Loaded Rectangular Slot Antenna

3.2.1 Multiband Operation using SRR

In this design, a novel SRR based square slot antenna is explained which provides triband operation and offers easy frequency tunability at the higher frequency bands, without affecting the main one. The higher frequency bands are obtained by loading the slot with two SRR structures that are optimally positioned within the slot. Desired bands of operation can be obtained by either changing the SRR or slot dimensions as each of the resonant band is either slot or SRR controlled.

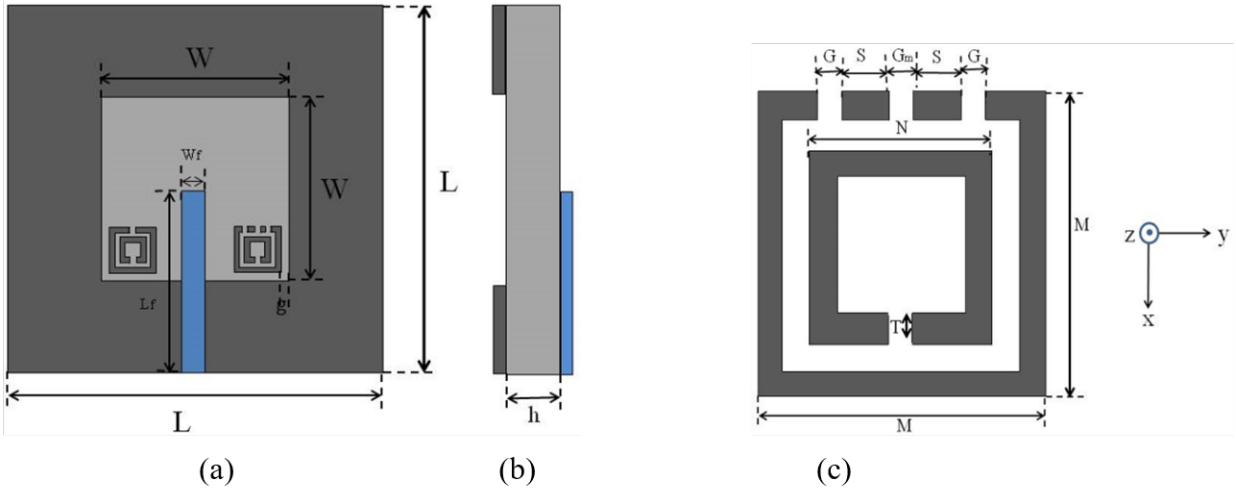

Figure 3.1: Geometry of the proposed antenna. (a) Topview (b) Sideview (c) SRR geometry. [W=33.2, L=60, Wf=3.6, Lf=29.4, M=6, N=4, T=0.6, S=0.9, G=0.5, Gm=0.6, g=0.3, and h=1.56](All in mm)

3.2.2 Antenna Design and principle of operation

The proposed tri-band antenna geometry is shown in Figure 3.1. The antenna is designed using an FR4 substrate of size 60X60 mm^2, permittivity (ϵ_r) = 3.6, height (h) = 1.56 mm and loss tangent = 0.02. The top side of the substrate consists of a square slot with side length 33.2 mm and two SRRs as shown in Figure 3.1(a). SRRs with single and multiple splits are used to create the two different resonant frequencies in addition to the slot main one. The bottom side of the substrate is printed with a suitably designed 50Ω microstrip feed line of width 3.6 mm and length 29.4 mm. The SRRs are placed symmetrically with respect to the feed line. Multiple splits of equal

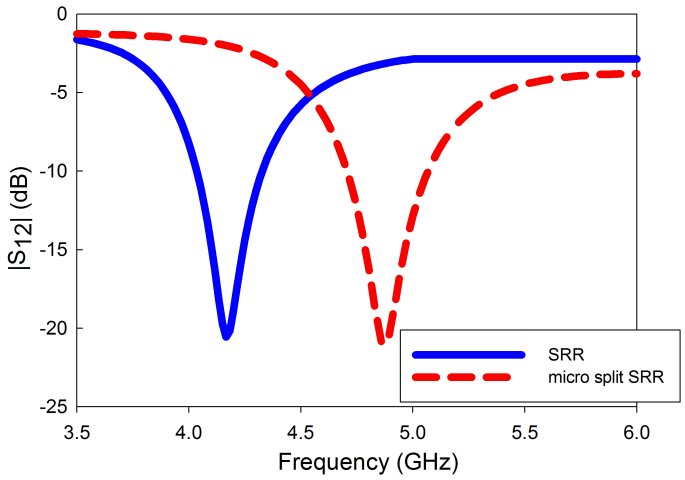

Figure 3.2: Transmission characteristics of the single and multisplit SRR

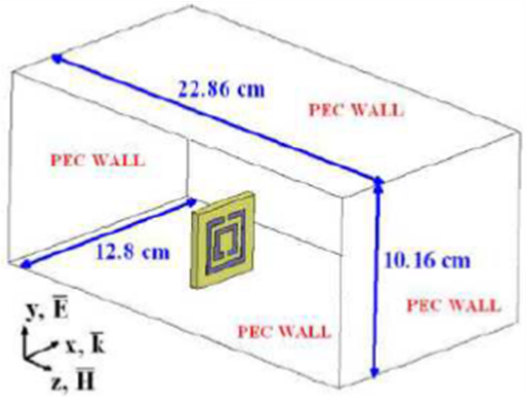

Figure 3.3: SRR unit cell characterization setup

width are introduced in one SRR to provide additional capacitive effects, which shifts the resonant frequency of the SRR to a higher value. The splits introduced here are of equal width of 0.5 mm, equally spaced at a distance of 0.9 mm from the edges of the main gap of the SRR as shown in Figure 3.1(c).

The square slot is excited to resonate at its fundamental resonant mode (TM_{01}). The resonant frequency (fr1) of the slot is found from Equation 3.1.

$$f_{r1} = \frac{c}{2w}\sqrt{\frac{2}{1+\epsilon_r}} \tag{3.1}$$

Here, c is the velocity of light. The square slot is designed to resonate at 2.6 GHz.

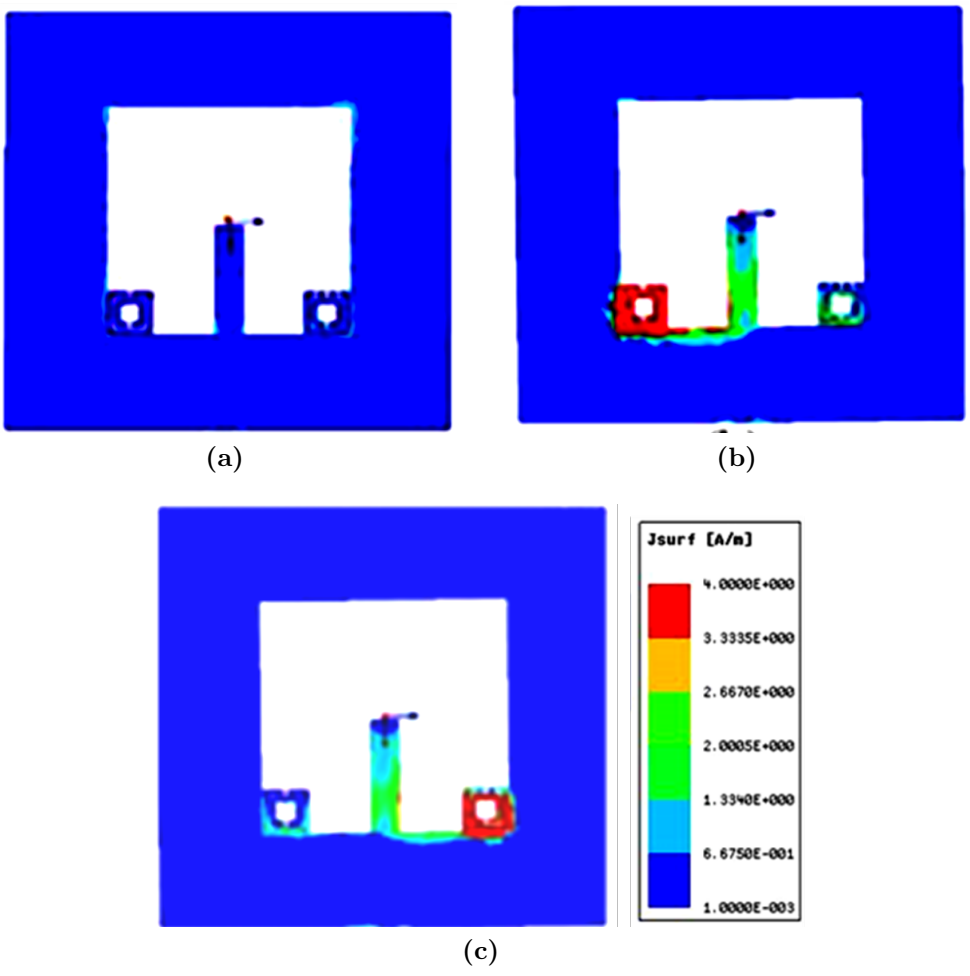

Figure 3.4: Surface current distribution of the proposed antenna at (a) 2.6 GHz (b) 4.2 GHz and (c) 4.7 GHz

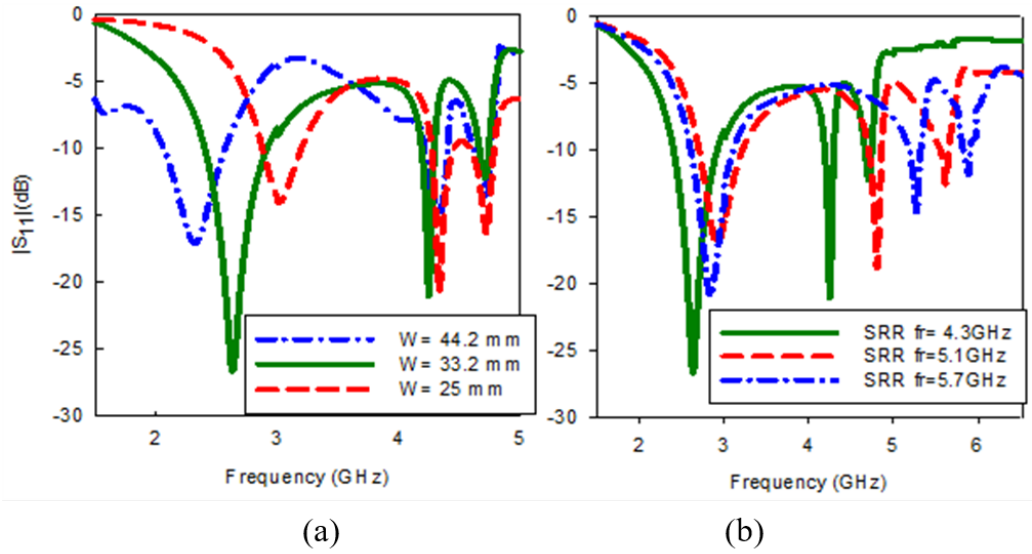

Figure 3.5: Effect of variation of SRR and slot parameters with resonance frequency. (a) SRR variation (b) slot dimensions variation

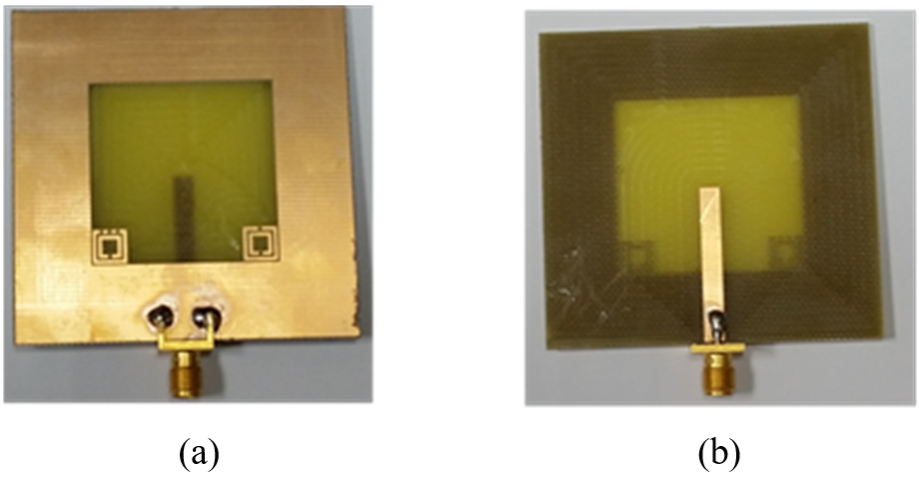

Figure 3.6: Photograph of the proposed antenna prototype (a) Front side (b) Back side

The resonant frequency of the SRR is calculated from (Ishikawa et al. (2007)). The SRR is designed to resonate at 4.2 GHz. The SRR is characterized using the technique given by Engheta and Ziolkowski (2006). The simulated transmission characteristics of SRRs with single split and multiple splits are shown in Figure 3.2. The experimental set up for the SRR unit cell characterization is given in Figure 3.3. It is observed that the SRR with multiple splits resonates at a higher frequency compared to the

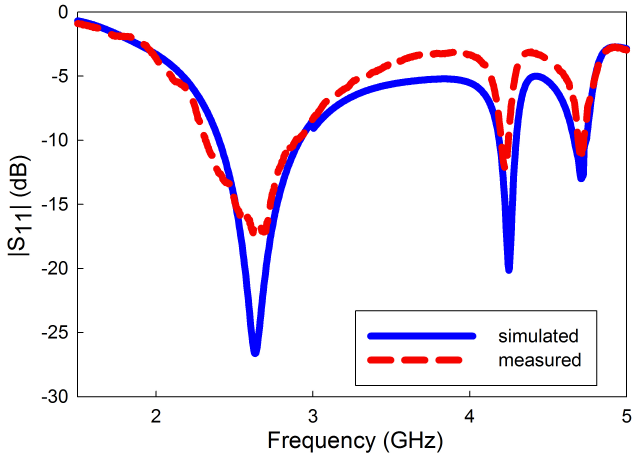

Figure 3.7: Measured and simulated reflection coefficient magnitudes of the proposed tri-band antenna

single split one. The placement of SRRs inside the slot allows for reasonably strong coupling of the magnetic field lines which pass perpendicular through the rings and hence facilitate SRR excitation.

The proposed antenna will radiate at the SRR controlled resonance bands of operation without largely affecting the slot resonance. Tri-band operation is thus achieved easily at 2.6, 4.2 and 4.7 GHz. The third band at 4.7 GHz can be fine-tuned by varying the width and position of the introduced micro splits (Ekmekci et al. (2009)). This can be implemented by electronically controlling the gap width using active devices such as varactor diodes.

The surface current distribution of the tri-band slot antenna is shown in Figure 3.4. It can be clearly seen that at 2.6 GHz, the magnitude of surface current distribution is concentrated in the slot. The peak surface current is observed on the single split SRR at 4.2 GHz. At 4.7 GHz the maximum magnitude of the surface current is observed around the multi-split SRR structure.

Further, to show the independent tuning of the resonant frequencies of the proposed tri-band antenna (an important feature that other designs lack), parametric studies were performed by varying one parameter while keeping the others constant. Figure 3.5 shows the simulated magnitude of the reflection coefficient of the antenna when varying the slot and SRR dimensions. It is observed that variation of the slot dimensions alone results in significant shift in the first resonant frequency at 2.6 GHz

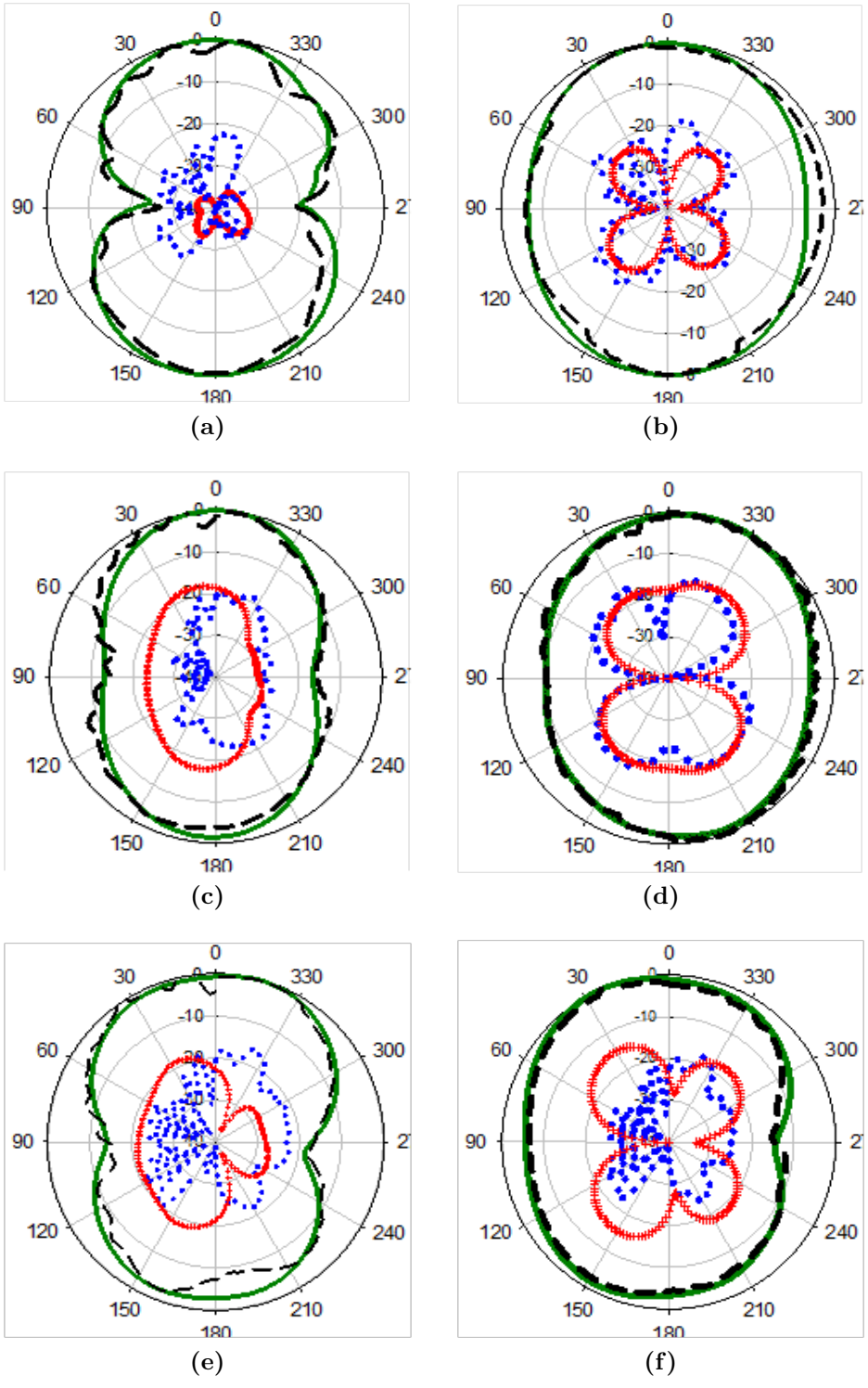

Figure 3.8: Simulated and measured radiation pattern plots of the proposed antenna at the three resonant frequencies 2.65 GHz (a)phi=0 (b)phi=90, 4.3 GHz (c)phi=0 (d)phi=90, 4.7 GHz (e)phi=0 (f)phi=90 (——measured co-pol, —simulated co-pol, —-measured cross-pol, +++simulated cross-pol)

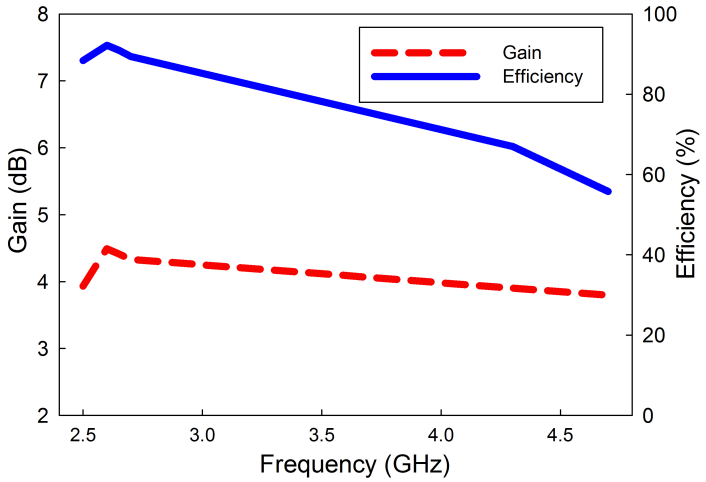

Figure 3.9: Measured maximum gain and efficiency plots of the proposed antenna

(Figure 3.5 (a)). Variation of the SRR dimensions results in a shift in the second and third frequency bands (Figure 3.5 (b)). The third frequency band is tuned by changing the split position and gap along the arms of the multi-split SRR. Therefore, the resonant frequencies of the proposed tri-band antenna can be independently tuned.

3.2.3 Results and Analysis

The proposed tri-band antenna was simulated using ANSYS HFSS 16.0 and was fabricated using an S103 LPKF machine then measured using an Agilent N9918A VNA at the AMSD lab at KFUPM. A photograph of the prototype of the proposed antenna is shown in Figure 3.6. The measured and simulated reflection coefficient magnitudes are shown in Figure 3.7. The simulated and measured results show good agreement. For the first band of operation of the antenna, the -10 dB measured bandwidth was 580 MHz (2.31 GHz - 2.89 GHz centered at 2.64 GHz). The second band of operation shows a measured bandwidth of 120 MHz (4.15 GHz - 4.27 GHz centered at 4.21 GHz) while the third band gives a measured bandwidth of 100 MHz (4.64 GHz - 4.74 GHz centered at 4.71GHz). The simulated and measured radiation patterns of the proposed antenna at the three resonance frequencies (for x-z, y-z planes) are shown in Figure 3.8. The antenna radiation characteristics were measured in a Satimo Star-Lab near-field chamber. The plots obtained in the x-z plane depict an omni-directional pattern. The measured efficiency and peak gain values at the three resonance frequen-

cies are 90.9% / 4.4dB, 67% / 3.9dB, 55.8% / 3.8dBi, respectively. Figure 3.9 shows the measured gain / efficiency versus frequency.

3.3 Pentaband Strip and SRR Loaded Slot Antenna Design

In this section, a novel compact slot antenna suitable for penta-band applications is proposed. The slot is loaded with an array of five copper strips on the top and an SRR with suitable configuration at the bottom to obtain different resonance bands. The antenna is found to resonate at frequencies of 1.51 GHz, 2.61 GHz, 3.11 GHz, 3.86 GHz and 6.26 GHz. Also, a gain higher that 2.4 dBi and a bandwidth of at least 80MHz are obtained for all the bands. This design offers a compact geometry due to the introduction of the SRR unit cell. It makes use of the frequency resonance obtained on excitation of the copper strips and SRR unit cell to obtain the multiband antenna design miniaturized by 78% compared to the pentaband antenna design by Gholamrezaei *et al.* (2014).

3.3.1 Antenna Design

The proposed penta-band antenna geometry is given in Figure 3.10. The antenna is designed on an FR4 substrate of height 1.56 mm, permittivity 4.4 and loss tangent 0.02. A slot, designed to operate at 2.46 GHz is etched out on top of the substrate and loaded with an array of five copper strips. On the bottom of the substrate the 50Ω microstrip feed line is situated. The SRR is also loaded at the bottom and positioned just below the corner of the slot such that the axial magnetic field lines excite it to produce resonance at 1.5 GHz. The other bands are produced upon excitation of the copper strip array.

The number of resonance bands produced depends on the number of copper strips loaded on the slot and on the number of odd multiples of half wavelength values obtained due to the lengths of the loaded strips. Also, the frequency bands slightly shift when altering the length of the strips. An increase in the length of the strips shifts the bands towards lower values, while a reduction in the length shifts the bands to higher resonance values. Only the SRR band remains unaffected at 1.5 GHz throughout, which changes only with the change in the dimensions of the SRR. Also changing the

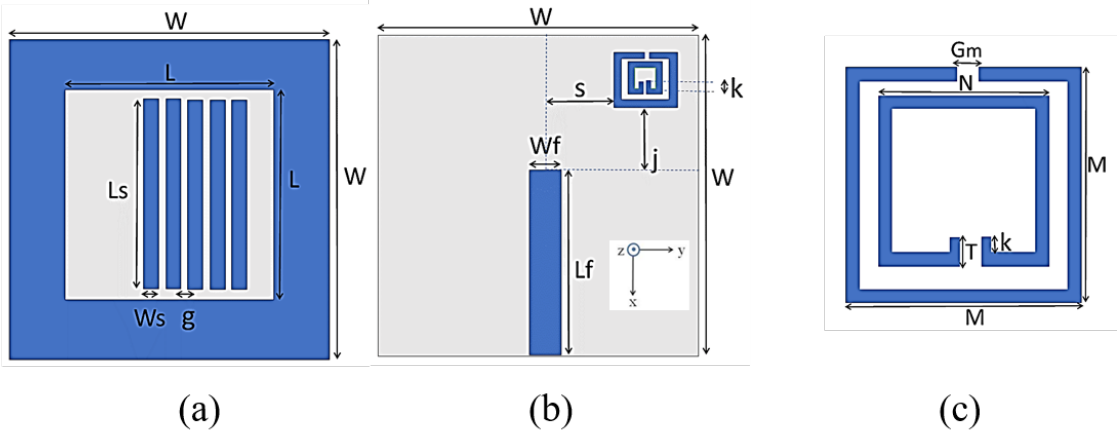

Figure 3.10: Antenna geometry (a) top view (b) bottom view (c) SRR geometry. [L=33.2, W=50, L_s=30.64, W_s=2.5, g=1.1, L_f=24.4, W_f=3.6, s= 8.6, j=8.4, k=1.65, M=6, N=4, T=0.6, G_m=0.6, h=1.56]. All dimensions in mm.

width of the strips affects the reflection coefficient magnitude values at the resonance frequencies (i.e. matching). The simulation and tuning of the antenna are performed using ANSYS HFSS.

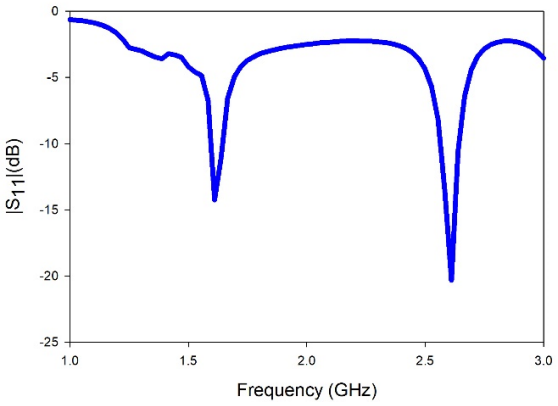

Figure 3.11: Simulated reflection coefficients of the proposed slot antenna loaded only with SRR

3.3.2 Results and Discussion

The antenna was simulated using ANSYS HFSS. The analysis was conducted by simulating the proposed antenna using different configurations. When loading the slot with the designed SRR unit cell, an additional resonance is obtained at 1.5 GHz

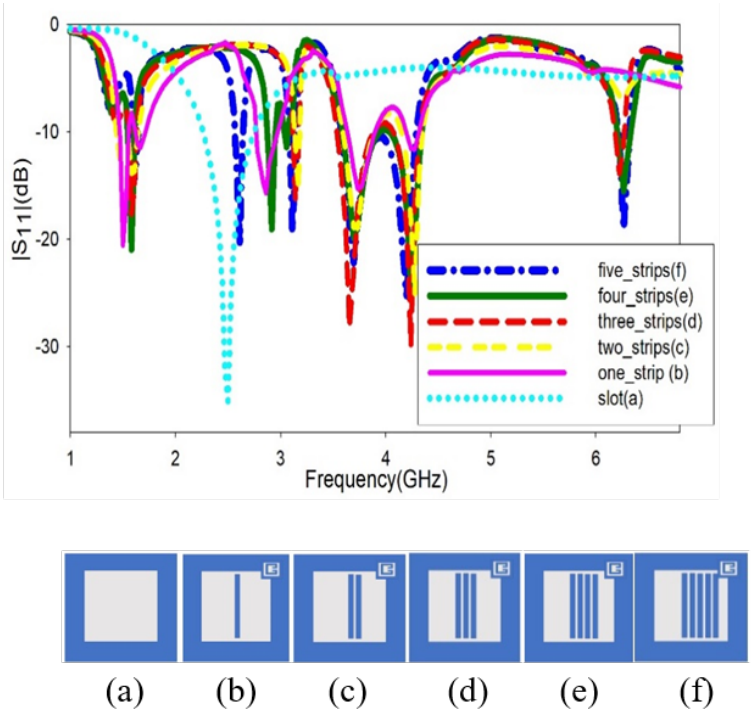

Figure 3.12: Simulated reflection coefficients of the proposed multiband antenna on varying number of copper strips

as seen in Figure 3.11. After loading the slot with different numbers of copper strips, the reflection coefficient curves are observed and plotted as shown in Figure 3.12. The current distribution for different resonance frequencies is plotted as shown in Figure 3.13. The effect of each of the strips on the resonance can be studied from the current density magnitudes. It can be seen from Figure 3.13 (a) that the maximum current density distribution is around the SRR at 1.6 GHz. The addition of one strip shifts the slot resonance to around 3.86 GHz which is seen in Figure 3.13 (d), where current density distribution is maximum around the slot. Loading of a second strip helps achieve the resonance at the third band (3.11 GHz) and with slight resonance at 6.29 GHz. This can be seen in Figure 3.13 (c) where maximum current density is found around the second strip. The addition of the remaining strips strengthens the resonance at 6.29 GHz, which is evident from the current distribution shown in Figure 3.13 (e), where the maximum current density is concentrated around the strips. The last two strips contribute to the resonance at the second band (2.61 GHz), which can be seen in Figure 3.13 (b) where current density distribution is observed to be maximum around the last two strips. Thus, the final reflection coefficient magnitude

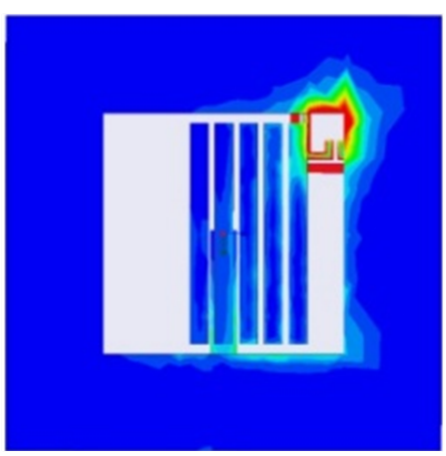

(a)

(b)

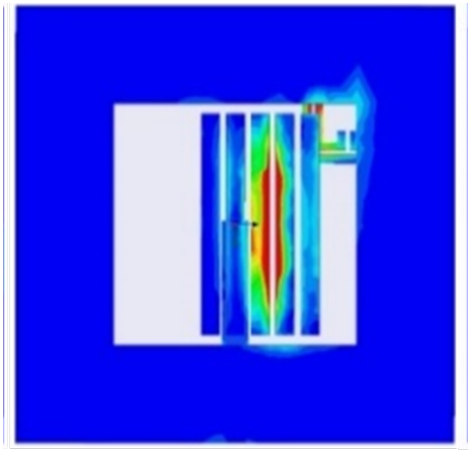

(c)

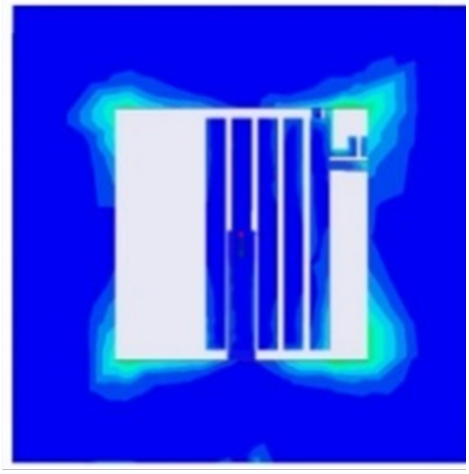

(d)

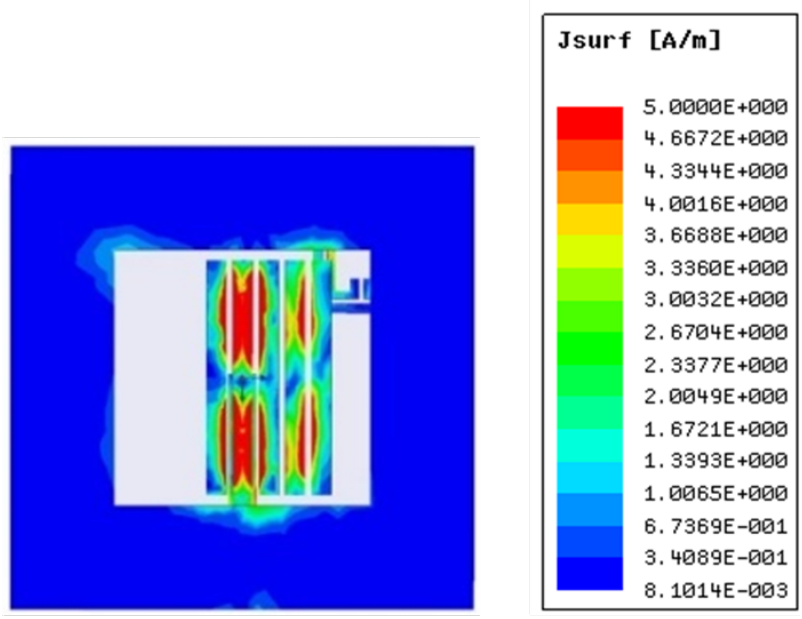

(e)

Figure 3.13: Surface current distribution of the proposed antenna at (a) 1.51 GHz, (b) 2.61 GHz, (c) 3.11 GHz, (d) 3.86 GHz, (e) 6.26 GHz

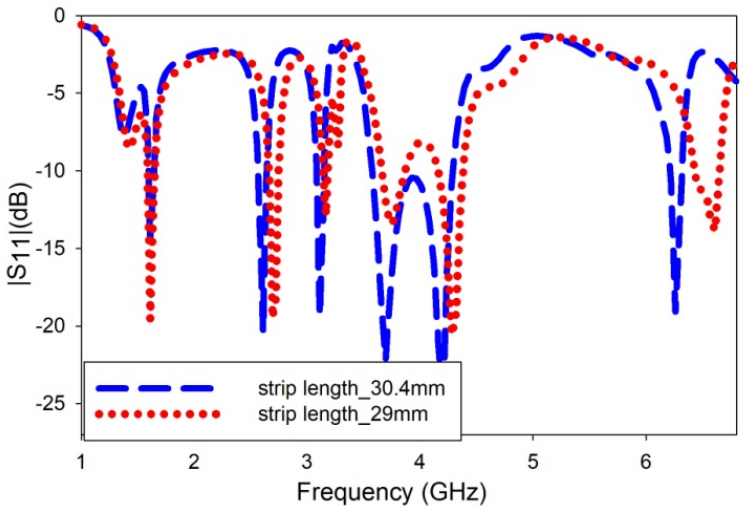

Figure 3.14: Simulated reflection coefficients of the proposed multiband antenna on varying length of copper strips.

curve obtained after loading the slot antenna with the five copper strips and the SRR can be understood by the study of Figure 3.12 and Figure 3.13. Also, upon altering

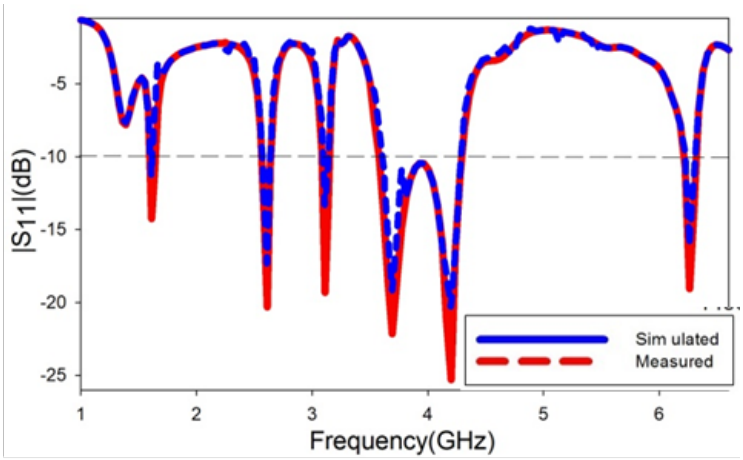

Figure 3.15: Measured and simulated reflection coefficients of the proposed penta-band antenna (5-strips).

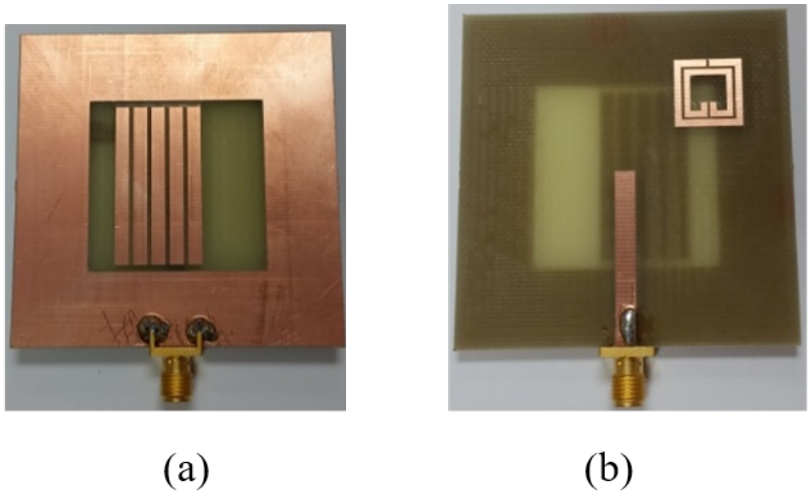

Figure 3.16: Fabricated prototypes of the proposed multiband antenna (a) Top view (b) Bottom view.

the dimensions of the copper strips, slight shift in the frequency bands is observed. Upon increasing the length of the copper strips, a slight shift in the bands towards lower frequencies is observed. When reducing the length of the strips, the bands are shifted towards higher bands. For all cases, the first band that is SRR controlled remains the same. This can be observed in Figure 3.14 which shows the simulated reflection coefficient characteristics for different strip length values. The proposed antenna was fabricated and tested using an LPKF S103 PCB milling machine and an Agilent N9918A VNA at the AMSD lab at KFUPM. The measured and simulated

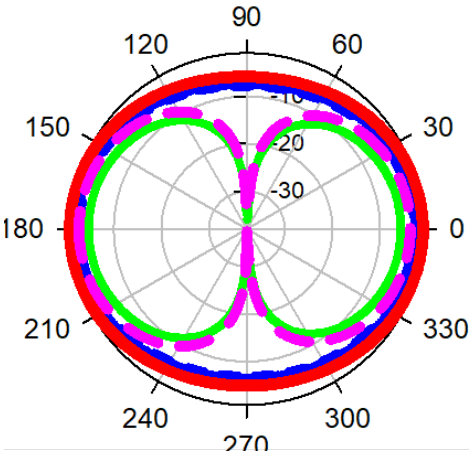
90
120
60
150
30
180
0
210
330
240
300
270
-20
-30

(a)

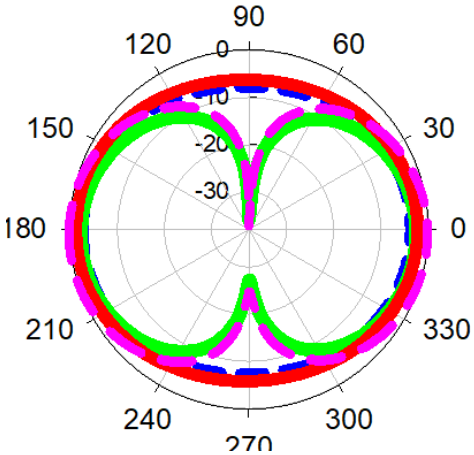
90
120
60
0
150
30
-20
-30
180
0
210
330
240
300
270

(b)

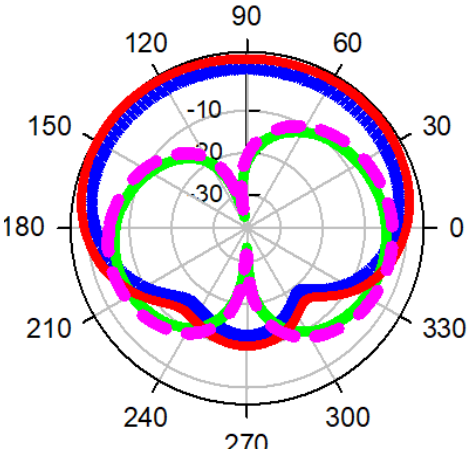
90
120
60
-10
150
30
-20
-30
180
0
210
330
240
300
270

(c)

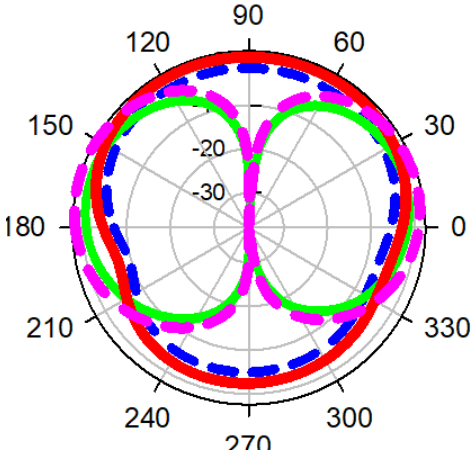
90
120
60
150
30
-20
-30
180
0
210
330
240
300
270

(d)

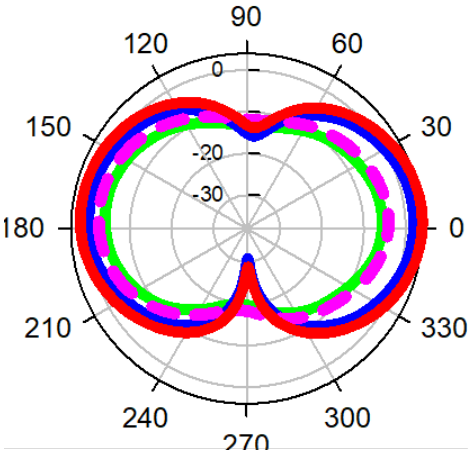
90
120
60
0
150
30
-20
-30
180
0
210
330
240
300
270

(e)

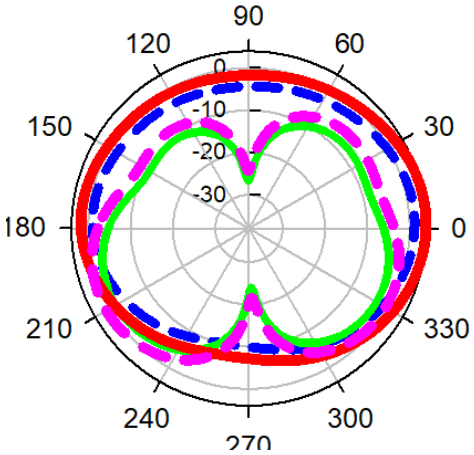
90
120
60
0
150
30
-10
-20
-30
180
0
210
330
240
300
270

(f)

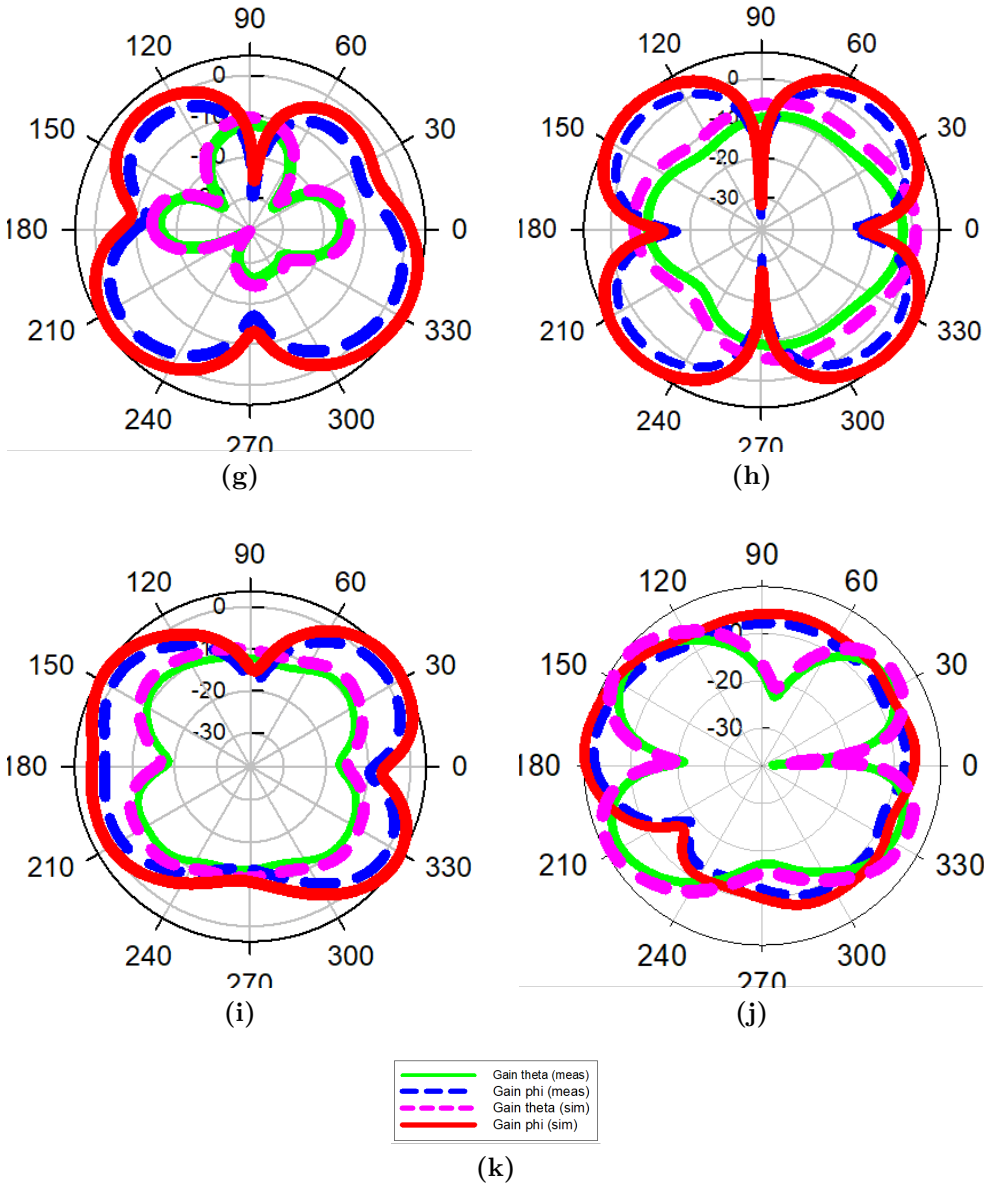

Figure 3.17: Simulated and measured radiation patterns of the proposed antenna at 1.51 GHz (a) phi=0 (b) phi=90 , 2.61 GHz (c) phi=0 (d) phi=90, 3.11 GHz (e) phi=0 (f) phi=90, 3.86 GHz (g) phi=0 (h) phi=90, 6.26 GHz (i) phi=0, (j) phi=90 and (k) legend

reflection coefficient magnitudes are shown in Figure 3.15,and the photographs of the fabricated prototypes are shown in Figure 3.16 . The simulation and measurement results are found to be in good agreement. The measured -10 dB bandwidths obtained are 210 MHz (1.35 GHz-1.56 GHz), 80 MHz (2.6 GHz-2.68 GHz), 70 MHz (3.07 GHz-3.14 GHz), 720 MHz (3.55 GHz-4.27 GHz), 108 MHz (6.102 GHz-6.21 GHz). The simulated radiation pattern plots at the resonance frequencies are shown in Figure 3.17. The efficiency and peak gain values obtained at the different resonant frequencies are 61%/2.5 dB, 64%/2.2 dB, 74%/2.7 dB, 80%/3.8 dB, 70%/2.4 dB.

3.4 Pentaband Strip Loaded Slot Antenna Design

In this work, a microstrip line fed pentaband square slot antenna is proposed which uses an array of copper strips whose periodicity and width are much smaller than the guide wavelength of the antenna. The various resonance bands are produced on excitation of the slot and the loaded copper strip array. The slot antenna is designed to radiate at 2.28 GHz. The slot is loaded with a uniform array of rectangular copper strips to produce the other resonances at 2.2 GHz, 3.4 GHz, 4.6 GHz, 5.4 GHz, 6.6 GHz. Impedance bandwidths of 500 MHz, 300 MHz, 600 MHz, 400 MHz, 600 MHz, a gain more than 3 dB and efficiency above 80% is obtained at all the frequency bands. The design offers a simple and compact geometry with more number of bands and wider impedance bandwidth values compared to previous works.

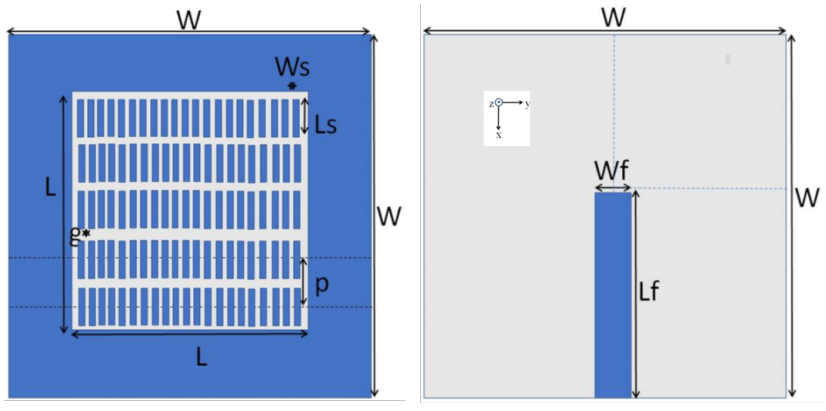

Figure 3.18: Antenna geometry (a) top view (b) bottom view. [L=33.2mm, W=50 mm, Wf=3.6mm, Lf=29.4mm, Ws=0.2mm, Ls=3mm, g=0.3mm, p=3.2mm].

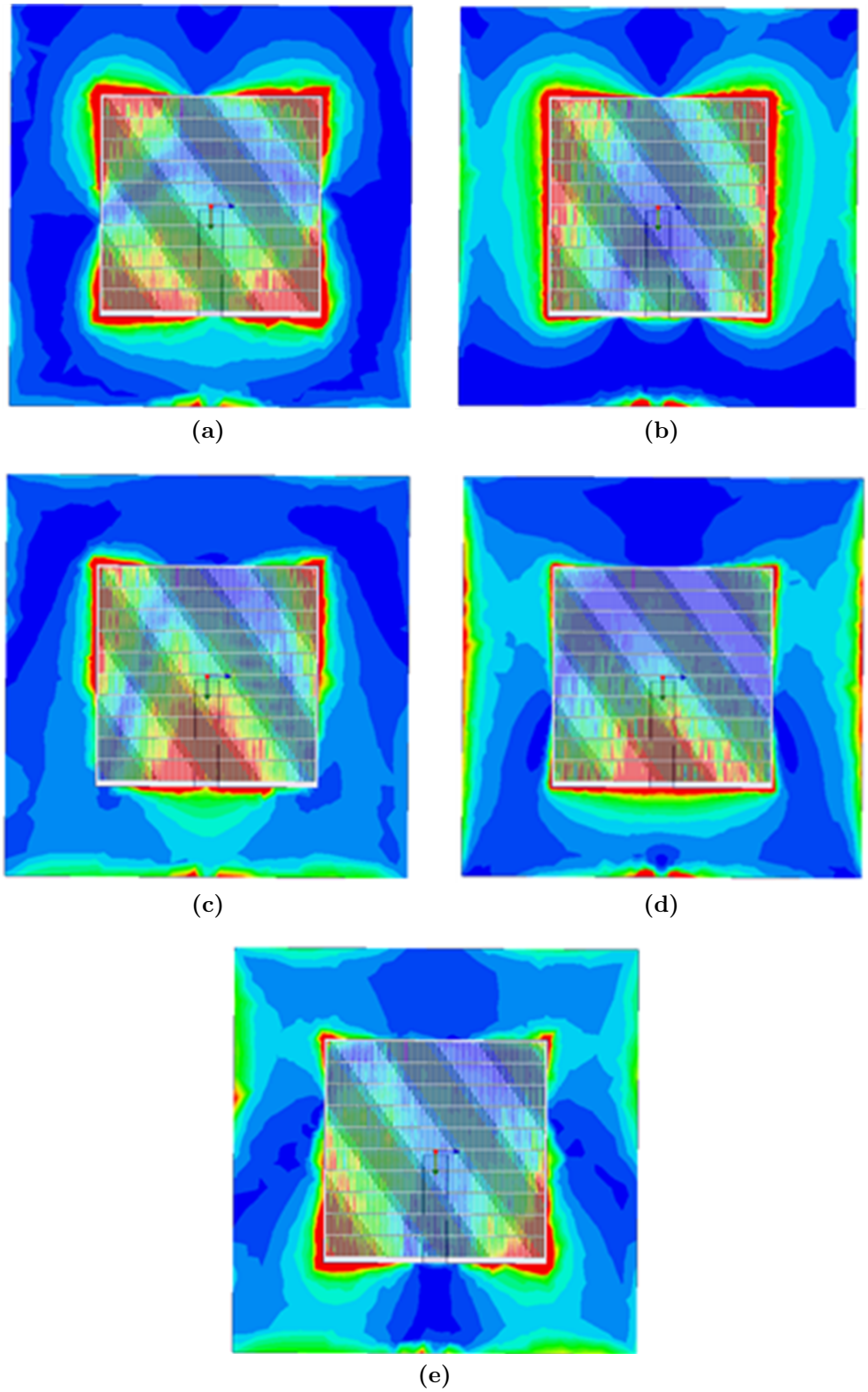

Figure 3.19: Simulated surface current distribution at (a) 2.2 GHz (b) 3.4 GHz (c) 4.6 GHz (d) 5.4 GHz (e) 6.6 GHz.

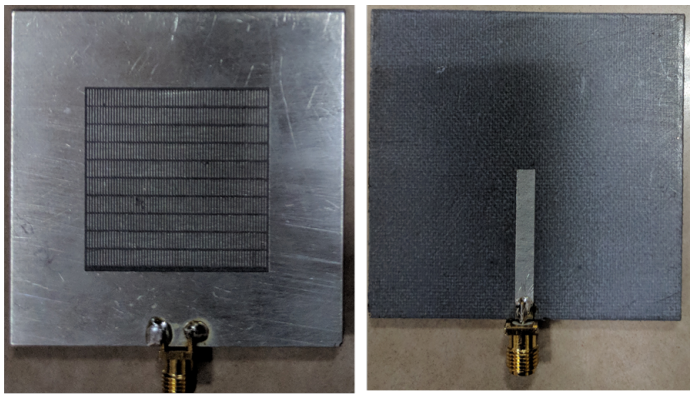

(a) (b)

Figure 3.20: Fabricated prototypes of the proposed multiband antenna (a) Top view (b) Bottom view.

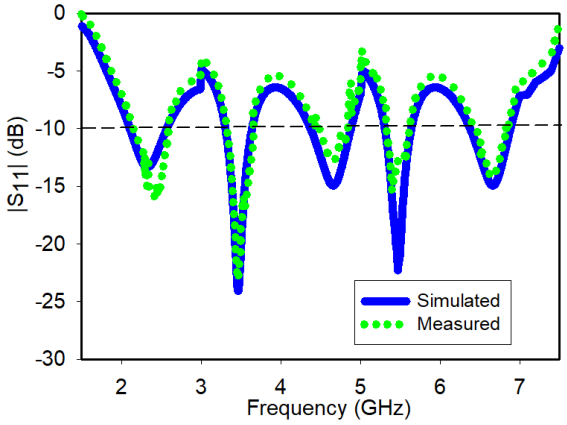

Figure 3.21: Measured and simulated reflection coefficients of the proposed antenna.

3.4.1 Antenna Design

The proposed antenna geometry is shown in Figure 3.18. The antenna is designed on a RT-Duroid 5880 substrate of permittivity 2.2, height 1.52 mm and loss tangent 0.02. On the top of the substrate, a square slot is etched out such that it operates at its fundamental resonant mode (TM_{01}). The resonant frequency (fr_1) of the square slot of dimension L is given by :

$$f_{r1} = \frac{c}{2L}\sqrt{\frac{2}{1+\epsilon_r}} \tag{3.2}$$

where, c is the speed of light and ϵ_r is the relative permittivity of the substrate.

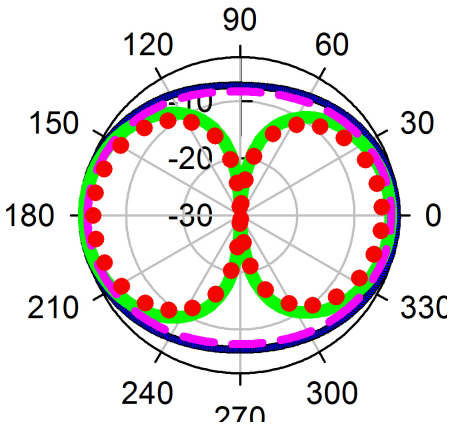
90
120
60
150
30
180
0
210
330
240
300
270
-20
-30

(a)

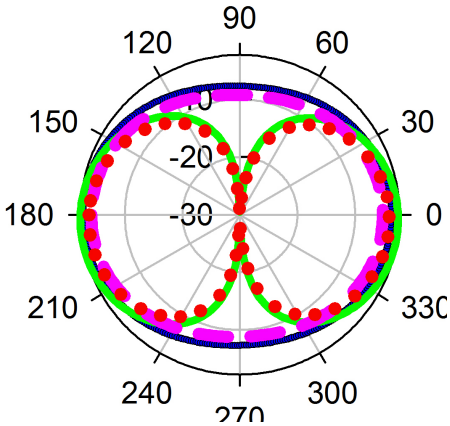
90
120
60
150
30
180
0
210
330
240
300
270
-20
-30

(b)

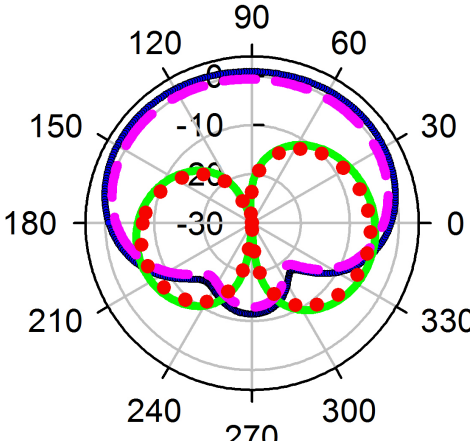
90
120
60
150
30
180
0
210
330
240
300
270
-10
-30

(c)

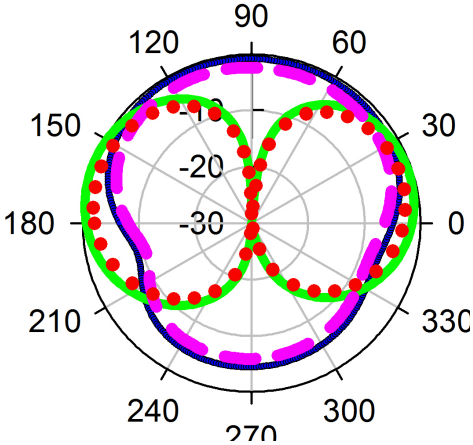
90
120
60
150
30
180
0
210
330
240
300
270
-20
-30

(d)

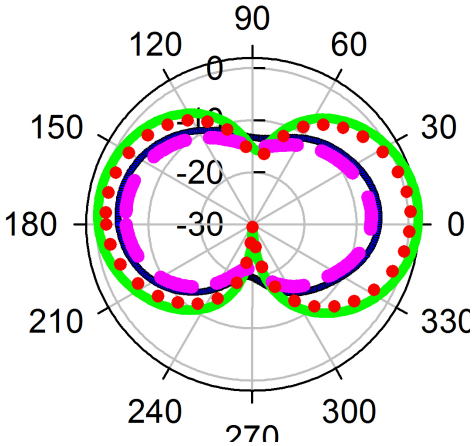
90
120
60
150
30
180
0
210
330
240
300
270
-20
-30

(e)

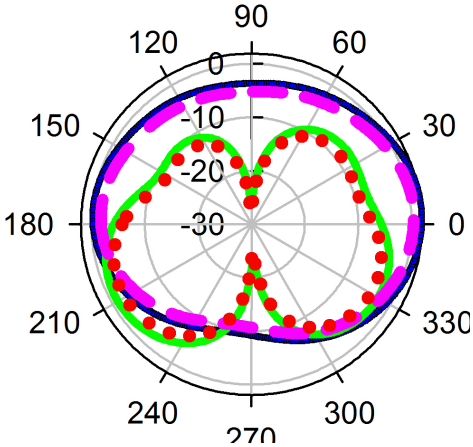
90
120
60
150
30
180
0
210
330
240
300
270
-10
-20
-30

(f)

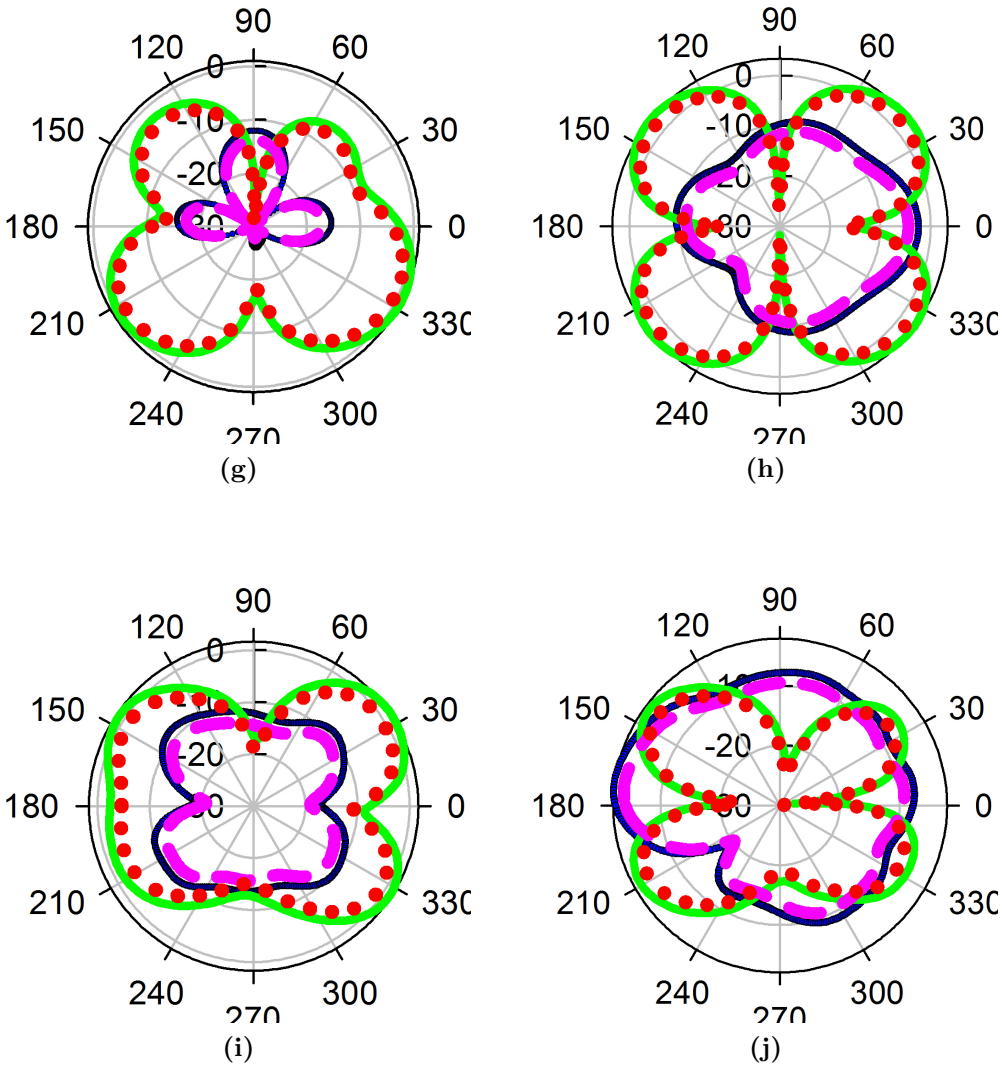

Figure 3.22: Simulated and measured radiation patterns of the proposed antenna at (a) 2.2 GHz (phi=0) (b) 2.2 GHz (phi=90) (c) 3.4 GHz (phi=0) (d) 3.4 GHz (phi=90) (e) 4.6 GHz (phi=0) (f) 4.6 GHz (phi=90) (g) 5.4 GHz (phi=0) (h) 5.4 GHz (phi=90) (i) 6.6 GHz (phi=0) (j) 6.6 GHz (phi=90).[——- -simulated co-pol, ——- - measured co-pol, —— - simulated cross-pol, ... - measured cross-pol]

Here the slot is designed to operate at 2.28 GHz and the slot is loaded with a uniform array of rectangular thin copper strips as shown in Figure 3.18 (a). A 50Ω microstrip line of width W_f is used to feed the slot as shown in Figure 3.18 (b). The loading of the copper strip array on the slot helps generate the remaining resonance frequencies without affecting the slot resonance. The uniform array of thin copper strips provide the negative permittivity effect when excited below their plasma frequency and hence helps to produce the additional resonances. The frequency at which the strip array resonates depends on the width of the strips and the side length of the cell lattice on which the strips are arranged. Therefore, depending on the number of copper strip rows that are excited, different lattice lengths are involved. Thus a series of different resonance frequencies are obtained giving a pentaband response in this case. The equations for the calculation of the plasma frequency is given in detail in Chapter 6.

3.4.2 Results and Analysis

The surface current distributions obtained on simulation of the proposed structure for the different resonance frequencies are give in Figure 3.19. It can be seen that at each frequency, different lengths of the strip array lattice are excited by the microstrip line fed slot to produce the different resonances. The proposed antenna was fabricated using an S103 LPKF machine and measured using an Agilent N9918A VNA at the AMSD lab at KFUPM. Photographs of the antenna prototype are shown in Figure 3.20. The measured and simulated reflection coefficient magnitudes of the copper strip array loaded slot antenna are shown in Figure 3.21. The measured and simulated results show good agreement. The measured -10dB bandwidths of operation of the antenna obtained at the five resonant frequencies are 500 MHz (2.1 GHz-2.6 GHz centred at 2.2 GHz), 300 MHz (3.3 GHz-3.6 GHz centred at 3.4 GHz), 600 MHz (4.3 GHz-4.9 GHz centred at 4.6 GHz), 400 MHz (5.2 GHz-5.6 GHz centred at 5.4 GHz) and 600 MHz (6.3 GHz-6.9 GHz centred at 6.6 GHz). The simulated and measured radiation patterns of the proposed antenna at the resonant frequencies for x-y and y-z planes are shown in Figure 3.22. The cross polarization gain values are observed to differ by at least -15 dB compared to co-polarization at the resonant frequencies. The simulated efficiency and peak gain values obtained at the different resonant frequencies are 90%/3 dB, 85%/3.2 dB, 87%/2.8 dB, 82%/3 dB, 88%/3.5 dB. The copper strip array loaded multiband slot antenna proposed here is seen to provide multiple bands of resonance with compact size, and good values of bandwidth, gain and efficiency

compared to earlier works. A comparison is provided in Table 3.1 which compares the performance parameters of different multiband slot antennas found in literature in terms of size, no of bands, -10 dB impedance bandwidth, peak gain and radiation efficiency values.

Table 3.1: Performance Comparison of Different Multiband Slot Based Antennas (λ_g-guided wavelength corresponding to the lowest resonant frequency.)

REF	SIZE	BANDS (GHz)	BW (Mhz)	GAIN (dBi)	EFF (%)
Gholamrezaei *et al.* (2014)	$0.205\lambda_g^2$	Five- 2.4, 4.3, 5.7, 6.9, 7.7	≈150	2.5-3.7	—
Cao *et al.* (2015)	$0.24\lambda_g^2$	Four- 1.58, 2.45, 3.5, 5.4	90, 145, 700, 760	3.5, 3.9, 5.02, 4.86	76.8, 80.1, 96.6, 85.5
Piao *et al.* (2017)	$0.193\ \lambda_g^2$	Four- 1.57, 2.4, 3.5, 5.5	50, 400, 390, 830	3, 3.1, 5, 4.2	70, 76, 80, 78
Kandasamy *et al.* (2016)	$2.1\lambda_g^2$	Two- 3.1, 4.7	400, 400	7.3,8.5	—
Proposed Paul *et al.* (2017)	$0.83\lambda_g^2$	Three- 2.6, 4.2, 4.6	580 , 120, 100	4.4, 3.9, 3.8	91, 67, 55.8
Proposed	$0.16\lambda_g^2$	Five- 1.41, 2.61, 3.11, 3.86, 6.26	55 , 80, 70, 720, 108	2.5, 2.2, 2.7, 3.8, 4, 2.4	62, 65, 75, 80, 70
Proposed	$0.2\lambda_g^2$	Five- 2.2, 3.4, 4.6, 5.4, 6.6	500, 300, 600, 400, 600	3, 3.2, 2.8, 3, 3.5	90, 85, 87, 82, 88

3.5 Summary

This chapter discusses the multiband SRR and strip loaded slot antennas.

- The first design is an SRR loaded tri-band square slot antenna that facilitates independent control of each of its resonant frequency bands is proposed. The frequency bands covered are 2.6, 4.2 and 4.7 GHz with measured bandwidths of 580, 120, 100 MHz in the three bands, respectively. The gain and efficiency were higher than 3.8 dBi and 58% in all bands. The negative permeability effects obtained from the SRR and micro split SRR are used to obtain the multiband operation

- The second design discusses a novel penta-band slot antenna designed to operate at 1.51 GHz, 2.61 GHz, 3.11 GHz, 3.86 GHz, 6.26 GHz. The antenna is loaded with a copper strip array and an SRR unit cell to obtain the necessary resonances. The frequencies can be altered on changing SRR and strip dimensions. The proposed compact SRR and strip loaded slot antenna offers 78% miniaturization at its lowest band of operation compared to the design proposed by Gholamrezaei *et al.* (2014). An impedance bandwidth of at least 80MHz, gain above 2.4 dB and efficiency greater than 60% is obtained at the frequency bands. Such a miniaturized design finds application in small multi-band antenna devices and terminals.

- In the third design, a pentaband square slot antenna is proposed using an array of copper strips whose periodicity and width are much smaller than the guide wavelength of the antenna. The loading of the slot with the array of thin copper strips yields to operation of the antenna at five resonant frequencies 2.2 GHz, 3.4 GHz, 4.6 GHz, 5.4 GHz, 6.6 GHz. The proposed antenna is found to have an impedance bandwidth above 300 MHz, peak gain more than 3 dB and efficiency of at least 80% at all the resonant frequencies. The design offers a simple and compact geometry of dimension 0.2 λ_g^2 with more number of bands and wider impedance bandwidth values compared to previous works (λ_g is the guide wavelength at the resonant frequency).

Chapter 4

WIDEBAND RECTANGULAR SLOT ANTENNA

4.1 Introduction

This chapter describes in brief the various wideband rectangular slot antenna designs proposed, the operating principle of the proposed designs, the simulation and measurement results obtained, and the conclusions drawn. The compact wideband slot antenna designed using an SRR loaded quarter wavelength slot to operate at dual bands is discussed in the first section. Bandwidth enhancement is achieved using active element integration on the narrow rectangular lot. The second section discusses an improvised version of the first design wherein a triband slot antenna is designed using a modified SRR and that exhibits wideband characteristics at its first resonant frequency band. Also, a comparison of these designs with the previous works is shown in a tabular form.

4.2 Compact Wideband Slot Antenna Using SRR

A compact dual-wideband slot antenna with independent tunability suitable for WLAN and WiMAX operation is proposed in this work. The slot antenna is microstrip line fed and loaded with an SRR to obtain dual-band operation. The wideband characteristic is obtained at the lower band by producing a fictitious short circuit at a certain point along the slot. The compactness is achieved by using an open slot antenna with quarter-wavelength. The slot is designed for a resonant frequency of 2.4 GHz.

This resonance merges with that produced due to the fictitious short circuit, hence providing a -10 dB wideband resonance of 2 GHz. Further, the impedance bandwidth is improved to 2.7 GHz by adding lumped capacitor across the slot. The second resonance is obtained at 5.9 GHz with a -10 dB bandwidth of 330 MHz that is SRR controlled. Independent control of each of the resonance frequencies is possible by changing either the slot or SRR dimensions. The proposed antenna is fabricated on an RT/ duroid 6002 substrate with a size of 50x25x1.52 mm^3.

4.2.1 Antenna Geometry

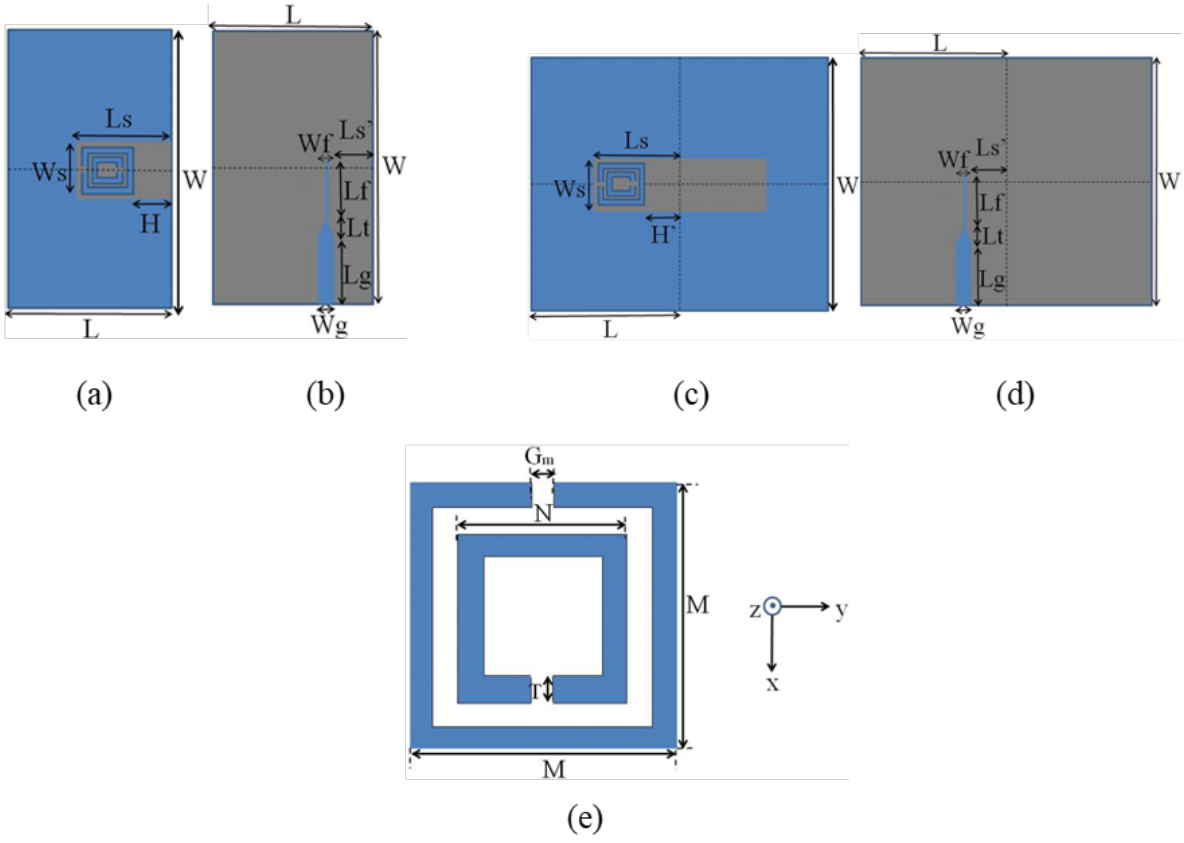

Figure 4.1: Antenna geometry: Open slot antenna (a) top view (b) bottom view, Half wavelength slot antenna (c) top view (d) bottom view, (e)SRR geometry. [L=30mm, W=60mm, Ls=18.5mm, Ws=6mm, H=12.05mm, H=11.05mm, Lf=11.35mm, Wf=0.8mm, Lg=18.75mm, Wg=3.91mm, Lt=2mm, Ls=12.9mm, M=5.2mm, N=3.2mm, T=0.6mm, Gm=0.6mm, h=1.52 mm].

The antenna is designed on a RT/duroid 6002 substrate of size 50mm x 25mm,

height 1.52 mm and permittivity 2.9. A narrow rectangular slot ($\lambda_g/4$) of length 18.5 mm and width 6 mm is etched out on the ground plane. The feed is printed at the bottom of the substrate and consists of a 110 Ω microstrip line of width 0.8 mm connected to a 50Ω line of width 3.91 mm via a tapered transition. A similar geometry is adopted for the half wavelength slot antenna design for comparison. Here, the slot is etched on a substrate of length 37 mm and width 6 mm. The top and bottom views of the antenna geometry are shown in Figure 4.1. The SRR dimensions are shown in Figure 4.1 (e) and is placed on the top of the substrate at one end of the slot and suitably positioned and oriented so as to be excited by the axial magnetic field and hence produce the required resonance.

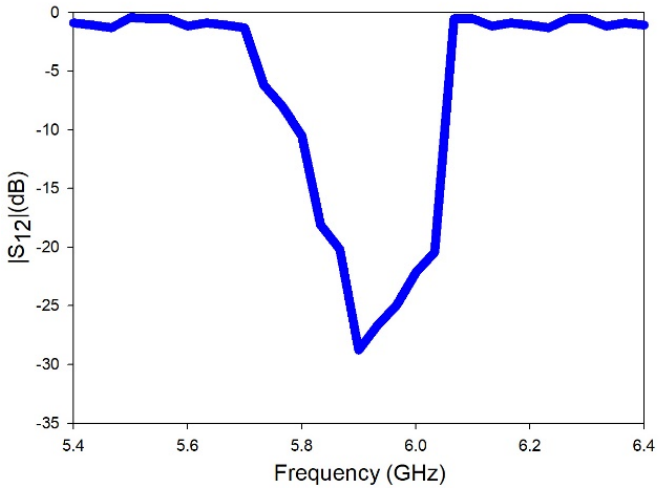

Figure 4.2: Simulated transmission coefficient magnitude of the SRR unit cell.

4.2.2 Operating Principle

At its first resonant frequency (2.4 GHz), the half-wavelength slot has an equivalent length of $\lambda_g/2$ (λ_g is the guided wavelength in the slot). In order to create a second resonance at a frequency close to the first resonance frequency, the dimensions of the microstrip feed line and its position along the slot ($L_s^{'}$) must be appropriately chosen so that the fictitious short circuit is created just above the slot resonance. This provides a wideband operation of the half-wavelength slot antenna (Behdad and Sarabandi (2005)) as seen in Figure 4.3 (a). The corresponding design is shown as an inset in the figure. The matching is largely determined by the length of the feed line portion

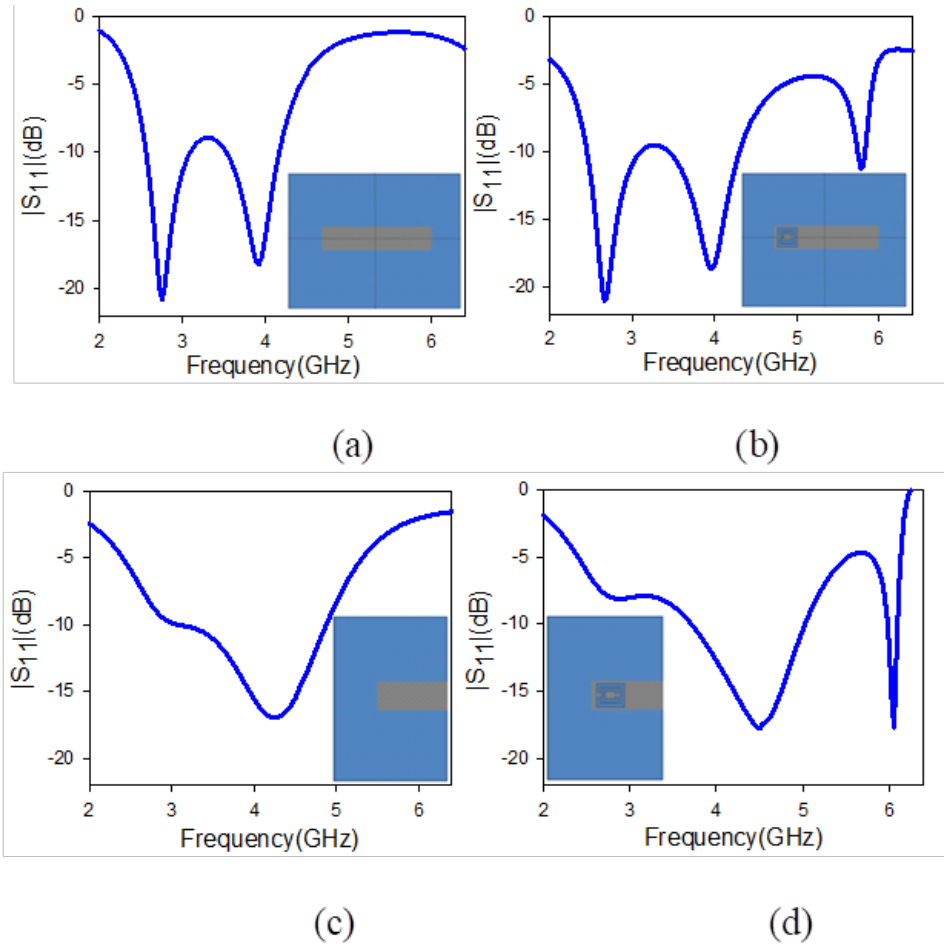

Figure 4.3: Simulated reflection coefficient magnitudes for the conventional (a) unloaded $\lambda_g/2$ slot (b) SRR loaded $\lambda_g/2$ slot (c) unloaded open $\lambda_g/4$ slot (d) SRR loaded $\lambda_g/4$ slot antenna.

above the slot, which is taken as 4.1 mm to obtain maximum resonance at the required frequency of operation. The second resonant frequency is obtained upon the excitation of the SRR which is tuned and designed to operate at 5.9 GHz. The calculation of the SRR frequency and its characterization follows the steps by Engheta and Ziolkowski (2006), Ishikawa *et al.* (2007). The simulated transmission characteristics of the SRR is shown in Figure 4.2 clearly showing its operating bandwidth around 5.9 GHz. The SRR is placed inside the slot to ensure maximum coupling of the magnetic field lines that pass perpendicular through the rings hence facilitating their excitation. Thus, a dual-band resonance with wideband characteristics is obtained using the SRR loaded half-wavelength slot antenna (Figure 4.3 (b)).

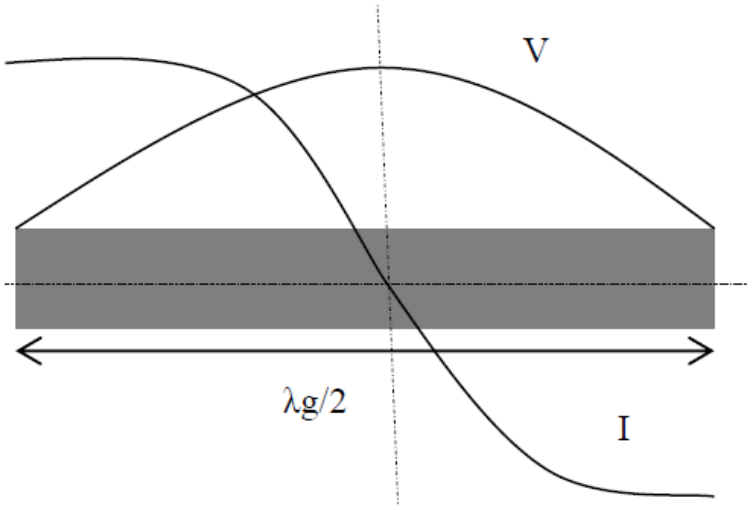

Figure 4.4: Variation of voltage and current along the half wavelength slot.

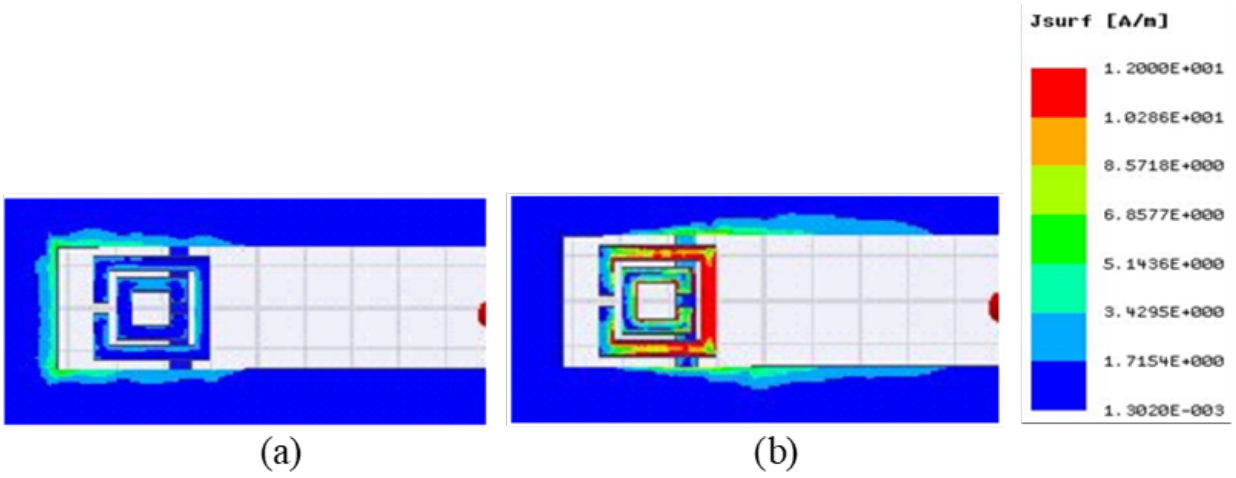

Figure 4.5: Surface current distribution of the proposed compact multiband open $\lambda_g/4$ slot antenna at (a) 2.4 GHz, (b) 5.9 GHz.

Compactness is achieved by using an open slot structure, with the length of $\lambda_g/4$. The length of the conventional $\lambda_g/2$ slot antenna structure is cut short by half and open circuited at one end to produce a voltage distribution along the slot that has a maximum value at the open end of the slot structure. The voltage and current distribution along a conventional slot antenna is shown in Figure 4.4. The voltage distribution along a conventional slot antenna follows a symmetrical pattern with respect to the centre of the slot and hence, a $\lambda_g/4$ slot would give rise to a similar field distribution and thus ensure that the resonant characteristics of the antenna remain

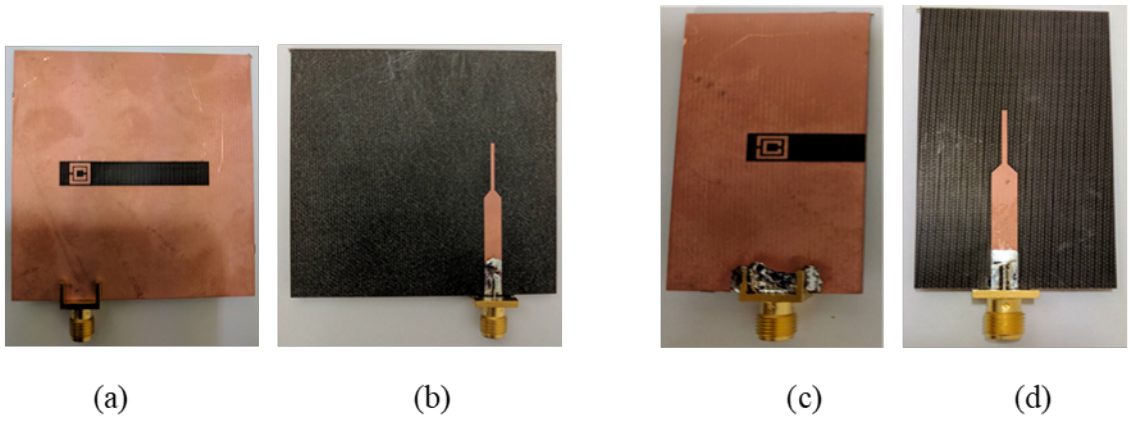

Figure 4.6: Photograph of the proposed multiband slot antenna prototypes- Half wavelength slot antenna (a) top view (b) bottom view, Compact open slot antenna (c) top view (d) bottom view

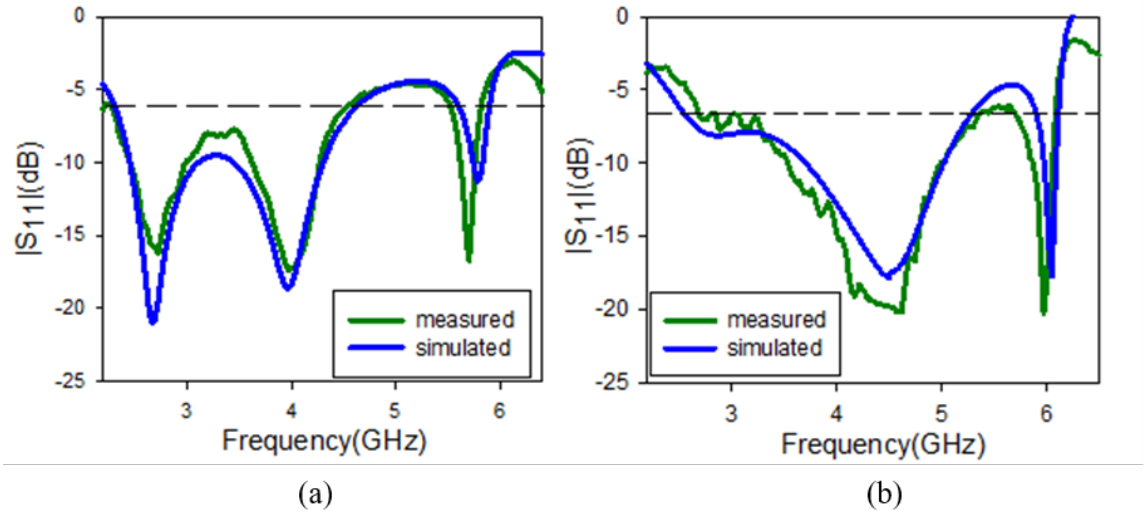

Figure 4.7: Measured and simulated reflection coefficient magnitudes of the proposed multiband antennas (a) half wavelength slot antenna (b) compact open slot antenna.

largely unaffected. This can be observed from Figure 4.3 (c) and Figure 4.3 (d) which show the simulated reflection coefficient magnitudes for the open slot antenna design (both unloaded and SRR loaded cases, respectively). In order to improve the -10 dB bandwidth of the compact open slot antenna, the capacitor is connected across the slot which in turn lowers the first resonant frequency of the slot. This helps to obtain a wide -10 dB resonance at 2.4 GHz. Thus, Figure 4.3 shows the evolution of the compact multiband antenna design from a conventional half wavelength slot antenna.

The study of the resonance characteristics for the half-wavelength and quarter-

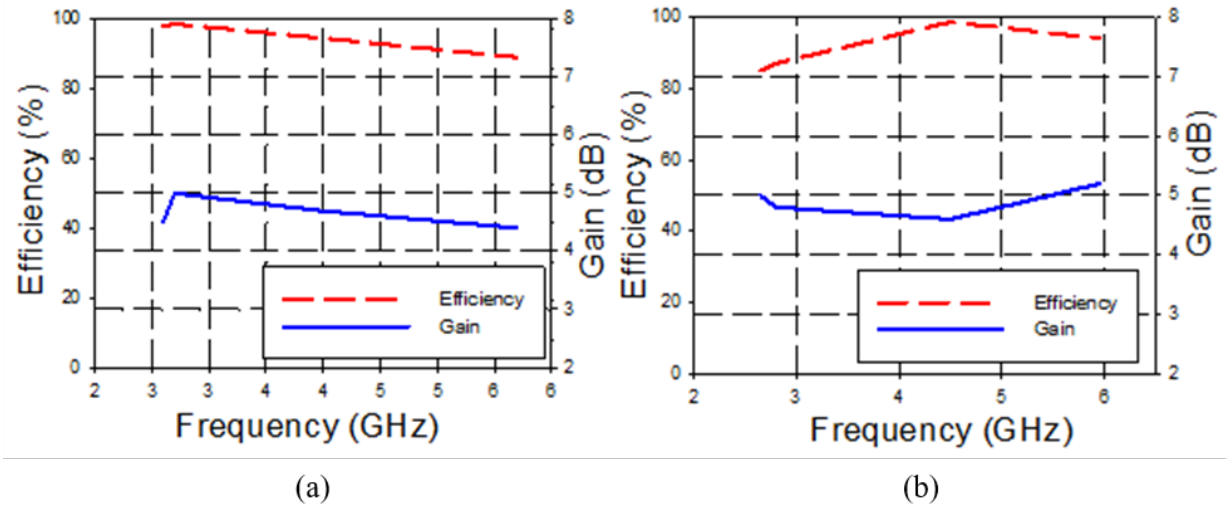

Figure 4.8: Measured maximum gain and efficiency of the proposed antennas (a) half wavelength slot antenna (b) compact open slot antenna.

wavelength slot antenna designs shows that the field distribution of the slot antenna makes it possible to have a compact structure with wideband characteristics. The surface current distribution as seen in Figure 4.5 clearly shows the contribution of the slot and SRR towards the independent operation of the dual bands of resonance. At the quarter wavelength resonance of 2.4 GHz, the surface current is at its maximum value around the slot (Figure 4.5(a)), while at the SRR resonant frequency of 5.9 GHz, the surface current distribution is around the SRR (Figure 4.5 (b)). Thus, the excitation of the slot and SRR provide us with two separate bands of resonance which can be independently controlled by changing the slot and the SRR dimensions.

4.2.3 Results and Analysis

Photographs of the prototyped antenna are shown in Figure 4.6. The measured and simulated results were plotted and compared in Figure 4.7 which show the reflection coefficient magnitudes. The measured -6 dB bandwidth obtained for the compact open slot design at the two bands of operation were 3.1GHz (2.4GHz 5.5GHz centered at 4.5GHz) and 450MHz (5.66GHz 6.11GHz centered at 5.96GHz), while the half wavelength slot antenna design provides a measured -6dB bandwidth of 2.28GHz (2.28GHz-4.56GHz) and 350MHz (5.48GHz-5.83GHz). The measured -10dB bandwidths on the other hand were 2GHz (3.2GHz 5.2 GHz) and 330MHz (5.72GHz

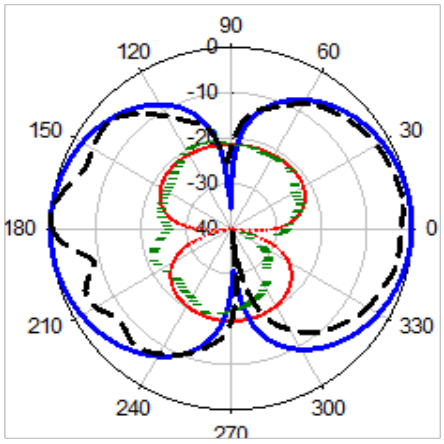
90
120
60
150
30
180
0
210
330
240
300
270
-10
-20
-30
-40

(a)

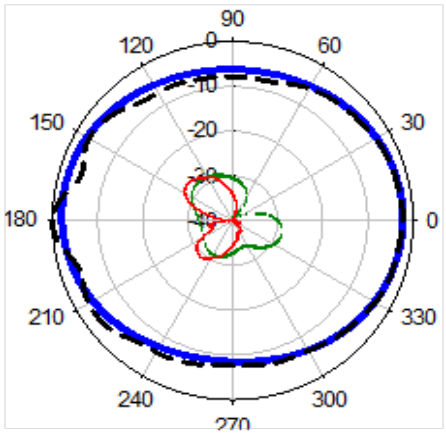
90
120
60
150
30
180
0
210
330
240
300
270
-10
-20
-30
-40

(b)

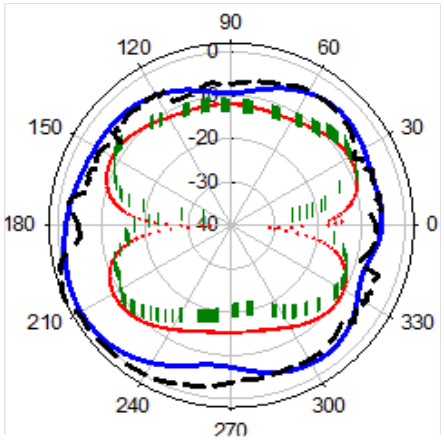
90
120
60
150
30
180
0
210
330
240
300
270
-10
-20
-30
-40

(c)

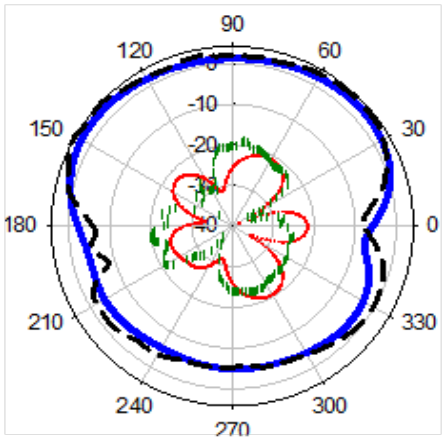
90
120
60
150
30
180
0
210
330
240
300
270
-10
-20
-30
-40

(d)

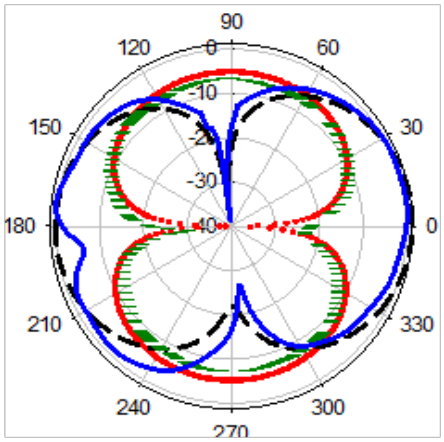
90
120
60
150
30
180
0
210
330
240
300
270
-10
-20
-30
-40

(e)

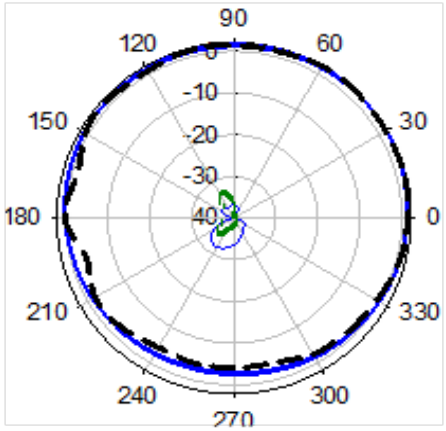
90
120
60
150
30
180
0
210
330
240
300
270
-10
-20
-30
-40

(f)

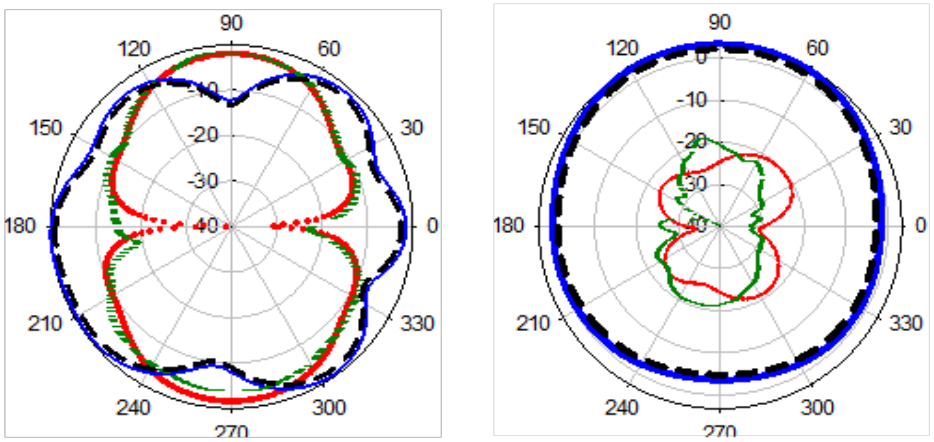

(g) (h)

(i)

Figure 4.9: Simulated and measured radiation pattern plots of the proposed antennas for x-z and y-z planes: $\lambda_g/2$ slot at 2.7GHz (a)phi=0 (b)phi=90, 5.69GHz (c)phi=0 (d)phi=90, $\lambda_g/4$ slot at 2.8GHz (e)phi=0 (f)phi=90, 5.96GHz (g)phi=0 (h)phi=90 (——measured co-pol, —simulated co-pol, ——measured cross-pol, +++simulated cross-pol) (i) Radiation Pattern measurement setups in a Satimo near-field chamber for$\lambda_g/2$ slot and $\lambda_g/4$ slot.

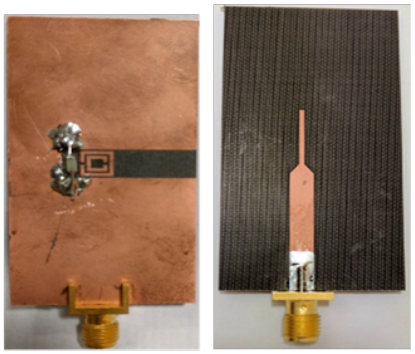

Figure 4.10: Capacitor loaded open slot antenna (a) Top view (b) Bottom view.

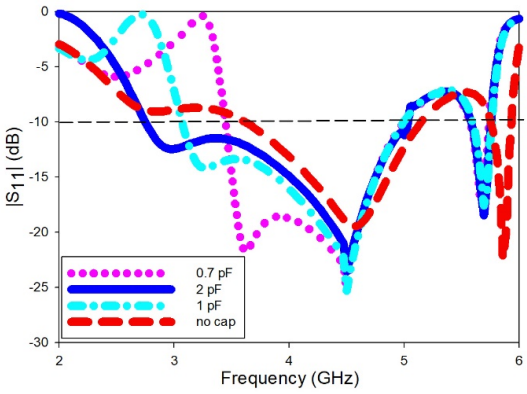

Figure 4.11: Simulated reflection coefficient magnitudes for capacitor and SRR loaded open slot antenna with different values of capacitances.

6.05 GHz) for the open slot design , and 1.98GHz (2.38GHz 4.36GHz) and 260MHz (5.52GHz 5.78GHz) for the half wavelength slot antenna design.

The gain and efficiency values of the proposed antenna were measured at the two resonance bands and plotted versus frequency as shown in Figure 4.8. The measured peak gain and efficiency values obtained for the open slot design at the resonance frequencies were 98.6% / 4.2 dB, 96% / 4.8 dB, respectively. For the full slot they were 96.6% / 4.4 dB, 89% / 4 dB. The simulated and measured radiation patterns of the proposed antennas at the resonance frequencies (for x-z, y-z planes) were plotted and compared as shown in Figure 4.9. The plots obtained in the x-z plane show an omni-directional pattern. The photographs of the radiation pattern measurement set-up can be seen as inset in Figure 4.9. Compactness, easy tunability of the resonance

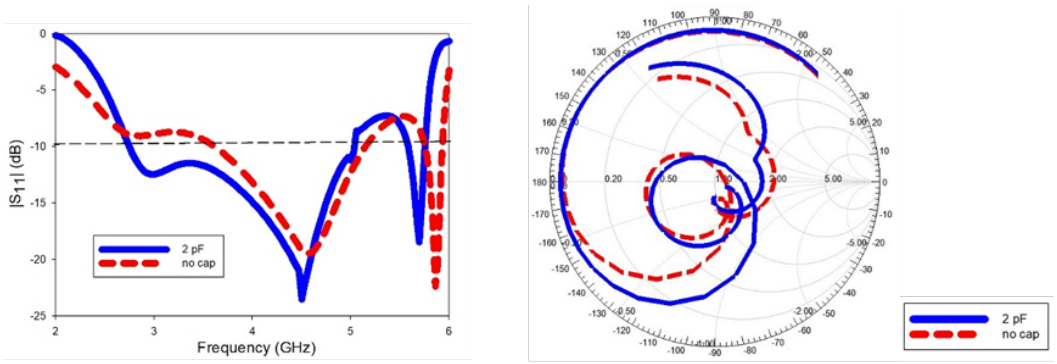

(a) (b)

Figure 4.12: (a) Reflection coefficient magnitudes and (b) Smith charts for open slot antenna loaded with SRR and 2 pF capacitor.

bands, wide bandwidth and high efficiency are the features of our proposed design as compared to other works in literature. Our proposed design is the first to adopt SRR loading of an open slot.

4.2.4 Bandwidth Enhanced Slot Antenna

The open slot antenna design is modified to enhance its -10 dB bandwidth by 35%. The slot is loaded with a capacitor at one end as shown in Figure 4.10. A lumped capacitor of 2 pF is connected across the slot at a distance of 0.2 mm from the closed end of the quarter wavelength slot.

The additional capacitance effect introduced across the slot helps to shift its resonant frequency to lower values, which in turn improves the operating bandwidth of the first resonant band. This can be seen from Figure 4.11, which shows the shift in resonance frequency on loading the slot with different capacitance values. Figure 4.12 (a) compares the reflection coefficient magnitude values for the open slot antenna with and without a 2 pF capacitor at one end. The simulated -10 dB bandwidth values obtained after loading the open slot antenna with a 2 pF capacitor are 2.7 GHz (2.5 GHz- 5.2 GHz) centred at 3.8 GHz and 380 MHz (5.6 GHz-5.98 GHz) centred at 5.8 GHz. The smith charts obtained on simulation of the open slot antenna for both cases (with and without capacitor load) are plotted and compared in Figure 4.12 (b). It can be observed that, when the open slot is loaded with capacitor, more number of frequency points of the lower band lie within the VSWR=2 circle as compared to

that in the open slot antenna without capacitor load. This explains the increase in bandwidth of the antenna on loading it with a 2pF capacitor. The introduction of capacitor helps reduce the inductive effect on the antenna characteristics due to the presence of the feed line and SRR, and hence shifts the frequency points such that a wider -10 dB bandwidth is obtained.

4.3 Triband SRR Loaded Compact Wideband Slot Antenna

In this section, a compact tri-band SRR loaded slot antenna is discussed which offers independent frequency tunability for operation at WLAN and WiMAX bands. The microstrip fed slot antenna is loaded with a modified SRR to obtain the triband resonance. The compactness is achieved by using an open slot antenna. The slot is designed to resonate at 2.4 GHz, which combines with the resonance obtained due to a fictitious short circuit produced at a certain point along the slot. This leads to the wideband property at the first band. The second and third resonances are obtained at 7.5 GHz and 9.3 GHz due to the excitation of the outer and inner rings of the modified SRR. A compact structure of area 0.2 λ_g^2 is obtained, where λ_g refers to the guide wavelength corresponding to the lowest resonant frequency. The resonances can be independently controlled by changing the slot and SRR dimensions. The first resonance can be controlled on changing the dimension of the slot. The second and third resonances depend on the dimensions of the modified SRR.

4.3.1 Antenna Design

The proposed antenna geometry is given in Figure 4.13. The multiband open slot antenna is designed on an FR-4 substrate of height 1.56 mm, permittivity 3.6 and loss tangent 0.02. An open rectangular slot is etched out on top of the substrate as shown in Figure 4.13 (a). The bottom of the substrate consists of the 50 Ω micro-strip feed line as shown in Figure 4.13 (b). The feed line is designed and positioned optimally along the slot to create the necessary fictitious short circuit resonance close to the first resonance frequency of the slot. The combination of the two resonances gives rise to the wideband property of the antenna. A modified SRR is suitably loaded on the slot as shown in Figure 4.13 (c) to be excited by the axial magnetic field

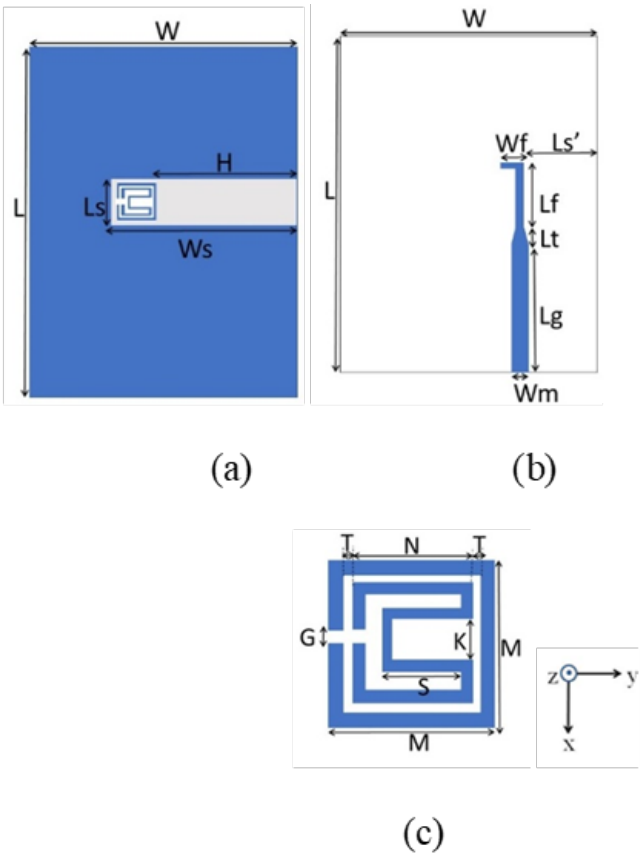

Figure 4.13: Antenna geometry (a)top view (b)bottom view (c)SRR geometry. [W=33.2, L=60,Ws=18.5, Ls=6, H= 14.5, Wf=3.6,Lf=3.1, Lt=2, Lg=18.75, Wm=3.91, Ls=13.7, M=6, N=4,T=0.6,G=0.5, K=0.6, S=1.56](All in mm)

lines. The excitation of the modified SRR creates the higher two resonances without affecting the slot resonance. The outer and inner rings of the SRR are responsible for producing the additional capacitive and inductive effects, which give rise to the second and third resonance frequencies respectively. These bands can be tuned depending on the dimensions of the modified SRR. The first resonance frequency and impedance bandwidth depend on the slot and feed dimensions and the feed position along the slot length. The antenna is modeled and simulated using ANSYS HFSS.

4.3.2 Results

The proposed multiband antenna was fabricated and tested using an LPKF S103 PCB milling machine and an Agilent N9918A VNA at the AMSD Lab at KFUPM. The

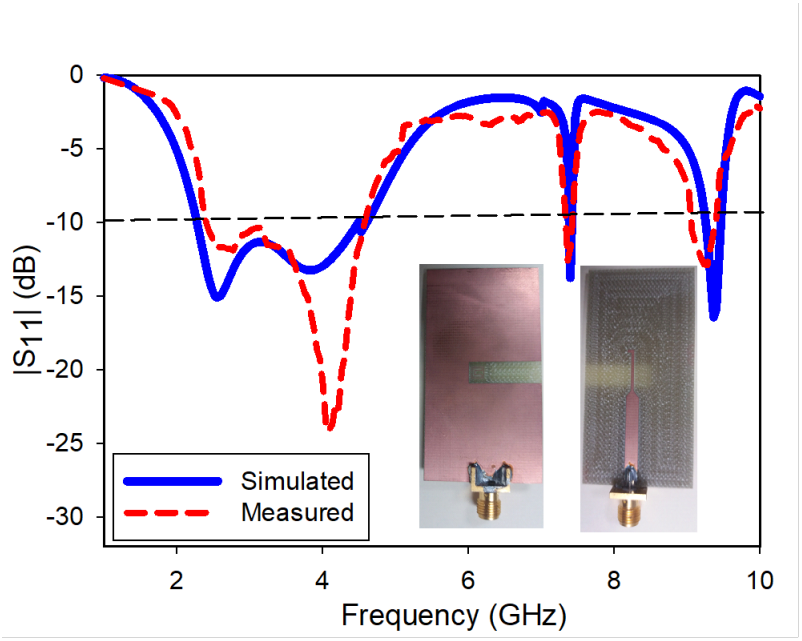

Figure 4.14: Simulated and measured reflection coefficients of the proposed multiband antenna (Fabricated prototypes shown in inset)

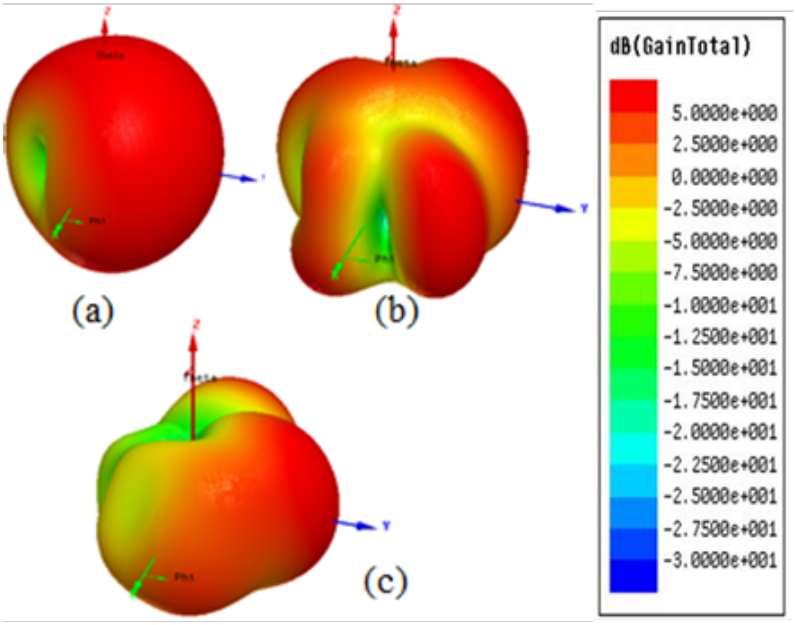

Figure 4.15: Simulated radiation patterns of the proposed antenna at (a) 2.4GHz (b) 7.5GHz (c) 9.3 GHz.

measured and simulated reflection coefficient magnitude curves of the antenna are plotted and shown in Figure 4.14. The -10dB measured bandwidths of the antenna are 2.4 GHz (2.23 GHz-4.63 GHz centered at 2.5 GHz), 50 MHz (7.38 GHz-7.88 GHz centered at 7.5 GHz) and 210 MHz (9.25 GHz-9.46 GHz centered at 9.3 GHz).

The measured and simulated curves are seen to be in good agreement. The fabricated prototypes are shown as inset in Figure 4.14. Figure 4.15 shows the simulated radiation patterns of the proposed antenna at the three resonance frequencies. The peak gain and efficiency values obtained are 2.8 dB/97.5%, 3.5 dB/ 86.8% and 3 dB/88.8%. The cross-polarization gain values are found to be less than -15 dB at all the three resonant frequencies.

Table 4.1: Performance Comparison of Different Multiband Slot Based Antennas with Wideband Characteristics (λ_g- guided wavelength corresponding to the lowest resonant frequency.)

REF	SIZE	BANDS (GHz)	BW (%)	NO. OF MTM UNITS	GAIN (dBi)	EFF. (%)	EASY TUNBLTY
Dang *et al.* (2010)	$0.28\lambda_g^2$	2.4, 5.2	25, 20	–	≈3-4	75, 80	NO
Hu *et al.* (2011)	$0.27\lambda_g^2$	2.5, 3.5, 5.6	21.6, 27, 17	–	3.8, 3.2, 5	–	NO
Sarkar *et al.* (2014)	$0.26\ \lambda_g^2$	1.65, 1.93, 2.2	4.2, 3.1, 12.7	1	1.1, 1.8, 2.9	–	NO
Kandasamy *et al.* (n.d.)	$2.2\ \lambda_g^2$	3.1, 4.7	13, 8.5	1	7.3, 8.5	–	YES
Proposed	$0.23\ \lambda_g^2$	2.4, 6.03	72.6, 6.5	1	4.2, 4.8	98.6, 96.8	YES
Proposed	$0.23\ \lambda_g^2$	2.4, 7.5, 9.3	96, 6.7 2.3	1	2.8, 3.5, 3	97.5, 86.8 88.8	YES

4.4 Summary

In this chapter, two wide band slot loaded antennas are presented:

- The first is a compact dual band slot antenna with an SRR loaded substrate that facilitates independent tuning of the resonance bands. A half wave and quarter wave versions of the design were prototyped, and good matching between the modeled and fabricated prototypes was obtained. Wideband characteristic is observed at the lower band. The proposed antenna operates at two bands with -10dB bandwidth of 2 GHz (3.2 GHz-5.2GHz) and 330 MHz (5.72GHz-6.05GHz), respectively, which makes it suitable for WLAN/WiMAX applications. Also, the -10 dB bandwidth of the first band is improved to 2.7 GHz on introducing capacitor across the slot. The gain and efficiency were higher than 4.3 dBi and 95% in all bands.

- The second design is a compact triband slot antenna with wideband characteristics at the first band. The antenna is designed to operate at the WLAN/WiMAX frequency range. The antenna is loaded with a modified SRR to obtain the triband operation. The resonant frequencies can be independently controlled by changing the dimensions of the slot and SRR. The quarter wavelength slot helps to achieve compactness in the proposed design compared to other existing multiband slot antennas. A minimum peak gain value of 2.5 dB and efficiency of 8% is obtained at all the three resonant frequencies.

Chapter 5

DISPERSION ENGINEERED TRANSMISSION LINES LOADED UWB SLOT ANTENNA

5.1 Introduction

In this section, an UWB wide square slot antenna design is presented where the concept of artificial transmission line is used to design and fabricate a dispersion engineered transmission line loaded square slot antenna. Periodically perturbed artificial transmission lines (TLs) are loaded on the microstrip line fed square slot antenna for ultra-wideband operation without modifying the square slot structure. The slot is designed to resonate at 2.4 GHz. The square slot is microstrip line fed and loaded with rows of transmission lines to achieve the ultra-wideband response from 2.1 GHz to 11.5 GHz. The transmission lines are dispersion engineered to resonate at desired frequencies so as to provide the wide band response. Loading of the engineered transmission lines on the square slot produce multiple resonances without affecting the fundamental mode of the slot antenna. Proposed antenna design is analyzed using transmission line dispersion relations and equivalent circuits. The proposed antenna is fabricated on a RT/Duroid 5880 substrate with a size of 50 x 50 x 1.52 mm^3. The antenna performance parameters including the impedance bandwidth, gain and efficiency values are experimentally verified. Good agreement is obtained between simulated and measured results.

5.2 Antenna Design

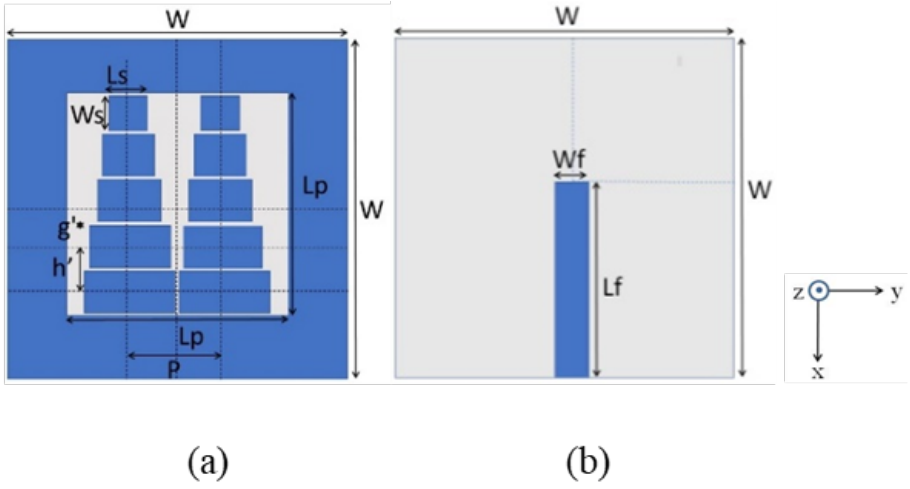

Figure 5.1: Antenna geometry (a) top view (b) bottom view. [Lp=44.2, W=50, Ws=4.5, Ls=6.5, g=0.2, p=14.7, Wf=4.4, Lf=24.6, h= 4.7] All in mm.

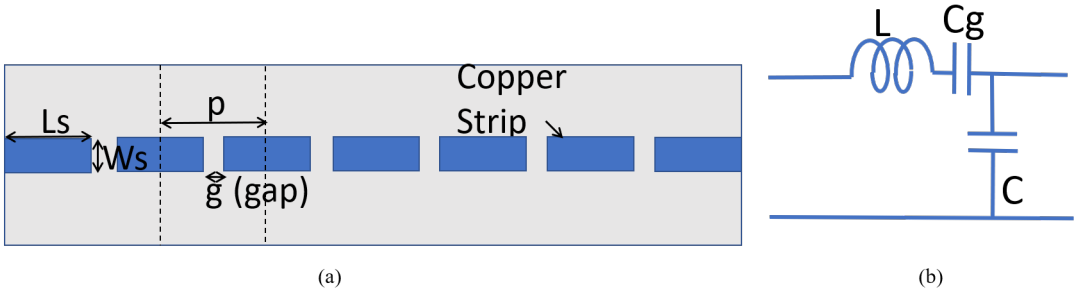

Figure 5.2: Transmission line with periodic gaps g (a) Structure (b) equivalent circuit.

The proposed UWB antenna geometry is shown in Figure 5.1. The antenna is designed using an RT/Duroid 5880 substrate of size 50X50 mm^2, permittivity (ϵ_r)= 2.2, height (h)= 1.52 mm and loss tangent=0.0009. The top view of the antenna is shown in Figure 5.1(a). A square slot of side length (L) 44.2 mm is etched out on top of the substrate so that the slot resonates at 2.6 GHz. Five rows of TLs with periodic gaps and whose lengths linearly reduce by 2 mm are loaded on the top of the substrate as shown in Figure 5.1(a). Each row of the TLs consists of metallic patches with uniform period p. This helps to achieve different resonant modes at the operating frequency range of the antenna. The bottom view of the antenna is shown

in Figure 5.1(b). A 50 Ω microstrip feed line is printed at the bottom of the substrate to excite the slot and TLs simultaneously.

5.3 Operating Principle

The 50Ω microstrip feed line excites the slot to resonate at its fundamental resonant mode. The resonance frequency is determined from Balanis (1992), as:

$$f_{r1} = \frac{c}{2L_p}\sqrt{\frac{2}{1+\epsilon_r}} \tag{5.1}$$

where L_p is the length of the slot and ϵ_r is the relative permittivity of the substrate.

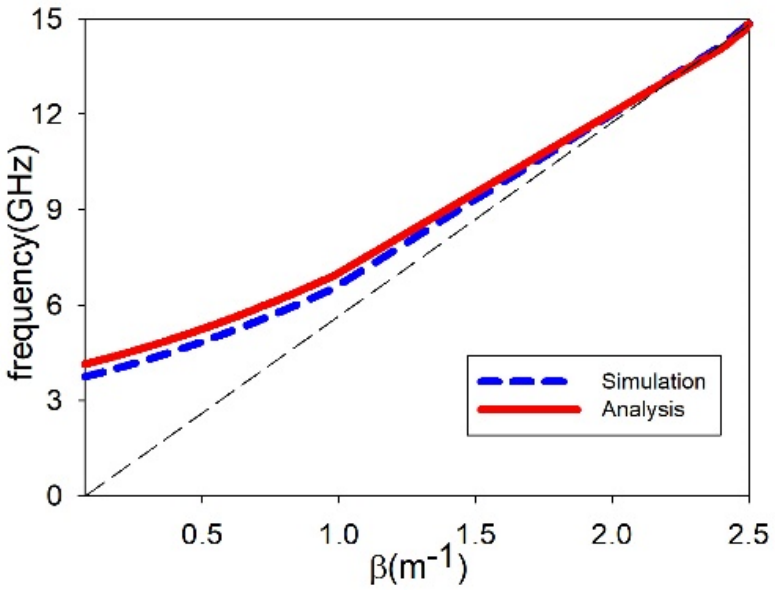

Figure 5.3: Dispersion curve (f vs β) for the lossless microstrip line with periodic gaps (fc=3.8 GHz).

TLs with periodic gaps loaded on the slot provide other resonances for the UWB operation of the antenna. Multi resonance behaviour of the proposed antenna is analysed using a microstrip TL with a set of periodic gaps in between as shown in Figure 5.2 (a) and its equivalent circuit is shown in Figure 5.2 (b). The gaps are placed with a periodicity p which is much smaller than the operating guided wavelength. The gaps are characterized by a capacitance (C_g) and the line is defined by the characteristic

impedance Z_0, the wave number k_z, the per unit length capacitance C and the per unit length inductance L. Then, as mentioned in Chapter 2, the propagation constant for a wave of frequency ω along the line is given by Balanis (1992)

$$\gamma = \alpha + j\beta = j\omega\sqrt{LC}\sqrt{1 - \frac{\omega_c^2}{\omega^2}} \tag{5.2}$$

When $\omega > \omega_c$ and $\alpha = 0$, then

$$\beta = \omega\sqrt{LC}\sqrt{1 - \frac{\omega_c^2}{\omega^2}} \tag{5.3}$$

Also

$$\omega_c = \frac{1}{\sqrt{C_g p L}} \tag{5.4}$$

where

$$L = \frac{k_z Z_0}{\omega} \ , \ C = \frac{k_z}{\omega Z_0} \tag{5.5}$$

The capacitance due to the gaps C_g depends on the width W_s of the microstrip line unit cells and the gap widths and is given by Kandasamy *et al.* (2015) as:

$$C_g = \frac{\epsilon_0(1+\epsilon_r)W_s}{\pi} \ln\left(\csc\frac{\pi g}{2W_s}\right) \tag{5.6}$$

The dispersion diagram for a microstrip line loaded with gaps with similar dimensions as the bottom most row of Figure 5.1(a) is plotted in Figure 5.3. It can be observed that above the cut-off frequency f_c, the wave propagates with propagation constant tending to approximately $\beta = \omega\sqrt{LC}$. From f_c and above, the dispersion curve is to the left of the dashed straight line. This portion of the bandwidth is responsible for radiation.

The equivalent circuit model for a TL loaded slot antenna is given in Figure 5.4. The equivalent circuit of the unloaded slot antenna is shown in Figure 5.4 (a) (Kandasamy *et al.* (n.d.)). The inductance of the lossless feed line and the equivalent inductance/capacitance of the slot are given by L_{se} and L_{sh}/C_{sh} , respectively. The loading of the TLs on the slot introduces the effect of mutual coupling given by M as seen in Figure 5.4 (b) which shows the equivalent circuit of the loaded slot antenna. Figure 5.4 (c) shows the simplified equivalent circuit where

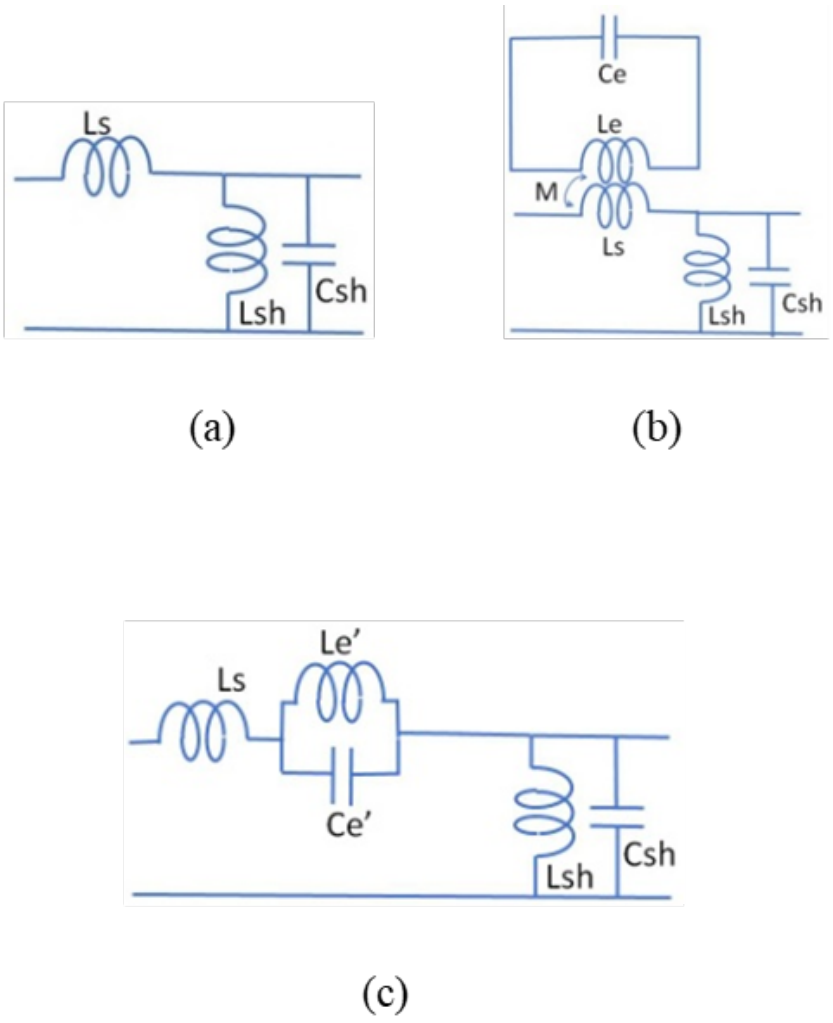

Figure 5.4: Equivalent circuits of (a) slot antenna (b) transmission line loaded slot antenna, and (c) simplified total equivalent circuit.

$$C_e^{'} = \frac{L_e}{\omega_e^2 M^2} \ , \ L_e^{'} = \omega_e^2 M^2 C_e \ , \ \omega_e^2 = \frac{1}{L_e C_e} \tag{5.7}$$

Le and Ce are the simplified equivalent inductance and capacitance of the TL. The equivalent model is verified for the proposed antenna loaded with one row of a TL (bottom row) using EM simulations. The return loss plots for the equivalent circuit model and full wave EM simulation match well as shown in Figure 5.5. The slot with one row of TL resonates at 2.6 GHz and 3.8 GHz. The bottom most row of TL loaded in the slot gives similar resonance effect as the microstrip TL in Figure 5.2. This is

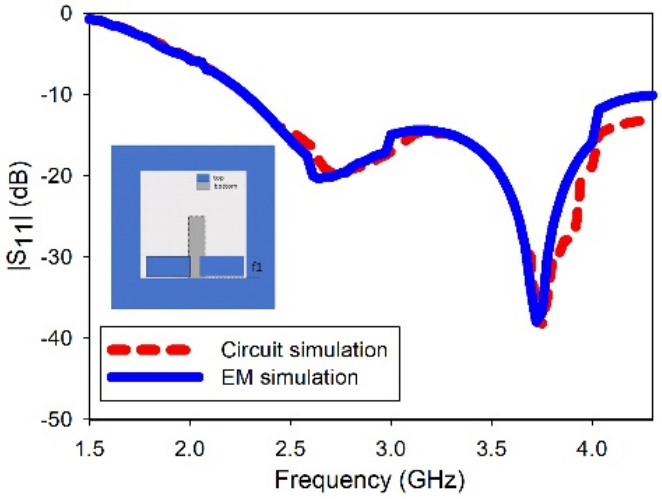

Figure 5.5: Reflection coefficient curves of the proposed antenna loaded with one transmission line (bottom row only) using the circuit model and EM simulation. (The calculated parameter values for 2.56 GHz and 3.8 GHz, were Lsh = 0.5 nH, Csh = 7.7 pF, Ce' = 5.8 pF, and Le' = 0.35 nH.)

attributed to the fact that the microstrip feed line at the bottom of the substrate acts as a partial ground plane for the loaded TLs.

The slot loaded with an array of TLs of varying lengths and gaps in between, leads to the excitation of different resonances namely, f_1, f_2 , f_3, f_4, f_5 as shown in Figure 5.6 (a) (each row). These resonances combine with that of the slot to give the UWB response. The operating principle of the proposed UWB antenna can further be explained based on the study of the simulated reflection coefficient characteristics obtained when loading the slot with different TLs. The bandwidth of the antenna increases with number of TLs as shown in Figure 5.6 (b). Finally, the UWB response is obtained due to the excitation of all the TLs. The simulated current distributions at different resonant frequencies of the proposed antenna are shown in Figure 5.6 (c). The slot mode is excited in case (i). Maximum current intensities along the different rows of TL elements are observed in cases (ii) and (iii) corresponding to their resonant frequencies.

In the above section, the proposed geometry has been analysed and studied using the microstrip TL model. In the next section, a detailed frequency response study of a microstrip TL is done and compared with the response of our geometry. This is done to justify and explain the relation of our design with the microstrip line model. The

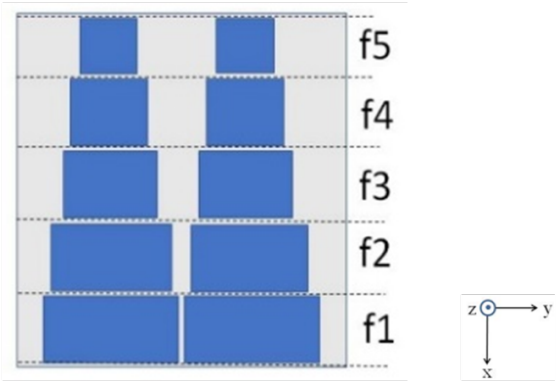
f5
f4
f3
f2
f1
z
y
x

(a)

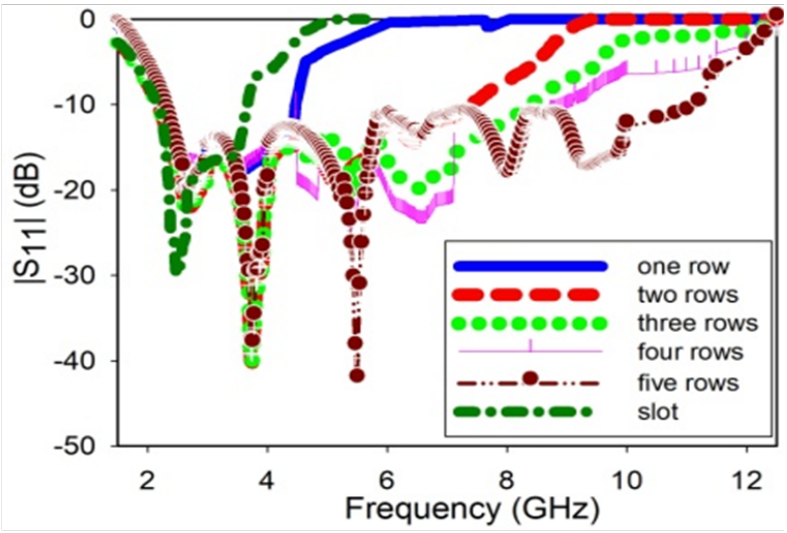
0
-10
-20
-30
-40
-50
|S11| (dB)
2
4
6
8
10
12
Frequency (GHz)
one row
two rows
three rows
four rows
five rows
slot

(b)

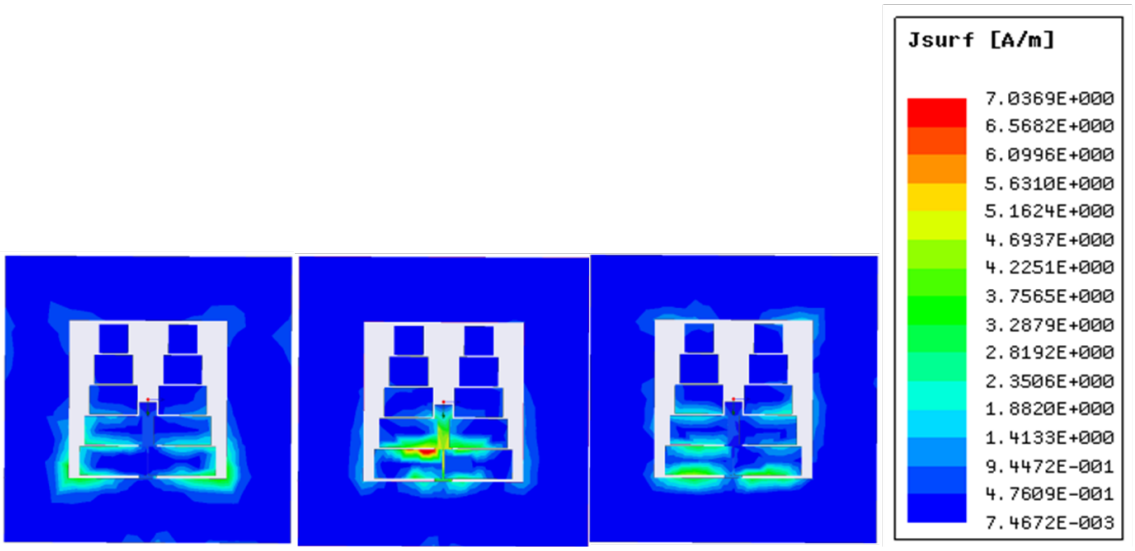

(i) (ii) (iii)

(c)

Figure 5.6: (a) Symbolic representation of the transmission lines loaded .slot with different resonant frequencies corresponding to each row. (b) Return loss plot for different configurations of the proposed wide band square slot antenna (c) Simulated current distributions at (i)2.6 GHz (ii)3.8 GHz (iii) 5.5 GHz.

goubau line (single wire conductor) response is also presented for analysis purpose.

5.4 Analysis of Microstrip and Goubau Transmission Lines

The transmission and reflection coefficient responses as well as the dispersion diagrams obtained from the simulation of a microstrip transmission line having a ground plane underneath and that of the single wire Goubau transmission line of similar dimensions that correspond to the last row of the dispersive transmission line in the proposed geometry are studied and plotted.

The two-port analysis for microstrip line and Goubau line is done for both the cases of continuous line and gap loaded line and the results obtained have been plotted and shown below.

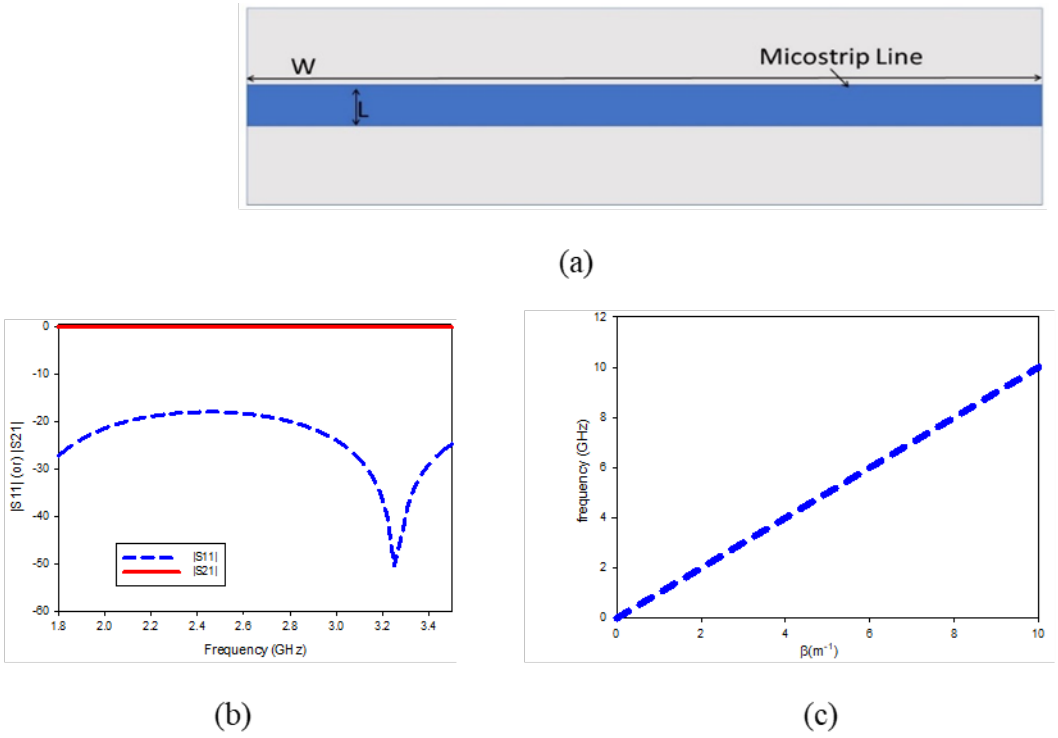

Figure 5.7: TL without gap loading (a) Schematic (b) Reflection and transmission coefficient magnitude charcateristics (c) Dispersion diagram.

5.4.1 Transmission lines without gap loading

1. **Microstrip line**

   The schematic of an unloaded microstrip transmission line of length W and width L, the reflection and transmission coefficient magnitude charcateristics and the dispersion digram obtained on simulation of the microstrip TL are shown in Fgure 5.7. The TL allows propagation over the entire simulated frequency band.

2. **Goubau Line**

   Similar analysis is done for a Goubau line of same dimensions. The schematic and the results obtained are shown in Figure 5.8. It is observed that the Goubau line (single conductor without ground plane) allows wave propagation in a similar manner as observed in the microstrip transmission line when gaps are not loaded on the transmission lines.

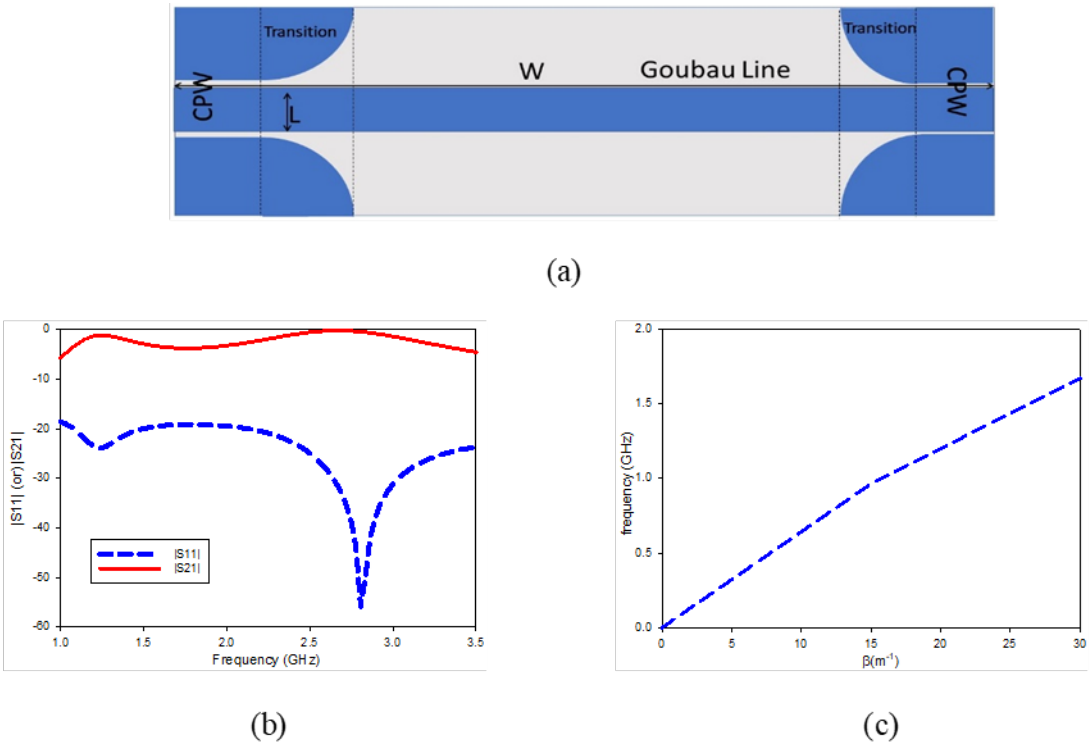

Figure 5.8: Single wire Goubau Line without gap loading (a) Schematic (b) Reflection and transmission coefficient magnitude charcateristics (c) Dispersion diagram.

5.4.2 Gap loaded transmission lines

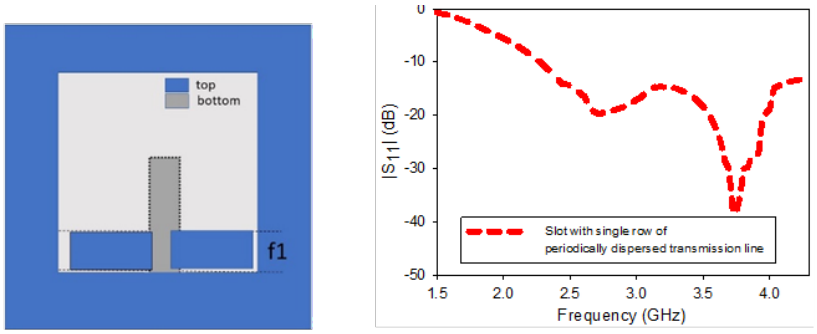

Figure 5.9: (a) Symbolic representation of the transmission line loaded slot (b) Return loss plot for the structure.

Gap loaded transmission lines (microstrip and Goubau line) with dimensions (W=14.5mm,

L= 4.5mm, p=14.7mm , g=0.2mm) similar to the bottom most row of the proposed antenna are analysed in Ansys HFSS Simulation software and the results are compared with the transmission line loaded slot antenna. Geometry and return loss plot of the slot antenna with one row of transmission line loading are shown in Figure 5.9 (a) and Figure 5.9 (b).

1. **Microstrip Line with Periodic Gaps** The geometry of the microstrip line

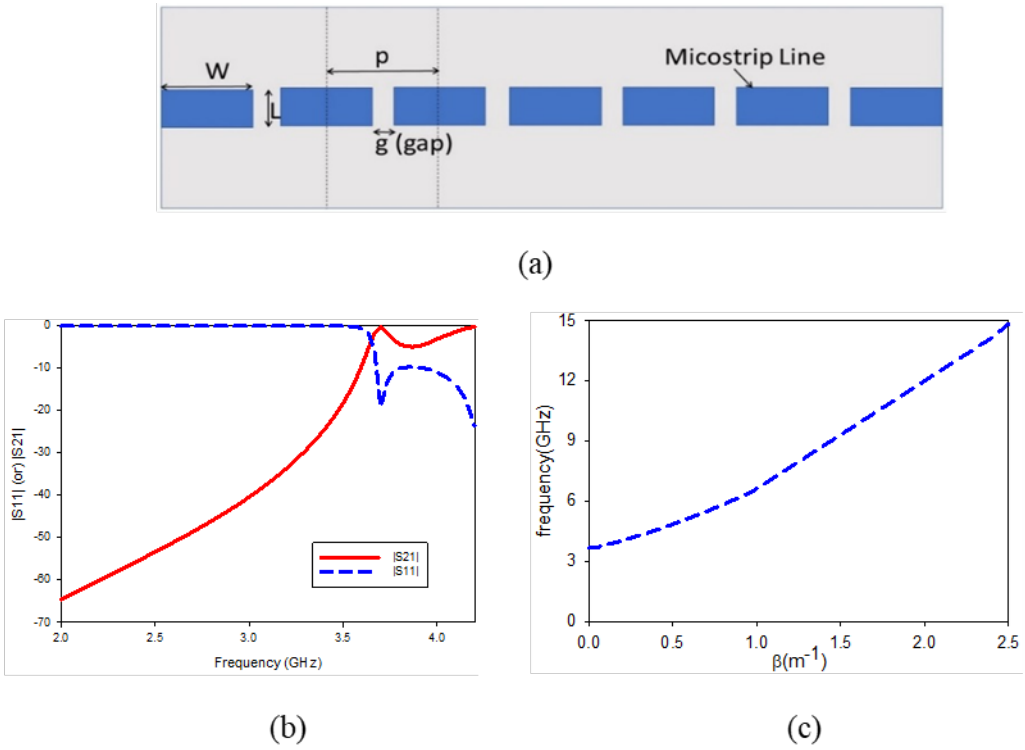

Figure 5.10: TL with gap loading (a) Schematic (b) Reflection and transmission coefficient magnitude charcateristics (c) Dispersion diagram.

which is loaded with peiodic gaps similar to the bottom most row of the proposed antenna is shown in Figure 5.10 (a). Simulated reflection and transmission coefficient curves and dispersion diagram of the microstrip line with gap loading are shown in Figure 5.10 (b) and Figure 5.10 (c). A cutoff frequency of 3.8 GHz is obtained in this case. This matches with the frequency of resonance obtained from the simulation of the single row transmission line loaded slot antenna. Hence, the proposed geometry for the periodically dispersed transmission lines loaded slot antenna can be modelled using the equations for the microstrip

transmission line. The analytical calculation for the cut-off frequency was done and a resonant frequency of around 3.9 GHz is obtained which matches well with the simulated results.

2. **Goubau Line with Periodic Gaps**

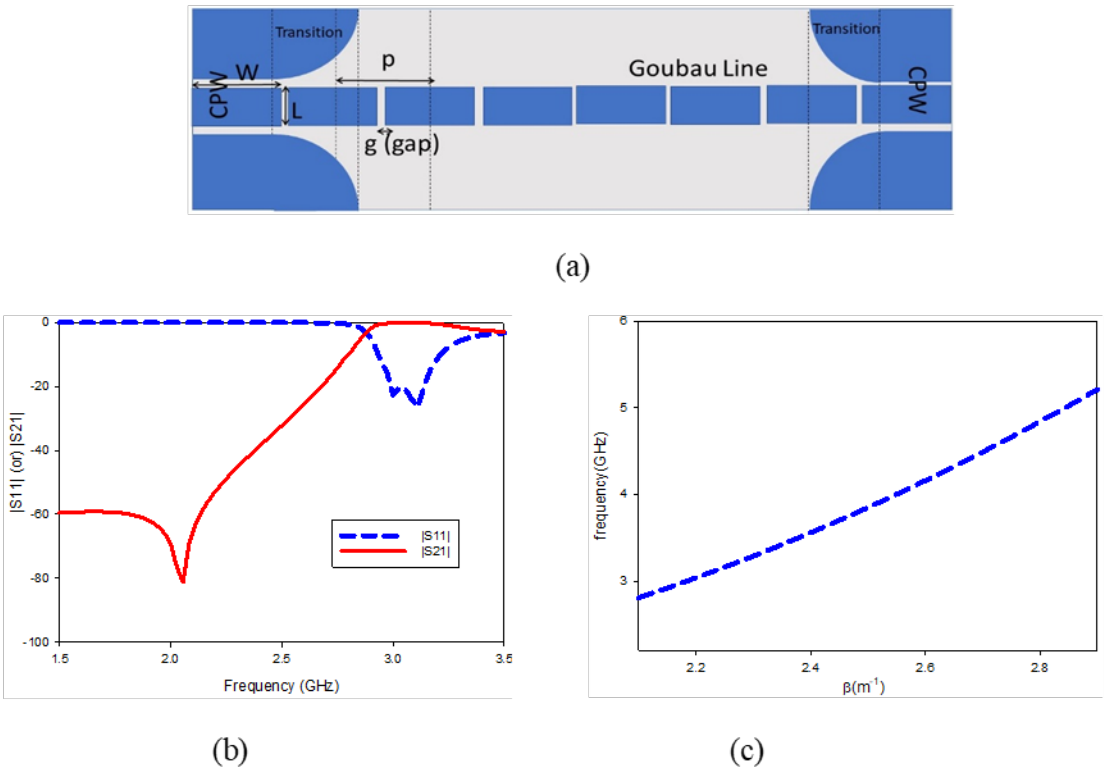

Figure 5.11: Single wire Goubau Line with gap loading (a) Schematic (b) Reflection and transmission coefficient magnitude charcateristics (c) Dispersion diagram.

S-parameter and dispersion characteristics of the single wire transmission line with gap (Figure 5.11 (a)) follow a similar pattern of reflection and transmission parameter as observed in the periodic dispersive transmission line with ground plane underneath, but with different cut off frequencies. A cut off frequency of 2.7 GHz is obtained here. This can be observed in Figure 5.11 (b) and Figure 5.11 (c).

Thus, upon comparison of the results obtained for the microstrip transmission line and the corresponding Goubau line model with our proposed structure, it can be concluded that the proposed geometry approximates a microstrip transmission line model. The microstrip line feed in the proposed UWB antenna

acts like a partial ground plane for dispersive transmission lines loaded on the slot providing the necessary potential gradient and effective capacitive effect. Thus, the resonance at around 3.8 GHz for the slot antenna simulation corresponds with the cut off frequency obtained for the transmission line analysis which shows that the proposed geometry can be analysed using the microstrip transmission line model.

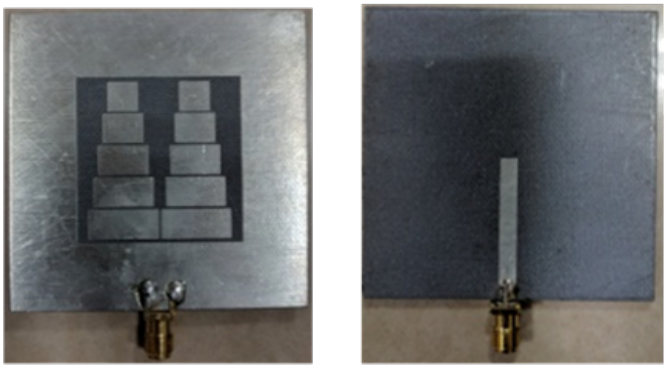

(a) (b)

Figure 5.12: Fabricated prototypes of the proposed UWB antennas (a) Top view (b) Bottom view.

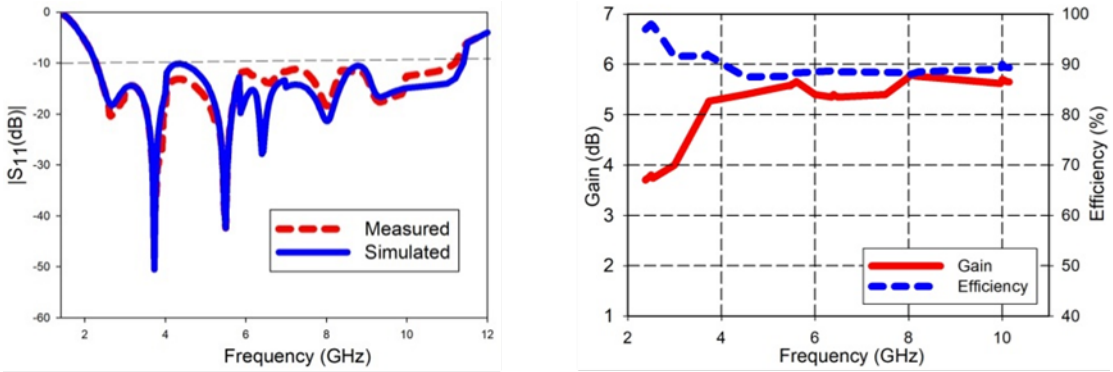

(a) (b)

Figure 5.13: (a) Measured and simulated reflection coefficient magnitudes of the proposed multiband antenna. (b)Measured maximum gain and efficiency of the proposed antenna.

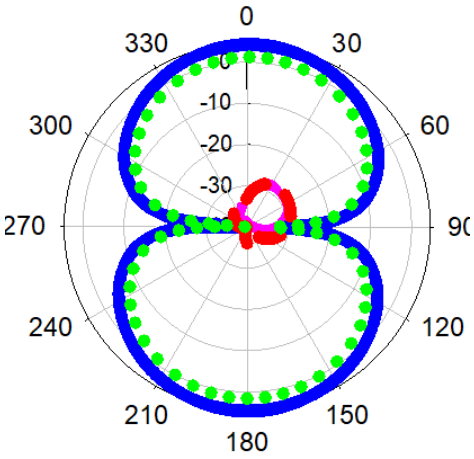
0
30
60
90
120
150
180
210
240
270
300
330
-10
-20
-30

(a)

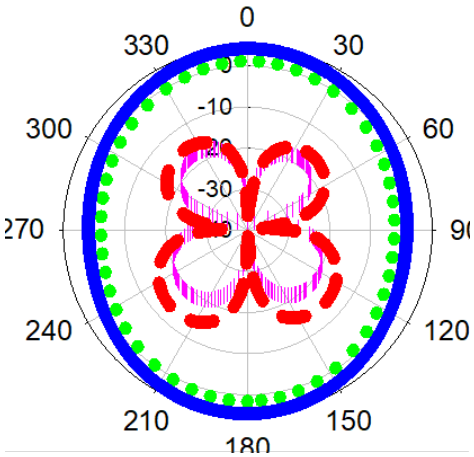
0
30
60
120
150
180
210
240
270
300
330
-10
-30

(b)

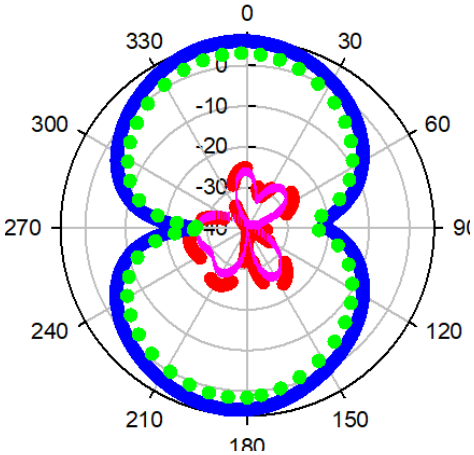
0
30
60
120
150
180
210
240
270
300
330
-10
-20
-30

(c)

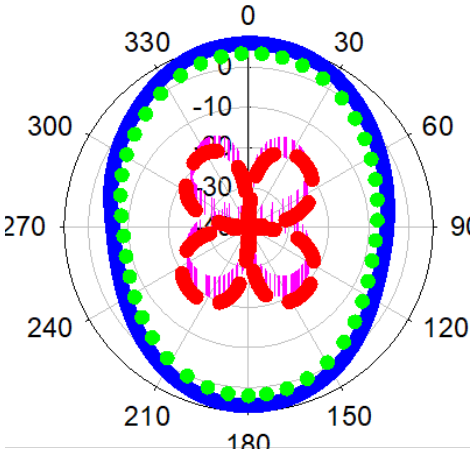
0
30
60
120
150
180
210
240
270
300
330
-10
-30

(d)

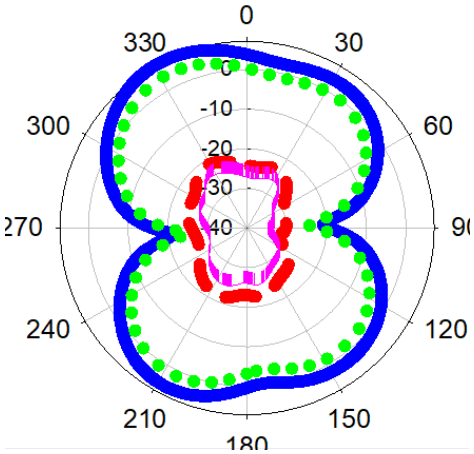
0
30
60
120
150
180
210
240
270
300
330
-10
-20
-30
-40

(e)

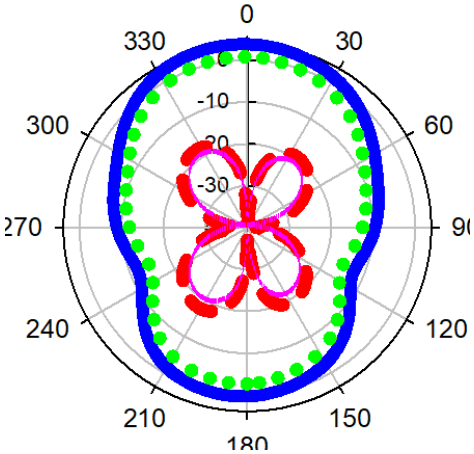
0
30
60
120
150
180
210
240
270
300
330
-10
-30

(f)

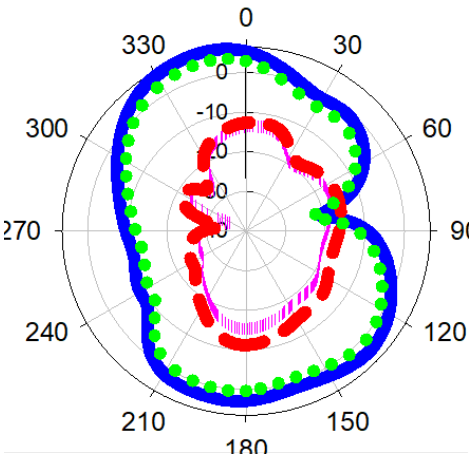
0
30
60
90
120
150
180
210
240
270
300
330
-10
-20
-30

(g)

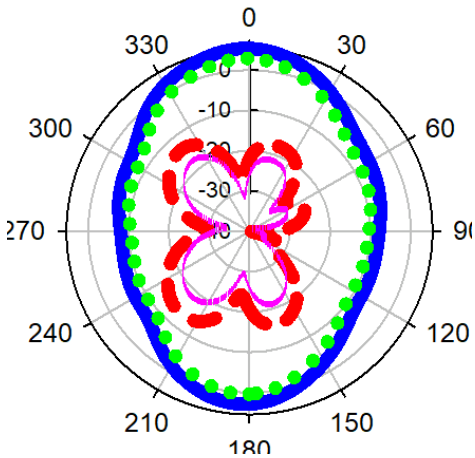
0
30
60
90
120
150
180
210
240
270
300
330
-10
-30

(h)

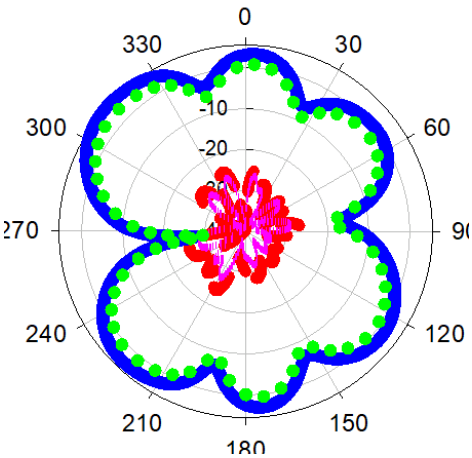
0
30
60
90
120
150
180
210
240
270
300
330
-10
-20

(i)

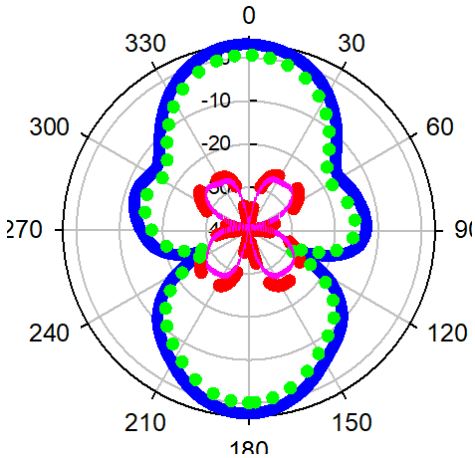
0
30
60
90
120
150
180
210
240
270
300
330
-10
-20

(j)

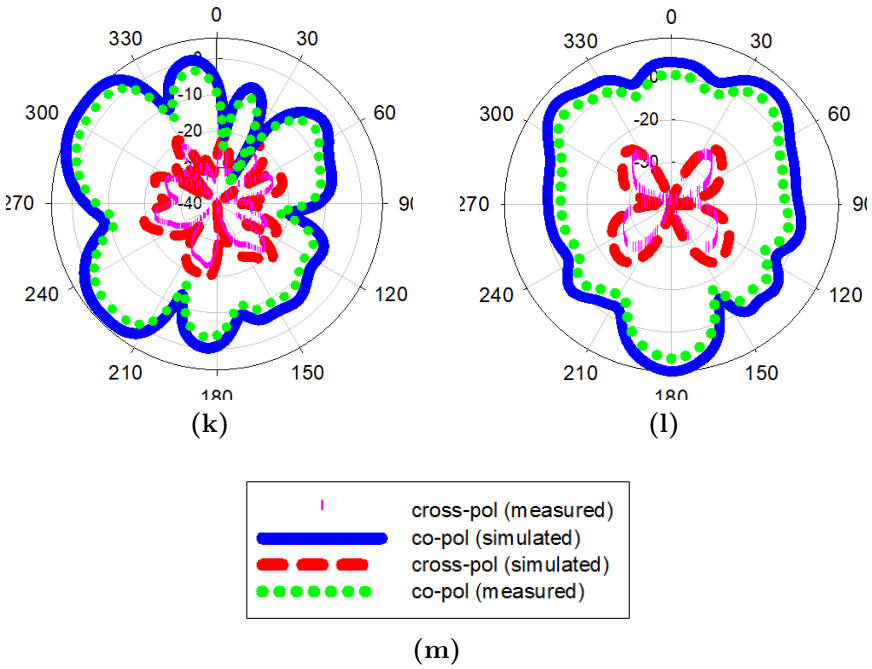

Figure 5.14: Simulated and measured radiation patterns of the proposed antenna at (a) 2.6 GHz (b) 3.8 GHz (c) 5.5 GHz (d) 6.4 GHz (e) 8.03 GHz (f) 10.5 GHz.

5.5 Results And Analysis

The proposed ultra-wideband antenna was simulated using ANSYS HFSS 16.0 and was fabricated using an S103 LPKF machine. A photograph of the prototype of the proposed antenna is shown in Figure 5.12. The reflection coefficient and radiation pattern were measured. The measured and simulated reflection coefficient magnitudes are shown in Figure 5.13 (a). The simulated and measured results show good agreement. The simulated and measured -10 dB impedance bandwidths obtained are 9.5 GHz (2.1 GHz 11.6 GHz centered at 1.5 GHz) and 9.4 GHz (2.1 GHz 11.5 GHz centered at 2.75 GHz) respectively.

The measured efficiency and peak gain values at the resonance frequencies over the band are 98% / 3.8 dB, 92% / 5.2 dB, 88% / 5.6 dBi, 90% / 5.4 dBi, 88% / 5.8 dBi, 90% / 5.7 dBi respectively. Figure 5.13 (b) shows the measured gain / efficiency versus frequency in a far field anechoic chamber using the gain substitution method. The simulated and measured radiation patterns of the proposed antenna at the six resonance frequencies (for x-z, y-z planes) over the resonant band for the x-z and y-z planes are shown in Figure 5.14. The cross-polarization values are below -15 dB. Table

5.1 gives a performance compariosn of different UWB slot based antennas. On comparison of the proposed design with other wideband slot based designs, compactness, high impedance BW values, good efficiency and gain values are the favorable features in the proposed design compared to other designs in literature.

Table 5.1: Performance Comparison of Different UWB Slot Based Antennas (λ_g-guided wavelength corresponding to the lowest resonant frequency.)

REF	SIZE	FBW (%)	GAIN (dBi)	EFFICIENCY (%)
Sung (2011)	$0.2\lambda_g^2$	118	1-5	——
Kumar *et al.* (2014)	$0.28\lambda_g^2$	122	2-4	>70
Lu and Zhu (2015)	$0.26\ \lambda_g^2$	31.5	≈5.2	—-
Hu *et al.* (2016)	$0.2\lambda_g^2$	109	1.8-4	>66
Hu *et al.* (2017)	$1.46\lambda_g^2$	46.1	≈5	—-
Proposed	$0.23\lambda_g^2$	138	3.8-5.8	88-98

5.6 Summary

This chapter presents a perturbed TL loaded wideband square slot antenna with compact size. The antenna is designed to operate over a wide band of frequency ranging from 2.21 GHz to 11.5 GHz with a measured impedance bandwidth of 9.4 GHz. A gain of 3.8 dB - 5.8 dB and efficiency of 88% - 98% is obtained over the resonance band. The different resonant frequencies over the entire band can be tuned by altering the dimensions and gap widths of the loaded gap dispersed TLs. The slot resonance remains unaffected. Thus, the proposed design offers compact size with wide impedance bandwidth and high gain values. The plot shows that an additional resonance is obtained at 3.7 GHz along with slot resonance mode at 2.7 GHz. This additional resonance is due to the loading of one row of transmission line on the slot antenna.

Chapter 6

CIRCULARLY POLARIZED SINGLE AND MULTIBAND SLOT ANTENNAS

6.1 Introduction

The first section of this chapter deals with the design and analysis of a simple coplanar waveguide (CPW) fed circularly polarized square slot antenna. A novel method is proposed to obtain CP for a CPW fed square slot antenna at the designed frequency. Complementary to the conventional method of using truncated corners in microstrip patch antenna to obtain orthogonal modes with 90° phase shift, here, circularly polarized waves are generated at the designed frequency by adding extensions to the slot corners. In the second section, a novel dual band square slot antenna is proposed which is designed to radiate at two circularly polarized bands centred at 2.4 GHz and 4.5 GHz. The slot is provided with two corner extensions and loaded with an array of inclined copper strips. The centre frequencies and sense of polarization at the frequencies can be controlled depending on the loaded strips and corner extensions of the slot.

The third proposed design involves the use of copper strips and SRR to design a compact multiband structure, which is altered by changing the orientation of the copper strips to form a triband CP slot antenna that offers compact structure compared to previous designs in literature. Also the sense of polarization can be reconfigured on shifting the orientation of the copper strips by 45°. In the fourth section, a novel

triband CP square slot antenna is proposed with improved axial ratio bandwidth (ARBW) and efficiency values. The antenna is fed with an F-shaped microstrip line, and loaded with an SRR and U-strip, to produce triband operation with centre frequencies at 1.5 GHz, 2.5 GHz, and 3.2 GHz. Impedance BWs of 12%, 9.1%, 7.3%, ARBWs of 9.3%, 7.3%, 8.5% and gains of 3.2 dB, 4.5 dB, and 3.5 dB are obtained at the three resonant frequencies, respectively. The orientation of the F-shaped feed line is used to control the sense of polarization of the antenna at the two operating bands. The proposed design offers compact size with wide impedance and AR bandwidth values.

In the fifth design, a Split Ring Resonator (SRR) loaded quad band microstrip slot antenna designed to operate at 2.42 GHz, 4.33 GHz, 8.46 GHz and 10.9 GHz is proposed. The additional resonant bands are generated by loading the square slot antenna with two pairs of SRR structures on either side of the feed line. The bands centered at 8.46 GHz and 10.9 GHz are found to exhibit wideband and circular polarization properties respectively. The resonance band at 8.46 GHz provides a wide bandwidth of 2.43 GHz. One pair of the loaded SRR structure consists of two spiral shaped connected SRRs. The excitation of these structures gives rise to a circularly polarized band at 10.9 GHz with 3-dB axial ratio bandwidth of 390 MHz. Comparison of the proposed designs with previous works in terms of impedance bandwdiths, ARBWs, gain, efficiency and size is provided at the end of the chapter.

6.2 Single Band Circularly Polarized Square Slot Antenna

A simple square shaped circularly polarized slot antenna with CPW feed is proposed here. The slot antenna is designed to radiate at 2.5 GHz. Small symmetric rectangular extensions are made on one pair of corners of the slot to produce the CP wave at 2.5 GHz. The slot is CPW fed thus, offering a planar design. The sense of polarization can be easily controlled by changing the position of extensions. The frequency of resonance can be controlled depending on the dimension of the slot. The proposed antenna is simulated, fabricated and tested. Good agreement is obtained between the measured and simulated results. An ARBW of 35% and a gain of 3.5 dB is obtained at the resonant frequency.

6.2.1 Antenna Design

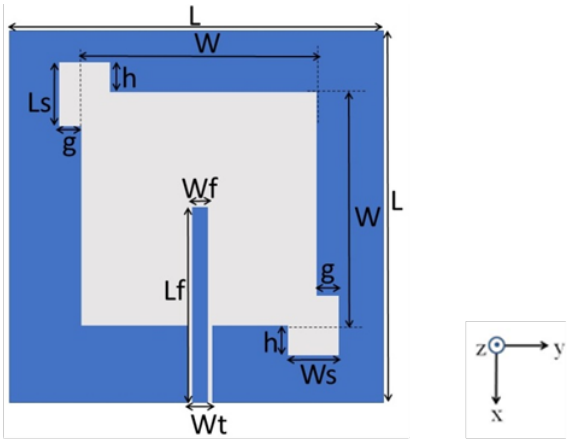

Figure 6.1: Antenna geometry (top view). [L=60 mm, W=40 mm, Wf=3.6 mm, Lf=29.4 mm, Wt=4 mm, Ws=1.6 mm, Ls=1.8 mm, g=0.5 mm, h=0.5 mm].

The proposed antenna geometry is shown in Figure 6.1. The antenna is designed on a RT-Duroid 5880 substrate of permittivity 2.2, height 1.52 mm and loss tangent 0.02. On the top of the substrate, a square slot is etched out such that it operates at its fundamental resonant mode (TM01). The resonant frequency (f_{r1}) of the square slot of dimension W is given by:

$$f_{r1} = \frac{c}{2W}\sqrt{\frac{2}{1+\epsilon_r}} \tag{6.1}$$

where c is the speed of light and ϵ_r is the relative permittivity of the substrate.

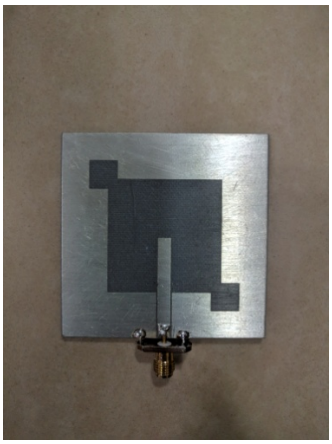

Figure 6.2: Photograph of the proposed antenna prototype.

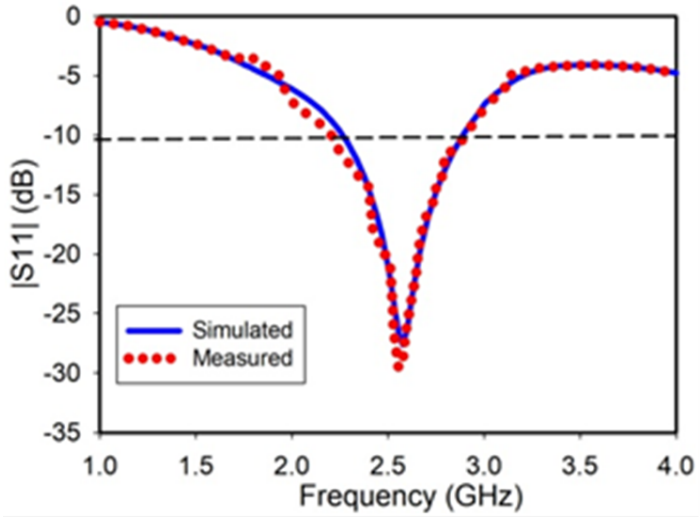

(a)

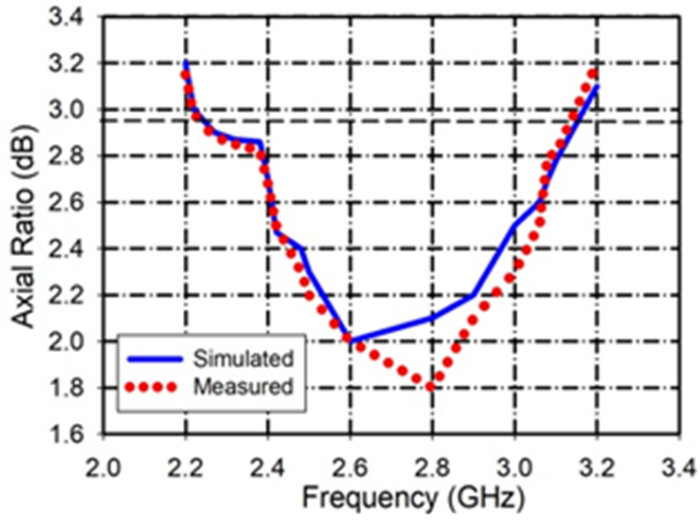

(b)

Figure 6.3: Measured and simulated (a)reflection coefficient magnitudes and (b) axial ratio values of the proposed antenna.

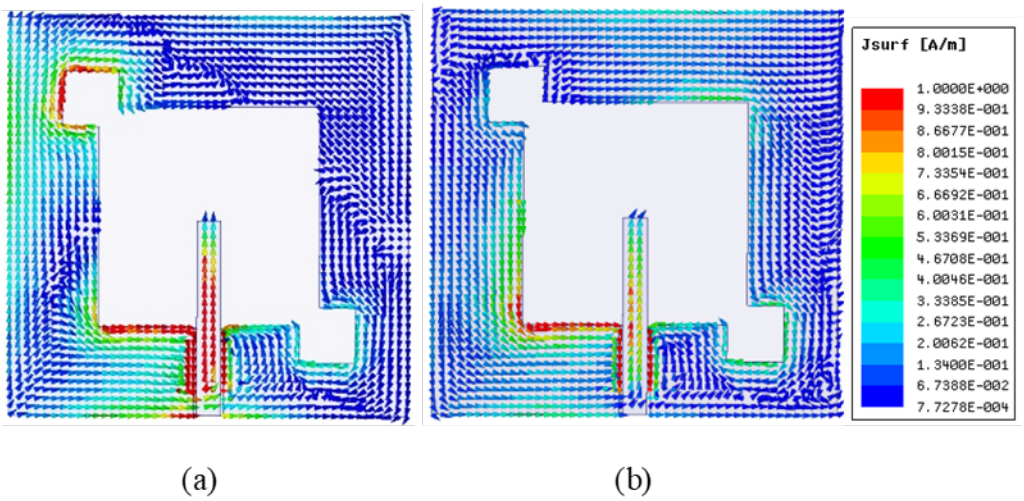

Figure 6.4: Simulated surface current distributions of the proposed antenna at 2.5 GHz for (a)phi=0 and (b)phi=90.

Here the slot is designed to operate at 2.5 GHz and two symmetric extensions are made on either end of the slot as shown in Figure 6.1. A 50Ω CPW line of width W_f is used to feed the slot. The loading of extensions on the slot creates the necessary phase shift without affecting the slot resonance. They provide the additional phase response to produce two orthogonal components with 90° phase shift. The sense of polarization can be rotated on shifting the position of extensions to the opposite corners. The antenna is simulated using ANSYS HFSS 17.0.

6.2.2 Results and Analysis

The proposed antenna was fabricated using an S103 LPKF machine and measured using an Agilent N9918A VNA. Photograph of the antenna prototype is shown in Figure 6.2.The measured and simulated reflection coefficient magnitudes are shown in Figure 6.3 (a). The -10dB bandwidths of operation of the antenna as obtained from the measured and simulated results are 0.88 GHz (2.1 GHz - 2.98 GHz centered at 2.5 GHz) and 0.8 GHz (2.17 GHz 2.98 GHz centered at 2.56 GHz) respectively. The measured and simulated axial ratio values are also plotted against frequency and shown in Figure 6.3 (b). The 3dB measured and simulated ARBW values obtained over the operating bandwidth were 35.2% (2.1 GHz– 2.98 GHz centered at 2.5 GHz) and 31.7% (2.17 GHz 2.98 GHz centered at 2.56 GHz) respectively. The current distribution obtained at the resonant frequency of 2.5 GHz is analyzed from the +z

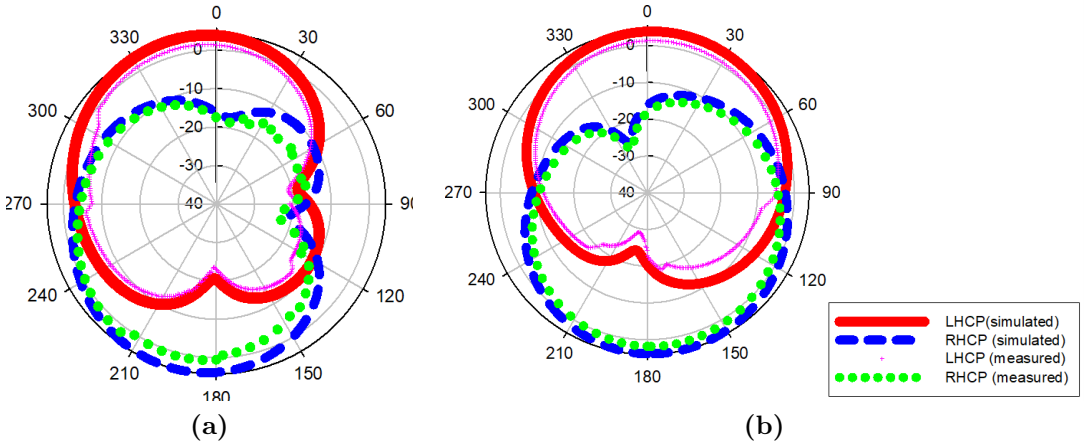

Figure 6.5: Measured and simulated radiation patterns of the proposed antenna at 2.5 GHz for (a) phi=0 (b) phi=90.

axis and plotted on the x-y plane in Figure 6.4. It can be seen that the vector current rotates anti-clockwise as the phase shifts by 90° which shows that the LHCP radiation is obtained at resonance. The measured and simulated radiation patterns of the proposed antenna at the resonant frequency for phi=0° and phi=90° planes are shown in Figure 6.5. The antenna radiates left hand circularly polarized (LHCP) waves in the upper hemisphere and right hand circularly polarized (RHCP) waves in the lower hemisphere. The cross polarization gain values are found to be less than -20 dB compared to co-polarization at the resonant frequency. Thus, the current distribution and radiation patterns show that LHCP radiation is obtained at the designed resonant frequency for this arrangement of slot extensions. When the extensions are shifted to opposite corners, the current distribution at resonance reverses and RHCP is obtained at the resonant frequency. The simulated efficiency and peak gain value at 2.5 GHz is 95% and 3.5 dB.

6.3 Dual Band CP Slot Antenna

A compact microstrip fed square slot antenna is proposed here with dual circularly polarized bands. The slot is designed to operate at 2.36 GHz. A pair of symmetric rectangular extension is introduced on opposite corners of the square slot to generate the lower circularly polarized band from 2.24 GHz to 2.62 GHz centered at 2.4 GHz with a 3 dB AR bandwidth of 15.7%. The square slot is loaded with an array of

inclined rectangular copper strips with truncated ends to generate the higher circularly polarized band from 3.26 GHz to 5.18 GHz centered at 4.52 GHz with a 3dB AR bandwidth of 45.5%. The bands can be independently tuned depending on the slot and strip dimensions respectively. Also, the sense of polarization at the two bands can be independently controlled depending on the position of the extensions and the orientation of the copper strips respectively. The proposed antenna is fabricated on a RT/Duroid 5880 substrate with a size of 50 x 50 x 1.52 mm^3. The antenna is prototyped and measured in terms of impedance bandwidth, ARBW, gain and efficiency. Fairly very good agreement can be observed between the simulated and measured results.

6.3.1 Antenna Geometry

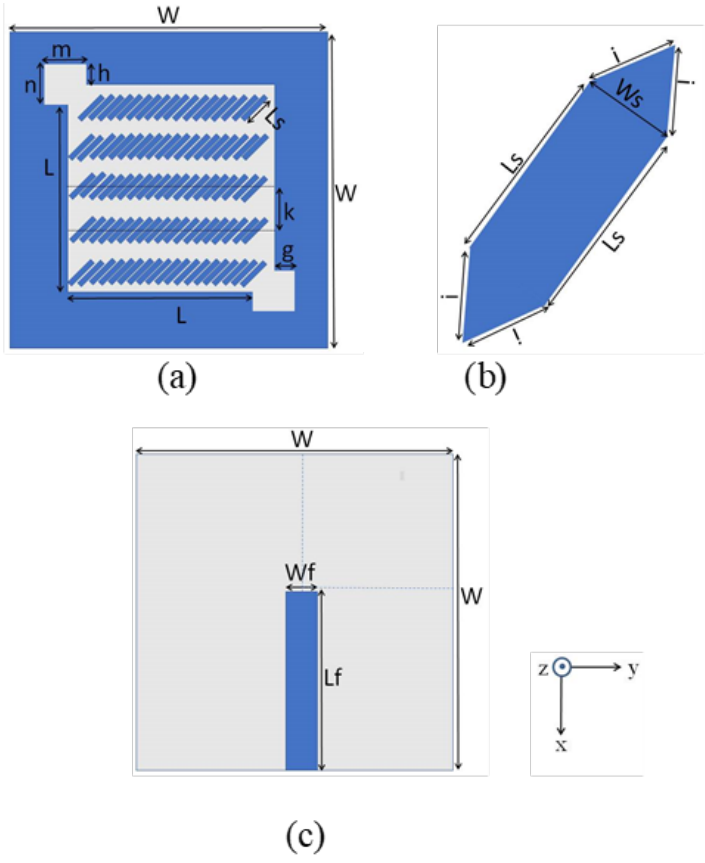

Figure 6.6: Proposed geometry depicts (a) upper surface (b) lower surface (c) dimensions of SRR. [L=40, W=50, Ls=6.15, Ws=0.65, g=0.5, h=0.5, k=9.5, m=1.6, n=1.8, i=0.65, Lf=31.2, Wf=3.6], All in mm.

The proposed dual band antenna geometry is shown in Figure 6.6. The antenna is designed on a RT/ Duroid 5880 substrate of size 50 x 50 mm^2, permittivity (ϵ_r)= 2.2, height = 1.52 mm and loss tangent= 0.02. A square slot is etched out on top of the substrate as shown in Figure 6.6 (a) so that the slot resonates at its fundamental resonant mode. A pair of symmetric rectangular extensions is made on one corner of the slot to generate the circularly polarized wave at the slot resonance. The slot is loaded with an array of closely spaced inclined rectangular copper strips of width smaller than operating wavelength and symmetrically truncated ends. The inclined strips are spaced at a centre to centre horizontal distance of d=1.7 mm. A detailed geometry of a single corner truncated rectangular copper strip is given in Figure 6.6 (b). The bottom view of the antenna is shown in Figure 6.6 (c). A 50 Ω microstrip feedline is printed at the bottom of the substrate to suitably feed the slot.

6.3.2 Operating Principle

The microstrip feedline excites the slot to resonate at its fundamental resonant mode TM01. The resonant frequency can be calculated as given in Equation 3.2. The slot is loaded with an array of copper strips which are excited by the magnetic and electric field lines produced on excitation of the slot. The copper strips are designed and spaced such that the array resonates around the plasma frequency where negative permittivity effects are observed. The effective angular plasma frequency of the copper strip array is given by Pendry *et al.* (1996).

$$\omega_p = \sqrt{\frac{N_{eff}q^2}{m_{eff}\epsilon_0}} \tag{6.2}$$

Here, N_{eff} and m_{eff} are the effective charge concentration and mass due to the effect of self inductance and are given by

$$N_{eff} = \frac{\pi(W_s/2)^2}{d^2}N \tag{6.3}$$

and

$$m_{eff} = \frac{N(W_s/2)^2\mu_0 q^2}{2}\ln\frac{d}{W_s/2} \tag{6.4}$$

where q is the electronic charge, N is the charge density, W_s is the width of the strips, d is the cell side of the lattice on which the strips are arranged, ϵ_0 and μ_0 refer

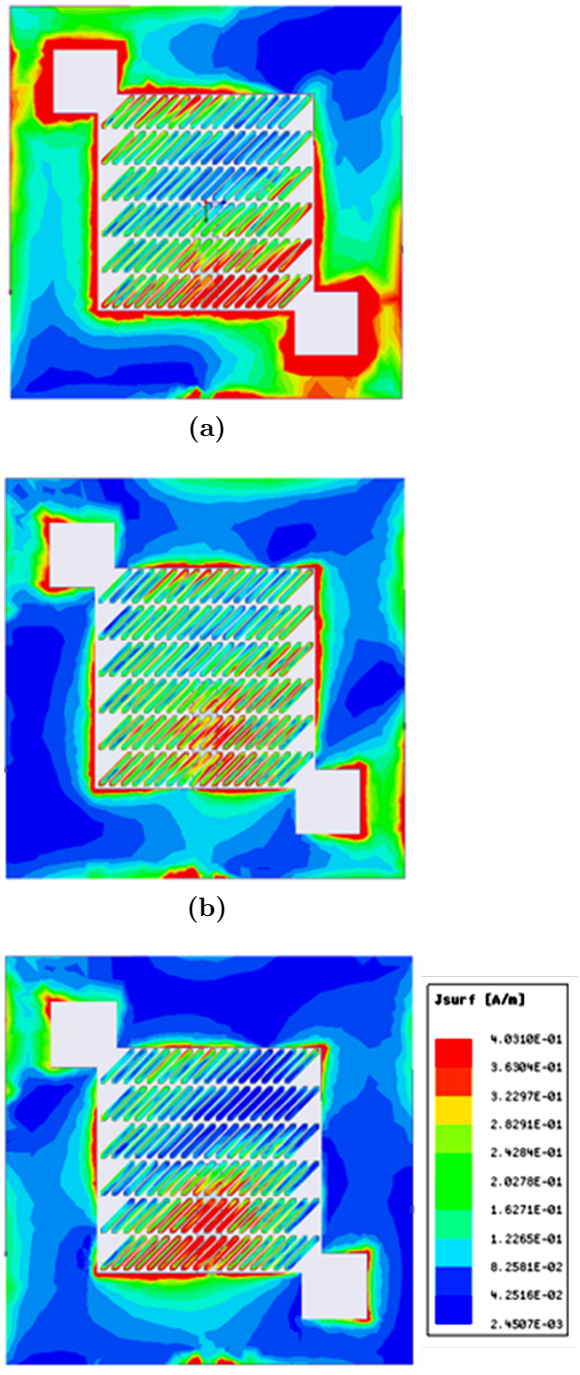

Figure 6.7: Simulated surface current distribution magnitude for the proposed antenna at (a) 2.4 GHz, (b) 4.2 GHz and (c) 4.8 GHz

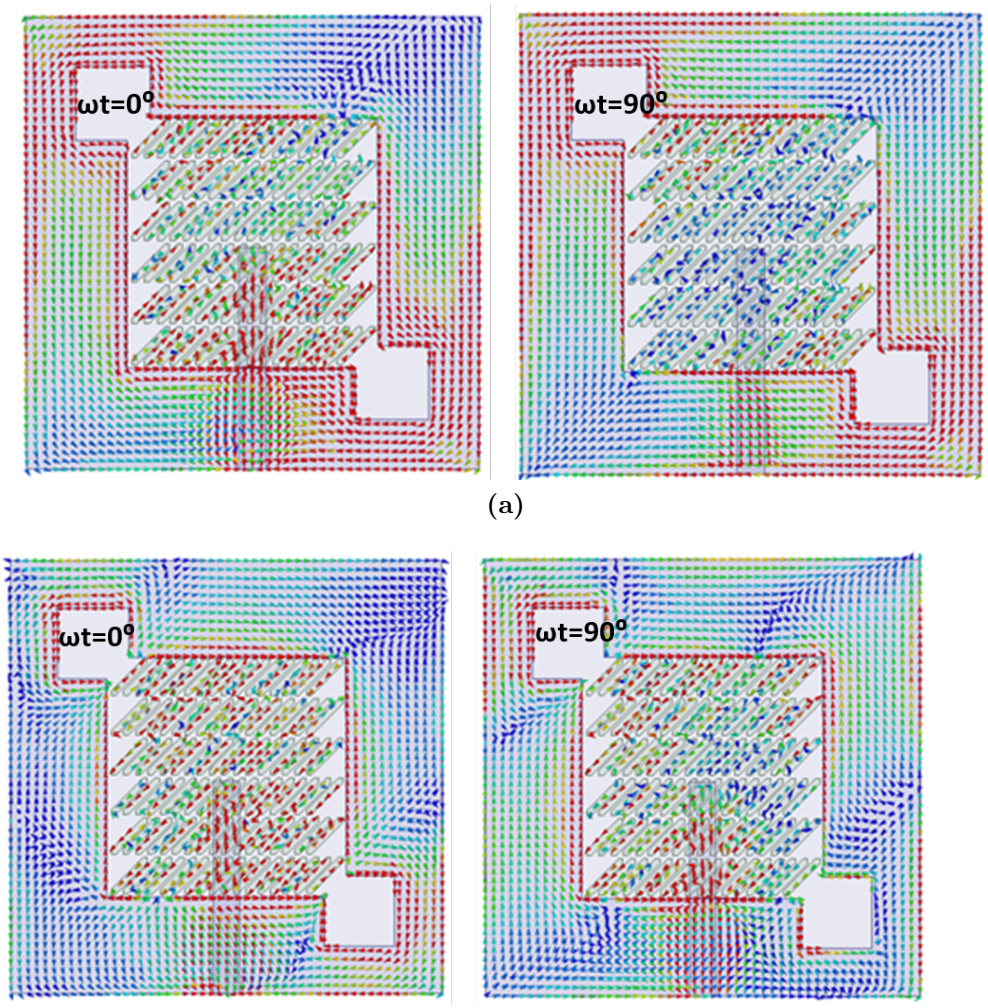

Figure 6.8: Simulated current distribution vector for the proposed antenna at (a) 2.4 GHz, (b) 4.5 GHz

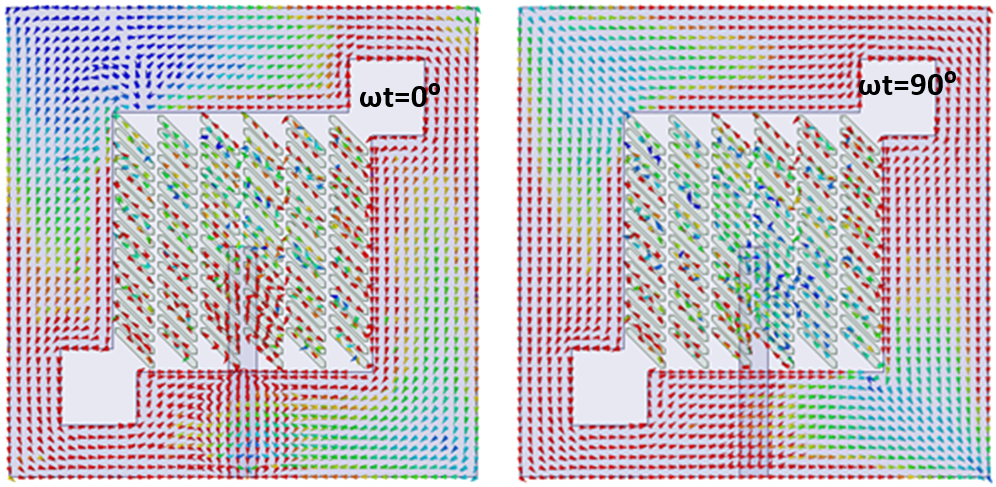

(a)

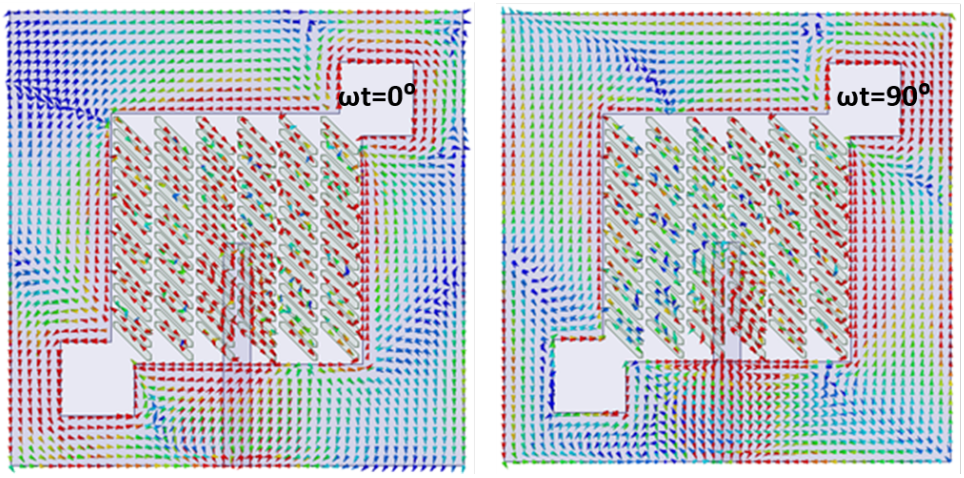

(b)

Figure 6.9: Simulated current distribution vector for the proposed antenna with orientation shift at (a) 2.4 GHz, (b) 4.5 GHz

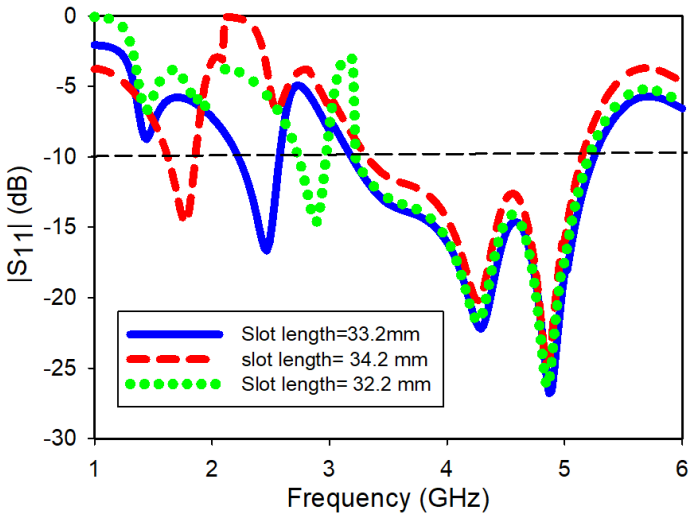

(a)

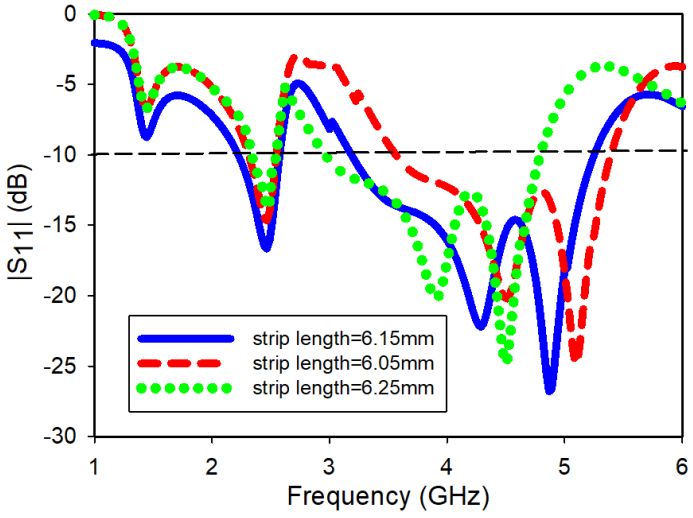

(b)

Figure 6.10: Simulated reflection coefficient magnitude values plotted against frequency for varying (a) slot and (b) strip dimensions.

to the absolute permittivity and permeability values. On substitution of the above values, the plasma frequency resonance can be calculated as :

$$f_p = \frac{1}{\sqrt{2\pi\mu_0\epsilon_0\epsilon_r d^2 ln(2d/W_s)}} \tag{6.5}$$

The dual band of operation can also be analysed based on study of the surface current distribution magnitudes obtained at the different resonant frequencies. The plots obtained on simulation are shown in Figure 6.7 for the resonant frequencies of (a) 2.4 GHz, (b) 4.2 GHz and (c) 4.8 GHz respectively. At 2.5 GHz, it can be seen that the resonance is obtained on excitation of the slot fundamental resonance mode and the strips near the corner extensions. The higher band is due to the combination of the resonance modes produced due to the excitation of the inclined strips. As seen from Figure 6.7(b), maximum current distribution can be observed around the inclined strip array at the resonance frequency of 4.2 GHz, while maximum current distribution is around the lower end of the array at the higher frequency of 4.8 GHz as seen in Figure 6.7(c). Thus, resonance frequency obtained can be observed to be inversely proportional to the cell side of the lattice as seen in equation (6.3).

6.3.2.1 CP Mechanism

Two rectangular extensions are made on the opposite corners of the slot which helps to generate the orthogonal frequency components with 90° phase shift. This gives rise to the circularly polarized band at the slot resonant frequency. This frequency band can be tuned depending on the slot dimension and the sense of polarization can be shifted on changing the position of the extensions to the opposite corners. The circular polarization is obtained at the higher bands on inclining the copper strips by 45° and truncating the corners. This helps to generate the orthogonal components required to produce the circularly polarized waves. This frequency band can be tuned depending on the length of the strips and the sense of polarization is altered on changing the inclination of the copper strips. The CP mechanism of the proposed dual band slot antenna is further explained based on the analysis of the current distributions obtained on simulation of the antenna at the different resonance frequencies. The current distributions are studied in the +z direction on the x-y plane for phases ωt =0° and ωt =90° as shown in Figure 6.8. Figure 6.8 (a) shows the current distribution at 2.4 GHz for both phases, while Figure 6.8 (b) shows the distributions at 4.5 GHz. It can

be seen that the the current distribution vector at the resonant frequencies rotates anti-clockwise as the phase changes by 90ωt. Hence, LHCP is obtained at both the centre resonant frequencies of the proposed antenna. The figure clearly shows that the CP operation at the resonant frequencies is obtained on excitation of the slot and the copper strips where maximum current distribution is observed. Also, it is observed that the direction of the current reverses when changing the position of the extensions and the orientation of the strips by 90°. Hence, RHCP is obtained at the resonant frequencies for this case as shown in Figure 6.9(a) and 6.9(b) where the simulated current distribution vectors are shown for the proposed antenna with orientation shift at (a) 2.4 GHz and (b) 4.5 GHz respectively .

6.3.2.2 Independent Tuning

The operating principle of the antenna is further explained using the reflection coefficient response of the antenna with change in slot and copper strip dimensions. Independent tuning of each of the bands is possible on changing the dimensions of the slot and the strips respectively. This can be observed from Figure 6.10 where the frequency response of one band remains unaffected irrespective of the change in the other. On changing the slot dimension, a shift in frequency values for the lower band was observed while the change in strip lengths affect the resonance frequencies at the higher band. This can be seen in Figure 6.10 (a) and Figure 6.10 (b) respectively.

6.3.3 Results And Analysis

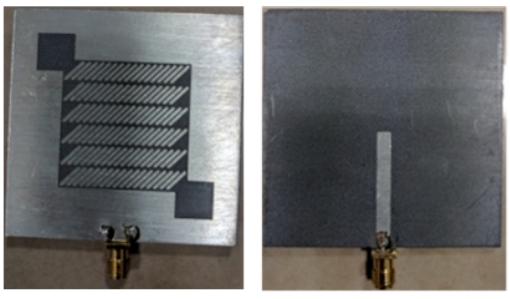

Figure 6.11: (a) Upper and (b) lower sights of the archetype.

The proposed dual-band CP slot antenna was simulated using ANSYS HFSS 16.0 and was fabricated using an S103 LPKF machine. The prototypes were then measured

for the reflection coefficient parameters using an Agilent N9918A VNA at NITK. A photograph of the prototype of the proposed antenna is shown in Figure 6.11. The measured and simulated reflection coefficient magnitudes and axial ratio plots are shown in Figure 6.12 (a) and Figure 6.12 (b). The simulated and measured results show good agreement.

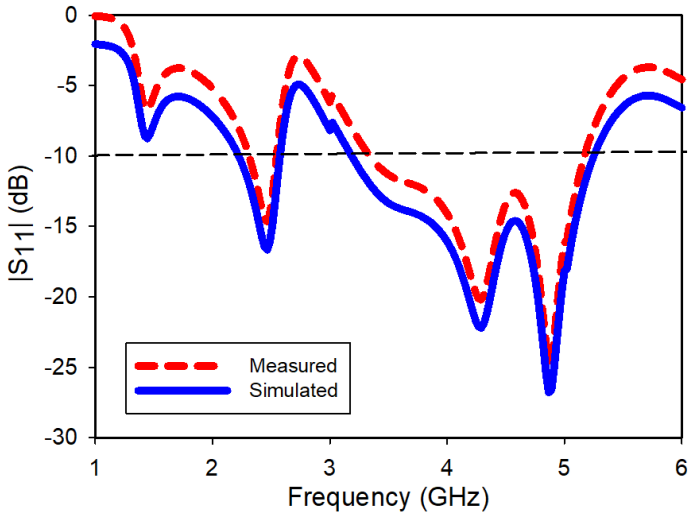

(a)

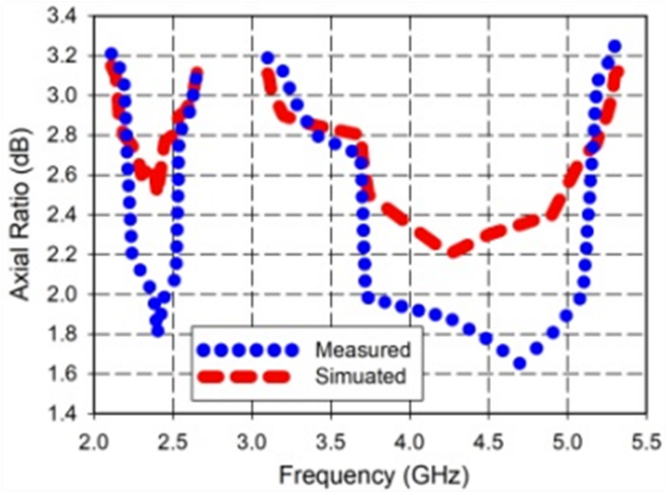

(b)

Figure 6.12: Plots of (a) reflection coefficient magnitudes and (b) axial ratio values obtained on simulation and measurement of the multiband antenna.

The measured -10 dB impedance bandwidths obtained were 15.6% (2.24 GHz 2.62 GHz with centre frequency of 2.43 GHz) and 42.4% (3.26 GHz 5.18 GHz with centre

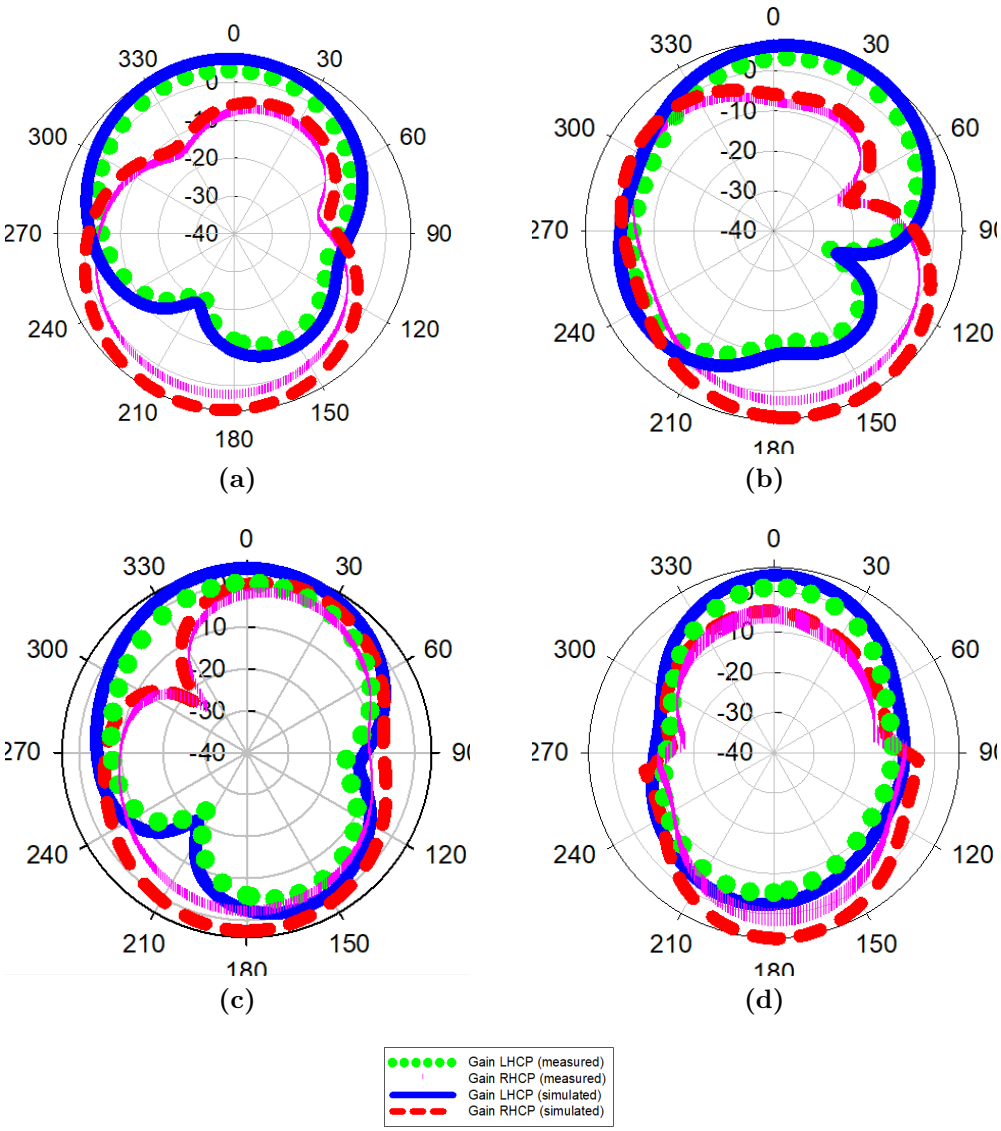

Figure 6.13: Radiation patterns of the proposed antenna at 2.4 GHz (a) phi=0 (b) phi=90, 4.5 GHz (c) phi=0 (d) phi=90 and (e) legend

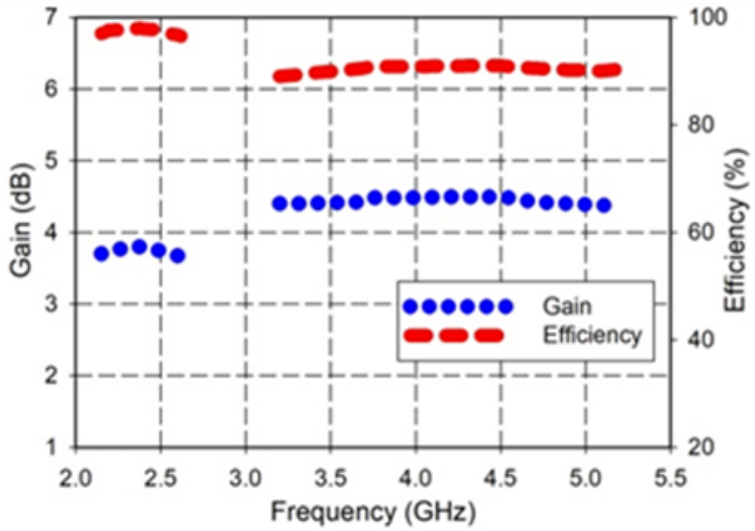

Figure 6.14: Maximum gain and radiation efficiency obtained on measurement of the proposed antenna.

frequency of 4.52 GHz), while the measured ARBWs were 15.7% (2.24 GHz 2.62 GHz centered at 2.41 GHz) and 45.5% (3.26 GHz 5.18 GHz centered at 4.32 GHz). The antenna radiation characteristics were measured in a Satimo Star-Lab near-field chamber. The simulated and measured radiation patterns of the proposed antenna at the three resonance frequencies (for x-z, y-z planes) are shown in Figure 6.13. From the radiation patterns it can be observed that the cross-polarization values at the resonant frequencies fall below -10 dB of the co-polarization values. In addition, it can be seen that LHCP wave is radiated in the upper hemisphere. Figure 6.14 shows the measured gain / efficiency versus frequency. The measured efficiency and peak gain values recorded at the resonance frequencies are 91% / 3.8 dB and 98% / 4.5 dB respectively. Compactness, ease of control in frequency bands and sense of polarization, high impedance BW and ARBW values, good efficiency and gain values are some of the desirable features in the proposed design compared to other dual band CP slot antenna designs in literature.

6.4 A Tri-Band Circularly Polarized Strip and SRR Loaded Slot Antenna

In this section, the design and analysis of a novel simple and compact multiband circularly polarized slot antenna loaded with metallic strips and a SRR is explained. The multiband operation is obtained via exciting the SRR and copper strips by the microstrip fed square slot antenna. The SRR resonates at 1.83 GHz, while the strips and the slot antenna provide resonances at 2.5 GHz and 3.1 GHz. Resonant modes of loaded SRR and strips combined with the fundamental mode of the slot produces circularly polarized waves at the resonance frequencies of the proposed antenna. The proposed antenna allows for independent tuning of the different bands via the use of the tilted strips and the SRR. Also, the sense of polarization at the resonance frequencies can be controlled by changing the orientation of the strips and the SRR with respect to the slot. The proposed antenna is fabricated on an FR-4 substrate of dimension 50x50x1.56 mm^3. Antenna performances in terms of 10 dB return loss bandwidth, 3 dB axial ratio bandwidth, gain and efficiency are validated experimentally and are in good agreement with simulated results. The proposed design provides wide CP resonance bands, wide ARBW values and compact size along with a mechanism to control the CP orientation compared to previous designs.

6.4.1 Antenna Geometry And Design

The proposed antenna geometry is given in Figure 6.15. The antenna is designed on an FR-4 substrate with ϵ_r =3.6, thickness (h) of 1.56 mm and loss tangent (tan δ) of 0.02. Figure 6.15 (a) shows the top view of the proposed antenna. A square slot with side length 33.2 mm, designed to operate at a resonant frequency of 2.5 GHz, is etched out on the top side of the substrate. The slot is loaded with an array of copper strips with varying lengths, all of which are inclined 45° with respect to the x-axis as shown in Figure 6.15 (a). The lengths of the copper strips are consistently reduced by 4 mm from the middle strip which is of length 36 mm to obtain the different resonance bands. Figure 6.15 (b) shows the bottom view of the proposed antenna. The bottom side of the substrate consists of a 50 Ω feed line and the SRR. The SRR is placed at the top right corner of the slot at distances 8.6 mm and 8.4 mm from the reference axes (x-y plane). The SRR geometry is shown in Figure 6.15 (c). It consists

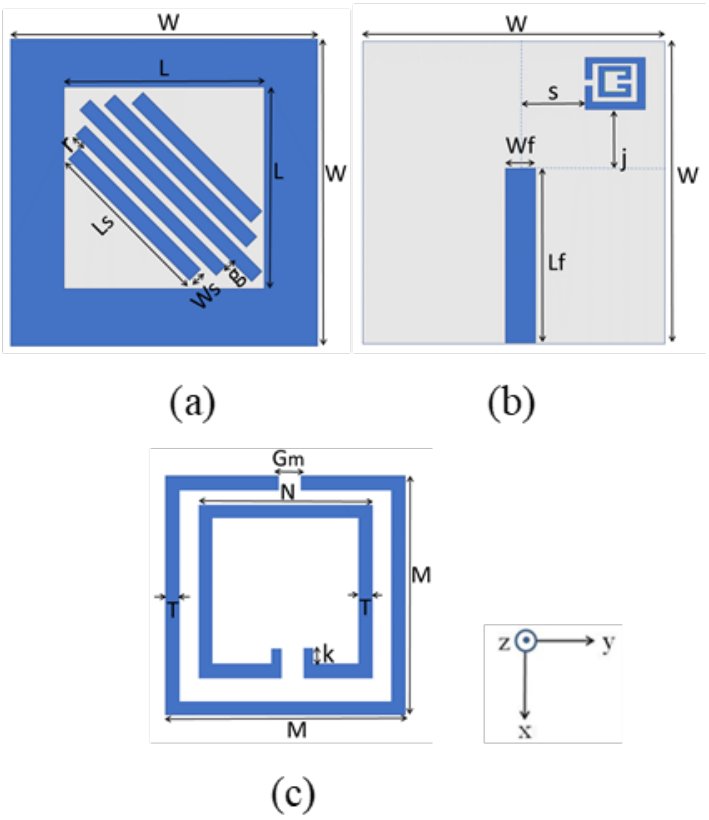

Figure 6.15: Antenna geometry (a) top view (b) bottom view (c) SRR geometry without stub. [L=33.2mm, W=50mm, Ls=26mm, Ws=2.5mm, g=1.1mm, r=2mm, Lf=24.4mm, Wf=3.6mm, s= 8.6mm, j=8.4mm, k=1.65mm, M=6mm, N=4mm, T=0.6mm, Gm=0.6mm, h=1.56 mm].

of concentric square rings with splits at opposite edges. The various dimensions of the SRR structure are given in the Figure 6.15 caption. Stubs of length 1.65 mm are added to the inner ring to improve the CP performance of the proposed antenna.

6.4.2 Operating Principle

6.4.2.1 Multiband Resonance

The microstrip feed line excites the slot to resonate at its fundamental resonant mode (TM01). The resonance frequency of the slot is given by Equation 3.1.

The different bands of operation of the proposed antenna design are obtained from the resonances produced by the SRR and the strips that are excited by the magnetic and electric fields of the microstrip line fed square slot antenna. When excited by the

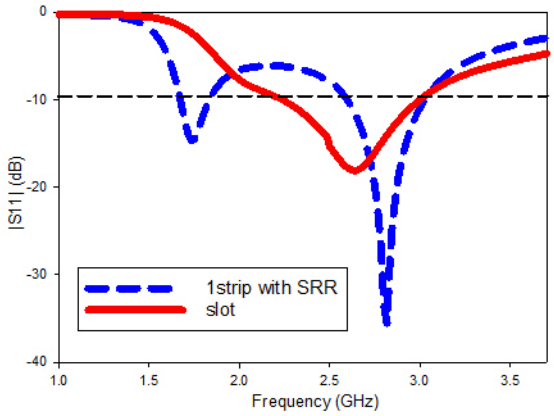

Figure 6.16: Simulated reflection coefficients of the proposed multiband antenna.

electric field lines along their axis, the strips resonate, and the resonant frequencies are determined by their lengths. These resonances combine with the slot mode to provide CP bands at the resonance frequencies 2.5 GHz and 3.16 GHz. The SRR is loaded such that its position and orientation allow for maximum coupling of axial magnetic field from the slot. The SRR can be modeled as an LC circuit. The inductance (L) and capacitance (C) values of the SRR equivalent circuit determine its frequency of operation (Ishikawa *et al.* (2007), Engheta and Ziolkowski (2006)). In the proposed antenna, the SRR is designed to resonate at 1.8 GHz as shown in Figure 6.16 (the first resonance). Thus, the SRR, which contributes to the lowest resonant band helps in obtaining miniaturization of the antenna structure.

The second and third resonances are mainly obtained by the excitation of the strips loaded inside the slot antenna. This can also be observed from the electric field distributions shown in Figure 6.17 for the different resonant frequencies. In particular, the second resonance is due to the slot mode and middle strip resonating around 2.45GHz and the third is due to the titled $\lambda_g/2$ strips of lengths 26mm and 32mm that provide a mid-band resonance around 3.1 GHz (the first has a resonance about 2.8GHz while the second at 3.4 GHz). The maximum field distributions are observed around the SRR and the middle strip for the first two resonance frequencies and around the strips at the ends for the third resonance. The selection of the strip lengths is done based on the guided wavelengths for different frequencies. The guide wavelength is given by (Balanis (1992)):

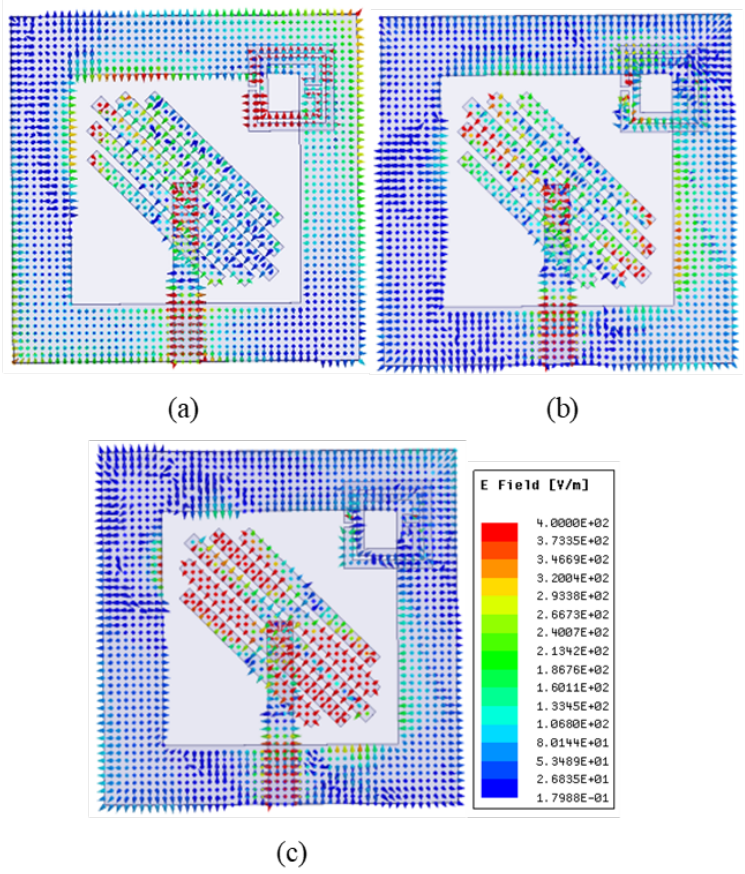

Figure 6.17: Simulated electric field distributions at (a) 1.83 GHz (b) 2.5 GHz (c) 3.1 GHz.

$$\lambda_g = \frac{300}{f_{r,GHz}\sqrt{\epsilon_{eff}}} \tag{6.6}$$

where dielectric constant ϵ_{eff} is calculated as follows:

$$\epsilon_{eff} = \frac{\epsilon_r + 1}{2} + \frac{\epsilon_r - 1}{2\sqrt{1 + 12(h/W_f)}} \tag{6.7}$$

W_f and h denote width of the feedline and thickness of the substrate. The length of the strips is taken to be approximately equal to 1/2 of the guide wavelength at the resonant frequencies.

Figure 6.18 shows the simulated reflection coefficient magnitudes for different configurations of the copper strips loaded slot antenna. It can be observed from Figure 6.18 (a) that the resonance of the middle strip coincides with the slot resonance con-

tributing to the middle band of operation of the proposed antenna design. The other two strips contribute to the third band of resonance as seen in Figure 6.18 (b) with improvement in reflection coefficient magnitude values owing to the third strip at the end (Figure 6.18 (c)). The addition of two more strips and the SRR leads to our final design shown in Figure 6.18 (e) with improved impedance bandwidth and ARBW values compared to the previous configurations as explained in the following sections.

6.4.2.2 CP mechanism

The variation of the axial ratio values with frequency for different configurations of the proposed slot antenna is plotted in Figure 6.19. It is evident from the plots that the excitation of the SRR along with the slot resonance provides CP characteristics at the first band. This could be attributed to the magnetic dipole-loop combination that excites orthogonal field components (Kraus and Marhefka (2001)). The lengths of the stubs on the inner ring are adjusted to ensure 90° phase difference between the field components. The CP wave at the first band is from 1.77 GHz to 1.85 GHz centred at 1.83 GHz.

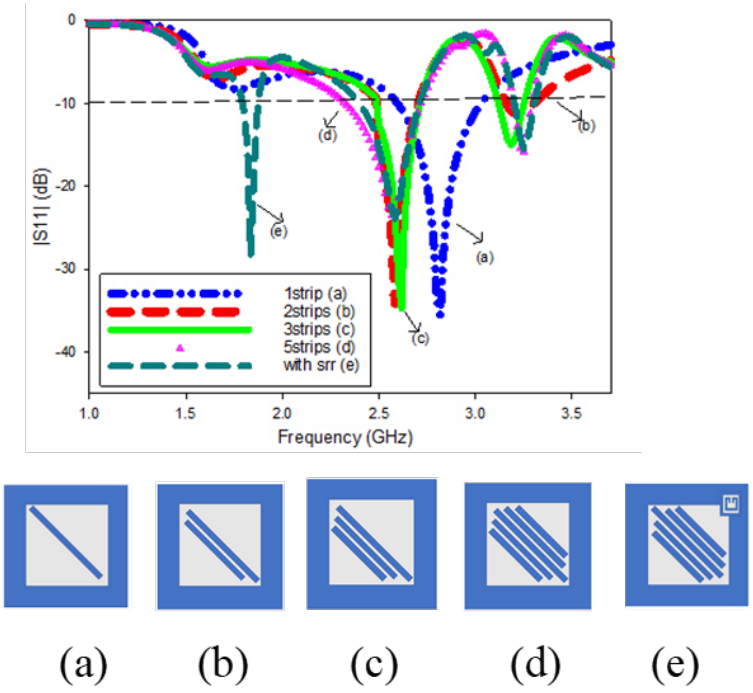

Figure 6.18: Simulated reflection coefficients for different configurations of the proposed multiband antenna.

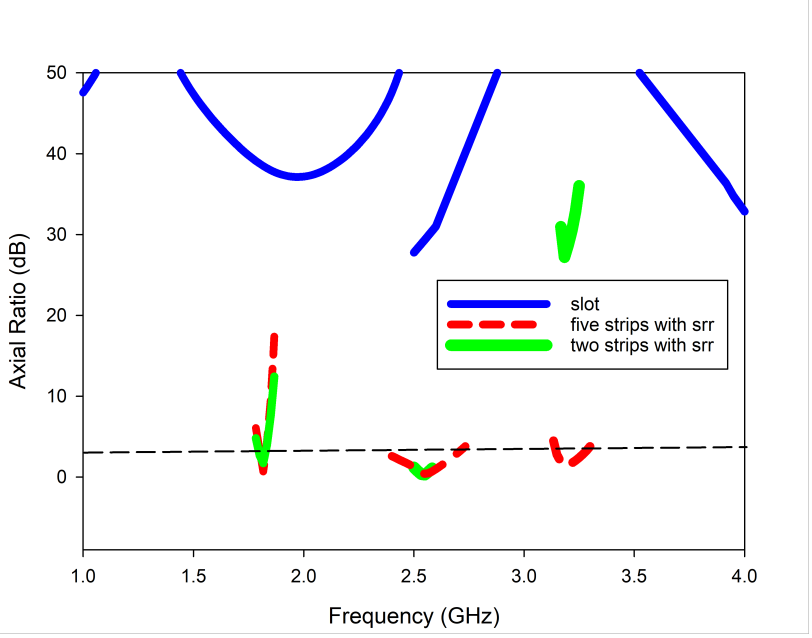

Figure 6.19: Simulated Axial Ratio values for different configurations of the proposed multiband antenna.

At the second band of resonance, the slot and centre strip mode combination produce the orthogonal field components. The degenerate modes help in realizing the circularly polarized waves. Thus, a second CP resonance band is obtained between 2.4 GHz 2.7 GHz, centred at 2.52 GHz, and is due to the excitation of the middle strip loaded slot. The resonances of the slot and the middle strip coincide hence producing CP at the middle band. The addition of more strips leads to improvement in the CP performance of the proposed antenna at the third band. The 45° oriented strips at the end resonate to produce the circularly polarized band from 3.04 GHz to 3.15 GHz with a centre frequency 3.08 GHz. The third strip at the end helps lower the AR values at this band as can be seen in Figure 6.19.

6.4.2.3 Parametric Analysis

A parametric study of the length of the strips, the gap between the strips and the width of the SRR on the reflection coefficient and AR values is shown in Figure 6.20. As observed from Figure 6.20 (a), when increasing the length of the strips, the second and third resonant frequencies shift to lower values and when reducing the strip lengths, they shift to higher values. Figure 6.20 (b) shows that there is no major

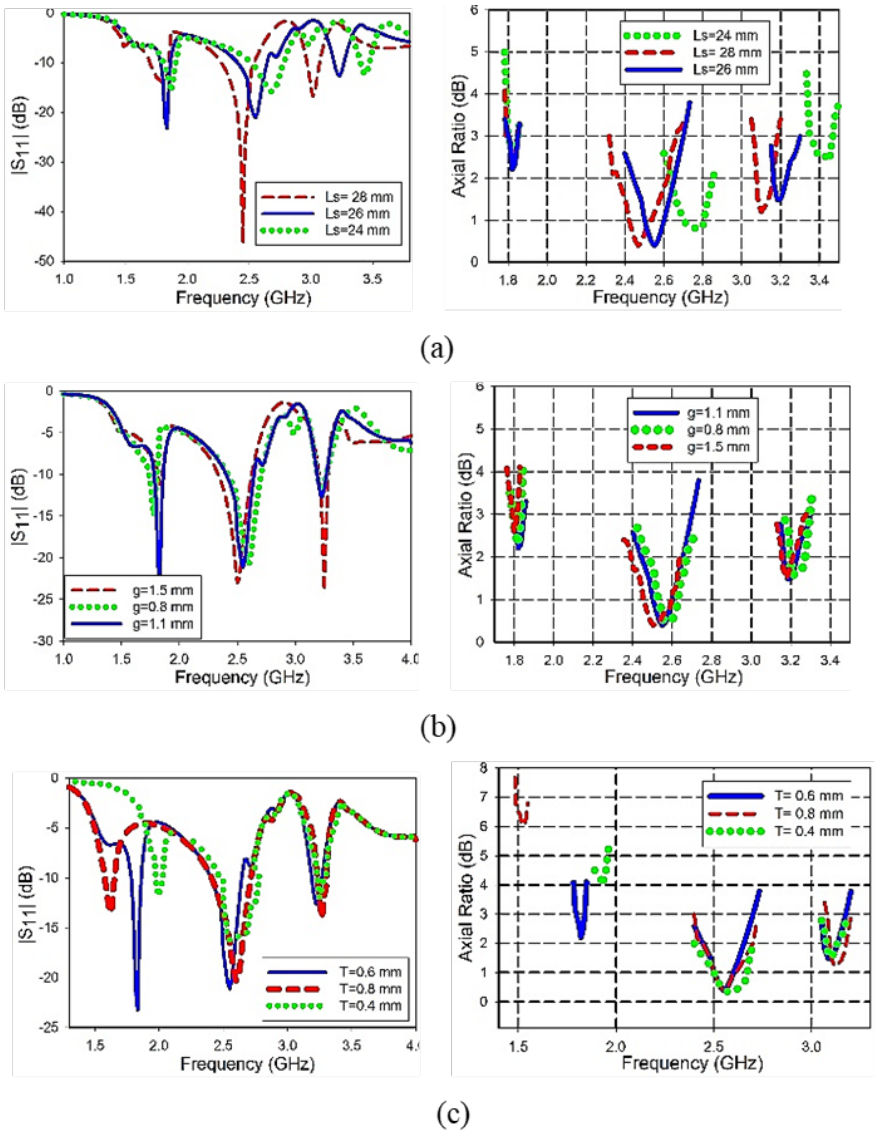

Figure 6.20: Simulated reflection coefficient and axial ratio values for parametric change in (a) length of strips (b) gap between strips (c) width of SRR metal ring.

shift in the resonance characteristics upon varying the gap between the strips. When varying the width of the SRR size, a shift in the first resonance can be observed as seen in Figure 6.20 (c). Also, the axial ratio values are found to increase in this case. Further, the second and third resonances can be independently tuned upon changing the dimensions of the middle and end strips respectively.

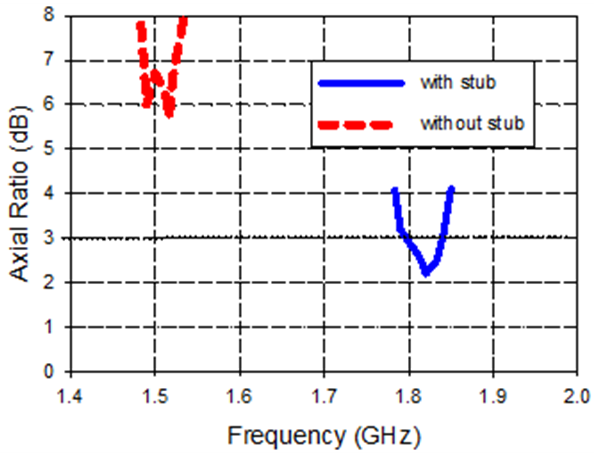

Figure 6.21: Simulated axial ratio values for for the proposed antenna for SRR with and without stub

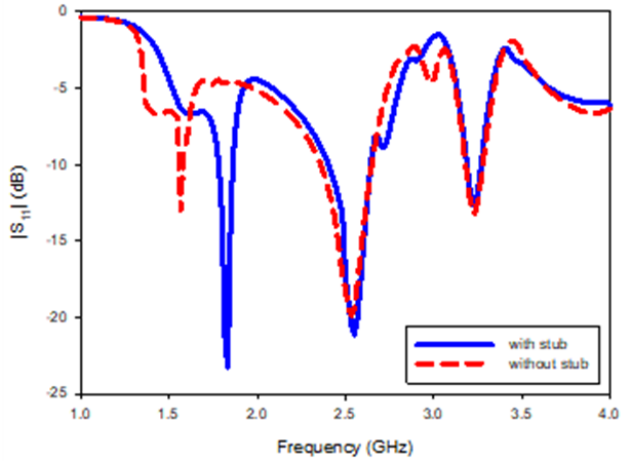

Figure 6.22: Simulated reflection coefficient magnitude values for the proposed antenna for SRR with and without stub

6.4.2.4 Effect of stubs

Here the AR values obtained for the proposed design is analysed in two cases: with and without stubs in the inner ring. It is observed that the AR values are lowered when the stubs are used. This can be seen in Figure 6.21. Also, a shift in the frequency of operation can be seen in Figure 6.22 (from 1.5 GHz without the stub to 1.8GHz with stub). This could be attributed to the fact that the additional stub in inner ring increases the effective inductive effect produced by the SRR structure. This leads to a slight change in resonance frequency and also the introduction of a phase shift. The stub length is so optimized to ensure 90° phase difference between the orthogonal

components; so that the AR value at resonance is reduced and circular polarization is achieved.

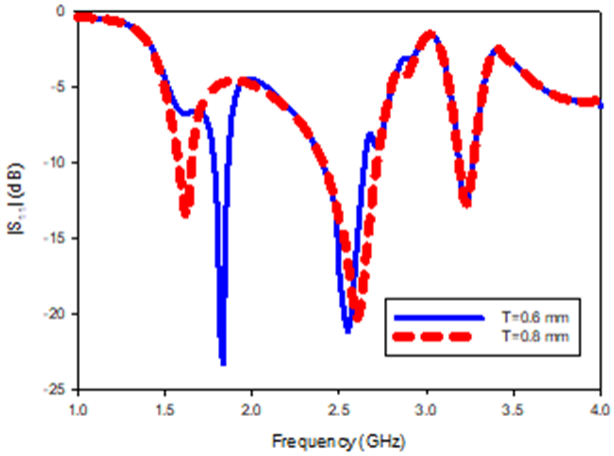

Figure 6.23: Simulated reflection coefficient magnitude values for the proposed antenna with change in SRR dimensions

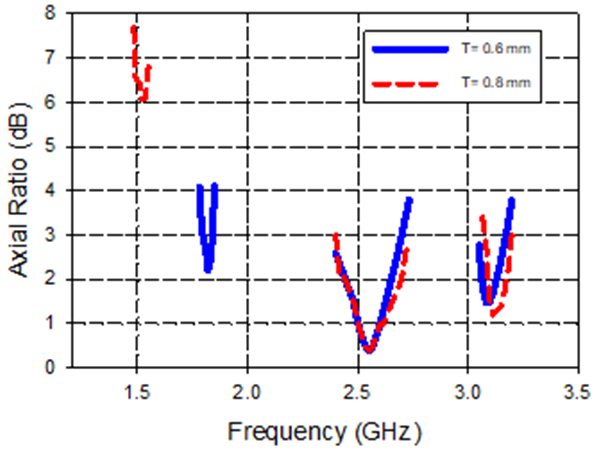

Figure 6.24: Simulated axial ratio values for for the proposed antenna with change in SRR dimensions

6.4.2.5 Independent Frequency Control

Here, the relation between dimensions of the strips and the SRR with the resonant frequencies obtained is studied. The variation in the resonance frequencies and the AR values with change in dimensions of the strips and the SRR show that each of the resonant bands can be independently controlled depending on the dimensions of the strips

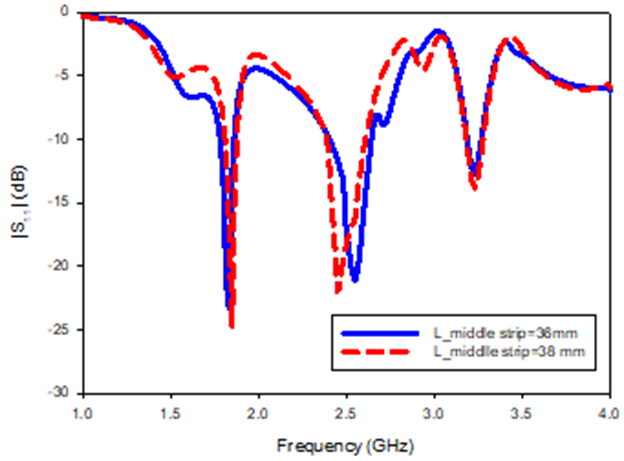

Figure 6.25: Simulated reflection coefficient magnitude values for the proposed antenna with change in middle strip dimensions

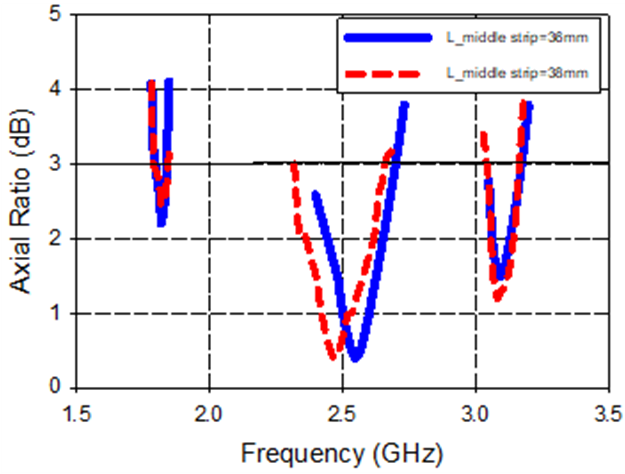

Figure 6.26: Simulated axial ratio values for the proposed antenna with change in middle strip dimensions

and the SRR. Figure 6.23 and Figure 6.24 show the variation in reflection coefficient and AR values with change in dimensions of the SRR. The first resonance is shifted to lower values upon increasing the width of the ring. Also, we observe an increase in the AR values. The AR values could be lowered to obtain CP on optimization of the stub length. The change in SRR parameter does not affect the operation of other two bands. Figure 6.25 and Figure 6.26 show the variation in reflection coefficient and AR values on changing dimensions of the middle strip. The second resonance is found to slightly shift towards lower value on increasing the strip length. The other two resonances remain more or less the same. The CP characteristics are maintained

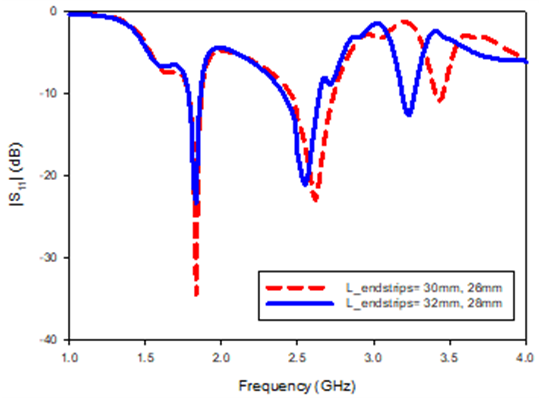

Figure 6.27: Simulated reflection coefficient magnitude values for the proposed antenna with change in dimensions of the strips at end

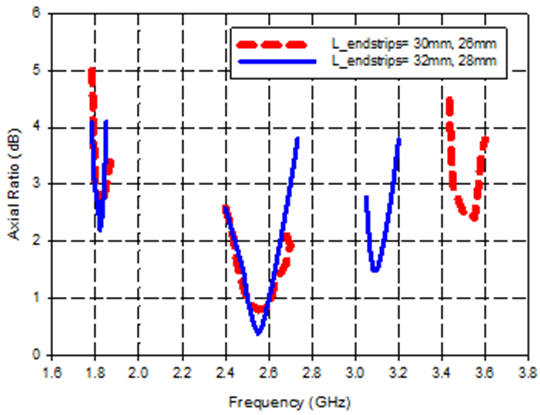

Figure 6.28: Simulated axial ratio values for the proposed antenna with change in dimensions of the strips at end

at all three resonant frequencies. Figure 6.27 and Figure 6.28 show the variation in reflection coefficient and AR values with change in dimensions of the other two strips. With change in length of the strips at the ends, the third resonance is found to mostly shift, with almost no shift in the resonance for the second and the first bands. The AR values slightly increase at third band but ARBW values remain almost the same for all frequencies.

6.4.2.6 Analysis of current distribution

The proposed antenna is simulated using ANSYS HFSS V15. The simulated current distributions at different resonance frequencies are analysed in the +z direction on the x-y plane to further understand the CP mechanism of the proposed antenna. The

current distribution is studied at phases t =0° and t =90° as shown in Figure 6.29. Figure 6.29 (a) shows the current distribution at 1.83 GHz for both phases, while Figure 6.29 (b) and Figure 6.29 (c) show the distributions at frequencies 2.5 GHz and 3.16 GHz, respectively.

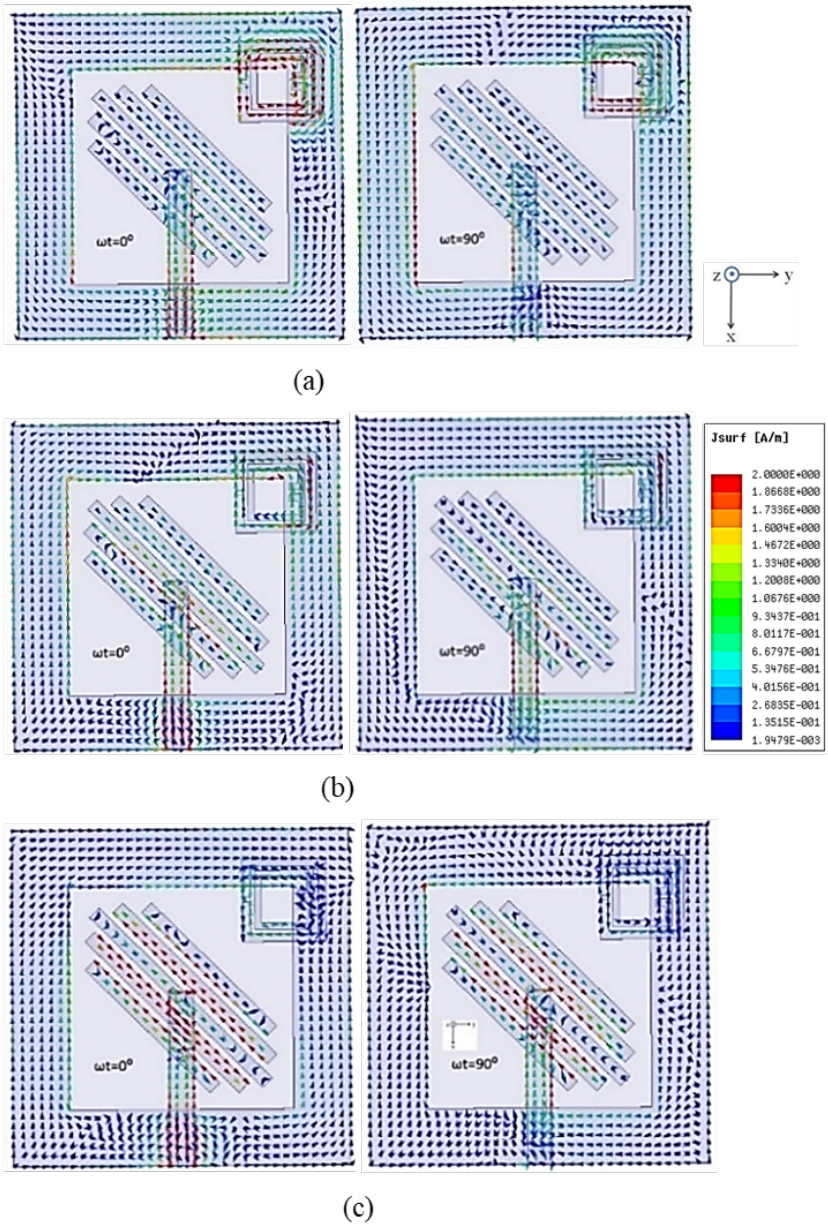

Figure 6.29: Simulated surface current distributions at (a) 1.83 GHz (b) 2.5 GHz (c) 3.16 GHz.

It is observed that as the phase changes by 90°, the current distribution vector at

all the resonant frequencies rotates clockwise when observed from the +z direction. Hence, RHCP is obtained at the three resonant frequencies of the proposed antenna. Also, it is observed that the direction of current reverses when changing the orientation of the strips by 90° and the SRR by 180°. The SRR is positioned to be suitably excited by the fields. Hence, LHCP is obtained at the three resonant frequencies for this configuration. It can be seen that the CP operation is obtained by a combination of the SRR and strip-slot configuration effects.

6.4.3 Simulation and Measurement Results

The proposed multi-band antenna was fabricated using an LPKF S103 PCB milling machine at AMSD lab at KFUPM and measured using an Agilent N9918A VNA. Photographs of the top and bottom sides of the fabricated prototype and the radiation pattern measurement setup are shown in Figure 6.30 The measured and simulated reflection coefficient characteristics and AR values are plotted and compared as shown in Figure 6.31 (a) and Figure 6.31 (b). Good agreement is obtained between the simulated and measured values. The slight shifts are due to fabrication tolerances.

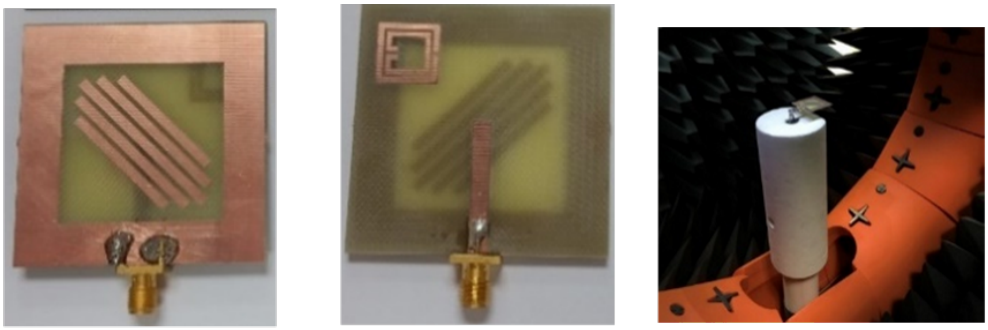

Figure 6.30: Fabricated prototypes of the proposed multiband antennas (a) Top view (b) Bottom view (c) Radiation pattern measurement setup.

The -10 dB measured impedance bandwidths obtained were 21.4% (1.48 GHz-1.87 GHz centered at 1.82 GHz), 12.8% (2.39 GHz-2.71 GHz centered at 2.5 GHz) and(4.5% (3.02 GHz-3.16 GHz centered at 3.1 GHz), while the simulated -10 dB bandwidths obtained were 4.9% (1.78 GHz-1.87 GHz centered at 1.83 GHz), 13.2% (2.38 GHz-2.71 GHz centered at 2.5 GHz) and 5.9% (3.21 GHz-3.4 GHz centered at 3.2 GHz). The 3dB measured ARBW values obtained were 4.37% (1.77 GHz-1.85 GHz, centred at

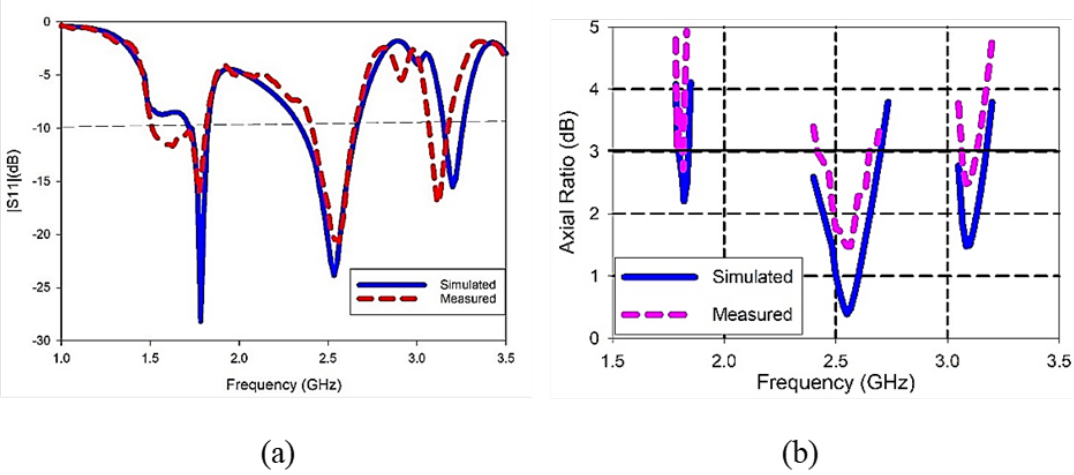

Figure 6.31: (a) Measured and simulated (a) reflection coefficients and (b) axial ratio values of the proposed multiband antenna.

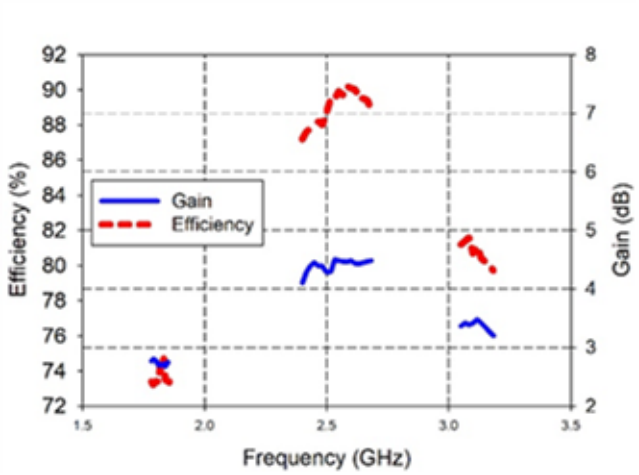

Figure 6.32: Measured gain and efficiency curves of the proposed multiband antenna.

1.83 GHz), 11.9% (2.4 GHz 2.7 GHz, centred at 2.52 GHz) and 3.57% (3.04 GHz - 3.15 GHz at centre frequency 3.08 GHz), while the simulated 3dB ARBW values obtained for the different resonance frequencies were 4.91% (1.79 GHz-1.86 GHz, centred at 1.83 GHz), 13.1% (2.39 GHz 2.72 GHz, centred at 2.52 GHz) and 5.48% (3.02 GHz to 3.19 GHz at centre frequency 3.1 GHz). The efficiency/gain values were also measured and plotted against the frequency as shown in Figure 6.32. The radiation patterns of the proposed antenna were measured in Satimo Star-Lab near-field chamber at MVG-Italy. Measured peak gains of 2.7 dBi, 4.2 dBi, 3.5 dBi and efficiencies of 75% , 90% , 82% were obtained at the resonant frequencies. Figure 6.33 compares the simulated

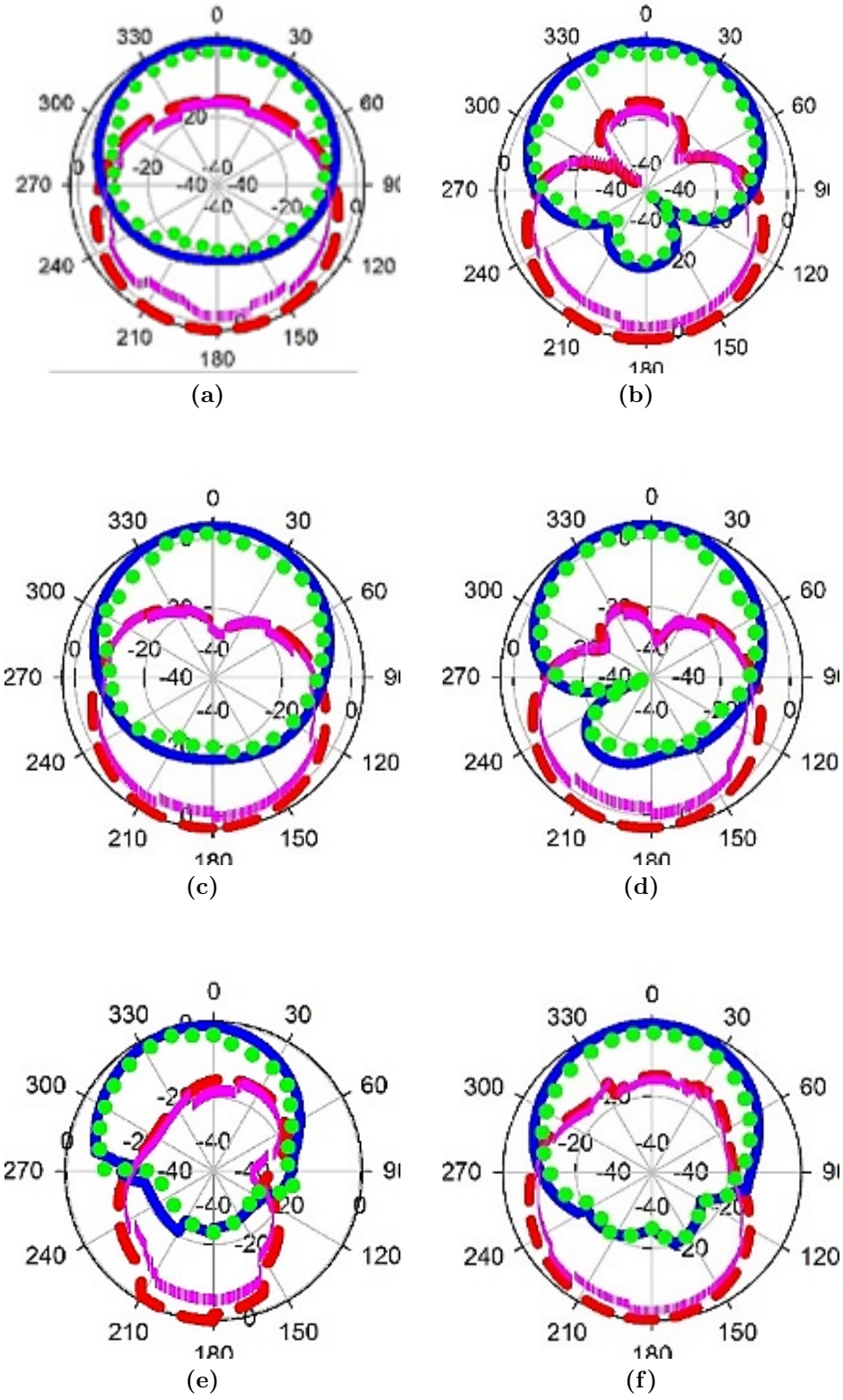

Figure 6.33: Simulated and measured radiation patterns of the proposed antenna at 1.85 GHz (a) phi=0, (b) phi=90, 2.5GHz (c) phi=0, (d) phi=90, 3.16 GHz (e) phi=0, (f) phi=90 (—-LHCP — RHCP —— LHCP(measured) .....RHCP (measured)

and measured radiation patterns in two principle planes. It is observed that simulated patterns match with the measurements at all the resonant frequencies. The antenna radiates RHCP in the upper hemisphere and LHCP in the lower hemisphere. Cross polarization levels are below -20 dB compared to the co-polarization as observed in the measured radiation patterns. The proposed antenna is smaller in size, provides wider impedance BW compared to other three band antennas, along with good efficiency and control of sense of polarization with wide ARBW.

6.4.4 Study on shifted strip and SRR orientation

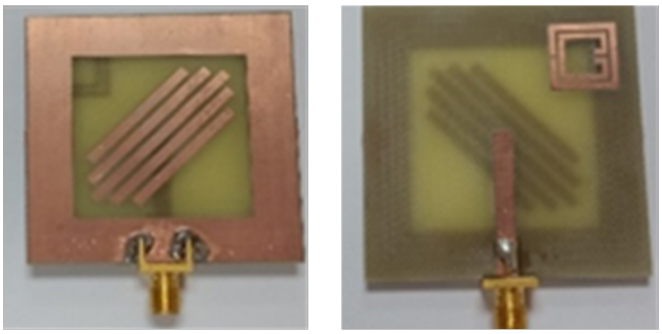

(a) (b)

Figure 6.34: Fabricated prototypes for the proposed antenna on shifting orientation of the strips and SRR (a) Top view (b) Bottom view.

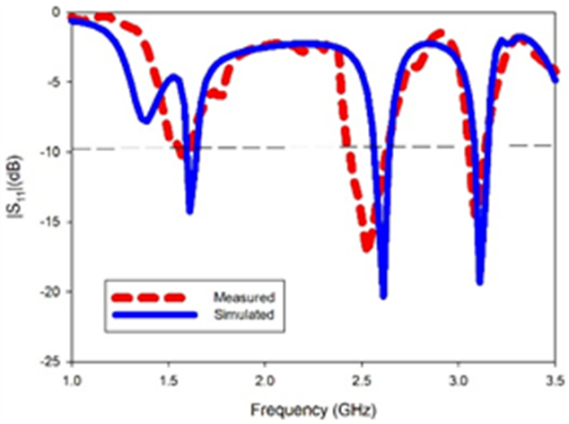

Figure 6.35: Measured and simulated reflection coefficients of the proposed multiband antenna on shifting orientation of the strips and SRR.

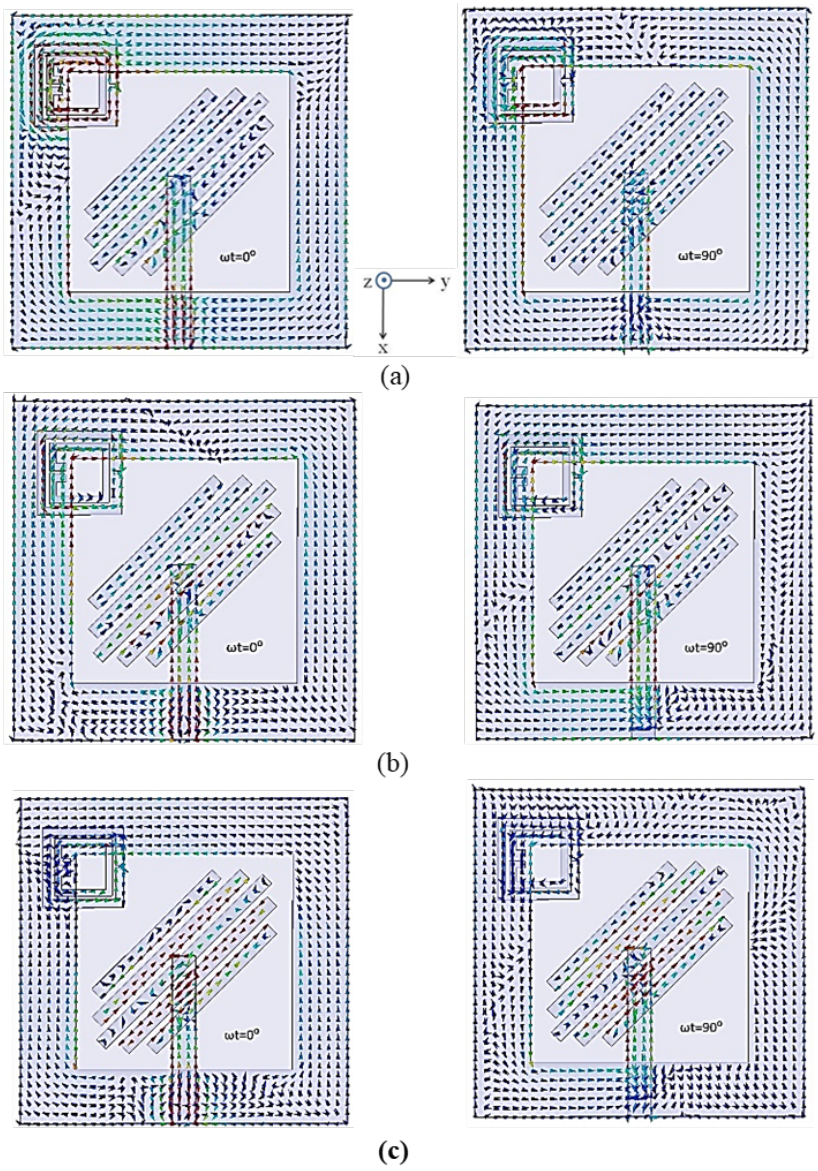

Figure 6.36: Simulated surface current distributions at (a) 1.65 GHz (b) 2.6 GHz (c) 3.2 GHz.

The orientation of the strips and SRR are shifted with respect to the slot and the reflection coefficient curves and surface current distributions obtained are studied. The top and bottom views of the fabricated prototpe are shown in Figure 6.34 (a) and Figure 6.34 (b). Figure 6.35 shows the simulated and measured reflection coefficient values obtained on simulation and measurement of the antenna prototype. The centre frequencies of resonance obtained are at 1.65 GHz, 2.6 GHz and 3.2 GHz. The current distributions are simulated and analysed at these frequencies. From Figure 6.36 it can

be seen that the direction of current reverses when changing the orientation of the strips by 90° and the SRR by 180°. Figure 6.36 (a) shows the current distribution at 1.65 while Figure 6.36 (b) and Figure 6.36 (c) show the distributions at frequencies 2.6 GHz and 3.2 GHz, respectively, for phases t =0° and t =90°. The SRR is positioned so as to be suitably excited by the fields. Hence, left hand circular polarization (LHCP) is obtained at the three resonant frequencies for this configuration. It can be seen that the CP operation is obtained by a combination of the SRR and strip-slot configuration effects.

6.5 A Multi-Band U-Strip and SRR Loaded Slot Antenna with Circular Polarization Characteristics

A compact multiband circularly polarized slot antenna is proposed in this section. An F-shaped microstrip feedline is used to excite the square slot antenna loaded with a U-shaped strip and a split ring resonator (SRR) to generate three circularly polarized bands at 1.5 GHz, 2.75 GHz and 3.16 GHz. A meandered slot is used in the feedline and the U-strip to improve the axial ratio bandwidth (ARBW). The meandered feedline excites the slot to produce resonance at 2.5 GHz. This resonance along with that of the F-shaped feed, loaded SRR and U-strip combine to give rise to three circularly polarized bands which can be tuned depending on the feed, SRR and U-strip dimensions. The orientation of the F-shaped feed decides the sense of polarization of the three circularly polarized bands of the proposed antenna. The proposed antenna is fabricated on a substrate of FR4 material with dimensions 50 x 50 x 1.56 mm^3. The antenna is prototyped and measured in terms of impedance bandwidth, ARBW, gain and efficiency. The simulated and measured results show reasonably good agreement.

6.5.1 Antenna Geometry

The proposed antenna geometry offering circularly polarized triple band operation is shown in Figure 6.35. The antenna is designed on an FR4 substrate of size 5050 mm^2, permittivity (ϵ_r)= 3.6, height (h)= 1.56 mm and loss tangent=0.02. The top view of

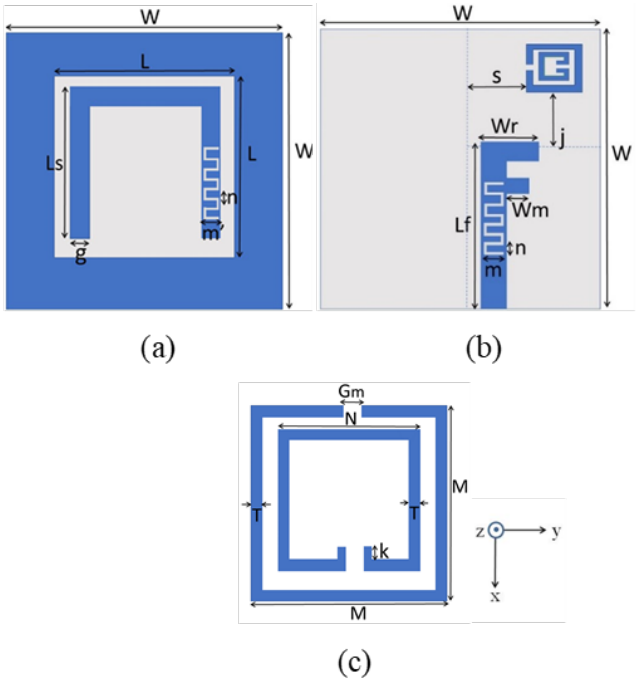

Figure 6.37: Geometry of the proposed multiband antenna (a) top view (b) side view (c) SRR structure. [L=33.2, W=50, Wr=9.6, Wm=5.3, Lr=18, Lm=25, Lf=31.2, g=4, r=2, Wf=3.6, s= 8.6, j=8.4, k=1.65, M=6, N=4, T=0.6, Gm=0.6, h=1.56, m=3, n=1.4, m=3.6, width of meander= 0.2], All in mm.

the antenna is shown in Figure 6.37 (a). A square slot of side length (L) of 33.2 mm is etched out on top of the substrate so that the slot resonates at 2.5 GHz. A U-shaped metallic strip is left in the slot. The bottom view of the antenna is shown in Figure 6.37 (b). A 50 ω feedline offset from the x- axis by 1.2 mm is printed at the bottom of the substrate. Two horizontal extension strips are attached to the top of the feedline to make an F-shaped feed. Meandered slots are etched on the right arm of the U-strip and the feedline. Also, an SRR is printed on the bottom layer as in Figure 6.37 (b) with its dimensions as shown in Figure 6.37 (c).

6.5.2 Operating Principle

The F-shaped meandered feedline excites the slot so that it produces resonance at its fundamental resonant mode (Balanis (1992)). The magnetic and electric field lines produced upon the excitation of the slot cause the U-strip and the SRR to resonate at their resonant frequencies. The SRR is placed and oriented in the slot such that it can

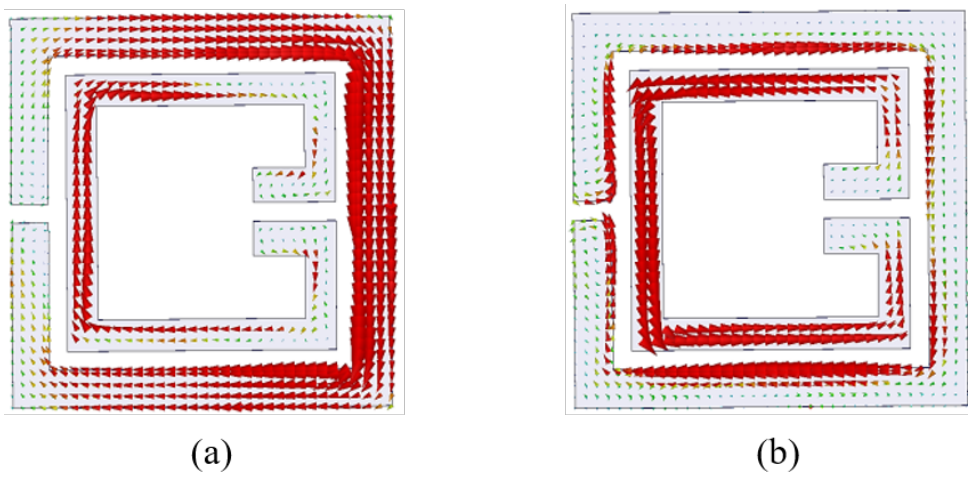

Figure 6.38: Surface current distribution for the SRR at (a) 1.6 GHz and (b) 2.89 GHz.

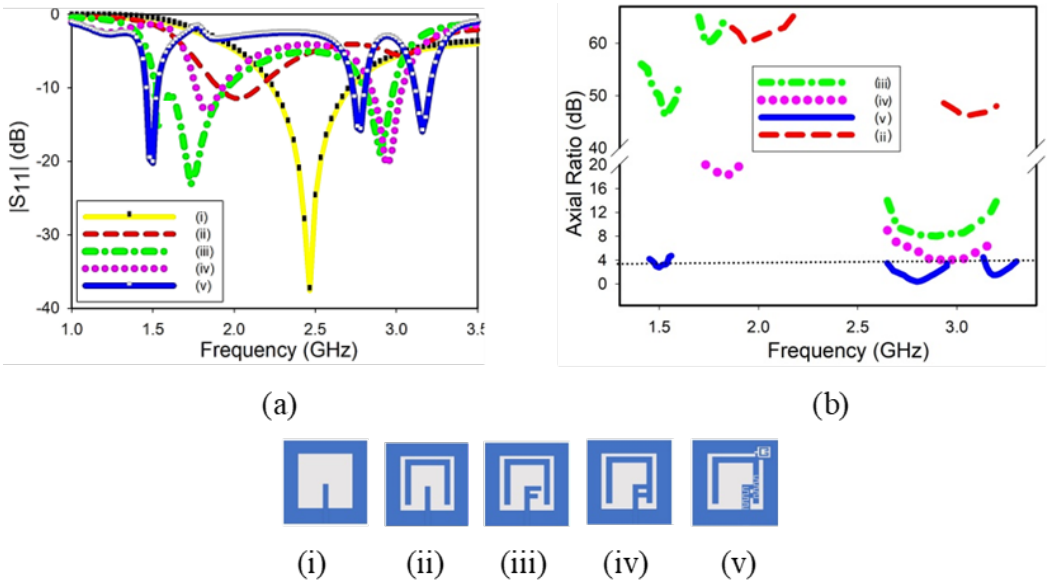

Figure 6.39: Design evolution of proposed antenna and its effects on the simulated :(a) reflection coefficient curves and (b) axial ratio values with frequency.

allow for maximum passage of the time varying axial magnetic field lines through it (Engheta and Ziolkowski (2006), Ishikawa *et al.* (2007)). The SRR structure acts as an LC resonator and can be modelled using the method given by Ishikawa *et al.* (2007). Here, the SRR dimensions are carefully chosen in order to produce resonance at 1.6 GHz upon field excitation. A higher order mode at 2.89 GHz is also observed. The

current distributions around the SRR and the inner ring of the SRR can be seen at the two resonance frequencies in 6.38 (a) and 6.38 (b) respectively. The maximum current distribution is observed around the inner ring for the higher resonance mode. The U-strip can resonate at different frequencies depending on its arm lengths. Combination of these with that of the slot and SRR gives rise to the circularly polarized bands of the proposed multiband antenna. The SRR contributes to the lowest resonance frequency hence leading to miniaturization of the proposed design.

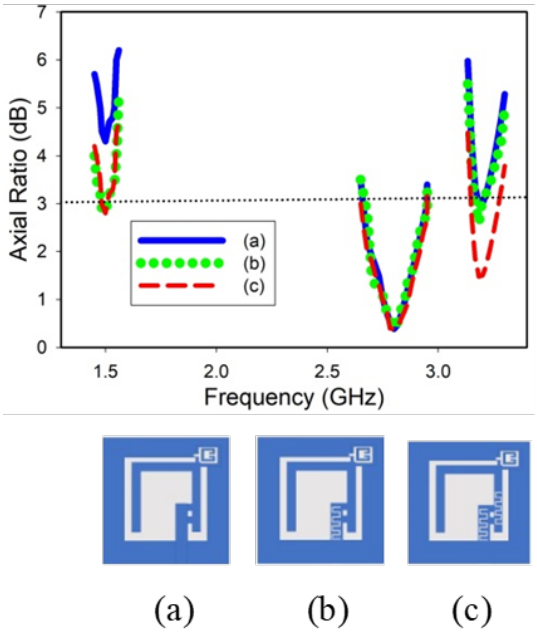

Figure 6.40: The effect of meandered slots on the simulated axial ratio values for the proposed antenna.

The design evolution and the effects of various parts of the antenna are shown in Figure 6.39. The slot initially resonates at 2.5 GHz when excited with the microstrip feed line. When loading the slot with the U-strip, the resonance is found to shift to 2 GHz. Also, a slight resonance is observed around 2.9 GHz. This could be due to the resonance introduced by the U-strip. The use of the F-shaped feed lowers the AR value at 2.9 GHz. This could be attributed to the CP wave obtained upon the combination of the resonances produced by the F-shaped feed and that of the U-strip. The offset at the feedline further improves the AR values. Also, the first resonance is now slightly shifted to 1.8 GHz. Thus, the modified feedline is used to improve the reflection coefficient and AR response of the initial dual-band antenna obtained

(without SRR loading). The horizontal stubs of the F shaped feedline and the offset introduce the necessary phase shift required for the orthogonal components that help improve the ARBW values. Besides, the addition of the y-directed horizontal stubs changes the input impedance to the extent that the —S11— response of the antenna is improved. The improvement in return loss characteristics is shown in 6.39. Now, loading the structure with an SRR and introducing the meandered slots, additional bands are produced at 2.7 GHz and 3.1 GHz. Also, the reflection coefficient values at 1.5 GHz are improved and the resonance at 2.9 GHz is shifted to 3.16 GHz due to the fundamental and higher order resonance modes of the SRR (Sarkar *et al.* (2014)). The fundamental resonance produces the CP resonance band at 1.5 GHz. The higher order mode of the SRR provides resonance at 2.75 GHz. Thus, the resonance bands can be tuned depending on the SRR, F-shaped feed and U-strip dimensions. The effect of meandering on the AR values of the resonance bands is shown in Figure 6.40. The introduction of meandered slots in the feedline and U-strip lower the AR values at the first and third bands respectively.

6.5.2.1 Surface Current Distribution

In order to better explain the CP operation of the proposed multiband antenna, the current distributions are simulated and studied at each of the three resonance frequencies. The antenna is placed on the x-y plane and the current density vectors are analyzed in the +z direction for phases t =0° and t =90° as shown in Figure 6.38. The distributions at the resonant frequencies 1.5 GHz, 2.75 GHz and 3.16 GHz for the different phases are shown in Figure 6.41 (a), Figure 6.41 (b) and Figure 6.41 (c) respectively.

The sense of polarization at the three bands is decided by observing the direction of rotation of the current distribution vector from the +z direction. In this case, it can be seen that at the resonant frequencies, the vectors rotate in the clockwise direction when there occurs an orthogonal shift in phase. This indicates the presence of right hand circularly polarized (RHCP) waves. The figure clearly shows that the CP resonance bands at the three resonant frequencies are obtained by exciting the SRR modes (fundamental mode) and U-strip excited by the F-shaped feed, the inner ring of the SRR (higher order mode) and U-strip, and the F-shaped feed and the U-strip. The different lengths of the U-strip when excited, produces the necessary resonance to combine with the other modes to generate the CP bands. In addition, on altering the

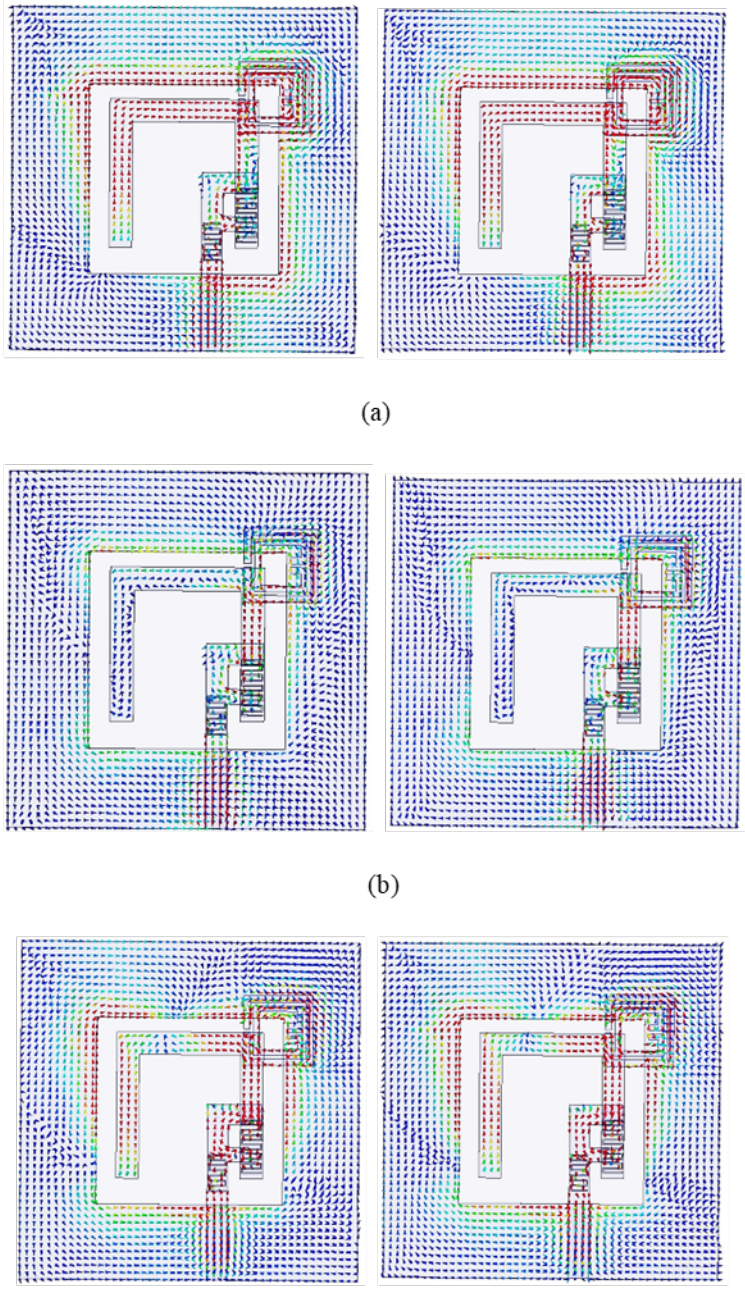

Figure 6.41: Simulated surface current distribution for the proposed antenna at: (a) 1.5 GHz, (b) 2.75 GHz, (c) 3.16 GHz

orientation of the F-shaped feed and the SRR by 90° and 180° respectively, reversal of the current direction occurs, hence giving rise to left hand circularly polarized (LHCP) waves at the resonant frequencies.

6.5.2.2 CP Mechanism

The CP mechanism is further analyzed by studying the frequency response at each band of operation. The U-strip can be thought of as resonating at different frequencies depending on the different lengths of the U-strip that are excited. The selection of the strip length is done based on the guided wavelengths for different frequencies. The guided wavelength (λ_g) for a resonance frequency of $f_{(r,GHz)}$ is given by Balanis (1992):

$$\lambda_g = \frac{300}{f_{r,GHz}\sqrt{\epsilon_{eff}}} \tag{6.8}$$

where effective dielectric constant ϵ_{eff} is calculated as follows:

$$\epsilon_{eff} = \frac{\epsilon_r + 1}{2} + \frac{\epsilon_r - 1}{2\sqrt{1 + 12(h/W_f)}} \tag{6.9}$$

W_f and h denote width of the feedline and thickness of the substrate. The lengths of the strip for different resonance frequencies is taken to be approximately equal to 1/2 λ_g at the corresponding frequencies.

The first CP response at 1.5 GHz is found to be obtained due to the fundamental resonance mode of the SRR at 1.6 GHz and the resonance obtained around 1.4 GHz is due to the excitation of the two arms (L-shape-52mm) of the U-shaped strip. The maximum surface current distribution can be seen around these regions for the first resonance band as shown in Figure 6.41 (a). The meanders at the feed line help to lower the AR values at this band.

The second CP band can be attributed to the higher order resonance mode of the SRR at 2.89 GHz and the right side of the U-strip of 26 mm which gives a 1/2 λ_g resonance at around 2.65 GHz. Thus, a mid-band CP resonance at 2.75 GHz is obtained. The surface current distribution for this frequency can be seen in Figure 6.41 (b).

The third CP band arises due to the slot fundamental resonance at 2.5 GHz and the resonance provided by the part of the strip of length 24 mm that corresponds to

a λ_g of 47.6 mm (It can be seen from the current distribution that the vectors cancel along the other regions of the U-strip). This value corresponds to a frequency of 3 GHz and hence, a mid-band resonance at around 2.8 GHz which shifts to 3.17 GHz due to the variation in current and field distributions upon the introduction of the SRR.

6.5.2.3 Effect of the meandered gaps

The effect of the meandered gaps on the frequency response of the proposed antenna is studied based on the design of the gaps and the capacitive effects produced due to them. Consider a set of meandered gaps where C_g represents the capacitance of one set of fingers to the ground and C_m the capacitance between two sets of fingers. Then for an array of N fingers having length l, the following equations can be defined:

$$C_g = NC_1 l/2 \tag{6.10}$$

$$C_m = NC_2 l/2 \tag{6.11}$$

where

$$C_1 = C_e \tag{6.12}$$

$$C_2 = 1/(2(C_o - C_e)) \tag{6.13}$$

Here C_o and C_e are defined as the odd mode and even mode capacitances respectively. They can be calculated depending on the dielectric characteristics, the characteristic impedance and phase velocity. It also depends on the finger width and finger separation (**?**).

The frequency shift due to the effect of the meandered gaps on a strip of length l_o can be relatively calculated as (**?**):

$$f_{r,new} = \sqrt{\frac{l_o}{l(N-1)}} f_r \tag{6.14}$$

Where $f_{(r,new)}$ is the new resonance frequency obtained after loading of the meandered gaps. In our proposed design, the fundamental resonance frequency of the slot which depends on the length of the slot L_{slot} and the dielectric constant of the substrate ϵ_r

is calculated as (Balanis (1992)):

$$f_{r,slot} = \frac{c}{2L_{slot}}\sqrt{\frac{2}{1+\epsilon_r}} \tag{6.15}$$

Here c is the speed of light in vacuum.

Upon the introduction of the meandered gaps in the feed line, the resonance frequency of the slot is found to shift to 1.59 GHz. Thus, lower AR values are observed at the first resonance frequency of 1.5 GHz when the gaps are introduced in the feed line.

The lower half of the U-strip of length 13 mm resonates at a half wavelength of the frequency 6 GHz which shifts to 3.08 when introducing the gaps. This frequency shift helps lower the AR values at the third band of resonance where the centre frequency obtained is around 3.17 GHz.

6.5.2.4 Equivalent Circuit Analysis

The equivalent circuit analysis is done using the circuit models for each electromagnetically coupled component of the design and extracting the corresponding circuit parameters. The equivalent circuit for the unloaded slot is shown in Figure 6.42 (a) where Ls and Lsh/Csh denote the series inductance of the lossless feedline and the equivalent inductive/capacitive effects of the slot. The equivalent circuit for a set of meandered gaps is shown in Figure 6.42 (b) where Ct corresponds to the capacitance of the strips. The total equivalent circuit for the proposed geometry is obtained after including the effect of the meandered gaps as well as that of the mutually coupled SRR which is denoted by a parallel L-C circuit (Le and Ce). The complete circuit is shown in Figure 6.42 (c). The magnetic coupling of the SRR with the slot is characterized by the coupling coefficient M. The series feed inductance of the offset F-shaped feed is denoted as Ls and that of the U-strip is defined as Lu. The different mutual capacitance effects and gap capacitances introduced by the meandered gaps on the feed and U-strip are denoted as Cm/Cg and Cm/Cg respectively.

The circuit can be simplified as shown in Figure 6.42 (d) using the equivalent circuit parameters denoted by Ce, Le and Ce. The parts A and B of the equivalent circuit in Figure 6.42 (c), show the effect of meandering on the simplified circuit. Upon extraction of the circuit parameters, the resonances for parts A and B are obtained to be around 1.5 GHz and 3.15 GHz which explains why the AR values are modified for

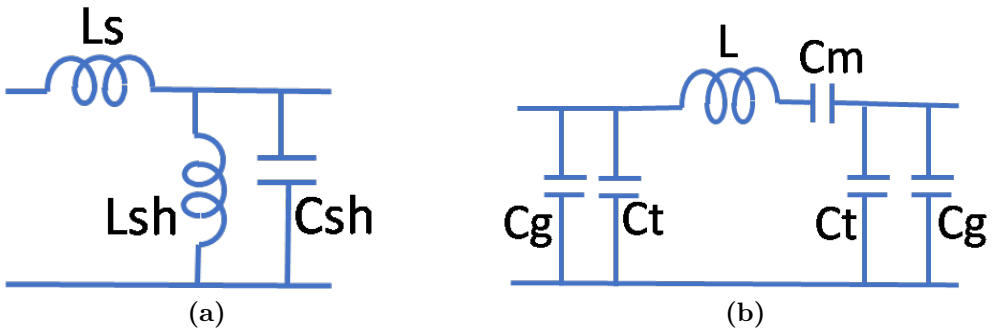

(a) (b)

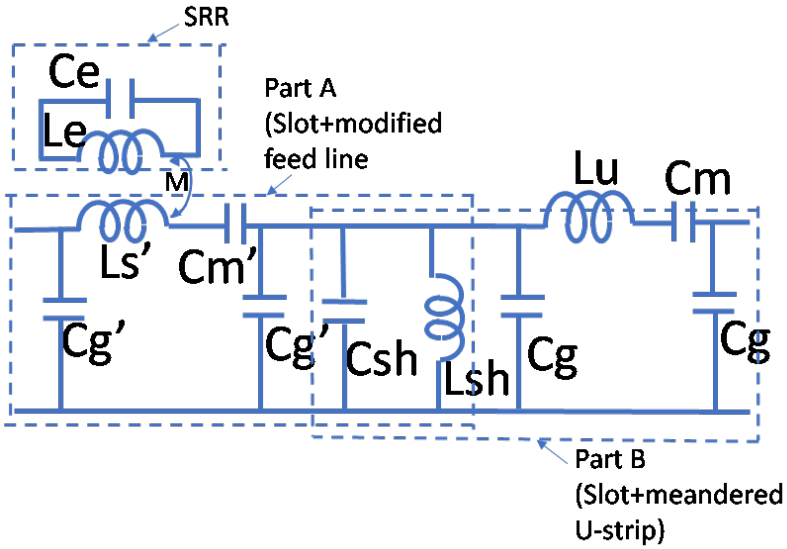

(c)

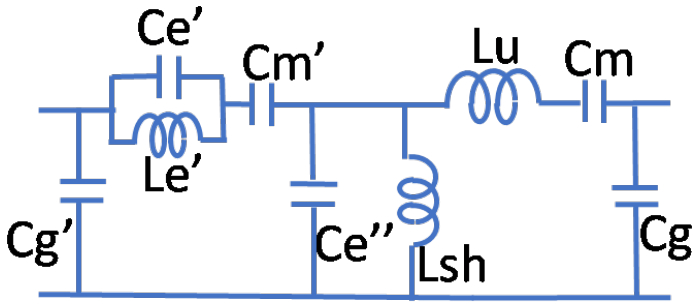

(d)

Figure 6.42: (a) Equivalent circuit of the unloaded slot with microstrip feed (b) Equivalent circuit model for interdigitated capacitors (c) Equivalent circuit of the proposed antenna (loaded with modified meandered feed, meandered U-strip and loaded SRR) (d) Simplified equivalent circuit for the proposed antenna.

these resonances due to the additional capacitive effects introduced by the meandering.

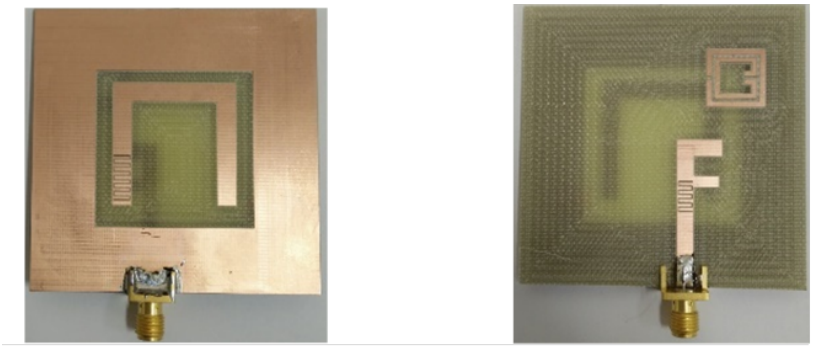

Figure 6.43: Fabricated prototypes (a) top, and (b) bottom views.

6.5.3 Results and Analysis

The proposed antenna was simulated, fabricated and measured for the reflection coefficient magnitudes and radiation patterns at the different resonant frequencies. For simulation, the ANSYS HFSS 16.0 software was used. Fabrication and measurement were done at the AMSD Lab at KFUPM using an S103 LPKF machine and an Agilent N9918A Vector Network Analyzer. The top and bottom views of the proposed antenna prototype are shown in Figure 6.43 (a) and Figure 6.43 (b). The effects on the simulated and measured reflection coefficient magnitudes and axial ratio values with change in frequency are plotted as shown in Figure 6.44 (a) and Figure 6.44 (b). The simulated and measured results can observed to be in fairly good agreement.

The -10 dB impedance bandwidths obtained on measurement of the reflection coefficient magnitudes at the resonant frequencies were 10% (1.37 GHz 1.52 GHz with centre frequency of 1.5 GHz), 9.1% (2.62 GHz 2.87 GHz with centre frequency at 2.75 GHz) and 7.3% (3.06 GHz 3.29 GHz with centre frequency at 3.14 GHz), while the measured ARBWs were 9.3% (1.37 GHz 1.51 GHz with centre frequency at 1.5 GHz), 7.3% (2.65 GHz 2.85 GHz with centre frequency at 2.75 GHz) and 8.5% (3.1 GHz 3.37 GHz with centre frequency at 3.15 GHz).

The variation in the AR values with the elevation angle (θ) is plotted and shown for the three resonance frequencies in Figure 6.44 (c). The AR values can be observed to be below 3dB for a minimum variation of +/-5° from the central axis for the three resonance frequencies. The radiation patterns for the proposed antenna at its

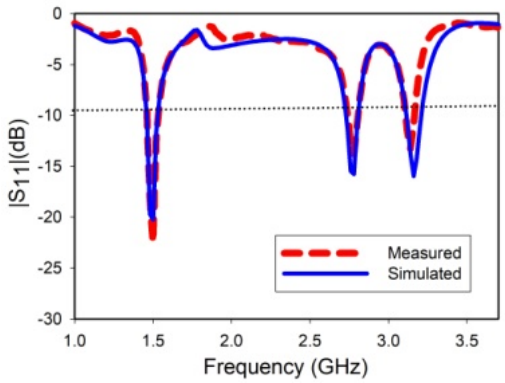

(a)

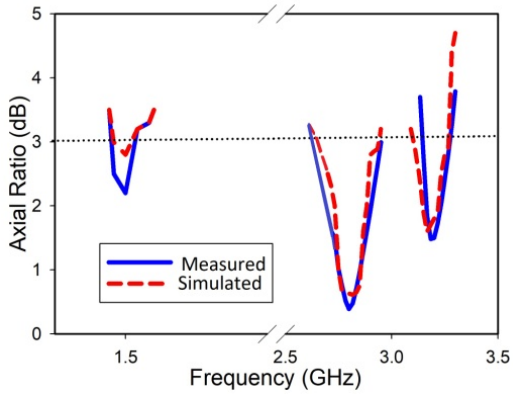

(b)

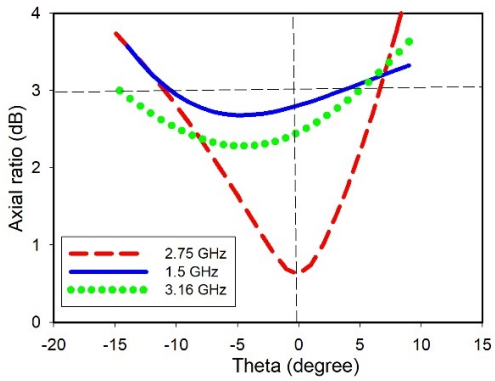

(c)

Figure 6.44: Variation in characteristics of the proposed antenna : (a) reflection coefficient magnitudes, and (b) axial ratio values, versus frequency (c) axial ratio values, versus theta.

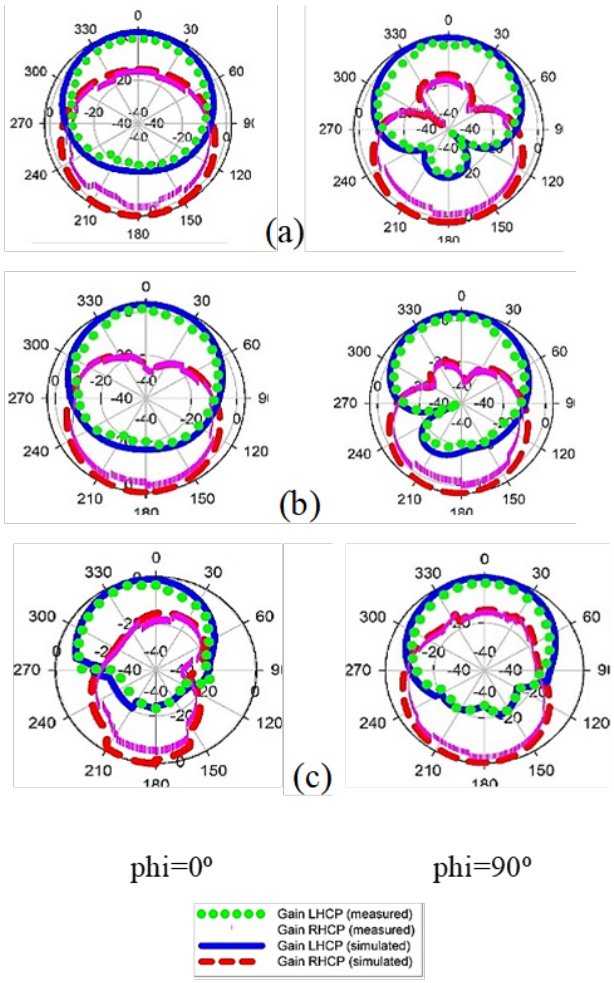

Figure 6.45: Radiation patterns obtained for the two orthogonal planes on simulation and measurement of the proposed antenna at: (a) 1.5 GHz, (b) 2.75 GHz, (c) 3.16 GHz

resonance frequencies were measured in a Satimo Star-Lab near-field chamber. The values obtained were plotted and compared against the simulated ones for phi=0° and phi=90° orthogonal planes as seen in Figure 6.45. The cross polarization values are below -20 dB. In addition, RHCP is radiated in the upper hemisphere. The radiation efficiency and peak gain values obtained on measurement were recorded at the three resonance frequencies as 80% / 3.2 dB, 94% / 4.5 dB, and 85% / 3.5 dB, respectively. The plot seen in Figure 6.46 shows the variation of the measured gain and efficiency values with frequency. Compactness, ease of control in sense of polarization, high impedance BW and ARBW values and good efficiency values are the favourable features in the proposed design compared to other designs in literature.

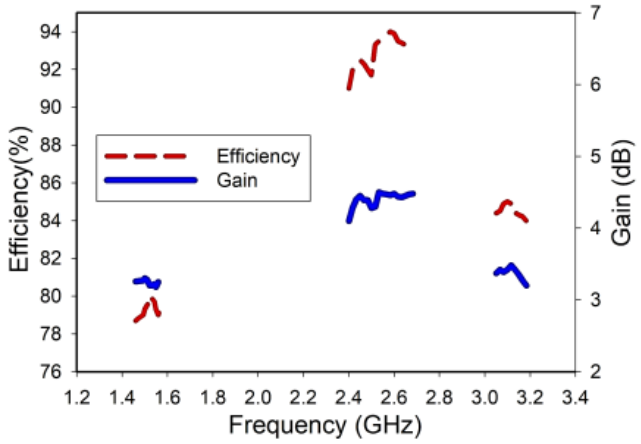

Figure 6.46: Measured peak gain and radiation efficiency values versus frequency for the proposed antenna.

6.6 Multiband Slot Antenna with Single Circularly Polarized Band Using SRRs

Here, in this section, a quad band SRR loaded square slot antenna is presented that resonates at 2.4 GHz, 4.33 GHz, 9 GHz and 10.9 GHz. The different bands of resonance can be attributed to the slot resonance and the resonant properties of the loaded SRRs. Here constant values of gain and efficiency are obtained throughout the bands of operation. Also, circular polarization can be observed at the highest frequency band due to the presence of the S-shaped resonator. The third resonance band offers wideband operation.

6.6.1 Antenna Geometry

The proposed antenna is designed on an Fr4 substrate of height (h) = 1.56 mm and permittivity (ϵ_r) = 3.6. A square slot of dimension 34mm x 34mm is cut out from the top of the substrate as shown in Figure 6.47 (a). The slot is designed to operate at 2.42 GHz. The feed line and SRRs are printed at the bottom of the substrate as shown in Figure 6.47 (b). The 50 Ω microstrip line is designed with length 30mm and width 3.05 mm. In order to obtain circular polarization, we design one pair of SRR with an S-shaped structure, with the rings connected to one another. The other pair of SRR is designed as a simple ring structure with split of width 0.6 mm. The SRR

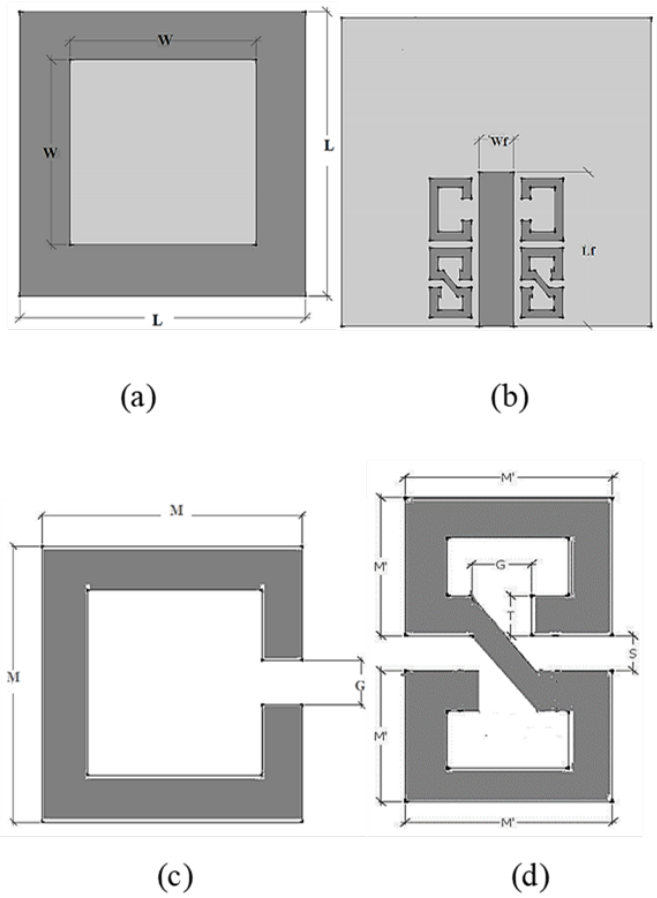

Figure 6.47: Antenna Geometry (a) Top view (b) Bottom view (c) Single ring SRR structure (d) S-shaped SRR structure.

structures are shown in Figure 6.47 (c) and Figure 6.47 (d).

6.6.2 Operation

The resonant frequency of the square slot which is excited to resonate at its fundamental TM01 mode can be given by Equation 3.1. The unloaded slot antenna structure when simulated can be found to resonate at 2.42 GHz. When loaded with each of the resonators, multiple bands of operation can be observed. A step by step approach is carried out to study the effect of the SRR loading on the slot antenna radiation. This can be seen from Figure 6.48 which shows the change in resonance behavior of the slot antenna for the different configurations. When the slot antenna is loaded with the simple square split ring resonators, an additional wideband resonance is observed from

6.43 GHz8.86 GHz. On the other hand, when the slot is loaded with the S-shaped connected resonators alone, additional bands at 4.3 GHz and 10.9 GHz are produced.

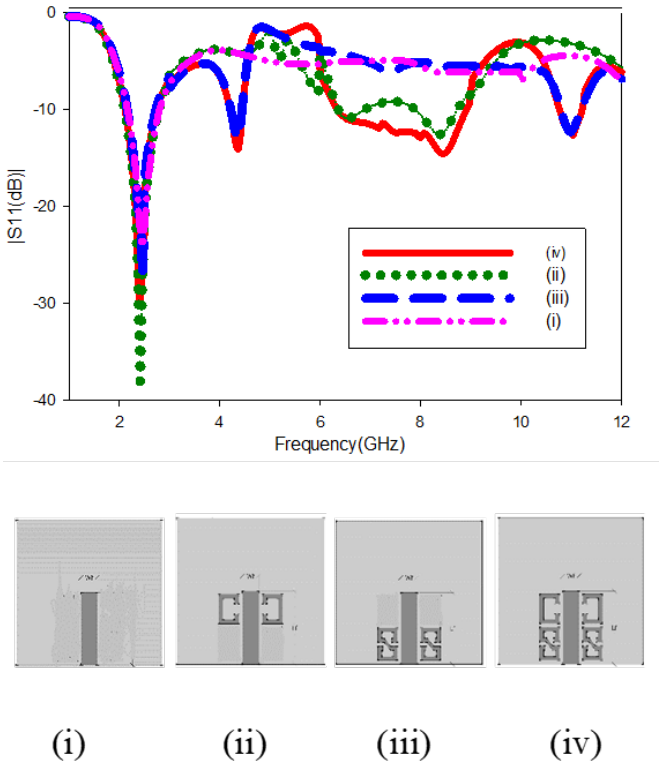

Figure 6.48: Effect of SRR loading on resonance of the proposed slot antenna : simulated reflection coefficient magnitudes for different configurations of the proposed quad band antenna.

Thus, the entire slot antenna structure loaded with the two pairs of SRR gives a quad band response. As the S- shaped SRR is shifted farther from the other pair of SRR and nearer to the feed line end, the impedance matching at 10.9 GHz is found to improve. This could be due to change in coupling of field lines of the pair of S-shaped SRRs with the slot field lines and also with those of the other pair of SRRs. The slot resonance is found to be largely unaffected by the loading of the SRRs.

Similar conclusions about the resonant behavior of the loaded slot antenna can be drawn on observation of the current distributions shown in Figure 6.49. At 2.42 GHz, the magnitude of surface current distribution is found to be maximum around the slot. It is evident that the S-shaped SRRs are excited at 4.3GHz and 10.9GHz as the peak surface current is observed around them at these frequencies. The maximum

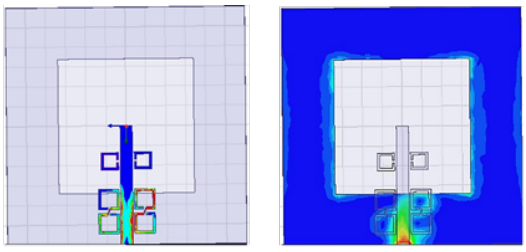

(a) 2.42GHz

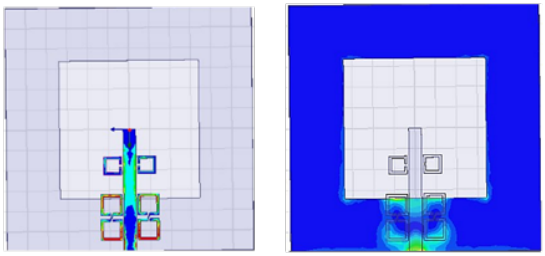

(b) 4.3GHz

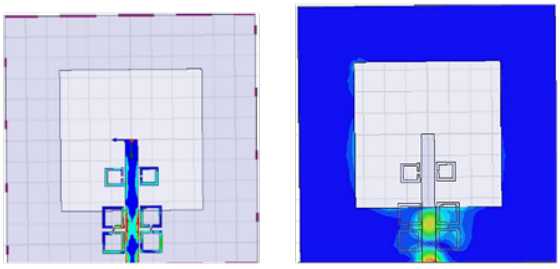

(c) 8.46 GHz

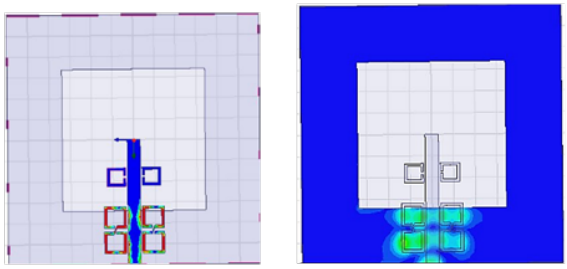

(d)10.9 GHz

Figure 6.49: Surface current distributions for the proposed antenna at diffferent frequencies.

excitation of the S-shaped SRR at 10.9 GHz could possibly cause the antenna to radiate circularly polarized waves around this frequency, as spiral resonators generally

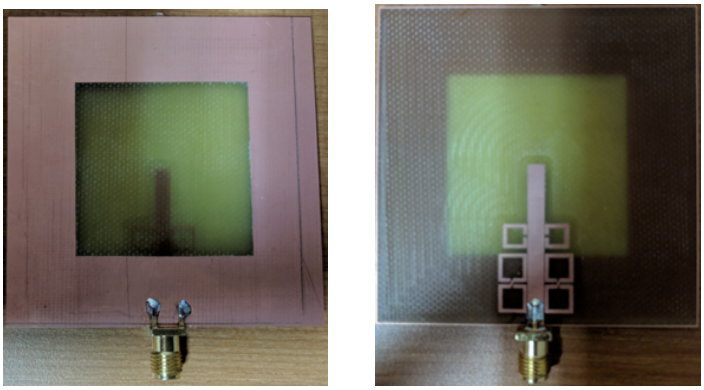

(a) (b)

Figure 6.50: Photographs of fabricated prototype (a) top view (b) bottom view.

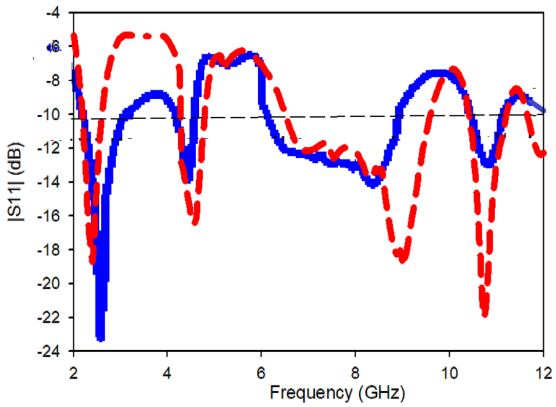

Figure 6.51: Simulated and measured reflection coefficient magnitudes for the proposed quad band antenna.

provide orthogonal components required for CP excitation. At 8.46GHz, it can be observed that the peak current flows along the simple SRR resonators which excite them to produce the third band of resonance. This helps to explain the quad band operation of the SRR loaded square slot antenna.

6.6.3 Results

The proposed quad band antenna was simulated using ANSYS HFSS software. The prototypes were fabricated using an LPKF machine at NITK. The photographs of the prototype are shown in Figure 6.50. The simulated and measured reflection coefficient magnitude curves obtained are shown in Figure 6.51. On simulation, the antenna is found to operate at four different bands with -10dB impedance bandwidth of 650 MHz

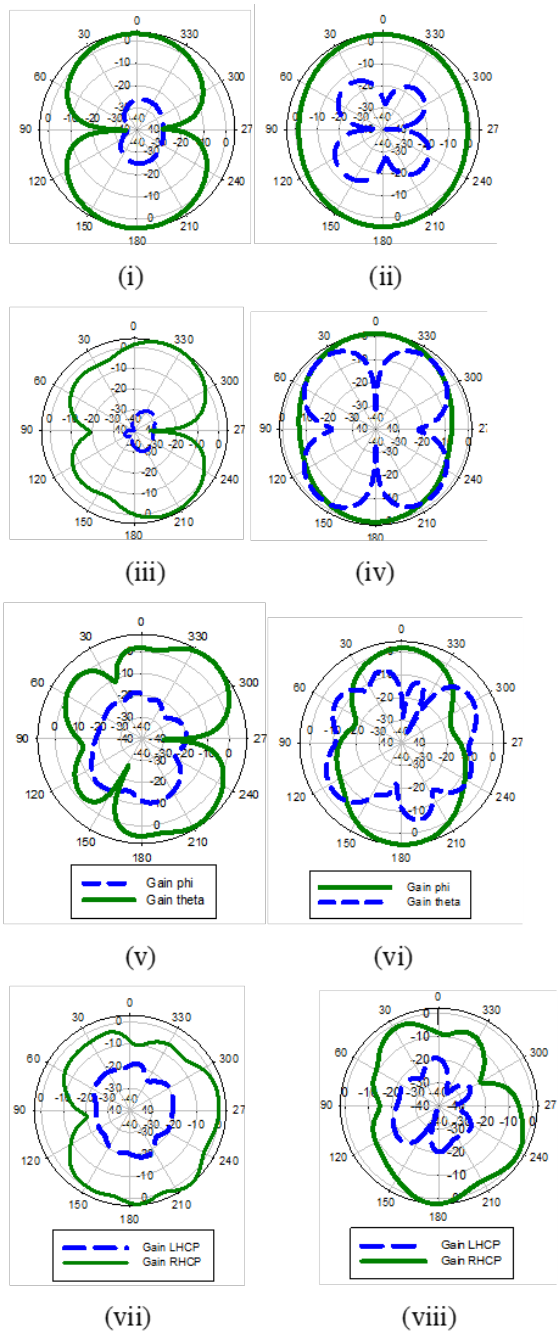

Figure 6.52: Gain Patterns at : 2.42GHz (i) phi=0 (ii) phi=90 , 4.3GHz (iii) phi=0 (iv) phi=90 , 8.46GHz (v) phi=0 (vi) phi=90, 10.9GHz (vii) phi=0 (viii) phi=90 (Gain LHCP, Gain RHCP)

(2.13 GHz 2.78 GHz centered at 2.42 GHz), 270 MHz (4.2 GHz 4.47 GHz centered at 4.33 GHz), 2.43 GHz (6.43 GHz 8.86 GHz with centre frequency at 8.46 GHz),

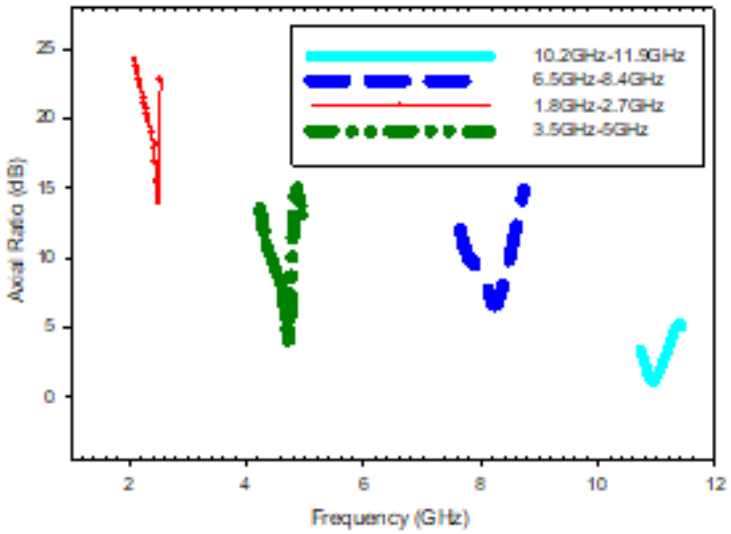

Figure 6.53: Simulated axial ratio results of proposed antenna.

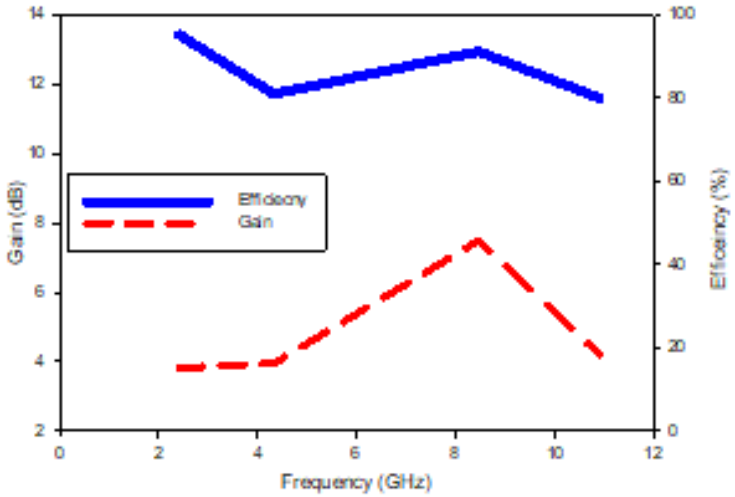

Figure 6.54: Simulated maximum gain and efficiency of the proposed antenna.

and 360 MHz (10.77 GHz 11.13 GHz centered at 10.9 GHz). The measured -10 dB bandwidths obtained were 550 MHz (2.13 GHz 2.68 GHz centered at 2.4 GHz), 320 MHz (4.2 GHz 4.52 GHz centered at 4.34 GHz), 3.2 GHz (6.5 GHz 9.7 GHz with centre frequency at 9 GHz), and 360 MHz (10.77 GHz 11.13 GHz centered at 10.9

GHz). The simulated radiation patterns at the four different resonance frequencies for the x-z and y-z planes are shown in Figure 6.52. The patterns depict typical slot antenna like radiation characteristics with slight beam tilting at the SRR resonant frequencies. The Gain LHCP and Gain RHCP patterns are plotted at 10.9 GHz. A Right Hand Circularly Polarized wave is obtained at 10.9 GHz. The simulated axial ratio versus frequency for the different bands of operation is shown in Figure 6.53. A 3-dB axial ratio bandwidth of 3.5% (10.76 GHz 11.15 GHz) is observed at resonance frequency 10.9 GHz. The simulated peak gain and efficiency values at the four centre frequencies are 3.82 dB / 95.14%, 3.95 dB / 81%, 7.5 dB / 91.2%, 4.2 dB / 80% respectively. The variation in simulated peak gain and efficiency values with frequency can be seen in Figure 6.54. A table of comparison is provided that highlights the advantages of the proposed designs over the existent multiband CP slot antenna designs.

Table 6.1: Performance Comparison of Different Multiband CP Based Slot Antennas (λ_g- guided wavelength corresponding to the lowest resonant frequency.)

REF	SIZE	BANDS (GHz)	IMP BW (%)	ARBW (%)	GAIN (dBi)	EFF. (%)	POLRZN SENSE TNBLTY
Hsieh *et al.* (2012)	0.6 λ_g^2	1.227, 1.575	3.7, 1.2	0.9, 0.6	1.1, 1.45	86.5, 80.7	NO
Baek and Hwang (2013)	1.74 λ_g^2	3.53, 5.08	33.16, 22.72	1.7, 3.86, 5.23	5.5, 4.63, 6.77	–	NO
Xu *et al.* (2017)	1.58 λ_g^2	3, 7.5	44, 70.9	35.9, 44, 6.3	4.2, 3.7, 3.5	–	NO
Wang *et al.* (2012)	0.5 λ_g^2	1.22, 1.57, 2.31	9, 2.5, 27	4.9, 1.2, 4.3	4, 4.6, 5.7	–	NO
Kandasamy *et al.* (2016)	2.1 λ_g^2	3.1, 4.7	12.9, 8.5	3.1, 4.2	7.3, 8.5	–	YES
Ghaffarian *et al.* (2017)	0.4 λ_g^2	3.2, 5	14, 14.5	27, 9	-4.7, 5.5	–	NO
Saraswat and Harish (2018)	0.3 λ_g^2	2.4, 3.5	37.52, 4.8	32.13, 2.17	3.2, 3.8	–	NO
Chen *et al.* (2018)	0.8 λ_g^2	2.4, 3.5	6.3, 8.1	10.2, 7.7	0.1, 0.2	–	NO
Proposed	0.2 λ_g^2	2.4, 4.2	42.4, 15.6	45.5, 15.7	3.8, 4.5	91, 98	YES
Proposed Paul *et al.* (2018)	0.3 λ_g^2	1.83, 2.5, 3.1	21.4, 12.8, 4.5	4.37, 11.9, 3.6	2.7, 4.2, 3.5	75, 90, 82	YES
Proposed	0.2 λ_g^2	1.5, 2.75, 3.16	10, 9.1, 7.3	9.3, 7.3, 8.5	3.2, 4.5, 3.5	80, 94, 85	YES

6.6.4 Summary

Several CP multiband SRR loaded designs were proosed in the chapter.

- The first design was a novel CPW fed circularly polarized slot antenna of dimension 0.2 λ_g^2, where λ_g is the guide wavelength at the resonant frequency. The slot antenna is made to extend symmetrically at opposite corners to generate the CP waves. The sense of polarization can be controlled by altering the position of the extensions. The antenna is simulated using the HFSS software and the results are compared with those of the measured ones. The proposed antenna is found to have an impedance bandwidth of 0.88 GHz, ARBW of 35.2%, peak gain of 3.5 dB and efficiency of 95% at the center frequency. An axial ratio value of less than 3 dB value is obtained over the entire operating bandwidth.

- The second design presents a copper strip array loaded square slot antenna with corner extensions. The frequencies of resonance obtained are 2.4 GHz and 4.52 GHz with measured impedance bandwidths of 42.4% and 15.7% and measured ARBWs of 45.5% and 15.7% in the two bands, respectively. Good agreement is obtained between measured and simulated results. The gain and efficiency values were higher than 3.5 dBi and 90% in all bands. Parametric analysis and study of current distributions were carried out at the resonant frequencies. The resonant frequency bands can be controlled depending on the slot and copper strip dimensions, while the sense of polarization at the resonant frequencies is changed by altering position of extensions and orientation of the copper strips. The proposed dual band CP square slot antenna offers compact size with wide impedance and ARBW and easy control of frequency bands compared to other dual band CP works found in literature.

- The third design presents a multiband circularly polarized slot antenna using copper strips and an SRR unit cell is designed to operate at resonant frequencies of 1.83 GHz, 2.5 GHz and 3.16 GHz has been proposed. The sense of polarization can be reversed by changing the orientation of the strips. A compact structure is obtained due to the resonance obtained from loading the slot with SRR and strips. A minimum impedance bandwidth of 4.5% and AR bandwidth of 3.2% are obtained in all the bands. The proposed antenna provides resonances at 1.83 GHz, 2.5 GHz, and 3.1 GHz with impedance bandwidths of 21.4%, 12.8%, 4.5%,

ARBWs of 4.37%, 11.9%, 3.6% and gains of 2.7, 3.2, 3.5, respectively. Thus, a novel, compact, SRR and strips loaded tri-band antenna with CP characteristics is proposed in this section.

- In the fourth design, a compact multiband slot antenna is proposed which operates at three circularly polarized bands and offers wide impedance bandwidth and ARBW is designed using a meandered F-shaped feed and by loading a meandered U-strip and SRR on the square slot. The frequencies of resonance obtained are 1.5 GHz, 2.75 GHz and 3.16 GHz with measured impedance bandwidths of 10%, 9.1% and 7.3% and measured ARBWs of 9.3%, 7.3% and 8.5% at the three resonant bands. A peak gain value of more than 3 dBi and a efficiency higher than 80% is obtained for the proposed antenna at all the operating bands. The resonant frequency bands can be controlled depending on the feed, U-strip and SRR dimensions, while the polarization sense at the resonant frequencies is controlled upon altering the direction of the F-shaped feed and the SRR. The proposed design is the smallest compared to the latest state of the art with multi-band coverage CP based slot antennas.

- The fifth design presents a simple SRR loaded square slot antenna that is designed to operate at four resonant frequencies. Two pairs of SRR are loaded on the substrate and the resonant properties of the SRR are used to provide multiple bands of operation which leads to quad band nature of the proposed slot antenna. The simulation results show that the antenna offers wideband and CP operation at the third and fourth bands respectively. The CP operation could be attributed to the electric field distribution at the spiral shape connected SRRs. Also, the peak gain and efficiency values were higher than 3.8 dBi and 78% at all the centre frequencies.

Chapter 7

CONCLUSION AND FUTURE WORK

The demand for antennas that could be integrated into various electronic devices that operate at different frequencies and used simultaneously for varying applications has considerably increased over the years. Similarly, there is an emerging need for antennas that could be reconfigured for various polarization states and operate over a wide range of frequencies for various applications in industry, satellite communication, military and medical fields. This research focuses on designing novel antenna structures of low profile and cost with desirable characteristics such as multiband and wideband properties in addition to frequency and polarization reconfigurability features. For this, the resonant properties of metamaterials and their ability to aid in configuring compact structures with tunable features will be utilized. The designs investigated in thesis aim for compact structures that can

1. Provide multiple bands of operation that could be easily tuned as per the application requirement.

2. Introduce desired properties at required frequency bands such as multiple polarization states and wideband operation.

3. Develop compact slot antenna designs that exhibit ultra-wideband resonance characteristics using the concept of artificial transmission lines.

7.1 Contributions

The major contributions of the thesis can be broadly classified into four depending on the application of the designs.

7.1.1 Multiband SRR and Strip Loaded Designs

The negative permeability and negative permittivity properties of the SRR and copper strip arrays when suitably excited have been used to obtain multiple bands of resonance in slot antennas. The fundamental slot mode is obtained due to the slot and can be tuned depending on the slot dimensions, while the additional resonance bands obtained due to the introduction of these MTM elements can be controlled by fine tuning the dimensions of these elements. They are suitably positioned and oriented along the slot geometry in order to obtain maximum resonance. Thus, these novel structures help to obtain compact multiband designs with independently tunable frequency bands.

A compact tri-band slot antenna with independent tuning capability of its resonant frequencies is proposed. A microstrip line fed square slot is loaded with SRRs to obtain multiband characteristics. The slot is designed to resonate at 2.6 GHz. Two SRRs with single and multiple splits are loaded with the slot, which provide additional resonances at 4.3 and 4.7 GHz, respectively. Parametric analysis of the antenna shows that its resonance frequencies are controlled independently. The proposed antenna is fabricated on an FR4 substrate with a size of 60 x 60 x 1.56 mm^2. The proposed design offers stable omnidirectional patterns and >3.8 dBi at all the resonating frequency bands.

A novel copper strip array loaded pentaband square slot antenna of dimension 0.2 λ_g^2 is proposed here, where λ_g is the guide wavelength at the resonant frequency. The loading of the slot with the array of thin copper strips yields to operation of the antenna at five resonant frequencies 2.2 GHz, 3.4 GHz, 4.6 GHz, 5.4 GHz, 6.6 GHz. The antenna is simulated using the HFSS software and the results are found to be in good agreement with those of the measured ones. The proposed antenna is found to have an impedance bandwidth above 300 MHz, peak gain more than 3 dB and efficiency of at least 80% at all the resonant frequencies.

A compact SRR and strip loaded slot antenna is proposed which offers 78% miniaturization at its lowest band of operation compared to the design proposed in [4]. Five

bands of operation are obtained by exciting the copper strips and the SRR unit cell.

7.1.2 Slot Antennas Exhibiting Wideband Characteristics

Compact multiband slot antennas are designed using quarter wavelength SRR loaded open slot antennas. The fictitious short circuit concept is used to obtain the wideband feature. Additional bands are obtained on loading the slot with SRR and modified SRR structures. Also, bandwidth enhancement is made possible by loading the slot capacitance elements. Independent tuning of each of the bands is possible by changing the slot and SRR dimensions. The dual band antenna is designed to operate at frequency bands centred at 2.4 GHz and 6.03 GHz with impedance bandwidths of 2.7 Ghz and 330 MHz respectively while the triband antenna was designed to operate at centre frequencies of 2.4 GHz, 7.4 GHz and 9.36 GHz offering impedance bandwidths of 2.4 GHz, 50 MHz and 210 MHz respectively.

7.1.3 UWB Slot Antenna Using Artificial Transmission Line

A UWB antenna is designed using the concept of artificial transmission lines. Here the slot is loaded with rows of transmission lines that have periodically dispersed gaps, The TLs are loaded such that the widths of the resonator elements and the periodicity at each row remain the same. Excitation of each of the transmission line row leads to the generation of a different resonance depending on the capacitance introduced by the gaps and the inductance of the resonator elements. The different resonances thus produced combines with the slot fundamental resonance mode to give a UWB response with good gain and efficiency values over the entire operating band. The proposed antenna offers a compact geometry of 0.23 λ_g^2 and operates from 2.1 GHz to 11.5 GHz with a fractional bandwdith of 138%. The gain varies from 3.8 dBi - 5.8 dBi over the operating bandwidth while the radiation efficiency ranges from 88% - 98%. Here λ_g corresponds to the lowest operating frequency.

7.1.4 SRR and Strip Loaded Multiband CP Based Antennas

A simple method is proposed to obtain CP for a CPW fed square slot antenna at the designed frequency. Complementary to the conventional method of using truncated corners in microstrip patch antenna to obtain orthogonal modes with 90° phase shift,

here, circularly polarised waves are generated at the designed frequency by adding extensions to the slot corners. The slot is CPW fed thus, offering a planar design. The sense of polarization can be easily controlled by changing the position of extensions. The frequency of resonance can be controlled depending on the dimension of the slot.

The proposed design describes a micro-strip fed square slot antenna of compact nature that operates at dual circularly polarized bands. A pair of symmetric rectangular extension is introduced on opposite corners of the square slot which is designed to radiate at 2.36 GHz. This produces the lower circularly polarized band which operates from 2.24 GHz - 2.62 GHz and centered at 2.4 GHz with a 3 dB AR (Axial Ratio) bandwidth of 15.7%. Besides, loading the square slot with an array of inclined and truncated rectangular copper strips helps produce a higher circularly polarized band. The band operates between 3.26 GHz - 5.18 GHz centered at 4.52 GHz with a 3dB AR bandwidth of 45.5%. These frequency bands can be independently tuned depending on the slot and strip dimensions respectively. However, independent control of the polarization sense at the two bands depends on the position of the extensions and the orientation of the copper strips respectively.

A novel multiband CP square slot antenna is proposed with improved ARBW and efficiency values. The antenna is fed with an F-shaped microstrip line, and loaded with an SRR and U-strip, to produce triband operation with centre frequencies at 1.5 GHz, 2.5 GHz, and 3.2 GHz. The different current distributions along the sot antenna geometry at the various frequencies are analysed and studied.

A novel, compact, SRR and strips loaded tri-band antenna with CP characteristics is proposed in this communication. The proposed antenna provides resonances at 1.83 GHz, 2.5 GHz, and 3.1 GHz with impedance bandwidths of 21.4%, 12.8%, 4.5%, ARBWs of 4.37%, 11.9%, 3.6% and gains of 2.7, 3.2, 3.5, respectively. The proposed design provides wide CP resonance bands, wide ARBW values and compact size along with a mechanism to control the CP orientation compared to other designs.

A quad band SRR loaded slot antenna is designed which exhibits circular polarization at one its bands due to the connected SRR ring. Wideband characteristic is also observed. The different resonances are obtained due to the excitation of the different pairs of SRRs arranged around the feed line at the substrate bottom.

7.2 Future Scope

The current technological era finds a surge in applications of multiband antennas for biomedical and communication purpose. The work presented in the thesis can be further extended by loading active elements such as pin diodes or varactor diodes that help in fine tuning of the different bands especially in case of micro split SRRs. The diodes when switched on/off help to create or close the micro splits which creates a change in the capacitive effects of the SRR. This in turn shifts the operating resonance frequency depending on the opearating state of the diode. Also, the dual band CP characteristics design can be extended to obtain CP over a wideband of frequencies. Besides, study is being carried out regarding the various works implemented for simple patch and monopole antenna designs, with an objective to design compact multiband antenna structures. In the case of biomedical applications, there have been multiple devices investigated for the need in detection of arrhythmia, sleep apnoea, cancer and other disorders. Besides, insertion of chips, spotting of the exact position of disorder and diseased tissues and their timely treatment requires the development and experimentation of such multiband compact antenna designs that can be easily simulated in bio-compatible environments and tested using body phantoms. Hence, there will be a greater need in future for miniaturized multiband antennas using metamaterials for such diversified applications and similarly in the field of space, defence, aviation, metamaterial science and physics.

In the area of wireless communication, millimeter wave technology is a promising sector where good reliability and high data rate are guaranteed for low cost, short range communication. This is implemented in the 60 GHz band using the CMOS (complementary metal-oxide-semiconductor) technology to realize the necessary integrated circuits. The high resolution, high gain and compactness of these antenna designs make them a suitable candidate for collision avoidance millimeter wave radar systems. In order to design highly sensitive biosensors, on-chip antennas that can operate at the Terahertz frequency range have been developed. Terahertz testing equipment and nano-fabrication techniques have facilitated the growth of this technology. Further developments in the wireless communication world would require suitable design of such nano sized antennas that can operate at higher frequency bands.

Hence antenna design is no longer limited to structuring an external hardware en-

tity for reception and transmission of signals, but the antenna system is required to be effectively incorporated into the concerned wireless communication system covering the required frequency standards. The size, number of operating bands, impedance bandwidths, availability of CP and UWB features provide constraints to the design while ensuring good antenna and gain values over the operating bandwidth. Reconfigurable and pattern diversity antennas that can radiate for MIMO systems at higher frequency range values are also being developed.

Publications based on the thesis

Refereed International Journals

1. **Princy Paul**, Krishnamoorthy Kandasamy and Mohammad Sharawi, "A tri-band slot antenna loaded with split ring resonators ", **Microwave and Optical Technology Letters, Vol. 59, No. 10, pp. 4595 - 4606, October 2017**.

2. **Princy Paul**, Krishnamoorthy Kandasamy and Mohammad Sharawi, "A Tri-band Circularly Polarized Strip and SRR Loaded Slot Antenna", **IEEE Transactions on Antennas and Propagation, Vol. 66, No. 10, pp. 5569 - 5573, October 2018**.

3. **Princy Paul**, Krishnamoorthy Kandasamy, Mohammad Sharawi and Basudev Majumder, "Dispersion Engineered Transmission Line Loaded Slot Antenna for UWB Applications", **IEEE Antennas and Wireless Propagation Letters, Vol. 18, N0. 2, pp. 323-327, December 2018**

4. **Princy Paul**, Krishnamoorthy Kandasamy and Mohammad Sharawi, "A Corner Expanded Slot Antenna Loaded with Copper Strips for Dual-band Circular Polarization Characteristics", **Microwave and Optical Technology Letters, 2019. (Minor revision submitted)**

5. **Princy Paul**, Krishnamoorthy Kandasamy and Mohammad Sharawi, "A Multi-Band U-Strip and SRR Loaded Slot Antenna with Circular Polarization Characteristics", **Advanced Electromagnetics, 2019. (Submitted)**

Conferences

1. **Princy Paul**, Krishnamoorthy Kandasamy and Mohammad Sharawi, "A Corner Expanded CPW-Fed Slot Antenna with Circular Polarization Characteristics

", **2019 European Conference on Antennas and Propagation (EuCAP), March 31 - April 05, 2019, Krakow, Poland**.

2. **Princy Paul**, Krishnamoorthy Kandasamy and Mohammad Sharawi, "A Copper Strip Array Loaded Multiband Square Slot Antenna ", **IEEE-INAE Workshop on Electromagnetics (IIWE), December 06 - 08, 2018, Trivandrum, India**.

3. **Princy Paul**, Krishnamoorthy Kandasamy and Mohammad Sharawi, "A Tri-Band SRR Loaded Half Slot Antenna with Wideband Properties ", **The IEEE Radio and Antenna Days of the Indian Ocean (RADIO), October 15-18, 2018, Mauritius**.

4. **Princy Paul**, Krishnamoorthy Kandasamy and Mohammad Sharawi, "A Multi-Band SRR and Strip Loaded Slot Antenna ", **2018 IEEE International Symposium on Antennas and Propagation and USNC-URSI Radio Science Meeting, July 8-13, 2018, Boston, Massachusetts**.

5. **Princy Paul**, Krishnamoorthy Kandasamy and Mohammad Sharawi, "SRR Loaded Slot Antenna for Multiband Applications ", **2017 IEEE AP-S Symposium on Antennas and Propagation and USNC-URSI Radio Science Meeting, July 9-14, 2017, San Diego, California, USA**.

6. **Princy Paul**, Krishnamoorthy Kandasamy and Mohammad Sharawi, "Quad Band SRR loaded Square Slot Antenna ", **The 9th IEEE GCC Conference and Exhibition, May 8-11, 2017, Manama, Bahrain**.

Curriculum Vitae

Princy Paul
Celin Cottage, Thiruvankulam P.O.,
Ernakulam, Kerala-682305
Email: princy7paul@gmail.com

Education:

- M.Tech in Tele-communication,
  National Institute of Technology, Calicut (June 2015)
  CGPA: 7.8/10

- B.Tech in Electronics and Communication Engineering,
  Rajagiri School of Engineering and Technology, Cochin
  Mahatma Gandhi University, Kerala (June 2013)
  CGPA: 78%

Bibliography

Baek, J. G. and Hwang, K. C. (2013). Triple-band unidirectional circularly polarized hexagonal slot antenna with multiple l-shaped slits, *IEEE Trans. Antennas Propag* **61**(9): 4831–4835.

Balanis, C. A. (1992). Antenna theory: A review, *Proceedings of the IEEE* **80**(1): 7–23.

Bao, X. and Ammann, M. (2008). Dual-frequency dual-sense circularly-polarized slot antenna fed by microstrip line, *IEEE Transactions on Antennas and Propagation* **56**(3): 645–649.

Basaran, S., Olgun, U. and Sertel, K. (2013). Multiband monopole antenna with complementary split-ring resonators for wlan and wimax applications, *Electronics Letters* **49**(10): 636–638.

Behdad, N. and Sarabandi, K. (2004). A multiresonant single-element wideband slot antenna, *IEEE Antennas and Wireless Propagation Letters* **3**(1): 5–8.

Behdad, N. and Sarabandi, K. (2005). A wide-band slot antenna design employing a fictitious short circuit concept, *IEEE Transactions on antennas and Propagation* **53**(1): 475–482.

Caloz, C. and Itoh, T. (2005). *Electromagnetic metamaterials: transmission line theory and microwave applications*, John Wiley & Sons.

Caloz, C., Itoh, T. and Rennings, A. (2008). Crlh metamaterial leaky-wave and resonant antennas, *IEEE Antennas and Propagation Magazine* **50**(5).

Cao, Y., Cheung, S. and Yuk, T. (2015). A multiband slot antenna for gps/wimax/wlan systems, *IEEE Transactions on Antennas and Propagation* **63**(3): 952–958.

Chen, S.-W., Wang, D.-Y. and Tu, W.-H. (2014). Dual-band/tri-band/broadband cpw-fed stepped-impedance slot dipole antennas, *IEEE Transactions on Antennas and Propagation* **62**(1): 485–490.

Chen, W.-L., Wang, G.-M. and Zhang, C.-X. (2009). Bandwidth enhancement of a microstrip-line-fed printed wide-slot antenna with a fractal-shaped slot, *IEEE Transactions on Antennas and Propagation* **57**(7): 2176–2179.

Chen, W.-S. and Ku, K.-Y. (2006). Broadband design of the non-symmetric ground $\lambda/4$ open slot antenna with small size, *2006 IEEE Antennas and Propagation Society International Symposium*, IEEE, pp. 2563–2566.

Chen, W.-S. and Ku, K.-Y. (2008). Bandwidth enhancement of open slot antenna for uwb applications, *Microwave and Optical Technology Letters* **50**(2): 438–439.

Chen, X., Han, L., Chen, X. and Zhang, W. (2018). Dual-band circularly polarized antenna using mu-negative transmission lines, *IEEE Antennas and Wireless Propagation Letters* .

Cheribi, H., Ghanem, F. and Kimouche, H. (2013). Metamaterial-based frequency reconfigurable antenna, *Electronics Letters* **49**(5): 315–316.

Chou, C., Lin, K. and Su, H. (2007). Broadband circularly polarised crosspatch-loaded square slot antenna, *Electronics Letters* **43**(9): 485–486.

Dang, L., Lei, Z. Y., Xie, Y. J., Ning, G. L. and Fan, J. (2010). A compact microstrip slot triple-band antenna for wlan/wimax applications, *IEEE Antennas and Wireless Propagation Letters* **9**: 1178–1181.

Deng, I.-C., Chen, J.-B., Ke, Q.-X., Chang, J.-R., Chang, W.-F. and King, Y.-T. (2007). A circular cpw-fed slot antenna for broadband circularly polarized radiation, *Microwave and Optical Technology Letters* **49**(11): 2728–2733.

Dong, Y., Toyao, H. and Itoh, T. (2011). Compact circularly-polarized patch antenna loaded with metamaterial structures, *IEEE transactions on antennas and propagation* **59**(11): 4329–4333.

Ekmekci, E., Topalli, K., Akin, T. and Turhan-Sayan, G. (2009). A tunable multi-band metamaterial design using micro-split srr structures, *Optics express* **17**(18): 16046–16058.

Eleftheriades, G. V. and Balmain, K. G. (2005). *Negative-refraction metamaterials: fundamental principles and applications*, John Wiley & Sons.

Engheta, N. and Ziolkowski, R. W. (2006). *Metamaterials: physics and engineering explorations*, John Wiley & Sons.

Fries, M. K., Grani, M. and Vahldieck, R. (2003). A reconfigurable slot antenna with switchable polarization, *IEEE Microwave and Wireless Components Letters* **13**(11): 490–492.

Futter, P. and Soler, J. (2017). Antenna design for 5g communications, *2017 Sixth Asia-Pacific Conference on Antennas and Propagation (APCAP)*, IEEE, pp. 1–3.

Garcia-Garcia, J., Bonache, J. and Martín, F. (2006). Application of electromagnetic bandgaps to the design of ultra-wide bandpass filters with good out-of-band performance, *IEEE Transactions on Microwave Theory and Techniques* **54**(12): 4136–4140.

Ghaffarian, M. S., Moradi, G. and Mousavi, P. (2017). Switchable dual/triple-band circularly polarised slot antenna by using artificial transmission line, *IET Microwaves, Antennas & Propagation* **11**(12): 1734–1741.

Gholamrezaei, M., Naser-Moghadasi, M. and Sadeghzadeh, R. (2014). An efficient frequency adjustable penta-band slot antenna, *Antennas and Propagation (EuCAP), 2014 8th European Conference on*, IEEE, pp. 2530–2533.

Gil, M., Bonache, J. and Martin, F. (2007). Metamaterial filters with attenuation poles in the pass band for ultra wide band applications, *Microwave and Optical Technology Letters* **49**(12): 2909–2913.

Gopikrishna, M., Krishna, D., Aanandan, C., Mohanan, P. and Vasudevan, K. (2008). Compact linear tapered slot antenna for uwb applications, *Electronics Letters* **44**(20): 1174–1175.

Gopikrishna, M., Krishna, D. D., Aanandan, C., Mohanan, P. and Vasudevan, K. (2009). Design of a microstip fed step slot antenna for uwb communication, *Microwave and Optical Technology Letters* **51**(4): 1126–1129.

Hoang, T. V., Le, T. T., Li, Q. Y. and Park, H. C. (2016). Quad-band circularly polarized antenna for 2.4/5.3/5.8-ghz wlan and 3.5-ghz wimax applications, *IEEE antennas and wireless propagation letters* **15**: 1032–1035.

Hrabar, S., Krois, I., Bonic, I. and Kiricenko, A. (2013). Ultra-broadband simultaneous superluminal phase and group velocities in non-foster epsilon-near-zero metamaterial, *Applied physics letters* **102**(5): 054108.

Hsieh, W.-T., Chang, T.-H. and Kiang, J.-F. (2012). Dual-band circularly polarized cavity-backed annular slot antenna for gps receiver, *IEEE Transactions on Antennas and Propagation* **60**(4): 2076–2080.

Hu, H.-T., Chen, F.-C. and Chu, Q.-X. (2016). A wideband u-shaped slot antenna and its application in mimo terminals, *IEEE Antennas and Wireless Propagation Letters* **15**: 508–511.

Hu, H.-T., Chen, F.-C. and Chu, Q.-X. (2017). Novel broadband filtering slotline antennas excited by multimode resonators, *IEEE Antennas and Wireless Propagation Letters* **16**: 489–492.

Hu, W., Yin, Y.-Z., Fei, P. and Yang, X. (2011). Compact triband square-slot antenna with symmetrical l-strips for wlan/wimax applications, *IEEE Antennas and Wireless Propagation Letters* **10**: 462–465.

Huang, X., Cheng, C. and Zhu, L. (2012). An ultrawideband (uwb) slotline antenna under multiple-mode resonance, *IEEE Transactions on Antennas and Propagation* **60**(1): 385–389.

Ishikawa, A., Tanaka, T. and Kawata, S. (2007). Frequency dependence of the magnetic response of split-ring resonators, *JOSA B* **24**(3): 510–515.

Jan, J.-Y. and Su, J.-W. (2005). Bandwidth enhancement of a printed wide-slot antenna with a rotated slot, *IEEE Transactions on Antennas and Propagation* **53**(6): 2111–2114.

Javan, D. S., Salari, M. A. and Ghoochani, O. H. (2008). Cross-slot antenna with u-shaped tuning stub for ultra-wideband applications, *International Journal of Antennas and Propagation* **2008**.

Jiang, X., Zhang, Z., Li, Y. and Feng, Z. (2013). A wideband dual-polarized slot antenna, *IEEE Antennas and Wireless Propagation Letters* **12**: 1010–1013.

Johnson, R. C. and Jasik, H. (1984). Antenna engineering handbook, *New York, McGraw-Hill Book Company, 1984, 1356 p. No individual items are abstracted in this volume.* .

Kandasamy, K., Majumder, B., Mukherjee, J. and Ray, K. (2015). Low-rcs and polarization-reconfigurable antenna using cross-slot-based metasurface, *IEEE Antennas and Wireless Propagation Letters* **14**: 1638–1641.

Kandasamy, K., Majumder, B., Mukherjee, J. and Ray, K. (n.d.). Dual-band circularly polarized split ring resonators loaded square slot antenna.

Kandasamy, K., Majumder, B., Mukherjee, J. and Ray, K. P. (2016). Dual-band circularly polarized split ring resonators loaded square slot antenna, *IEEE Trans. Antennas Propag* **64**(8): 3640–3645.

Kanno, H. (2007). Compact ultra-wideband antenna based on broadband radiating ground slit fed by microstrip line, *2007 IEEE Antennas and Propagation Society International Symposium*, IEEE, pp. 4645–4648.

Karimian, R., Oraizi, H., Fakhte, S. and Farahani, M. (2013). Novel f-shaped quad-band printed slot antenna for wlan and wimax mimo systems, *IEEE Antennas and Wireless Propagation Letters* **12**: 405–408.

Khan, M., Sharawi, M. et al. (2014). A 2× 1 multiband mimo antenna system consisting of miniaturized patch elements, *Microwave and Optical Technology Letters* **56**(6): 1371–1375.

Ko, S.-T., Park, B.-C. and Lee, J.-H. (2013). Dual-band circularly polarized patch antenna with first positive and negative modes, *IEEE Antennas and Wireless Propagation Letters* **12**: 1165–1168.

Kraus, J. D. and Marhefka, R. J. (2001). Antennas for all applications 3rd ed.

Kumar, R., Khokle, R. and Krishna, R. R. (2014). A horizontally polarized rectangular stepped slot antenna for ultra wide bandwidth with boresight radiation patterns, *IEEE Transactions on Antennas and Propagation* **62**(7): 3501–3510.

Latif, S. I., Shafai, L. and Sharma, S. K. (2005). Bandwidth enhancement and size reduction of microstrip slot antennas, *IEEE Transactions on Antennas and Propagation* **53**(3): 994–1003.

Lee, C.-H., Chen, S.-Y. and Hsu, P. (2009). Isosceles triangular slot antenna for broadband dual polarization applications, *IEEE Transactions on Antennas and Propagation* **57**(10): 3347–3351.

Li, M., Lu, M. and Cui, T. J. (2008). Novel miniaturized dual band antenna design using complementary metamaterial, *2008 International Workshop on Metamaterials*.

Li, Y. S., Yang, X. D., Liu, C. Y. and Jiang, T. (2010). Compact cpw-fed ultra-wideband antenna with dual band-notched characteristics, *Electronics Letters* **46**(14): 967–968.

Liang, X. and Michael, C. Y. W. (2000). Microstrip-fed wide-band slot array with finite ground.

Lim, S., Caloz, C. and Itoh, T. (2004). Metamaterial-based electronically controlled transmission-line structure as a novel leaky-wave antenna with tunable radiation angle and beamwidth, *IEEE Transactions on Microwave Theory and Techniques* **52**(12): 2678–2690.

Lu, W.-J. and Zhu, L. (2015). Wideband stub-loaded slotline antennas under multimode resonance operation, *IEEE Trans. Antennas Propag.* **63**(2): 818–823.

Lui, W., Cheng, C., Cheng, Y. and Zhu, H. (2005). A novel broadband multislot antenna fed by microstrip line, *Microwave and Optical Technology Letters* **45**(1): 55–57.

Luk, K.-M. (2011). The importance of the new developments in antennas for wireless communications, *Proceedings of the IEEE* **99**(12): 2082–2084.

Majumder, B., Kandasamy, K., Mukherjee, J. and Ray, K. (2015). Wideband compact directive metasurface enabled pair of slot antennas, *Electronics Letters* **51**(17): 1310–1312.

Marques, R., Martel, J., Mesa, F. and Medina, F. (2002). Left-handed-media simulation and transmission of em waves in subwavelength split-ring-resonator-loaded metallic waveguides, *Physical Review Letters* **89**(18): 183901.

Martel, J., Bonache, J., Marques, R., Martin, F. and Medina, F. (2007). Design of wide-band semi-lumped bandpass filters using open split ring resonators, *IEEE Microwave and Wireless Components Letters* **17**(1): 28–30.

Martin, F. (2015). *Artificial transmission lines for RF and microwave applications*, John Wiley & Sons.

Mo, T. T., Xue, Q. and Chan, C. H. (2007). A broadband compact microstrip rat-race hybrid using a novel cpw inverter, *IEEE transactions on microwave theory and techniques* **55**(1): 161–167.

Ntaikos, D. K., Bourgis, N. K. and Yioultsis, T. V. (2011). Metamaterial-based electrically small multiband planar monopole antennas, *IEEE Antennas and Wireless Propagation Letters* (10): 963–966.

Pan, C.-Y., Horng, T.-S., Chen, W.-S. and Huang, C.-H. (2007). Dual wideband printed monopole antenna for wlan/wimax applications, *IEEE Antennas and Wireless Propagation Letters* **6**: 149–151.

Paul, P. M., Kandasamy, K. and Sharawi, M. (2017). A tri-band slot antenna loaded with split ring resonators, *Microwave and Optical Technology Letters* **59**(10): 2638–2643.

Paul, P. M., Kandasamy, K. and Sharawi, M. S. (2018). A triband circularly polarized strip and srr-loaded slot antenna, *IEEE Transactions on Antennas and Propagation* **66**(10): 5569–5573.

Pendry, J. B., Holden, A. J., Robbins, D. and Stewart, W. (1999). Magnetism from conductors and enhanced nonlinear phenomena, *IEEE transactions on microwave theory and techniques* **47**(11): 2075–2084.

Pendry, J. B., Holden, A., Stewart, W. and Youngs, I. (1996). Extremely low frequency plasmons in metallic mesostructures, *Physical review letters* **76**(25): 4773.

Perruisseau-Carrier, J., Bongard, F., Fernandez-Bolanos, M. and Ionescu, A. M. (2011). A microfabricated 1-d metamaterial unit cell matched from dc to millimeter-waves, *IEEE Microwave and Wireless Components Letters* **21**(9): 456–458.

Piao, H., Jin, Y., Tak, J. and Choi, J. (2017). Compact mobile quad-band slot antenna design for gps l1, wimax, and wlan applications, *Journal of electromagnetic engineering and science* .

Rajkumar, R. and Kiran, K. U. (2016). A compact metamaterial multiband antenna for wlan/wimax/itu band applications, *AEU-International Journal of Electronics and Communications* **70**(5): 599–604.

Rao, P., Fusco, V. and Cahill, R. (2000). A broadband antenna for pcn/umts applications, *High Frequency Postgraduate Student Colloquium, 2000*, IEEE, pp. 2–5.

Row, J., Lee, T. and Chen, M. (2011). Circularly-polarized ring slot antenna fed by a v-shaped coupling strip, *IEEE transactions on antennas and propagation* .

Sadat, S., Fardis, M., Geran, F., Dadashzadeh, G., Hojjat, N. and Roshandel, M. (2006). A compact microstrip square-ring slot antenna for uwb applications, *2006 IEEE Antennas and Propagation Society International Symposium*, IEEE, pp. 4629–4632.

Sadat, S., Javan, S. et al. (2007). Design of a microstrip square-ring slot antenna filled by an h-shape slot for uwb applications, *2007 IEEE Antennas and Propagation Society International Symposium*, IEEE, pp. 705–708.

Saraswat, K. and Harish, A. R. (2018). Dual-band cp coplanar waveguide-fed split-ring resonator-loaded g-shaped slot antenna with wide-frequency ratio, *IET Microwaves, Antennas & Propagation* **12**(12): 1920–1925.

Sarkar, D., Saurav, K. and Srivastava, K. (2014). Multi-band microstrip-fed slot antenna loaded with split-ring resonator, *Electronics Letters* **50**(21): 1498–1500.

Sharawi, M. S., Khan, M. U., Numan, A. B. and Aloi, D. N. (2013). A csrr loaded mimo antenna system for ism band operation, *IEEE Transactions on antennas and propagation* **61**(8): 4265–4274.

Sharawi, M. S., Numan, A. B., Khan, M. U. and Aloi, D. N. (2012). A dual-element dual-band mimo antenna system with enhanced isolation for mobile terminals, *IEEE antennas and wireless propagation letters* **11**: 1006–1009.

Sim, C., Chen, H., Chiu, K. and Chao, C. (2012). Coplanar waveguide-fed slot antenna for wireless local area network/worldwide interoperability for microwave access applications, *IET Microwaves, Antennas & Propagation* **6**(14): 1529–1535.

Sun, X., Zeng, G., Yang, H.-C. and Li, Y. (2012). A compact quadband cpw-fed slot antenna for m-wimax/wlan applications, *IEEE Antennas and Wireless Propagation Letters* **11**: 395–398.

Sung, Y. (2011). A printed wide-slot antenna with a modified l-shaped microstrip line for wideband applications, *IEEE Transactions on Antennas and Propagation* **59**(10): 3918–3922.

Sze, J.-Y., Wong, K.-L. and Huang, C.-C. (2003). Coplanar waveguide-fed square slot antenna for broadband circularly polarized radiation, *IEEE Transactions on antennas and propagation* **51**(8): 2141–2144.

Verbiest, J. and Vandenbosch, G. (2006). Low-cost small-size tapered slot antenna for lower band uwb applications, *Electronics Letters* **42**(12): 670–671.

Wang, C.-J. and Chen, C.-H. (2009). Cpw-fed stair-shaped slot antennas with circular polarization, *IEEE Transactions on Antennas and Propagation* **57**(8): 2483–2486.

Wang, L., Guo, Y.-X. and Sheng, W. (2012). Tri-band circularly polarized annular slot antenna for gps and cnss applications, *IEEE Antennas and Wireless Propagation Letters* .

Wong, K.-L., Huang, C.-C. and Chen, W.-S. (2002). Printed ring slot antenna for circular polarization, *IEEE Transactions on Antennas and Propagation* **50**(1): 75–77.

Xu, R., Li, J., Qi, Y.-X., Guangwei, Y. and Yang, J.-J. (2017). A design of triple-wideband triple-sense circularly polarized square slot antenna, *IEEE Antennas and Wireless Propagation Letters* **16**: 1763–1766.

Yoon, I.-J., Kim, H., Chang, K., Yoon, Y. J. and Kim, Y.-H. (2004). Ultra wideband tapered slot antenna with band-stop characteristic, *Antennas and Propagation Society International Symposium, 2004. IEEE*, Vol. 2, IEEE, pp. 1780–1783.

Zhang, X., Jiao, Y. and Wang, W. (2012). Compact wide tri-band slot antenna for wlan/wimax applications, *Electronics letters* **48**(2): 64–65.

Zheng, Z.-A., Chu, Q.-X. and Huang, T.-G. (2010). Compact ultra-wideband slot antenna with stepped slots, *Journal of Electromagnetic Waves and Applications* **24**(8-9): 1069–1078.

Zheng, Z.-A., Chu, Q.-X. and Tu, Z.-H. (2011). Compact band-rejected ultrawideband slot antennas inserting with and resonators, *IEEE Transactions on Antennas and Propagation* **59**(2): 390–397.

Zhou, J., Koschny, T. and Soukoulis, C. M. (2007). Magnetic and electric excitations in split ring resonators, *Optics express* **15**(26): 17881–17890.

Zhou, L., Liu, S., Wei, Y., Chen, Y. and Gao, N. (2010). Dual-band circularly-polarised antenna based on complementary two turns spiral resonator, *Electronics letters* **46**(14): 1.

Zhu, L., Fu, R. and Wu, K.-L. (2003). A novel broadband microstrip-fed wide slot antenna with double rejection zeros, *IEEE antennas and wireless propagation letters* **2**(1): 194–196.